

**UNIVERSITÄTSKLINIKUM HAMBURG-EPPENDORF**

Institut für Experimentelle Pharmakologie und Toxikologie

Prof. Dr. med Thomas Eschenhagen

**Utilizing Engineered Heart Tissue to Evaluate Anti-Fibrotic Strategies for  
Treating Cardiac Fibrosis**

**Dissertation**

zur Erlangung des Doktorgrades PhD

an der Medizinischen Fakultät der Universität Hamburg.

Durch

**Aaltje Maria Stella Stoter**

Aus Apeldoorn

Hamburg 2024

**Datum der Disputation:** 25.11.2024

**(wird von der Medizinischen Fakultät ausgefüllt)**

**Angenommen von der**

**Medizinischen Fakultät der Universität Hamburg am:** \_\_\_\_\_

**Veröffentlicht mit Genehmigung der**

**Medizinischen Fakultät der Universität Hamburg.**

**Prüfungsausschuss, der/die Vorsitzende:** Prof. Dr. med. Thomas Eschenhagen

**Prüfungsausschuss, zweite/r Gutachter/in:** Prof. Dr. rer. nat. Dipl.-Med. Boris Fehse

**Prüfungsausschuss, dritte/r Gutachter/in:** Prof. Dr. rer. nat. Tanja Zeller

Universitätsklinikum Hamburg-Eppendorf

# Table of contents

1.	Introduction.....	1
1.1	Heart function .....	1
1.2	Cellular composition.....	2
1.2.1	Cardiomyocytes .....	2
1.2.2	Cardiomyocyte differentiation.....	4
1.2.3	Cardiac fibroblasts .....	5
1.2.4	Cardiac fibroblast differentiation.....	6
1.3	Cardiac fibrosis .....	6
1.3.1	The 3 phases of reparative cardiac fibrosis .....	7
1.3.2	Active role of fibroblasts.....	8
1.3.3	TGF- $\beta$ 1 .....	9
1.3.4	RAAS .....	10
1.3.5	A 4 <sup>th</sup> phase .....	11
1.4	Models of cardiac fibrosis.....	12
1.4.1	Existing fibrosis models .....	12
1.4.2	State-of-the-art 3D hiPSC-derived cardiac fibrosis model.....	14
1.5	The role of enhancers in gene regulation.....	15
1.5.1	RUNX1.....	17
1.5.2	CRISPR/Cas9 .....	18
1.6	In summary.....	19
1.7	Study concept.....	20
2.	Materials and Methods .....	22
2.1	Compositions.....	22
2.1.1	Media Compositions.....	22
2.1.2	Buffer compositions.....	24
2.2	2D cell culture.....	26
2.2.1	Coating.....	26
2.2.2	Stem cell culture .....	27
2.2.3	(Cardiac) fibroblasts.....	29
2.3	Differentiation .....	29
2.3.1	Cardiomyocyte differentiation.....	29
2.3.2	Cardiac fibroblast differentiation.....	31
2.4	EHT generation .....	33

2.4.1 Contractility analysis.....	34
2.4.2 Electrical pacing.....	35
2.4.3 Harvesting.....	35
2.5 Molecular analysis.....	36
2.5.1 Gene expression.....	36
2.5.2 Collagen quantification.....	39
2.5.3 Protein expression.....	40
2.5.4 Flow cytometry.....	40
2.6 Nanoindentation.....	42
2.7 Statistics.....	42
3. Results.....	43
3.1 Results I: Development of an <i>in vitro</i> fibrosis model.....	43
3.1.1 Fibroblast differentiation.....	43
3.1.2 Serum concentration.....	50
3.1.3 CF percentage.....	55
3.1.4 2D fibroblast activation.....	60
3.1.5 3D fibroblast activation.....	61
3.1.6 SB-431542 treatment.....	63
3.1.7 TGF- $\beta$ 1 treatment.....	65
3.1.8 Timing of treatment.....	67
3.1.9 The <i>in vitro</i> fibrosis model.....	71
3.2 Results II: Implementation of the <i>in vitro</i> fibrosis model.....	75
3.2.1 Quality control.....	75
3.2.2 Effects of an <i>enh35232</i> or <i>RUNX1</i> knockout in 2D culture.....	79
3.2.3 Effects of an <i>enh35232</i> or <i>RUNX1</i> knockout in 3D culture.....	83
3.2.4 Effects of an <i>enh35232</i> or <i>RUNX1</i> knockout in ERC001.....	92
4. Discussion.....	101
4.1 Fibrosis model development.....	101
4.1.1 Quiescent baseline.....	101
4.1.2 Fibroblast activation.....	104
4.1.3 Fibrosis model validation.....	105
4.2 Assessment of potential anti-fibrotic genetic interventions in the fibrosis model.....	107
4.2.1 2D cultured cardiac fibroblasts.....	107
4.2.2 The 3D EHT based fibrosis model.....	108

4.3 Global outlook .....	111
4.4 Conclusion and future perspectives .....	116
5. Summary – Zusammenfassung.....	118
6. List of abbreviations .....	120
7. References .....	124
8. Curriculum vitae .....	149
9. Acknowledgements .....	151
10. Supplements.....	152
10.1 Supplementary figures .....	152
10.1.1 Fibroblast differentiation .....	152
10.1.2 Serum concentration .....	155
10.1.3 CF percentage .....	158
10.1.4 2D fibroblast activation .....	160
10.1.5 3D fibroblast activation .....	161
10.1.6 SB-431542 treatment .....	163
10.1.7 TGF- $\beta$ 1 treatment .....	166
10.1.8 Timing of treatment .....	169
10.1.9 The <i>in vitro</i> fibrosis model .....	175
10.1.10 Quality control .....	184
10.1.11 Effects of an <i>enh35232</i> or <i>RUNX1</i> knockout in 2D culture .....	187
10.1.12 Effects of an <i>enh35232</i> or <i>RUNX1</i> knockout in 3D culture .....	189
10.1.13 CF-EHTs composed of 75% cardiomyocytes and 25% cardiac fibroblasts .....	191
10.1.14 Effects of an <i>enh35232</i> or <i>RUNX1</i> knockout in ERC001.....	193
10.1.15 <i>Enh35232</i> sequence data .....	197
10.2 Devices, materials and substances .....	198
10.2.1 Devices.....	198
10.2.2 Software .....	199
10.2.3 Materials and equipment .....	199
10.2.4 Cell culture medium and serum .....	200
10.2.5 Reagents .....	201
10.2.6 Kits .....	203
10.2.7 Composition of reagents and solutions.....	203
10.2.8 Antibody list.....	204
11. Declaration of academic integrity – Eidesstattliche Versicherung .....	205



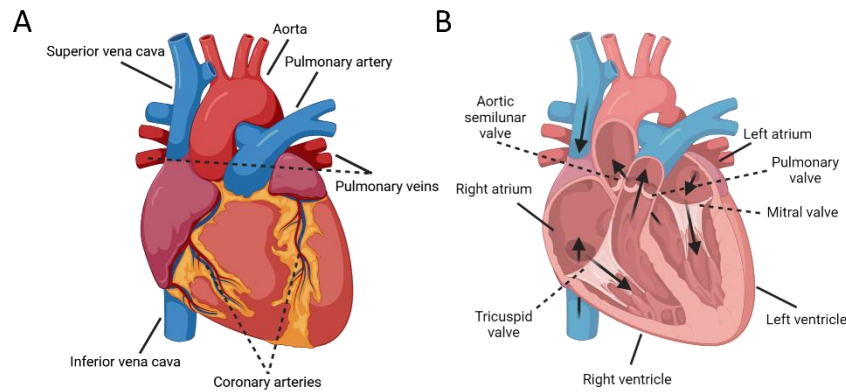
## 1. Introduction

Heart failure, a condition in which the heart is no longer able to provide the body with sufficient oxygen and nutrients, affects more than 60 million people worldwide (Becher et al., 2022). Though the mortality rate is decreasing, still an average of 33% of patients diagnosed with heart failure die within the first year of diagnosis (Emmons-Bell et al., 2022). Myocardial infarction (MI), in which an area of the heart is not provided with sufficient oxygen, is the most common cause of heart failure (Talman & Ruskoaho, 2016). Cardiac fibrosis, one of the consequences of MI, is amongst the primary causes of end-stage heart failure (Hinderer & Schenke-Layland, 2019). Despite the high prevalence and serious consequences of cardiac fibrosis, treatment options are currently limited. Fibrosis is defined as the excessive formation of fibrous connective tissue, or deposition of extracellular matrix (ECM), usually as a reparative response to injury. When fibrosis is formed as a result of injury, it is often referred to as scarring. In fibrosis, fibroblasts already present in the respective organ are activated, causing them to deposit more ECM components. Fibrosis can occur in every organ, though the pathological process is slightly different depending on the location. The injury that can lead to fibrosis is often the same, e.g., an infarction, or reduced blood flow to an area of tissue. Fibrosis is often found in the lungs as pulmonary fibrosis, in the liver as liver cirrhosis, and in the heart as cardiac fibrosis (Robertson, 2023). Though it is important to note that fibrosis can occur in each organ, here, we will focus on cardiac fibrosis.

In this work we aimed to engineer a reliable *in vitro* model of cardiac fibrosis and investigate the role of potential pro-fibrotic enhancer sequences. Therefore, this introduction will focus on the heart, cardiac fibrosis, the role of enhancer sequences in gene expression regulation and on the current state and limitations of cardiac fibrosis models.

### 1.1 Heart function

Fibrosis can compromise regular heart function. In a physiological setting, oxygen-poor blood enters the adult heart from the superior and inferior vena cava into the right atrium (Figure 1). During contraction, the blood is pumped through the tricuspid valve into the right ventricle and then out of the heart, through the pulmonary valve into the pulmonary artery and into the lung capillaries. After gas exchange through the capillary wall, oxygenation and the exhalation of carbon dioxide, the blood re-enters the heart through the pulmonary veins into the left atrium. It is then pumped through the mitral valve into the left ventricle and subsequently out of the heart through the aortic semilunar valve into the aorta and into the rest of the body. The first branches of the aorta are the coronary arteries, these provide the blood flow to the heart itself (Betts et al., 2022).



*Figure 1: Anatomy of the heart. A, frontal view of the heart, including the superior and inferior vena cava, the pulmonary artery, the pulmonary vein, the aorta and coronary arteries. B, section of the heart through the frontal plane, depicting the blood flow through the heart. Blood enters the heart from both venae cavae into the right atrium. From the right atrium blood is pumped through the tricuspid valve into the right ventricle. From the right ventricle blood is pumped out of the heart through the pulmonary valve into the pulmonary artery, through the lungs and back into the heart via the pulmonary veins into the left atrium. Blood is then pumped through the mitral valve into the left ventricle and out of the heart through the aortic semilunar valve into the aorta. Created with BioRender.com.*

## 1.2 Cellular composition

The heart consists of different cell types. The largest populations are cardiomyocytes, cardiac fibroblasts, mural cells, endothelial cells and immune cells. The atria and ventricles have been reported to consist of 30%/49% cardiomyocytes, 24%/16% cardiac fibroblasts, 17%/21% mural cells, 12%/8% endothelial cells and 10%/5% immune cells, respectively, as measured via single cell genomics (Litviňuková et al., 2020). The amount of endothelial cells has, however, also been reported to be as high as 45% (Lothar et al., 2021) and the amount of cardiomyocytes in the ventricles has been reported to be as low as 18%, as measured by cardiomyocyte nuclei staining and stereology (Bergmann et al., 2015).

### 1.2.1 Cardiomyocytes

Though generally representing less than a third of the number of cells present in the heart, cardiomyocytes constitute 70-85% of the volume of the heart (Bergmann et al., 2015; Y. Tang et al., 2009). A cardiomyocyte is conceived as a contractile, excitable heart cell; the heart (cardio) muscle (myo) cell (cyte) (Keepers et al., 2020). In the human heart, cardiomyocytes most often contain 1 nucleus, but around 25% of cardiomyocytes are binucleated (Bergmann et al., 2015; Derks & Bergmann, 2020), and they contain an abundance of sarcomeres. In other species, such as mice, the majority of cardiomyocytes are binucleated (Raulf et al., 2015) or, for example in pigs, contain up to 10 nuclei (Velayutham & Yutzey, 2022). As the smallest contractile units in each cell, sarcomeres enable the contraction of the cardiomyocytes (Brodsky et al., 1991; Miko et al., 2017).

Contraction of the multitude of cardiomyocytes in a heart needs to be synchronous. As exhibited in Figure 2, pacemaker cells in the sinoatrial node send an electrical signal, the action potential (AP), through conduction pathways, a network of specialized conductive cardiomyocytes, and from cardiomyocyte to cardiomyocyte via gap junctions, until the AP has reached the atrioventricular node, to enable a synchronous contraction of the atria. After the AP has reached the atrioventricular node, it



travels through the ventricles via larger structures of the specialized conduction system, the bundle of His and Purkinje fibres, causing a synchronous contraction of the ventricles, after which the ventricles need to repolarise (Avissar, Choi, et al., 2016; Gilbert et al., 2020).

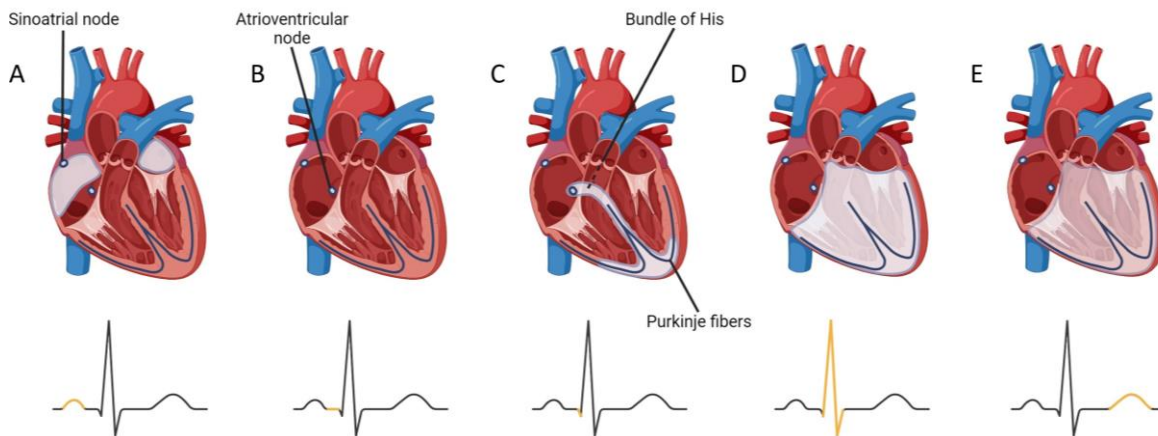


Figure 2: Conductivity through the heart. A, pacemaker cells send an AP from the sinoatrial node through the atria to facilitate synchronous contraction of the atria. B, the AP travels through the atria until it reaches the atrioventricular node. C, from the atrioventricular node the AP travels through the bundle of His and Purkinje fibres, D, to synchronously contract the ventricles. E, the repolarization of the ventricles (based on a figure by Avissar, Choi, et al., 2016). Created with BioRender.com.

In a resting state, cardiomyocytes are negatively charged. Their resting membrane potential is around -70 mV to -90 mV for atrial and ventricular cardiomyocytes, respectively. It is determined by an electrochemical gradient of potassium ( $K^+$ ) and sodium ( $Na^+$ ) maintained by the  $Na^+-K^+-ATPase$ , which exchanges 3  $Na^+$  ions out of the cardiomyocyte, for 2  $K^+$  into the intracellular space. When the AP reaches a cardiomyocyte via gap junctions, the cell membrane is passively depolarized to -40 mV, which activates  $Na^+$  channels. This causes an influx of  $Na^+$  ions into the cardiomyocyte along the gradient across the membrane, further depolarizing the cell. The membrane potential threshold is then reached, at which time  $Ca^{2+}$  channels are activated, leading to an influx of  $Ca^{2+}$  into the cardiomyocyte, again along the pre-existing gradient. This increase stimulates the release of additional  $Ca^{2+}$  from the sarcoplasmic reticulum (SR) within the cell, a process called  $Ca^{2+}$ -induced  $Ca^{2+}$  release. The  $Ca^{2+}$  binds to  $Ca^{2+}$  binding sites on the sarcomeres, troponin C coupled to actin filaments, ultimately leading to conformational changes in the troponin complex and exposure of cross-bridge binding sites. This enables the main motor protein, myosin, to bind to the actin filaments and travel across the actin filaments, leading to the contraction of each sarcomere and ultimately the entire cardiomyocyte (Avissar, Belardo, et al., 2016; Gilbert et al., 2020; M. X. Li et al., 2005; Lindert et al., 2012).

After each depolarization and contraction, repolarization and relaxation of the cardiomyocytes occurs. First,  $Ca^{2+}$  is both actively eliminated from the cytoplasm into the SR by sarcoplasmic/endoplasmic reticulum  $Ca^{2+}$  ATPase 2 (SERCA2) and exchanged for  $Na^+$  by  $Na^+/Ca^{2+}$  antiporters (NCX) for elimination out of the cardiomyocytes. Repolarization is mainly determined by  $K^+$  outflow from the cytoplasm into the extracellular space, following its concentration gradient. Finally,  $Na^+-K^+-ATPase$  restores the balance between  $Na^+$  and  $K^+$  across the cell membrane (Gilbert et al., 2020).

During the growth from newborn to adult, neither the principal anatomy of the heart nor the amount of cells present in the heart changes substantially, as postnatal cardiomyocytes possess minimal proliferation capacities. Nevertheless, during this time the heart does grow substantially in size. This growth is mainly caused by enlargement of cardiomyocytes, which is called maturational hypertrophy. The process is responsible for an up to 30-fold increase in size. The hypertrophy is necessary to meet

the increasing demand as the body grows, such as the increased oxygen demand and the increased blood volume that needs to be circulated through the body (Y. Guo & Pu, 2020; M. T. Zhao et al., 2020).

### 1.2.2 Cardiomyocyte differentiation

Myocardial cells, including primary human cardiomyocytes, originate from the mesoderm. The mesoderm appears from the primitive streak during gastrulation (Kuhn & Wu, 2010; Rawles, 1943). Due to a limited availability of primary human cardiomyocytes, it is important to be able to robustly differentiate cardiomyocytes from hiPSCs for cardiac research.

Induced PSCs were first introduced to science in 2006 (Takahashi & Yamanaka, 2006). This offered a great breakthrough in the possibility to engineer and study disease in *in vitro* models. Prior to this stem-cell revolution, animal models were often the only means available to study certain aspects of diseases. Though animal models are a valuable source of information, only limited translation is possible, attributable to the physiological differences between animal models and humans. Embryonic stem cells (ESCs) have been used to engineer human models since 1998, but ESCs are associated with severe ethical concerns. ESCs are obtained from viable human embryos, which are destroyed during the harvest procedure of the ESCs (Thomson et al., 1998).

Induced PSCs are adult cells, often fibroblasts, reprogrammed to form pluripotent cells. This procedure was first conducted with mouse fibroblasts in 2006. The produced iPSCs exhibited the same proliferation and morphological properties as ESCs. The iPSCs could be differentiated into cell types of all 3 germ layers in a teratoma assay, which proved the pluripotent potential of the iPSCs (Takahashi & Yamanaka, 2006). In 2007 reprogramming of adult cells into iPSCs was first performed with human fibroblasts, which yielded similar results (Takahashi et al., 2007).

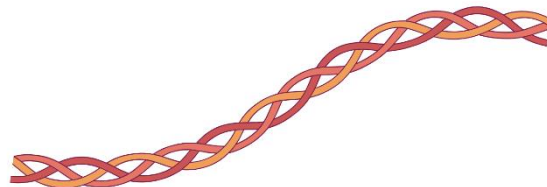
Another important advantage of the use of hiPSCs to engineer disease models is the possibility to use patient specific cells.

Multiple approaches to differentiate cardiomyocytes from hiPSCs have been published, including approaches employing the use of a 2D monolayer or 3D embryoid bodies (EBs). In this work the 3D EB method will be used. EBs are small cell aggregates formed in suspension by overnight continuous stirring of the cell culture. After the EBs are formed, hiPSCs are first manipulated with regard to Wnt/ $\beta$ -catenin activation, inducing mesodermal development of the cells. This is achieved by treatment with bone morphogenetic protein-4 (BMP-4), activin A and basic fibroblast growth factor (bFGF). After a few days, cardiac differentiation is initiated by inhibiting the Wnt/ $\beta$ -catenin signalling with XAV-939. At the end of differentiation, the EBs are enzymatically dissociated into single cells by collagenase II (Breckwoldt et al., 2017; D. Li et al., 2022; Nosedá et al., 2011; Tzahor, 2007).

To determine the purity of cardiomyocytes within the dissociated single cells for quality control, the amount of cells expressing sufficient cardiac troponin T can be measured via flow cytometry. The 3D EB protocol yields predominantly ventricular cardiomyocytes. A potential disadvantage of the use of hiPSC-derived cardiomyocytes from this and other protocols is the yield of rather immature cardiomyocytes (Y. Guo & Pu, 2020).

### 1.2.3 Cardiac fibroblasts

Though not the most prevalent in the heart, cardiac fibroblasts are one of the most important cell types. They are located in the cardiac interstitium, which represents the complex 3D formation of the ECM components (Borg et al., 1996). Cardiac fibroblasts are spindle-shaped and flat in structure, with an oval nucleus (Banjeree et al., 2006; Baudino et al., 2006). Fibroblasts are traditionally defined as cells able to produce collagen. They represent the most common cell type in connective tissue. Cardiac fibroblasts are able to express collagen types I, III, V and VI. Collagens are the most abundant ECM proteins, of which, in the heart, types I and III are most prevalent, with type I accounting for 85% and type III for 11% of all collagen present (Nikolov & Popovski, 2022). Type I collagen is a heterotrimeric triple-helix structure (Figure 3), made up of 2  $\alpha 1$  subunits, encoded by the collagen1a1 (*COL1A1*) gene, and 1  $\alpha 2$  subunit, encoded by the collagen1a2 (*COL1A2*) gene (Goffin et al., 2010; Henriksen & Karsdal, 2016). Type III collagen is also a triple-helix structure, but is a homotrimer consisting of 3  $\alpha 1$  subunits, encoded by the collagen3a1 (*COL3A1*) gene, supercoiled around each other (Nielsen & Karsdal, 2016).



*Figure 3: A triple-helix structure with 3 subunits supercoiled around each other. Collagen I is a heterotrimeric triple-helix structure, with 2  $\alpha 1$  subunits and 1  $\alpha 2$  subunit. Collagen III is a homotrimeric triple-helix structure, composed of 3  $\alpha 1$  subunits. Created with BioRender.com.*

Cardiac fibroblasts are primarily responsible for the synthesis and remodelling of the ECM. The ECM forms the scaffold and thereby the mechanical support for the heart. The ECM also represents a signalling platform. Cardiac fibroblasts express multiple ion channels and connexins and are able to influence the conduction of the action potential across the heart (Vasquez et al., 2011). Balanced production and regulation of the collagen network by cardiac fibroblasts is required to ensure the regular conductivity and rhythmicity of the heart (Tallquist & Molkenin, 2017).

Cardiac fibroblasts are able to communicate with the ECM via integrins and discoidin domain receptors (DDR), which represent important cell surface receptors. Via this communication, various cellular responses can be induced, such as proliferation and migration (Goldsmith et al., 2014). Cardiac fibroblasts are also able to communicate with cardiomyocytes, indirectly by maintaining ECM homeostasis, or directly via paracrine signalling (Cartledge et al., 2015).

Cardiac fibroblasts are challenging to define, due to a lack of specific markers. As the model described in this work consists of hiPSC-derived cardiomyocytes and hiPSC-derived cardiac fibroblasts, markers for cardiac fibroblast are an important part of quality control of the differentiated cells.

Markers that are often used include fibroblast specific protein (FSP1), vimentin, DDR2, thymus cell antigen 1 (Thy1, also called CD90), transcription factor 21 (TCF21) and platelet-derived growth factor receptor  $\alpha$  (PDGFR $\alpha$ ). Unfortunately, none of these markers is entirely specific for cardiac fibroblasts. FSP1 is not expressed by all cardiac fibroblasts and is also expressed by smooth muscle cells, endothelial cells, CD45+ immune cells and cardiomyocytes (Moore-Morris et al., 2014). Vimentin is expressed by

all cardiac fibroblasts, but also by cells of the entire endothelial lineage. DDR2 is not present in all cardiac fibroblasts and is also expressed by smooth muscle cells (Bursac & J. Kim, 2014). Thy1 is expressed by 65-85% of cardiac fibroblasts, but also expressed by immune cells and cells from the endothelial lineage (Hudon-David et al., 2007). TCF21 is a marker for mesenchyme derived cells and is therefore present in the majority of cardiac fibroblasts and is a rather specific marker. It is, however, also expressed in other cell types from the proepicardial lineage (H. Hu et al., 2020). PDGFR $\alpha$  is highly expressed by cardiac fibroblasts, but is also expressed by cardiomyocytes, smooth muscle cells and cardiovascular progenitor cells (Doppler et al., 2017; Smith et al., 2011).

As mentioned above, cardiac fibroblasts are able to communicate with cardiomyocytes, for example by paracrine signalling. Cardiac fibroblasts can express transforming growth factor- $\beta$  (TGF- $\beta$ ), which can lead to hypertrophic remodelling of cardiomyocytes (Dobaczewski et al., 2011; Pellman et al., 2016). This communication is not unidirectional. By expressing TGF- $\beta$ , cardiomyocytes can stimulate the transdifferentiation of cardiac fibroblasts into myofibroblasts, an activated phenotype of fibroblasts which produce increased amounts of ECM proteins and are able to contract (Koitabashi et al., 2011). Myofibroblasts express  $\alpha$ -smooth muscle actin ( $\alpha$ SMA) and periostin, which can be used as markers of activation (Czubryt, 2019).

Within certain limits, cardiac fibroblasts are able to transduce electrical signalling, i.e. carry the AP across the heart. In an *in vitro* experiment on a heterocellular monolayer culture of primary rat cardiomyocytes and cardiac fibroblasts, it was possible to propagate an electrical signal across cardiac fibroblasts for up to 300  $\mu$ m (Gaudesius et al., 2003). In scar tissue, cardiac fibroblasts are able to directly regulate cardiac excitation and can cause arrhythmogenesis (Y. Wang et al., 2023).

#### 1.2.4 Cardiac fibroblast differentiation

Similar to primary cardiomyocytes, there is limited availability of primary cardiac fibroblasts. Thus, the ability to robustly differentiate cardiac fibroblasts from hiPSCs was of equal importance for this work. For the differentiation of cardiac fibroblasts, Wnt/ $\beta$ -catenin signalling in the hiPSCs has to be activated, for example by treatment with CHIR99021, a glycogen synthase kinase 3 $\beta$  (GSK3 $\beta$ ) inhibitor. The activation induces mesodermal development of the cells (H. Zhang et al., 2019, 2022). This is followed by the inhibition of the Wnt pathway, which can be achieved by treatment with IWR-1. The inhibition induces the formation of cardiac progenitor cells. The formation of epicardial cells can then be achieved by subsequent exposure to CHIR99021, retinoic acid and the TGF- $\beta$ 1 receptor inhibitor SB-431542. The differentiation of epicardial cells into quiescent cardiac fibroblasts can then be reached by treatment with SB-431542 and bFGF (H. Zhang et al., 2019, 2022).

#### 1.3 Cardiac fibrosis

In accord with minimal proliferation properties, the adult human heart also has minimal regenerative properties. This means that after an injury, cardiac tissue is susceptible to the formation of scar tissue, cardiac fibrosis, in lieu of replacement of injured or apoptotic cardiomyocytes with healthy cardiomyocytes.

Cardiac fibrosis can have different causes, including chronic diseases such as diabetes, hypertension and even aging alone, but the most common cause is an acute injury caused by myocardial infarction (Raziyeva et al., 2022).

### 1.3.1 The 3 phases of reparative cardiac fibrosis

Reduced or discontinued coronary artery perfusion during MI causes oxygen deprivation, called ischemia. The tissue responds to this injury in 3 partially overlapping phases (Figure 4). First, the ischemia leads to necrosis and apoptosis of cardiomyocytes and degradation of the ECM. This triggers an immune response, called the inflammatory phase. In this phase, fibroblasts acquire an inflammatory phenotype and secrete interleukin-1 $\beta$  (IL-1 $\beta$ ). IL-1 $\beta$  plays an essential role to recruit leukocytes, including neutrophils and mononuclear cells, to the infarct area to phagocyte necrotic cells and matrix debris (Bujak et al., 2008). Neutrophils are short lived cells which undergo local apoptosis after maximally 4 days. Apoptotic neutrophils are phagocytosed by macrophages (Prabhu & Frangogiannis, 2016). These macrophages secrete anti-inflammatory cytokines, such as IL-10, and profibrotic mediators such as TGF- $\beta$ 1. The expression of TGF- $\beta$ 1 starts the second phase, the proliferative phase, in which TGF- $\beta$ 1 initiates the transdifferentiation of cardiac fibroblasts into myofibroblasts. Myofibroblasts then participate in increased ECM production by depositing mainly collagen I and III, causing the scar formation. Besides initiating the transdifferentiation of fibroblasts, the cytokines expressed by the macrophages also promote angiogenesis, which is required as a reaction to the high metabolic demand of the infarct area (W. Chen & Frangogiannis, 2013). The proliferative phase is followed by the third phase, the maturation phase, where the scar matures due to cross-linking of the ECM. In this phase, the myofibroblasts become quiescent and are referred to as matrifibrocytes (Eschenhagen, 2018; Fu et al., 2018). The exact mechanism that leads to this quiescence is unknown, but a decreased local concentration of TGF- $\beta$ 1 might be an essential component. The myofibroblasts are cleared from the site of injury over time, presumably due to apoptosis (Frangogiannis et al., 2000). The mechanism responsible for the induction of apoptosis in this process also remains unknown (Humeres & Frangogiannis, 2019). Though the scar does not actively contribute to heart function, a mature scar resulting from these phases is essential to maintain structural integrity of the heart, which is necessary for survival. Without the scar formation and maturation, the tensile strength of the wound area would be reduced, which can lead to further adverse remodelling of the heart, such as dilation or even rupture (Huebener et al., 2008).



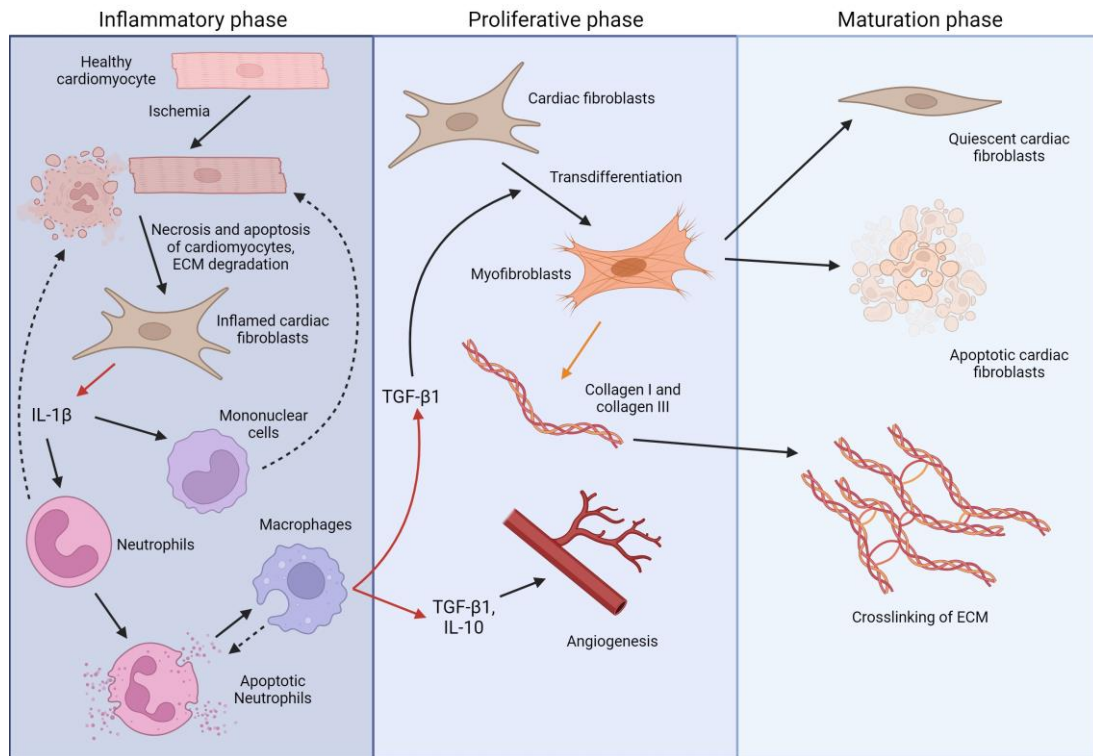


Figure 4: The 3 phases of fibrosis formation. In the first phase, the inflammatory phase, ischemia leads to necrosis and apoptosis of cardiomyocytes and the degradation of the ECM, which in turn leads to inflammation of cardiac fibroblasts. Inflammatory cardiac fibroblasts secrete IL-1 $\beta$ . IL-1 $\beta$  recruits neutrophils and mononuclear cells to phagocytose the necrotic and apoptotic cardiomyocytes and the ECM debris. After maximally 4 days the neutrophils undergo apoptosis, which recruits macrophages. These macrophages phagocytose apoptotic neutrophils and secrete TGF- $\beta$ 1 and IL-10. The expression of TGF- $\beta$ 1 initiates the second phase, the proliferative phase, in which cardiac fibroblasts transdifferentiate into myofibroblasts. Myofibroblasts deposit predominantly collagen I and collagen III. Both the TGF- $\beta$ 1 and IL-10 expressed by the macrophages stimulate angiogenesis. In the third phase, the maturation phase, the myofibroblasts become quiescent and/or leave the infarct site, possibly due to apoptosis, through unknown mechanisms. Crosslinking of the ECM in the infarct area leads to the formation of a mature scar (based on a figure by Humeres & Frangogiannis, 2019). Created with BioRender.com.

### 1.3.2 Active role of fibroblasts

The previous paragraph suggests a rather passive role of the cardiac fibroblasts after MI. This is however, a too narrow perspective. Cardiomyocytes are extremely sensitive to ischemia, causing a massive loss of cardiomyocytes after MI. (X. Zhang et al., 2001). Though the majority of cardiac fibroblasts in the infarct region likely also undergo apoptosis, cardiac fibroblasts from the border zone are able to infiltrate the infarct region within 1 day (Fu et al., 2018). The position of these cardiac fibroblasts in the cardiac interstitium renders them ideal to sense the changes in the cardiac microenvironment following MI and to initiate the inflammatory response. Reactive oxygen species (ROS) are generated as a consequence of ischemia after MI (Hori & Nishida, 2009). ROS both directly and indirectly modulate the function of fibroblasts and induce the expression of cytokines (including IL-1) and chemokines, which trigger the inflammatory response and the recruitment of leukocytes. These cytokines and chemokines are also expressed by other cells, including endothelial cells (W. Chen & Frangogiannis, 2013). The cytokines, especially IL-1 $\beta$ , trigger more fibroblasts to migrate towards the site of injury, intracellularly mediated through mitogen-activated protein kinase (MAPK) cascades (Mitchell et al., 2007). Different possible origins of the migrated fibroblasts have been investigated. According to popular hypotheses, the fibroblasts could be recruited from bone-marrow derived cells (Möller et al., 2006), from the endothelial lineage (E. M. Zeisberg et al., 2007) or from the epithelial

lineage (X. Yang et al., 2014). This has however been refuted. More recently, it could be demonstrated that the fibroblasts present in the infarct area are largely of epicardial origin (Moore-Morris et al., 2018). As mentioned before, the macrophages recruited to phagocyte the apoptotic neutrophils, secrete cytokines that clear the way for the proliferative phase. It is unknown whether the fibroblasts themselves also secrete cytokines to inhibit the inflammatory response.

During the proliferative phase, fibroblasts become the most abundant cell type in the infarct site (W. Chen & Frangogiannis, 2013). The transdifferentiation into myofibroblasts causes the cells to undergo major phenotypic differences. The fibroblasts increase the synthesis of ECM components and become more proliferative and migratory. Phenotypically, myofibroblasts resemble smooth muscle cells more closely than fibroblasts, as they extensively form contractile stress fibres (W. Chen & Frangogiannis, 2013). The transdifferentiation into myofibroblasts is paired with an increased expression of multiple smooth muscle cell proteins, including  $\alpha$ SMA and transgelin (Brønnum & Kalluri, 2012). The stress fibres in myofibroblasts consist of cytoplasmic actin. At the stage where myofibroblasts express stress fibres, but do not yet express  $\alpha$ SMA, they are also referred to as proto-myofibroblasts (Tomasek et al., 2002). These proto-myofibroblasts promote ECM remodelling, which in turn promotes the development of proto-myofibroblasts towards fully differentiated myofibroblasts, which express  $\alpha$ SMA. The  $\alpha$ SMA expression is largely controlled by TGF- $\beta$ 1. The expression of  $\alpha$ SMA and the incorporation of  $\alpha$ SMA into the stress fibres further promotes the cellular contractility, which is needed for physiological tissue remodelling (W. Chen & Frangogiannis, 2013; Roche et al., 2016; X. Yang et al., 2014).

### 1.3.3 TGF- $\beta$ 1

A pivotal marker of myofibroblasts is the expression of  $\alpha$ SMA, which is largely induced by TGF- $\beta$ 1. TGF- $\beta$ 1 can induce the expression of  $\alpha$ SMA in both a Smad-dependent (canonical) or Smad-independent (non-canonical) pathway. In the Smad-dependent pathway (Figure 5), TGF- $\beta$ 1 binds to TGF- $\beta$  receptor II (TGF- $\beta$ 1RII) present on the cell membrane, which phosphorylates its heterotetramer partner, TGF- $\beta$  receptor I activin receptor-like kinase 5 (TGF- $\beta$ 1RI ALK5), activating the intracellular kinase domain of ALK5 (H.-H. Hu et al., 2018). In turn, ALK5 phosphorylates the transcription factors Smad2 and Smad3 present in the cytoplasm, which together form a heterodimer. Smad4 binds to this heterodimer, forming a heterotrimer. This trimer is able to translocate to the nucleus, where it can bind to TGF- $\beta$  target genes, such as  $\alpha$ SMA, and activate transcription (Derynck & Zhang, 2003; H.-H. Hu et al., 2018; Yue et al., 2017). In line with this mechanism, after treatment with neutralizing TGF- $\beta$ 1 antibodies, a decrease in synthesis of  $\alpha$ SMA was measured in both quiescent and activated fibroblasts. The expression of  $\alpha$ SMA promotes the transdifferentiation of fibroblasts into myofibroblasts (Desmoulibre et al., 1996; X. Yang et al., 2014).

The Smad-dependent pathway includes a negative feedback loop, which negatively regulates the phosphorylation of Smad2 and Smad3 (H.-H. Hu et al., 2018). Smad3 is activated by the binding of TGF- $\beta$  to the TGF- $\beta$ 1RII, which in turn upregulates Smad7. Smad7 inhibits the activation of Smad2 and therefore negatively regulates the Smad2/3 pathway, also visualized in Figure 5 (Humeres et al., 2022).

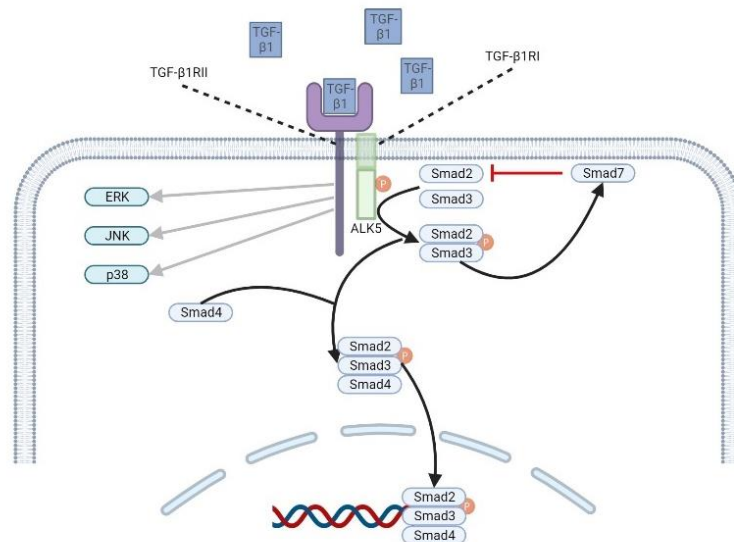


Figure 5: The Smad-dependent pathway of TGF- $\beta$ 1. TGF- $\beta$ 1 binds to TGF- $\beta$ 1RII, which phosphorylates TGF- $\beta$ 1RI (ALK5). Smad2/3 present in the cytoplasm are phosphorylated in turn by ALK5 and form a heterodimer. Smad4, also present in the cytoplasm, binds to the heterodimer, forming a heterotrimer. The heterotrimer is able to translocate to the nucleus, bind to TGF- $\beta$ 1 target genes and activate transcription. Binding of TGF- $\beta$ 1 to TGF- $\beta$ 1RII activates Smad 3, which upregulates Smad7. Smad7 inhibits the activation of Smad2, negatively regulating the Smad2/3 pathway; the negative feedback loop. The phosphorylation of TGF- $\beta$ 1RI (ALK5) also stimulates the 3 MAPK cascades; ERK, JNK and p38 (based on a figure by H.-H. Hu et al., 2018). Created with BioRender.com.

In the Smad-independent pathway, TGF- $\beta$ 1 stimulates fibrosis through MAPK cascades. The binding of TGF- $\beta$ 1 to the TGF- $\beta$ 1RII and subsequent phosphorylation of TGF- $\beta$ 1RI (ALK5) causes the stimulation of the 3 known MAPK cascades: the extracellular signal-related kinase (ERK) pathway, the c-Jun N-terminal kinase (JNK) pathway and the p38 pathway (Figure 5). Among others, these pathways are also involved in the regulation of collagen production (Papakrivopoulou et al., 2004; M. Tang et al., 2007; Wojciechowski et al., 2017). The p38 MAPK pathway is also related to myofibroblast proliferation, similarly to the Smad-dependent pathway (Yue et al., 2017).

### 1.3.4 RAAS

Stressed fibroblasts produce angiotensin-converting enzyme (ACE), a protease which generates angiotensin II (AngII) from the less active angiotensin I (AngI), in the renin-angiotensin-aldosterone system (RAAS) (Hafizi et al., 1998). The RAAS is of outstanding importance in regulating ion and water homeostasis and maintaining haemodynamic stability in the body. After MI, this stability is disturbed and the acutely lowered organ perfusion is sensed by the kidneys and leads to activation of the RAAS (Dargie & Byrne, 1995). Renin is produced by the kidneys and converts circulating angiotensinogen into AngI. ACE then converts AngI to AngII (AlQudah et al., 2020).

AngII is an important activator of cardiac fibroblasts, promoting proliferation of fibroblasts (Sadoshima & Izumo, 1993), an increase of ECM production (Crabos et al., 1994) and transdifferentiation of cardiac fibroblasts into myofibroblasts (Swaney et al., 2005). A big part of these effects can be explained by the induction of TGF- $\beta$ 1 expression attributed to AngII, or by the induction of ROS by AngII (Bertaud et al., 2023). However, AngII is also able to directly cause fibroblast proliferation after binding to angiotensin receptor 1 (AT1). Periostin is one of the downstream products of direct AngII-induced fibroblast



activation and its expression is elevated after TGF- $\beta$  treatment (Bertaud et al., 2023; Kim et al., 2013). AngII moreover inhibits the activity of matrix metalloproteinase 1, an important contributor to interstitial collagen degradation (Brilla et al., 1994). Furthermore, AngII activated rat cardiac fibroblasts expressed connective tissue growth factor (CTGF, encoded by *CCN2*), which additionally promoted fibroblast proliferation (Ahmed et al., 2004).

### 1.3.5 A 4<sup>th</sup> phase

The 3 phases following MI, the inflammation phase, the proliferative phase and the maturation phase, are crucial for stable repair of the injury site. In some cases, a 4<sup>th</sup> phase takes place. This phase is called the late phase and can contribute to adverse fibrosis formation, cardiac remodelling and even heart failure. Moreover, independently of previous MI, adverse fibrosis formation is found in patients with both common types of heart failure: heart failure with a preserved ejection fraction (HFpEF) and heart failure with a reduced ejection fraction (HFrEF) (Frangogiannis, 2021). Multiple mechanisms contribute to the 4<sup>th</sup> phase and modulate its outcome.

One such important factor is a bigger infarct area and subsequent greater inflammatory response. With larger affected areas, it is possible that the overwhelming inflammatory response cannot be sufficiently resolved, resulting in chronic inflammation, which can lead to ventricular dilation (Prabhu & Frangogiannis, 2016).

Another possible factor is wall stress: due to the wound healing after MI and the reparative remodelling of the site resulting in reduced elasticity of the affected tissue, there is an increased amount of wall stress in the surrounding, non-infarcted, myocardial wall. This can cause fibroblasts to be activated in these neighbouring parts of the myocardial wall, leading to an increase in ECM production where it is neither needed nor wanted. Thus, reduced function is able to spread across the myocardial wall (Humeres & Frangogiannis, 2019).

Myofibroblasts which do not sufficiently leave the infarct area after the acute injury has been resolved, are another possible contributor to the 4<sup>th</sup> phase. These myofibroblasts may retain their properties of increased ECM deposition, which can lead to tissue deformation. The scar can become hypertrophic and lead to contracture of the tissue, which in turn can cause arrhythmia (AlQudah et al., 2020). Sustained excessive ECM production can additionally promote arrhythmia through diffuse stiffening of the cardiac wall. All processes combined can ultimately lead to fatal heart failure (W. Chen & Frangogiannis, 2013).

Aside from MI and ischaemia-related heart failure, several other cardiac conditions are associated with fibrosis. One prominent example is chronic hypertension, which can cause interstitial fibrosis and perivascular fibrosis. In interstitial fibrosis, collagen is diffusely deposited between groups of cardiomyocytes. In perivascular fibrosis, there is an increase of collagen deposition around blood vessels. Both types of fibrosis have also been associated with obesity, diabetes and aging (Alex et al., 2023; Christine et al., 2010; Horn & Trafford, 2016; Ytrehus et al., 2018). Interstitial fibrosis has also been associated with genetic defects (Frangogiannis, 2021).

## 1.4 Models of cardiac fibrosis

Many of the mechanisms behind the development of cardiac fibrosis remain unclear (Frangogiannis, 2021). Therefore, it remains continuously important to study cardiac fibrosis. One way to study cardiac fibrosis is to use reliable cardiac fibrosis models.

### 1.4.1 Existing fibrosis models

Multiple models have been established to research fibrosis, including animal models, based on both small and large animals.

Established models include MI, which leads to cardiac fibrosis, induced in rat and mice (Blankestijn et al., 1997; Tao et al., 2016). Cardiac fibrosis can surgically also be induced in rats and mice via transverse aortic transcription (TAC). With TAC, the transverse aortic arch is constricted with a suture, which leads to pressure overload and subsequent cardiac fibrosis (Y. Wang et al., 2022). Cardiac fibrosis was also established indirectly *in vivo* in rats through treatment with aldosterone (Lijnen & Petrov, 2000), and fibrosis as a consequence of cardiomyopathy was induced in mice by treatment with the cardiotoxic agent doxorubicin (Tao et al., 2016).

Larger animal models of MI induced cardiac fibrosis were also studied, including models of miniature pigs (Yuan et al., 2019) and regular sized pigs (Gabisonia et al., 2019; Ma et al., 2023).

Though not yet employed as cardiac fibrosis models, the possibility to combine human cells with animal models has also been investigated. For example, engineered tissue sheets of hiPSC-derived cardiomyocytes, endothelial cells and vascular mural cells, were transplanted onto MI rat hearts. Cardiac function was improved after transplantation compared to control MI rats, as the transplanted sheets functioned as a form of cardiac regenerative therapy (Masumoto et al., 2014). Fibrin based engineered heart tissue patches were also transplanted onto MI guinea pig hearts, which resulted in partial remuscularization. In a proof of principle study, similar patches on a human-scale were successfully transplanted onto healthy pig hearts (Querdel et al., 2021; von Bibra et al., 2023).

*In vitro* models based on primary cardiac fibroblasts with or without cardiomyocytes represent another important research tool. In an early model, cardiac fibrosis was induced *in vitro* in primary rat cardiac fibroblasts co-cultured with cardiomyocytes through treatment with AngII (Fullerton & Funder, 1994). In another model, primary mouse cardiomyocytes and cardiac fibroblasts were harvested for co-culture in a dish to mimic cardiac fibrosis (van Spreeuwel et al., 2017). Cell cultures with only primary rat cardiac fibroblasts were created to study the response of cardiac fibroblasts to different stimuli (Kong et al., 2019; H. Zhao et al., 2014), similar to 2D studies of primary human cardiac fibroblasts (Palano et al., 2020). Numerous 3D models of cardiac fibrosis which consisted of a co-culture of primary rat cardiomyocytes and cardiac fibroblasts on a hydrogel basis have been engineered (Y. Li et al., 2017; Sadeghi et al., 2017; Saini et al., 2015). Another hydrogel model was engineered from human cardiac stromal cells (Ragazzini et al., 2022). A similar technique to engineer a cardiac fibrosis model was based on 3D vascularized spheroids from rat ventricular heart cells (Figtree et al., 2017). Some of the previously mentioned animal models could be directly compared to results acquired in a study of primary human cardiac fibroblasts obtained from patients suffering from dilated cardiomyopathy (Tao et al., 2016). Similarly, the findings from the research with miniature pigs could be translated to *in vitro* plated primary human cardiac fibroblasts (Yuan et al., 2019).

Animal models are associated with a number of limitations, both for ethical concerns and the inability to directly translate the findings from animal models to humans. *In vitro* models engineered from harvested cells could provide a solution. Due to the aforementioned sparsity of primary human cardiomyocytes and cardiac fibroblasts, a reliable cardiac fibrosis model consisting of (mostly) stem cell differentiated cells would be desirable.

In an engineered model, ESC-derived cardiomyocytes and mesenchymal stem cells were combined to form a 3D cardiac sphere platform for the study of cardiac fibrosis. Following treatment with TGF- $\beta$ 1, the mesenchymal stem cells successfully developed a fibrotic reaction (Lee et al., 2019). While this study conveyed the feasibility of employing ESC-derived cells, for ethical reasons and the possibility to create patient specific cell lines, models composed of hiPSC-derived cells would be preferable. A 3D hydrogel cardiac fibrosis model based on primary human foetal cardiac fibroblasts (Bracco Gartner et al., 2019), was later expanded by including hiPSC-derived cardiomyocytes (hiPSC-CMs) (Bracco Gartner et al., 2022, 2023). Another research group engineered a fibrosis-on-a-chip-model in which hiPSC-CMs were co-cultured with primary human cardiac fibroblasts (Mastikhina et al., 2020). hiPSC-CMs were co-cultured with hiPSC-derived endothelial cells, hiPSC-derived pericytes and/or primary human cardiac fibroblasts in another 3D model (Szepes et al., 2020). 3D human cardiac organoids to model MI were engineered by combining hiPSC-CMs with primary human cardiac fibroblasts, human umbilical vein endothelial cells and human adipose-derived stem cells (Richards et al., 2020). An engineered human myocardium model consisting of hiPSC-CM and primary human foreskin fibroblasts has been used as a heart failure model, but has not been used to systematically investigate cardiac fibrosis (Tiburcy et al., 2020).

Despite the aforementioned advances, the biggest limitation currently is the lack of cardiac fibrosis models comprised solely of hiPSC-derived cells. One model used a combination of hiPSC-CMs and non-cardiomyocytes at different ratios. Human iPSCs underwent a cardiomyocyte differentiation protocol, after which the obtained cells were separated into cardiomyocytes and non-cardiomyocytes by magnetic-activated cell sorting. The non-cardiomyocytes were positive for different cell markers, including the mesenchymal marker vimentin and the endothelial cell marker CD31, though their exact cell type(s) remained unknown. In this model, the cells were cultured together on a 2D cell culture dish (Iseoka et al., 2021). Another 2D model comprised hiPSC-CM and hiPSC derived cardiac fibroblasts (hiPSC-CF) to study the influence of hiPSC-CF on mechanical functions of the hiPSC-CM (Stempien et al., 2024). Lastly, a model comprised a 3D co-culture of hiPSC-CM and hiPSC-CF. This was a first example of a similar model as established in this work. Importantly however, the authors did not employ this model to study cardiac fibrosis (Aalders et al., 2024).

The abovementioned models have provided valuable insights into the mechanisms behind cardiac fibrosis. However, while models which are solely composed of hiPSC-derived cells have been published, these models were mostly not employed to study cardiac fibrosis, while models that were employed to study cardiac fibrosis were not solely composed of hiPSC-derived cells. Additional knowledge can therefore still be gained by engineering a 3D model specifically to mimic cardiac fibrosis, composed of hiPSC-CMs and hiPSC-CF, as is the basis of the model discussed in this work.

### 1.4.2 State-of-the-art 3D hiPSC-derived cardiac fibrosis model

The basis of the 3D engineered heart tissue (EHT) model which will be used in this work, was first described by Eschenhagen et al in 1997. Embryonic chick cardiomyocytes were mixed with collagen and cast between 2 glass tubes to form a first 3D EHT (Eschenhagen et al., 1997). Since then, EHTs have evolved tremendously (Figure 6) to different shapes and sizes e.g., towards circular EHTs (Zimmermann et al., 2002) and squared, patch EHTs (Bian et al., 2009). In the group of Prof. Eschenhagen, instead of collagen, a fibrin-based hydrogel currently forms the EHT matrix. The standard fibrin based EHT is cast between 2 flexible silicon posts in a 24-well format, as developed in 2010. The liquid fibrinogen polymerizes upon the addition of thrombin during the casting process, creating a fibrin cell block (Hansen et al., 2010; Schaaf et al., 2014). The cardiac fibrosis model described in this work will be developed on the basis of this model.

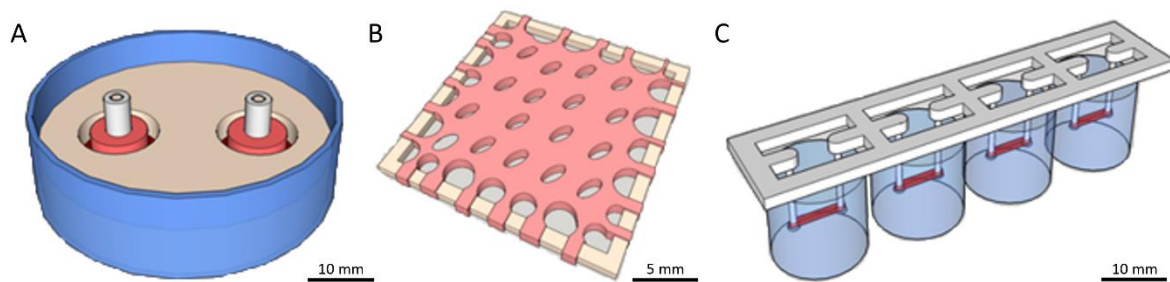


Figure 6: Different formats of EHT. A, ring EHTs. B, patch EHT. C, fibrin-based EHTs cast between flexible posts. Adapted from Weinberger et al., 2017.

The posts between which the EHTs are cast are flexible. This flexibility allows the contraction of the EHTs to deflect the posts with each beat. As the stiffness of the posts is known (and can be adjusted), this deflection can be quantified and converted to force generated by the EHT (Hansen et al., 2010).

Though EHTs at present are most commonly used as monocultures of cardiomyocytes, a co-culture of cardiomyocytes and cardiac fibroblasts has previously been developed (Werner, 2018). Previous research had suggested that cardiomyocyte-cardiac fibroblast EHTs (CF-EHTs) could potentially be used as an *in vitro* model of fibrosis. However, to be able to investigate the dynamic development of fibrosis under different activation conditions, a non-fibrotic baseline was to be established. One advantage of the EHT based fibrosis model over standard 2D fibroblast culture is an inherent property of the model: the fibroblasts in the EHTs are embedded in flexible 3D constructs, rather than being attached to a stiff (plastic) surface. This will provide favourable starting conditions for a non-fibrotic baseline of the embedded fibroblasts, as fibroblasts are known to become activated when cultured on a stiffer 2D surface versus flexible surfaces or in a 3D culture (Htwe et al., 2015; Solon et al., 2007).

Spontaneous activation after differentiation and activation by undefined serum components normally present in EHT culture medium was to be considered. By preventing activation during differentiation or early after the process, a non-fibrotic baseline after differentiation can be obtained. Following an established protocol, this can be achieved through the presence of the TGF- $\beta$ 1 receptor inhibitor SB-431542 (H. Zhang et al., 2019). Successive continuous exposure to SB-431542 can furthermore be employed to maintain quiescence during EHT culture.

SB-431542 is a small molecule that binds to TGF- $\beta$ 1R1 and inhibits the Smad-dependent TGF- $\beta$ 1 pathway (Hjelmeland et al., 2004). SB-431542 has been reported to be sufficiently specific to the TGF-

$\beta$ 1R1 kinase (ALK5), but depending on the source has also been reported to inhibit other type 1 receptors, such as ALK4 and ALK7, both also able to bind and react to TGF- $\beta$ . The inhibition of these receptors in turn has been reported to alleviate fibrosis (M. Chen et al., 2022; Liu et al., 2022; Loomans & Andl, 2016). The half maximal inhibitory concentration of SB-431542 was reported as 0.75  $\mu$ M for ALK5, 1  $\mu$ M for ALK4 and 2  $\mu$ M for ALK7 (SB-431542, 2023; SB-431542 [301836-41-9], 2023). SB-431542 has no effect on the ERK, JNK or p38 pathways, which are all part of the Smad-independent activation pathways. Of the 7 known ALK receptors, SB-431542 has not been reported to exert an effect on the other 4, which instead recognize bone morphogenetic proteins (BMPs) (Inman, Nicolás, Callahan, et al., 2002).

Undefined serum components in the EHT culture medium can activate the fibroblasts and stimulate collagen synthesis. These undefined components of the (horse) serum which activate the fibroblasts could comprise hormones or growth factors. The regular amount of serum in EHT culture medium is 10%, referred to in this work as 'high serum' (Hansen et al., 2010). Fibroblasts cultured under high serum conditions regularly transdifferentiate into myofibroblasts (Swaney et al., 2005). To obtain a non-fibrotic baseline during the EHT culture, the CF-EHTs can be cultured under low serum conditions, in 0.5% serum containing medium. Low serum has been previously used in models to investigate activation of cardiac fibroblasts (Tao et al., 2016). In this work, one of the tasks was finding an optimal balance between maintaining fibroblast quiescence and cardiomyocyte integrity, both in terms of the time and the extent of serum reduction or withdrawal.

Vice versa, as the presence of a high serum concentration can activate fibroblasts, increasing the serum level in the culture medium is one of several possible fibrosis inducing conditions in *in vitro* models. Another well-known method is the addition of TGF- $\beta$ 1, as there are multiple pathways through which TGF- $\beta$ 1 can activate cardiac fibroblasts, as discussed above.

The advantage of establishing both a clearly non-fibrotic baseline and pro-fibrotic conditions, is a high dynamic range of regulation in this model, rendering the model suitable to investigate differences in the development of fibrosis with high sensitivity. This provided us with the unique opportunity to study whether compound interventions, mechanical or genetic interventions, such as the absence of pro-fibrotic enhancer sequences, attenuated fibrosis formation in the model.

## 1.5 The role of enhancers in gene regulation

For protein synthesis, genes encoded in the DNA need to be transcribed to RNA, which in turn is translated into proteins.

For a gene to be transcribed, RNA polymerase II needs to bind to the promotor sequence on the DNA, located directly upstream (in the conventional direction of DNA from 5' to 3' end of its backbone) of the gene. General transcription factors need to bind to the promotor for RNA polymerase II to be able to bind. The first transcription factor locates to a region called the TATA box, which consists solely of thymine and adenine base pairs, or a related sequence. This is trailed by the binding of more transcription factors to the promoter and the first transcription factor, after which RNA polymerase II associates to the transcription factors, together forming the transcription initiation complex. RNA polymerase II can then 'walk across' a DNA strand, unwinding the DNA helix as it goes, and transcribe the gene located downstream into newly synthesized RNA. After processing and nuclear export, the RNA can be translated into proteins (Alberts et al., 2002).

Enhancer sequences are non-coding genomic sequences that regulate gene transcription (Panigrahi & O'Malley, 2021; Pennacchio et al., 2013). By definition, enhancer sequences are not essential for the transcription of a gene, but they can increase transcriptional activity of the gene substantially when activated (Pennacchio et al., 2013).

Enhancer sequences can be located thousands to a million base pairs away from the gene whose transcription they enhance (Lettice et al., 2003). They can be located both upstream and downstream of the target gene and within introns in the regulated gene or neighbouring genes (Pennacchio et al., 2013). Physical interaction between enhancer sequence, enhancer binding proteins and the site of transcription is necessary for enhancer activity. Thus, as enhancer sequences can be remote from their target gene, chromatin loops need to be formed to bend the DNA strand to enable the enhancer sequences to reach their target gene (Krivega & Dean, 2012).

For well characterized T cell specific enhancer sequences, it has been demonstrated that RNA polymerase and general transcription factors are recruited towards these enhancer sequences. It is hypothesized that a similar mechanism is at play throughout the genome in each cell (Koch et al., 2011). By chromatin looping, the RNA polymerase or general transcription factors that stimulate RNA polymerase binding to the promotor region, can be directed to the promotor region. Other ways in which enhancer sequences can stimulate transcription include the removal of repressive marks from the promotor or the removal of pausing factors of RNA polymerase from the target gene (Beagrie & Pompo, 2016).

Due to the wide spread of possible locations of the enhancer sequence pertaining to the target gene, it is challenging to definitively identify which target gene an enhancer belongs to (Krivega & Dean, 2012). Enhancer sequences are therefore often referred to as gene related enhancer sequences.

Multiple tools are available to identify enhancer sequences. One such tool is chromatin immunoprecipitation sequencing (ChIP-seq), which is a genome-wide profiling technique, used to analyse DNA-binding proteins and histone modifications (Park, 2009). Enhancers can be identified as they are often marked by an epigenetic modification of histone 3, called H3 lysine 4 mono-methylation (H3K4me1) and by the histone acetyltransferase p300 (Ghisletti et al., 2010). The modification of histone H3K27ac is also a well-recognized marker for the identification of active enhancers (T. Zhang et al., 2020). In 2022, MoMotif was developed, which can identify alterations to core binding motifs, at single base-pair resolution (Lebeau et al., 2022). Circularized chromosome conformation capture (4C) is a method to map out genomic folding patterns, such as chromatin looping, based on proximity ligation (Karasu & Sexton, 2021). Inverse PCR is used to quantify the DNA contact frequencies (Krijger et al., 2020). By detecting genomic regions that are in each other's vicinity, high-throughput chromosome conformation capture (Hi-C) can analyse the 3D structure of the genome. Enhancers can then be identified by applying multi-dimensional scaling (MDS) to the 3D structure (Ishibashi & Taguchi, 2021). By amplifying 'unwrapped' accessible DNA between nucleosomes, assay for transposase-accessible chromatin with high-throughput sequencing (ATAC-seq) can be used to map the chromatin accessibility at genome level (Dillinger, 2021).

As activation of enhancer sequences elevates the transcriptional activity of their target gene, genomic deletion (knockout; KO) of an enhancer sequence can potentially reduce transcription of the target gene, rendering enhancer sequences a pertinent area of research. By knocking out enhancer sequences, pathologically upregulated genes could potentially be downregulated (H. Li et al., 2021).

### 1.5.1 RUNX1

The RUNX1 protein, encoded by the gene of the same name, is part of the RUNT domain containing family of proteins, which consists of RUNX1, RUNX2 and RUNX3 (Levanon et al., 1994). The RUNX proteins are a part of core binding (transcription) factors. Core binding factors (CBFs) contain an  $\alpha$  subunit (CBF $\alpha$ ) and a  $\beta$  subunit (CBF $\beta$ ). The proteins encoded by *RUNX1*, -2 and -3 are the 3 possible CBF $\alpha$ s (Post et al., 2015). These proteins all contain a RUNT domain on the N-terminal. The RUNT domain can bind to the promotor of the protein's target gene. The CBF $\beta$  subunit binds to the CBF $\alpha$  subunit to form a heterodimeric complex. CBF $\beta$  itself does not bind to the promoter, but the binding of CBF $\beta$  to DNA bound CBF $\alpha$  significantly increases the transition enthalpy, the energy necessary to destabilize the bond between CBF $\alpha$  and the DNA (Post et al., 2015; Tahirov et al., 2001).

The *RUNX1* gene is located on chromosome 21 and spans 261 kb. There are 3 major isoforms that can be transcribed from the *RUNX1* gene. Isoform 1A and 1B are transcribed by the proximal promotor P2, isoform 1C is transcribed by the distal promotor P1 (Sood et al., 2017). The different isoforms are differentially expressed in different development stages and in different cell types (de Bruijn & Dzierzak, 2017). Different enhancers elevate the transcription of *RUNX1*, of which enhancer eR1 was identified first. This enhancer is located in the first intron between the 2 promotors. As multiple enhancer sequences have been identified in the region, the region was classified as a super-enhancer (Liau et al., 2017; Nottingham et al., 2007).

As a transcription factor, the RUNX1 protein, CBF $\alpha$ 2, plays an essential role in haematopoiesis related gene expression regulation (Okuda et al., 1996). The eR1 enhancer mediates early hematopoietic expression of *RUNX1* (Nottingham et al., 2007). *RUNX1* is also known as acute myeloid leukaemia 1 (*AML1*), as mutations in *RUNX1* are often found in patients suffering from leukaemia. In familial platelet disorder with predisposition to AML, the *RUNX1* mutations are often the initiating event (Bellissimo & Speck, 2017).

In the developmental phase of a mouse embryo, RUNX1 is necessary for the generation of the first definitive haematopoietic stem cells (Nottingham et al., 2007). RUNX1 is also essential for the transition from endothelial cells to haematopoietic progenitors (M. J. Chen et al., 2009). RUNX1 is not only needed for embryonic development of haematopoiesis, but also for its maintenance (de Bruijn & Dzierzak, 2017; Ichikawa et al., 2013).

In recent years, interest regarding the role of *RUNX1* in fibrosis formation has arisen. In lungs, treatment with TGF- $\beta$  led to higher mRNA abundance of *RUNX1*. The inhibition of *RUNX1* (using siRNA) resulted in a block in the transdifferentiation of fibroblasts into myofibroblasts. *RUNX1* also appears important in the epigenetic memory of the lung mesenchyme. This epigenetic memory is formed when pulmonary mesenchymal cells are repeatedly injured, for example by exposure to pathogens, particles and/or noxious gases. Repeated injuries can lead to fibrosis (Dubey et al., 2022; Jones et al., 2022; O'Hare et al., 2021). Thus, the role of *RUNX1* does not seem limited to a marker, but it seems to actively contribute to fibrosis pathophysiology, as *RUNX1* also promoted TGF- $\beta$  mediated fibrosis by stimulating the epithelial-to-mesenchymal transition in renal fibrosis (Zhou et al., 2018). In both renal and hepatic fibrosis, *RUNX1* was overexpressed. In the liver, *RUNX1* expression was able to activate the Smad-dependent TGF- $\beta$  pathway (Z. Guo et al., 2023; Zhou et al., 2018). Similar results were obtained with regard to cardiac fibrosis in animal models of MI (M. Sharma & Bhatt, 2022). In a rat MI model, *Runx1*



was the most differentially expressed gene related to the injury. Its overexpression resulted in a decreased cardiac contractile function (Ni et al., 2021). In a mouse MI model, adverse cardiac remodelling following injury was blunted in *Runx1* deficient mice, compared to control mice (McCarroll et al., 2018), suggesting an adverse role of *Runx1*.

A high expression of *RUNX1* led to an increase in myofibroblast differentiation and extracellular matrix expression in cardiac cells expressing PDGFR- $\beta$ . These cells were, amongst others, vascular smooth muscle cells and interstitial cells (Kuppe et al., 2022; Seifert et al., 1998). Moreover, *RUNX1* was generally highly expressed in the region bordering a MI (Martin et al., 2022). As discussed above, the region bordering the injury is an important site of adverse cardiac remodelling.

These findings have turned *RUNX1* into an interesting potential therapeutic target against detrimental cardiac fibrosis (M. Sharma & Bhatt, 2022).

### 1.5.2 CRISPR/Cas9

The fibrosis model described in this work was to be employed to study whether fibrosis formation is attenuated in the absence of pro-fibrotic enhancer sequences. The state-of-the art tool for genetic deletion of any sequence, including enhancer sequences, is the CRISPR/Cas9 nuclease system.

CRISPR/Cas was initially discovered in prokaryotes, where it functions as an innate defence mechanism against foreign elements which threaten to alter the genome, such as integrating viruses (Barrangou et al., 2007). CRISPR/Cas9 was adapted in 2013 to manipulate the genome of eukaryotes in a highly sequence-specific manner. CRISPR/Cas9 consists of 2 components: The Cas9 protein, responsible for creating a double-stranded break in the DNA, and a guide RNA that is able to recognize the sequence of DNA that is to be edited or knocked out by sequence homology (Figure 7). The guide RNA is composed of 2 parts, each with a distinct function; a homologous sequence to recognize the target DNA and a sequence which enables the guide RNA to bind to the Cas9 protein. For experimental genome editing, the CRISPR/Cas9 complex is introduced into the cell by transfection of the coding sequence or by direct introduction of the proteins, where the guide RNA then locates the target sequence of DNA (Doudna & Charpentier, 2014). After recognition, the unwinding of the DNA helix is initiated and the guide RNA can now pair with the target sequence. The Cas9 protein can subsequently cut the DNA, enabling the genome to be edited, a new sequence to be introduced, or a sequence to be knocked out (J.-X. Tang et al., 2018).

For a sequence to be knocked out, 2 different guide RNAs can be introduced into the cells, where the guide RNAs target sequences on either side of the desired deletion, as depicted in Figure 7. Cas9 can cut the DNA at both places and the desired sequence is then deleted, or knocked out. After deletion of a sequence, non-homologous end-joining will join the separate ends of the DNA strand (Caillaud et al., 2022; *CRISPR/Cas9*, 2023; Ran et al., 2013).



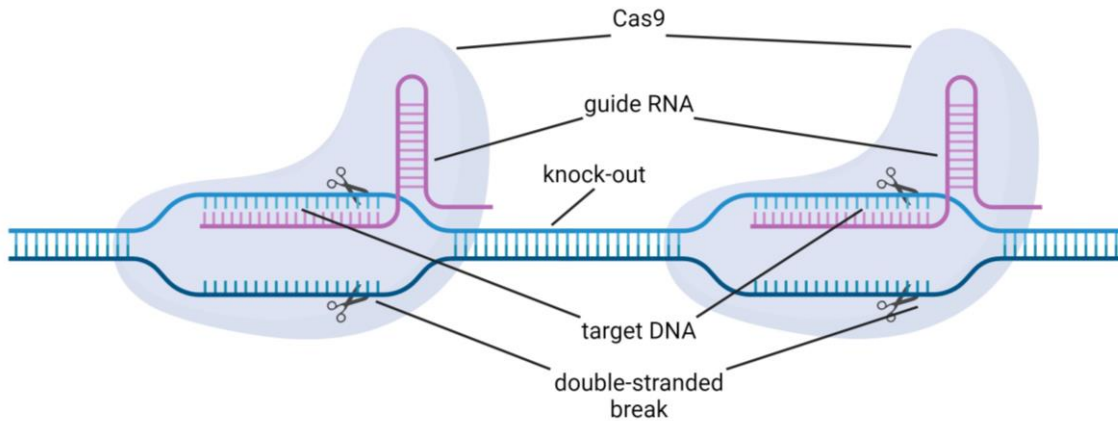


Figure 7: By introducing 2 different CRISPR/Cas9 components into the cell, of which the guide RNAs bind to target DNA on either side of a sequence, the Cas9 protein can create a double-stranded break on either side of the sequence and delete the sequence from the DNA. Created with BioRender.com.

## 1.6 In summary

Cardiac fibrosis is in essence a necessary reparative process following an injury such as MI. Cardiac fibrosis is formed in 3 phases, the inflammatory phase, the proliferative phase and the maturation phase. A potential 4<sup>th</sup> phase, called the late phase, can contribute to adverse fibrosis formation with detrimental effects such as heart failure. The late phase can occur for example due to chronic inflammation caused by a large injury and an exaggerated inflammatory response, which can be the consequence of an increase in wall stress in the myocardial wall surrounding the injury, or myofibroblasts pathologically remaining at the infarct site after the acute injury has resolved. Non-injury related cardiac conditions, such as chronic hypertension and heart failure, both associated with increased wall tension, can also lead to detrimental fibrosis formation.

Multiple models exist to study cardiac fibrosis, both in animals and *in vitro*, which have provided valuable insights into the mechanisms behind cardiac fibrosis. More insight can still be gained by engineering an *in vitro* 3D EHT based model comprising a co-culture of hiPSC-derived cardiomyocytes and hiPSC-derived cardiac fibroblasts to mimic cardiac fibrosis, as was to be the basis of the model described in this work.

The model was to be designed to allow for a high dynamic range of regulation, owing to a strictly non-fibrotic baseline vs. pro-fibrotic treatment conditions. The high dynamic range of regulation renders this model suitable to study the effect of genetic interventions, such as the knockout of pro-fibrotic enhancer sequences, with sufficient sensitivity. CRISPR/Cas9 can manipulate the genome in a highly sequence-specific manner and can therefore be employed to delete enhancer sequences.

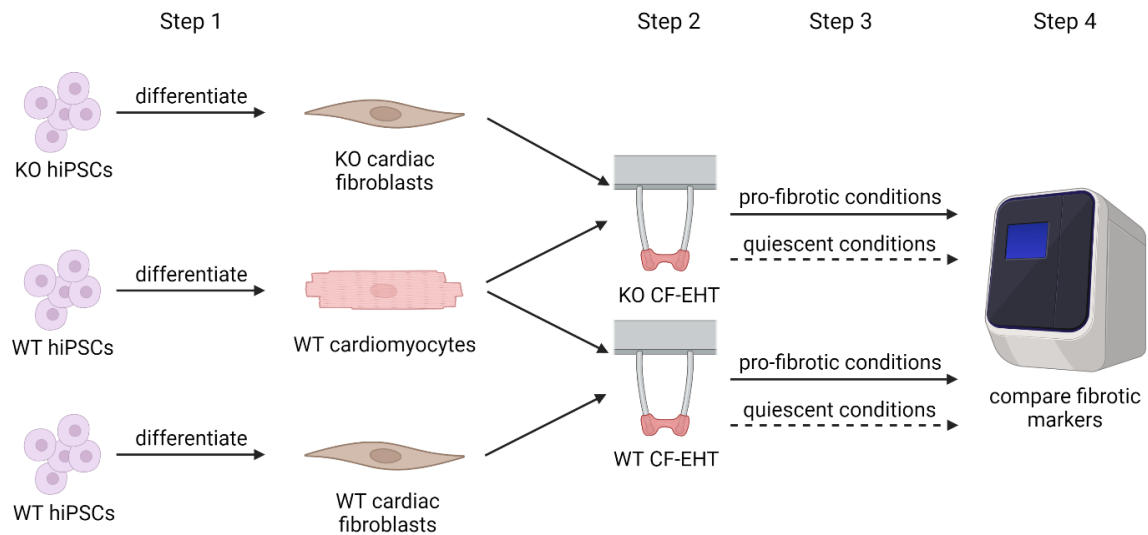
Interest regarding *RUNX1* with regard to fibrosis formation has recently arisen. In pulmonary, renal, hepatic and cardiac fibrosis, *RUNX1* was highly expressed. In cardiac fibrosis, the high expression of *Runx1* in mice resulted in decreased cardiac contractile function.

## 1.7 Study concept

This work was part of a consortium, consisting of 4 partners, conducting 4 work packages. In the first work package, Dr. Paola Cattaneo (Milan, Italy) collected primary murine cardiac fibroblasts from TAC-treated mice and sham mice and primary human cardiac fibroblasts treated either with TGF- $\beta$ 1 or a vehicle control. In the second work package, Dr. Luis Luna-Zurita (Madrid, Spain) epigenomically profiled these cardiac fibroblasts. To this end, RNA-seq, H3K27ac ChIP-seq and ATAC-seq were conducted. The data obtained with the bioinformatics analysis was investigated for differentially expressed genes in the primary murine cardiac fibroblasts obtained from the TAC-treated mice compared to the primary murine cardiac fibroblasts obtained from the sham mice and in the TGF- $\beta$ 1 treated primary human cardiac fibroblasts compared to the vehicle control treated primary human cardiac fibroblasts. Expression data was layered with the epigenetic data. From these analyses, *RUNX1* was identified as being upregulated in the TAC and TGF- $\beta$ 1 activated cardiac fibroblasts. Enhancer *enh35232*, located close the *RUNX1* gene, was one of the most prominent examples of an enhancer with significantly different accessibility and activation state between groups. In the third work package, Dr. Thomas Moore-Morris and Dr. Alenca Harrington (Montpellier, France) created 2 different cell lines in which they deleted (or knocked out) *RUNX1* or *enh35232*, respectively, from episomal line A18945 hiPSCs. This work is part of the last work package, in which we engineered a cardiac fibrosis model to evaluate the influence of either deletion on fibrosis formation in this model.

As previously discussed, a major limitation to modelling cardiac fibrosis *in vitro* was the lack of a model composed solely of hiPSC-derived cells. A model comprising hiPSC derived cells only has the advantage of overcoming the limited availability of primary cardiomyocytes and cardiac fibroblasts. Moreover, an hiPSC model offers the possibility to render the model patient specific and/or introduce genomic alterations. The model engineered in this work therefore consists of only hiPSC-derived cells.

To study the effect of either the *RUNX1* (Gene) or the *enh35232* (Enh) deletion on fibrosis formation in the model, the first step was to differentiate cardiac fibroblasts from KO hiPSCs and wild-type (WT) hiPSCs and cardiomyocytes from WT hiPSCs, as depicted in Figure 8. The second step was to establish CF-EHTs composed of either KO cardiac fibroblasts and WT cardiomyocytes (Enh KO or Gene KO CF-EHTs), or of WT cardiac fibroblasts and WT cardiomyocytes (WT CF-EHTs). In the next step, CF-EHTs from each genotype were to be subjected to both pro-fibrotic conditions and quiescent conditions. In the last step, the effect of the *RUNX1*-related enhancer KO and the *RUNX1* gene KO on fibrosis formation was to be measured by comparing signs of fibrosis in activated CF-EHTs versus inhibited CF-EHTs. To investigate for signs of fibrosis formation, among others, contractility parameters of the CF-EHTs and the mRNA abundance of multiple fibrosis markers in the CF-EHTs were analysed.



*Figure 8: Simplified schematic representation of how to investigate the effect of genetic interventions in the model described in this work. In step 1, cardiac fibroblasts will be differentiated from KO and WT hiPSCs, and cardiomyocytes will be differentiated from WT hiPSCs. In step 2, EHTs will be engineered from KO cardiac fibroblasts with WT cardiomyocytes (KO CF-EHTs) and from WT cardiac fibroblasts with WT cardiomyocytes (WT CF-EHTs). In step 3, both the KO CF-EHTs and the WT CF-EHTs will be subjected to pro-fibrotic or quiescent conditions. In step 4, fibrotic markers expressed by the KO CF-EHTs and the WT CF-EHTs will be measured and compared. Created with BioRender.com.*

## 2. Materials and Methods

### 2.1 Compositions

#### 2.1.1 Media Compositions

Table 1: Media compositions, in order of appearance.

Medium	Composition
FTDA	DMEM/F-12 -glutamine (Gibco) 2 mM L-Glutamine (Gibco) 5 mg/l Transferrin (Sigma-Aldrich) 6.6 µg/l Sodium selenite (Sigma-Aldrich) 1% (v/v) Human serum albumin (HSA, Biological Industries) 0.1% (v/v) Lipid mix (Sigma-Aldrich) 5 mg/l Insulin (Sigma-Aldrich) 50 nM Dorsomorphin (Tocris) 2.5 µg/l Activin A (R&D Systems) 0.5 µg/l Transforming growth factor-β 1 (TGF-β1, Peprotech)  The medium was sterile filtered and stored for up to 2 weeks at 4 °C. 30 µg/l bFGF (R&D Systems) was freshly supplemented immediately before usage
10% Serum containing EHT medium	DMEM-low glucose (Sigma-Aldrich) 1% (v/v) Penicillin/streptomycin (Gibco) 10% (v/v) Heat inactivated horse serum (Life Technologies) 10 mg/l Insulin 33 mg/l Aprotinin (Genaxxon BioScience) 200 µM Trans-4-(aminomethyl)cyclohexane carboxylic acid (TA, Sigma-Aldrich)  The medium was freshly prepared before usage
0.5% Serum containing EHT medium	DMEM-low glucose 1% (v/v) Penicillin/streptomycin 0.5% (v/v) Heat inactivated horse serum 10 mg/l Insulin 33 mg/l Aprotinin 40 ng/ml Hydrocortisone (Sigma-Aldrich) 0.5 ng/ml Triiodo-L-thyronine sodium salt (T3, Sigma-Aldrich) 200 µM TA  The medium was freshly prepared before usage

10% Serum containing NKM	DMEM-low glucose 1% (v/v) Penicillin/streptomycin 10% (v/v) Heat inactivated horse serum 1% (v/v) GlutaMax (Gibco)  The medium was freshly prepared before usage
0.5% Serum containing NKM	DMEM-low glucose 1% (v/v) Penicillin/streptomycin 0.5% (v/v) Heat inactivated horse serum 1% (v/v) GlutaMax 40 ng/ml Hydrocortisone 0.5 ng/ml T3  The medium was freshly prepared before usage
EB formation medium (Stage 0 medium)	FTDA 4 g/l Polyvinyl alcohol in 1x DPBS (Sigma-Aldrich) 10 µM Y-27632 (Biaffin)  The medium was sterile filtered and stored for up to 1 week at 4 °C. 30 µg/l bFGF was freshly supplemented immediately before usage
Mesoderm induction medium (Stage 1 medium)	RPMI 1640 (Gibco) 4 g/l Polyvinyl alcohol in 1x DPBS 10 mM HEPES, pH 7.4 (Roth) 5 mg/l Transferrin 6.6 µg/l Sodium selenite 0.05% (v/v) HSA 0.1% (v/v) Lipid mix 10 µM Y-27632 250 µM Phosphoascorbate (PAA, Sigma-Aldrich)  The medium was sterile filtered and stored for up to 1 week at 4 °C. Supplemented immediately before usage with: 5 µg/l bFGF 3 µg/l Activin A 10 µg/l BMP-4 (R&D Systems)
Cardiac differentiation medium I (FDM medium)	RPMI 1640 0.5% (v/v) Penicillin/streptomycin 10 mM HEPES, pH 7.4 5 mg/l Transferrin 6.6 µg/l Sodium selenite 0.5% (v/v) HSA 0.1% (v/v) Lipid mix

	<p>1 <math>\mu</math>M Y-27632 250 <math>\mu</math>M PAA</p> <p>The medium was sterile filtered and stored for up to 1 week at 4 °C. 1 <math>\mu</math>M XAV-939 (Tocris) was freshly supplemented immediately before usage</p>
Cardiac differentiation medium II (Stage 2 medium)	<p>RPMI 1640 0.5% (v/v) Penicillin/streptomycin 10 mM HEPES, pH 7.4 1 <math>\mu</math>M Y-27632 500 <math>\mu</math>M 1-Thioglycerol (Sigma-Aldrich)</p> <p>The medium was sterile filtered and stored for up to 2 weeks at 4 °C. Supplemented immediately before usage with: 1 <math>\mu</math>M XAV-939 2% (v/v) B27 + insulin</p>
Cardiac differentiation medium III (RDM medium)	<p>RPMI 1640 0.5% (v/v) Penicillin/streptomycin 10 mM HEPES, pH 7.4 1 <math>\mu</math>M Y-27632 500 <math>\mu</math>M 1-Thioglycerol</p> <p>The medium was sterile filtered and stored for up to 1 week at 4 °C. 2% (v/v) B27 + insulin was freshly supplemented immediately before usage</p>
Epi-medium	<p>RPMI 1640 0.5% (v/v) Penicillin/streptomycin 0.1% (v/v) Lipid mix 1 <math>\mu</math>M Y-27632 250 <math>\mu</math>M PAA 0.01% Transferrin-selenium</p> <p>The medium was sterile filtered and stored for up to 2 weeks at 4 °C.</p>

### 2.1.1.2 Buffer compositions

Table 2: Buffer compositions, in alphabetical order.

Buffer	Composition
Blocking buffer (for dissociation of EBs)	<p>RPMI 1640 6 ml/l DNase II type V (Sigma-Aldrich) 1% (v/v) Penicillin/streptomycin</p>

Dissociation buffer	HBSS (-) calcium/magnesium (Gibco) 200 U/ml Collagenase II (Worthington) 1 mM HEPES 30 µM N-benzyl-p-toluenesulfonamide (BTS, TCI) 10 µM Y-27632
Electrophoresis buffer (10x)	30.2 g Trizma base (Sigma-Aldrich) 144 g Glycine (Roth) 10 g 20% Sodium dodecyl sulfate (SDS, Roth) Top up to 1 l with water
FACS buffer	DPBS 5% (v/v) Foetal bovine serum (FBS, Biochrom)
Kranias buffer	2 ml 1.5 M Tris (pH 8.8, Roth) 1 ml 0.5 M Titriplex III (ethylenedinitrilotetraacetic acid disodium salt dihydrate; EDTA, Roth) 6 ml 500 mM NaF (Merck) 15 ml SDS 10 ml Glycerol (Roth) 100 ml Deionized water
Laemmli buffer (6x)	1.2 g SDS 6 mg Bromophenol blue (Merck) 6 g Glycerol 1.2 ml 0.5 M Tris (pH 6.8, Roth) 0.93 g 1,4-Dithiothreitol (DTT, Roth) Top up to 10 ml with water
Separation gel SDS-PAGE (10%, 10 ml)	4.8 ml Water 2.5 ml 40% Acrylamide (Bio-Rad Laboratories) 2.5 ml 1.5 M Tris pH 8.8 100 µl 10% (w/v) SDS 100 µl 10% (w/v) Ammoniumpersulfate (APS, Bio-Rad Laboratories) 4 µl N,N,N',N'-Tetramethylethylenediamine (TEMED, Bio-Rad Laboratories)
Stacking gel SDS-PAGE (10 ml)	6 ml Water 1.25 ml 40% Acrylamide 2.5 ml 0.5 M Tris pH 6.8 100 µl 10% (w/v) SDS 100 µl 10% (w/v) APS 4 µl TEMED
TAE buffer	242 g Trizma base 37.2 g EDTA 57.1 ml Concentrated acetic acid Top up to 1 l with water, pH 8.5
TBS (10x)	1 M Trizma base or Tris-HCl (Roth) 1.5 M NaCl Water; pH 7.5 (adjust with 35% HCl)

Western blot transfer buffer (1x)	200 ml Western blot transfer buffer (5x) 200 ml Methanol (Fisher Bioreagents) Top up to 1 l with water
Western blot transfer buffer (5x)	29 g Trizma base 145 g Glycine Top up to 2 l with water

## 2.2 2D cell culture

For the majority of the experiments discussed in this work, the commercially available episomal hiPSC line A18945 (Thermo Fisher Scientific) was used (<https://www.thermofisher.com/order/catalog/product/A18945>). The cell line was generated from cord blood-derived CD34+ progenitor cells. Episomal stem cells are somatic cells, reprogrammed into iPSCs via non-integrative episomal vector methods rather than integrative methods, such as a lenti- or retrovirus (A. Y. L. Wang & Loh, 2019). Global gene expression analyses demonstrated that molecularly, the stem cells were indistinguishable from human embryonic stem cells. The hiPSCs had been able to differentiate into cells from the ectodermal, endodermal and mesodermal lineage. For the second part of the results, modified hiPSCs from this cell line with either the *RUNX1*-related enhancer '*enh35232*' or the *RUNX1* gene knocked out via CRISPR, were kindly provided by Dr. Thomas Moore-Morris and Dr. Alenca Harrington (Institute for Regenerative Medicine & Biotherapy, Montpellier, France).

For certain specific experiments, the in-house established control hiPSC lines ERC001 or ERC018 were used. These cell lines were registered as UKEi001-A or UKEi003-C, respectively (<https://hpscereg.eu/cell-line/UKEi001-A>, <https://hpscereg.eu/cell-line/UKEi001-A>). The cell lines had been previously generated from skin biopsies by the UKE Stem Cell Core Facility with the CytoTune-iPS Sendai Reprogramming kit (Thermo Fisher Scientific), also a non-integrative reprogramming method. The Ethics Committee of the Hamburg Physicians' Chamber, responsible for the UKE, approved the studies in which these hiPSC lines were used (Az. PV4798/28.10.2014).

### 2.2.1 Coating

All 2D cell culture was performed on coated cell culture vessels. For the culture of hiPSCs the cell culture vessels were coated with Geltrex (GTX, Gibco), diluted 1:100 in RPMI 1640 for 24 hours at room temperature. For the differentiation of hiPSCs into cardiac fibroblasts, the cell culture vessels were coated with GTX or Matrigel (MG, Corning), as specified in the cardiac fibroblast differentiation section. MG was diluted 1:60 in RPMI 1640 and the cell culture vessels were coated for 24 hours at room temperature. For the culture of (cardiac) fibroblasts, the cell culture vessels were coated with laminin (Sigma-Aldrich), diluted 1:50 in DPBS and coated for 24 hours at 4 °C. The cell culture vessel coating volumes are listed in Table 3.



Table 3: Cell culture vessel coating volumes.

	<b>GTX</b>	<b>MG</b>	<b>Laminin</b>
T175 cell culture flask	16 ml	16 ml	n/a
T75 cell culture flask	7 ml	7 ml	n/a
6-well plate	1 ml/well	1 ml/well	800 µl/well
12-well plate	n/a	n/a	400 µl/well
24-well plate	n/a	n/a	200 µl/well

### 2.2.2 Stem cell culture

All cell culture was performed under sterile conditions, while wearing surgical gloves. Human iPSC culture was performed without the use of antibiotics, while wearing a face mask and plastic arm covers.

Human iPSCs were cultured under hypoxic conditions (37 °C, 5% O<sub>2</sub>, 5% CO<sub>2</sub> and 95% humidity), in GTX coated cell culture vessels, generally in T75 cell culture flasks but occasionally in 6-well plates. Human iPSCs were seeded at a density of 4.5-6.5 x 10<sup>6</sup> hiPSCs/T75 cell culture flask and cultured in FTDA medium for 4 or 3 days respectively, until 100% confluency was reached. The hiPSCs were then passaged, usually twice per week. Fresh FTDA medium was added daily, and twice per day when close to confluency. When the medium of the hiPSCs was changed twice in 1 day, only half the medium was removed and replaced with fresh FTDA during the first medium change.

Table 4: Schedule for the medium change of hiPSCs.

	<b>4.5 x 10<sup>6</sup> hiPSC/T75 cell culture flask</b>	<b>6.5 x 10<sup>6</sup> hiPSC/T75 cell culture flask</b>
Seeding day (day 0)	15 mL FTDA + 10 µM Y-27632	20 mL FTDA + 10 µM Y-27632
Day 1	20 mL FTDA	20 mL FTDA
Day 2	20 mL FTDA	½ Medium removal + 15 mL FTDA; 25 mL FTDA
Day 3	½ Medium removal + 15 mL FTDA; 25 mL FTDA	Passage
Day 4	Passage	

#### 2.2.2.1 Passaging

To passage the hiPSCs, the cell culture vessels were washed with DPBS and incubated with Accutase (Sigma-Aldrich) + 10 µM of the kinase ROCK1/2 inhibitor Y-27632 for 5-10 minutes, to dissociate the cells into single cells. FTDA + 10 µM Y-27632 was added to the Accutase in a 1:1 ratio for neutralization, after which the cell suspension was centrifuged at 1000 rpm for 3 minutes. After the supernatant was removed, the cell pellet was resuspended in fresh FTDA + 10 µM Y-27632. The total hiPSC number was calculated using Trypan Blue (Biochrom) and a Neubauer counting chamber, and the hiPSCs were seeded in a fresh, GTX coated T75 cell culture flask at the desired cell density.

#### 2.2.2.2 Freezing and thawing of hiPSCs

In addition to further culturing hiPSCs after dissociation with Accutase, hiPSCs could alternatively be frozen. After obtaining the desired amount of cells, the cell suspension was centrifuged at 1000 rpm for 4 minutes and the supernatant was removed. The cells were then resuspended in 1 ml heat-

inactivated FBS containing 10% dimethyl sulfoxide (DMSO, Sigma-Aldrich) per  $1.5 \times 10^6$  hiPSCs, aliquoted into cryotubes and slowly frozen in an isopropanol-based freezing device (called a Mr. Frosty) at  $-80^\circ\text{C}$  for 24 hours. After 24 hours the cryotubes were transferred to  $-150^\circ\text{C}$  for long-term storage.

To thaw the hiPSCs, the cryotubes were placed in a water bath at  $37^\circ\text{C}$  for 2-3 minutes, until the remaining frozen part was around 5 mm in diameter. The cryotubes were then sprayed with 70% ethanol and placed in a sterile hood. 5 ml of  $37^\circ\text{C}$  FTDA +  $10\ \mu\text{M}$  Y-27632 was pipetted with a 5 ml pipet, the pipet was placed in the cryotube and the 1 ml of cell suspension was additionally aspirated. The cell suspension was then slowly transferred to a 15 ml tube, at around 1 drop per second. The 15 ml tube was centrifuged at 1000 rpm for 3 minutes, the supernatant was removed and the cells were resuspended in FTDA +  $10\ \mu\text{M}$  Y-27632, after which they were seeded into 2 wells of a GTX-coated 6-well plate.

### 2.2.2.3 Mycoplasma test

The hiPSCs were examined for mycoplasma. 1 ml of cell culture medium, which had not been refreshed for at least 3 days, was collected, incubated at  $100^\circ\text{C}$  for 10 minutes and centrifuged at 1200 rpm for 5 minutes.  $2\ \mu\text{l}$  of the supernatant was added to a PCR mastermix. Contaminated supernatant was used as a positive control and water was used as a negative control. The recommended PCR program was run and gel electrophoresis on 1% (w/v) agarose (Invitrogen) gels with TAE buffer, was used to analyse the PCR products. Mycoplasma tests were kindly performed by June Uebeler (IEPT, UKE, Hamburg).

Table 5: Reaction mix for PCR mycoplasma test

Component	Quantity (total of 50 $\mu\text{l}$ )
Nuclease-free water	25.75 $\mu\text{l}$
Q-solution	10 $\mu\text{l}$
10x buffer	5 $\mu\text{l}$
$\text{MgCl}_2$ (25 mM)	4 $\mu\text{l}$
Sample	2 $\mu\text{l}$
Primer pool Myco-dw (10 pM)	1 $\mu\text{l}$
Primer pool Myco-up (10 pM)	1 $\mu\text{l}$
dNTPs	1 $\mu\text{l}$
Taq DNA polymerase	0.25 $\mu\text{l}$

Table 6: Thermocycling conditions for PCR mycoplasma test

	Temperature	Time
40 cycles	$95^\circ\text{C}$	15 minutes
	$94^\circ\text{C}$	30 seconds
	$56^\circ\text{C}$	30 seconds
	$72^\circ\text{C}$	1 minute
	$72^\circ\text{C}$	10 minutes
	$4^\circ\text{C}$	Indefinitely

#### 2.2.2.4 Giemsa-banding

Cytogenetic analysis by Giemsa-banding was used to produce a visible karyogram of the different episomal line A18945 genotypes. For each genotype, 3 wells of a GTX coated 6-well plate were seeded with  $1 \times 10^6$  hiPSCs each and cultured under standard conditions. Once the hiPSCs had reached a confluency of 70%, they were transferred to the Institute of Human Genetics (UKE, Hamburg) where Giemsa-banding and analysis were conducted (Breckwoldt et al., 2017).

#### 2.2.3 (Cardiac) fibroblasts

(Cardiac) fibroblasts were cultured in laminin coated cell culture vessels, generally 6-well plates, 12-well plates or 24-well plates. The (cardiac) fibroblasts were seeded at a density of  $1.4 \times 10^5$  (cardiac) fibroblasts/cm<sup>2</sup> and cultured in either 10% (horse) serum containing EHT medium, 0.5% serum containing EHT medium, 10% serum containing NKM + 0.25  $\mu$ M PAA or 0.5% serum containing NKM + 0.25  $\mu$ M PAA. The culture medium was changed on Mondays, Wednesdays and Fridays.

### 2.3 Differentiation

#### 2.3.1 Cardiomyocyte differentiation

Once hiPSCs had reached 100% confluency, they were detached to start the process of differentiation into cardiomyocytes. The differentiation was performed according to a previously published in-house protocol, where hiPSCs were first cultivated in spinner flasks for 24 hours to allow for embryoid body (EB) formation, after which the EBs were subjected to mesoderm induction followed by cardiac differentiation (Breckwoldt et al., 2017).

Before detaching the confluent hiPSCs, the hiPSCs were pre-treated with 10  $\mu$ M Y-27632 for 1 hour, to increase cell survival. The T75 cell culture flasks containing the hiPSCs were then washed with DPBS, after which they were dissociated into single cells with 0.5 mM EDTA and incubated for 5-10 minutes. After collection by centrifugation, the hiPSCs were resuspended in EB-formation medium (stage 0 medium). The hiPSCs were then counted using Trypan Blue and a Neubauer counting chamber, after which they were transferred into spinner flasks at a density of  $30\text{-}35 \times 10^6$  hiPSCs/100 ml stage 0 medium. To stimulate EB formation, the cell suspension was placed on a magnetic stirrer, stirring at 40 rpm, for 24 hours in a hypoxic incubator. To prepare for the next step, T175 cell culture flasks were coated with 1% (w/v) Pluronic F-127 (Sigma-Aldrich).

After 24 hours, on day 1, the Pluronic coated T175 cell culture flasks were washed with DPBS twice. The stirring of the EBs was stopped, which allowed the EBs to settle and to be washed. The EB volume was then estimated with a 15 ml centrifuge tube. 200-250  $\mu$ l of EBs was resuspended in 46 ml mesoderm induction medium (stage 1 medium) and added to each Pluronic coated T175 cell culture flask. The stage 1 medium contained 10 ng/ml BMP4, 3 ng/ml activin A and 5 ng/ml bFGF to induce differentiation into the mesoderm stage. The cells were cultured under hypoxic conditions in stage 1 medium for 3 days, with a daily change of half the medium volume, i.e. 23 ml used medium was removed and 23 ml fresh medium was added.

On day 4, the cells were directed towards cardiac differentiation, using the Wnt-signalling inhibitor XAV-939. The EBs from the T175 cell culture flasks were combined. To this end, the T175 cell culture flasks containing the EBs were placed in V-racks, allowing the EBs to settle in 1 corner. The used medium was then removed and the EBs were combined. The EBs were then washed with cardiac differentiation medium I (FDM medium). The EB volume was again estimated with a 15 ml centrifuge tube. 200-250  $\mu$ l of EBs was resuspended in 46 ml FDM medium and added to the used T175 cell culture flasks. The cells were cultured under normoxic conditions (21% O<sub>2</sub>, 5% CO<sub>2</sub>) for 3 days, with a daily change of half the medium. On day 7, the FDM medium was completely removed and replaced with cardiac differentiation medium II (stage 2 medium). The cells were further cultured under normoxic conditions for 4 days, with a daily change of half the medium. Spontaneous contractions starting between day 9 and day 11 indicated a successful differentiation. On day 12, the stage 2 medium was completely removed and replaced with cardiac differentiation medium III (RDM medium), which did not contain XAV-939. The cells were further cultured under normoxic conditions for at least 5 days, with a daily change of half the medium. This period could be extended to 12 days of culture in RDM medium.

To dissociate the EBs into single cardiomyocytes, the EBs from the different T175 cell culture flasks were combined; the T175 cell culture flasks containing the EBs were placed in V-racks, which allowed the EBs to settle in 1 corner, the RDM medium to be removed and the EBs to be combined. The EBs were then washed twice with HBSS and resuspended in dissociation buffer. The cell suspensions in the T175 cell culture flasks were incubated for 2-3 hours and regularly microscopically assessed for the dissociation of the EBs. Further dissociation of the EBs was attained by rapidly pipetting the cell suspension. Once the EBs were sufficiently dispersed, i.e. sufficient collagenase digestion had taken place, the same volume of blocking buffer as the dissociation buffer was added to the T175 cell culture flasks. The cells were then centrifuged at 800 rpm for 10 minutes, after which the cells were washed twice with RPMI 1640 and counted using Trypan Blue and a Neubauer counting chamber.

The cells could now be cryopreserved, i.e. frozen, or used for flow cytometry analysis or other experiments.

#### *2.3.1.1 Freezing and thawing of cardiomyocytes*

As it was not always possible to cast (CF-)EHTs immediately after dissociation of the cardiomyocytes, for standardization reasons, it was decided to freeze all cardiomyocytes and thaw them when the (CF-)EHTs were cast.

Cardiomyocytes were frozen similar to hiPSCs. After collection of cardiomyocytes by centrifugation at 800 rpm for 10 minutes, the cardiomyocytes were resuspended in heat inactivated FBS + 10% DMSO. Aliquots of 25-45 x 10<sup>6</sup> cardiomyocytes were frozen in cryotubes in 1 ml FBS + 10% DMSO each. The cryotubes were slowly frozen in an isopropanol-based freezing device at -80 °C for 24 hours. After 24 hours the cryotubes were transferred to -150 °C for long-term storage.

Thawing cardiomyocytes was more precarious than thawing hiPSCs. To thaw cardiomyocytes, cryotubes were placed in a water bath at 37 °C for 2-3 minutes, until a frozen portion of around 5 mm diameter remained. The cryotubes were then sprayed with 70% ethanol and placed in a sterile hood. The cell suspension was pipetted into a 15 ml tube in a dropwise manner. 1 ml of 37 °C 10% serum containing NKM + 10  $\mu$ M Y-27632 was pipetted into the cryotube for washing, and added to the 15 ml tube, at around 1 drop per 4-5 seconds. Next, 2 ml of 37 °C 10% serum containing NKM + 10  $\mu$ M Y-

27632 was added to the 15 ml tube over 30 seconds. Finally, 5 ml of 37 °C 10% serum containing NKM + 10 µM Y-27632 was added to the 15 ml tube over 30 seconds. The 15 ml tube was then centrifuged at 800 rpm for 5 minutes, the supernatant was removed and the cells were resuspended in 10% serum containing NKM + 10 µM Y-27632, after which they were counted using Trypan Blue and a Neubauer chamber and used for (CF-)EHT casting.

### 2.3.2 Cardiac fibroblast differentiation

Multiple cardiac fibroblast differentiation protocols were followed and compared.

#### 2.3.2.1 EB cardiac fibroblast differentiation protocol

The EB cardiac fibroblast differentiation protocol (in short the EB protocol) was followed as described in a previous doctoral thesis from the IEPT (Pan, 2022), which was adapted from another previous doctoral thesis from the IEPT (Werner, 2018), which in turn was adapted from a previous publication (Witty et al., 2014).

The formation of EBs and subsequent induction of the mesoderm stage was performed as described in the cardiomyocyte differentiation protocol. On day 4, immediately after the mesoderm stage, the epicardial differentiation was initiated. 50-55 µl of EBs was transferred to a GTX coated T75 cell culture flask, to which the cells were able to attach and form a monolayer. The cells were cultured in 20 ml Epi-medium + 10 ng/ml BMP4, 5 ng/ml VEGF (R&D Systems), 4 µM CHIR99021 (Cayman) and 5.4 µM SB-431542 (MedChemExpress) for 2 days. After these 2 days, the cells were cultured in Epi-medium + 5 ng/ml VEGF for 8 days, with a medium change every second day.

On day 15, the epithelial-to-mesenchymal transition started. Collagenase II + 0.05% trypsin (Gibco) was used to detach the EBs and dissociate them into single cells. The cells were seeded into GTX coated T75 cell culture flasks at a density of  $2 \times 10^6$  cells/T75 cell culture flask in 20 ml Epi-medium + 10 µM Y-27632. From day 16 to day 24, the cells were cultured in Epi-medium + 10 ng/ml bFGF, with a medium change every second day. On day 24, the cardiac fibroblasts were harvested using Accutase + 10 µM Y-27632, similarly to how hiPSCs were passaged.

#### 2.3.2.2 Quiescent cardiac fibroblast differentiation protocol

The quiescent cardiac fibroblast differentiation protocol (in short the quiescent protocol) was adapted from a previously published protocol (H. Zhang et al., 2019).

For certain runs of the quiescent protocol, the hiPSCs were cultured in Essential E8 medium + supplements (Thermo Fisher Scientific) prior to the start of the differentiation protocol.

After hiPSCs had reached 70-80% confluency on 6-well plates, the mesoderm induction was initiated. The medium was removed from the plates and replaced with RPMI 1640, containing 2% B27 without insulin, and 6 µM CHIR99021, a Wnt activator. The cells were then left undisturbed for 2 days under hypoxic conditions.

After 2 days, the cells were pushed to differentiate into cardiac progenitor cells. This was achieved first by removing the CHIR99021 from the culture medium. The RPMI 1640 containing the CHIR99021 was

replaced with fresh RPMI 1640, containing 2% B27 without insulin. The cells were cultured for another day under hypoxic conditions. On day 3, the medium was removed and replaced with fresh RPMI 1640, containing 2% B27 without insulin, and 5  $\mu$ M IWR-1 (Selleckchem), a Wnt inhibitor. The cells were then left undisturbed for 2 days under hypoxic conditions. On day 5, the IWR-1 was removed from the culture medium. The RPMI 1640 containing the IWR-1 was replaced with fresh RPMI 1640, containing 2% B27 without insulin. The cells were cultured under hypoxic conditions for another day.

From day 6, the cardiac progenitor cells were pushed to differentiate into proepicardial cells. The cells were first detached from the 6-well plates using Accutase + 10  $\mu$ M Y-27632. The cells were gently pipetted to dissociate them, counted using Trypan Blue and a Neubauer counting chamber and resuspended in Advanced DMEM/F12 (Gibco), containing 1% glutamine, 5  $\mu$ M CHIR99021, 2  $\mu$ M retinoic acid (Sigma-Aldrich), 5  $\mu$ M Y-27632 and 1% heat-inactivated FBS. The cells were seeded in GTX coated T75 cell culture flasks at a density of  $1.5 \times 10^6$  cells/T75 cell culture flask. The flasks were incubated under hypoxic conditions overnight to allow for cell attachment. On day 7, the medium was removed and replaced with Advanced DMEM/F12, containing 1% glutamine, 5  $\mu$ M CHIR99021 and 2  $\mu$ M retinoic acid. The cells were then again left undisturbed for 2 days under hypoxic conditions. On day 9, the medium was removed and replaced with Advanced DMEM/F12 containing 1% glutamine. The cells were again left undisturbed for 2 days under hypoxic conditions. On day 11 the cells were detached from the T75 cell culture flasks using Accutase + 10  $\mu$ M Y-27632. The cells were gently pipetted to dissociate them, counted using Trypan Blue and a Neubauer counting chamber and resuspended in Advanced DMEM/F12, containing 1% glutamine and 2  $\mu$ M SB-431542. The cells were seeded in GTX coated T75 cell culture flasks at a density of  $1.5 \times 10^6$  cells/T75 cell culture flask. On day 12, the medium was removed and replaced with fresh Advanced DMEM/F12, containing 1% glutamine and 2  $\mu$ M SB-431542.

From day 14, the proepicardial cells were pushed to differentiate into cardiac fibroblasts. The cells were first detached from the T75 cell culture flasks using Accutase + 10  $\mu$ M Y-27632. The cells were gently pipetted to dissociate them, counted using Trypan Blue and a Neubauer counting chamber and resuspended in Fibroblast Growth Medium 3 + supplements (PromoCell), containing 20 ng/ml bFGF and 10  $\mu$ M SB-431542. The cells were seeded in GTX coated T75 cell culture flasks at a density of  $1.5 \times 10^6$  cells/T75 cell culture flask. The flasks were incubated under hypoxic conditions overnight to allow for cell attachment. On day 16, the medium was removed and replaced with fresh Fibroblast Growth Medium 3 + supplements, containing 20 ng/ml bFGF and 10  $\mu$ M SB-431542. On day 18 the cells were detached from the T75 cell culture flasks using Accutase + 10  $\mu$ M Y-27632. The cells were gently pipetted to dissociate them, counted using Trypan Blue and a Neubauer counting chamber and resuspended in Fibroblast Growth Medium 3 + supplements, containing 20 ng/ml bFGF and 10  $\mu$ M SB-431542. The cells were seeded in GTX coated T75 cell culture flasks at a density of  $1.5 \times 10^6$  cells/T75 cell culture flask.

From day 20, the cardiac fibroblasts were either passaged or harvested. Both were conducted using Accutase + 10  $\mu$ M Y-27632. After harvesting the cardiac fibroblasts were either cryopreserved or immediately used for further experiments.

### *2.3.2.3 Hybrid cardiac fibroblast differentiation protocol*

The hybrid cardiac fibroblast differentiation protocol (in short the hybrid protocol) contained elements of both the EB protocol and the quiescent protocol.

For some runs of the hybrid protocol, the cells were not seeded onto GTX coated, but onto Matrigel coated cell culture vessels.

The formation of EBs and subsequent induction of the mesoderm stage was performed as described in the cardiomyocyte differentiation protocol. On day 4, immediately after the mesoderm stage, the cells were pushed to differentiate into proepicardial cells. 50-55  $\mu$ l of EBs was resuspended in Advanced DMEM/F12, containing 1% glutamine, 5  $\mu$ M CHIR99021, 2  $\mu$ M retinoic acid, 5  $\mu$ M Y-27632 and 1% heat-inactivated FBS. The EBs were seeded in a GTX coated T75 cell culture flask. From this point, the quiescent protocol was followed, and the cells were treated in analogy to day 6 of the quiescent protocol.

### *2.3.2.4 Freezing and thawing of cardiac fibroblasts*

As it was not always possible to cast CF-EHTs immediately after harvesting the cardiac fibroblasts, it was decided to standardize the procedure and freeze all cardiac fibroblasts after harvesting and thaw the cardiac fibroblasts when the CF-EHTs were cast.

Cardiac fibroblasts were frozen similar to hiPSCs. After collection of cells by centrifugation at 800 rpm for 4 minutes, they were resuspended in heat inactivated FBS + 10% DMSO.  $2.5-6.5 \times 10^6$  cardiac fibroblasts were frozen in 1 ml FBS + 10% DMSO in a cryotube. The cryotubes were slowly frozen in an isopropanol-based freezing device at -80 °C for 24 hours. After 24 hours the cryotubes were transferred to -150 °C for long-term storage.

To thaw the cardiac fibroblasts, the cryotubes were placed in a water bath at 37 °C for 2-3 minutes, until the diameter of the remaining frozen part was around 5 mm. The cryotubes were then sprayed with 70% ethanol and placed in a sterile hood. 3 ml of 37 °C 10% serum containing NKM + 10  $\mu$ M Y-27632 was aspirated with a 5 ml pipet, the pipet was placed in the cryotube and the cell suspension was additionally aspirated. The cell suspension was then slowly transferred to a 15 ml tube at around 1 drop per second. Additionally, 1 ml of 10% serum containing NKM + 10  $\mu$ M Y-27632 was added to the cryotube for washing, aspirated and added to the 15 ml tube, at around 1 drop per second. The tube was then centrifuged at 800 rpm for 4 minutes, the supernatant was removed and the cells were resuspended in 10% serum containing NKM + 10  $\mu$ M Y-27632. The cells were then counted using Trypan Blue and a Neubauer chamber and used for CF-EHT casting or 2D culture.

## 2.4 EHT generation

(CF-)EHTs were generated according to a slightly adapted previously published in-house protocol (Breckwoldt et al., 2017). The protocol was adapted to include 10% cardiac fibroblasts, unless otherwise specified.

To cast the (CF-)EHTs, casting molds were prepared by placing polytetrafluoroethylene (PTFE) spacers into 24-well plates, filled with 1.5 ml/well 60 °C 2% agarose (in DPBS). The 2% agarose was left to solidify at room temperature for around 15 minutes. During this time, the (CF-)EHT mastermix (Table



7) was prepared on ice. Generally, a ratio of 9:1 cardiomyocytes:cardiac fibroblasts was adhered to. All cells were thawed prior to the generation of the mastermix. The cells were resuspended in 10% serum containing NKM, and 2x DMEM (Gibco), fibrinogen (Sigma-Aldrich) and Y-27632 were added to the mastermix in the appropriate quantities. The cell suspension was mixed gently but thoroughly.

Table 7: Mastermix for 1 CF-EHT

Component	Quantity
Cardiomyocytes	0.9 x 10 <sup>6</sup> cells
Cardiac fibroblasts	0.1 x 10 <sup>6</sup> cells
10% Serum containing NKM	97.6 µl
2x DMEM	6.2 µl
Fibrinogen	2.8 µl
Y-27632	0.1 µl

By the time the mastermix was prepared, the agarose had solidified and the PTFE spacers could be gently removed. PDMS racks were placed into the generated agarose molds. 100 µl mastermix was pipetted into 200 µl microtubes containing 3 µl thrombin (100 U/ml, Sigma-Aldrich) and mixed quickly and gently, but thoroughly. 100 µl mastermix + thrombin was then carefully pipetted between the 2 posts of the PDMS racks, into the agarose casting molds. The (CF-)EHTs were then incubated (37 °C, 7% CO<sub>2</sub>, 40% O<sub>2</sub>, 95% humidity) for 1.5 hours to allow for the polymerization of the fibrin. 400 µl of 37 °C medium was layered on top of the (CF-)EHTs before they were incubated for another 30 minutes, to allow the (CF-)EHTs to detach from the agarose molds. The (CF-)EHTs could then be removed from the agarose molds and transferred to a 24-well plate filled with 1.5 ml/well of fresh 10% serum containing EHT medium. The (CF-)EHTs were kept in the incubator and the medium (either 10% serum containing EHT medium or 0.5% serum containing EHT medium) was changed on Mondays, Wednesdays and Fridays.

#### 2.4.1 Contractility analysis

1.5 to 2 hours after the medium of the (CF-)EHTs was changed, the spontaneous contractions of the (CF-)EHTs were measured according to a previously established automated video-optical recording procedure (Hansen et al., 2010). A 24-well plate containing (CF-)EHTs was placed in a specialized incubator (37 °C, 7% CO<sub>2</sub>, 40% O<sub>2</sub>, 95% humidity) equipped with a glass roof. The 24-well plate was placed on top of 24 white LEDs, to illuminate the (CF-)EHTs. A video camera mounted onto a motorised XYZ-axis above the transparent roof recorded a video of the contractions of each individual (CF-)EHT. The contractions of the (CF-)EHTs were analysed from this video by CTMV-Software (Consulting Team Machine Vision, Pforzheim), a pattern recognition software, which detected post deflection and could automatically convert the post deflection into multiple parameters of contraction. These parameters included but were not limited to the force of the contractions, the beating frequency, kinetics (including relaxation time and -velocity) and resting length of the (CF-)EHTs. Additionally, still images of each (CF-)EHT during relaxation and contraction were taken. The width of (CF-)EHTs was measured at the smallest part of the (CF-)EHT, perpendicular to the (CF-)EHT based on the respective image of the relaxed (CF-)EHT using ImageJ (NIH, Figure 9).



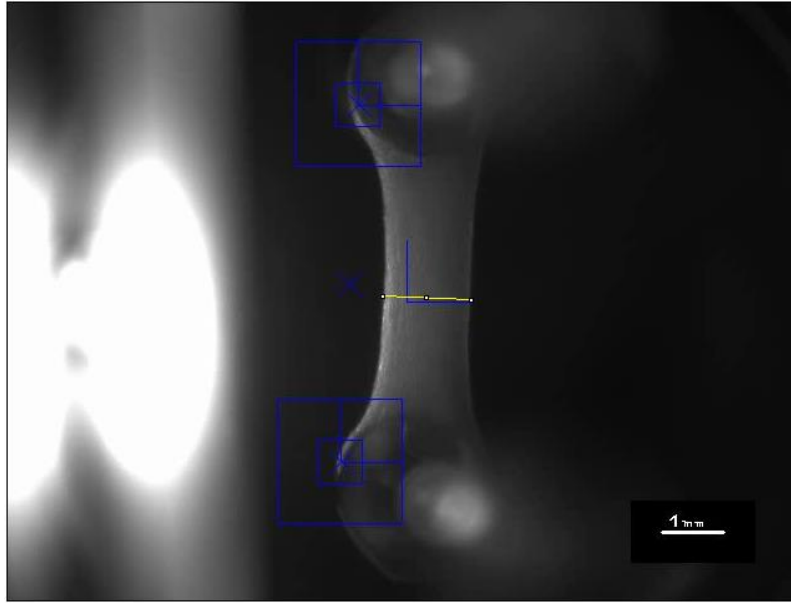


Figure 9: The width of the (CF-)EHTs was measured at the smallest part of the (CF-)EHT, perpendicular to the (CF-)EHT, using ImageJ, scale bar is 1 mm.

We set 0.2 mN as the threshold for sufficient force development. When (CF-)EHTs generated a force lower than 0.2 mN, those (CF-)EHTs were excluded from further contractility analysis. It is mentioned in the text when less than 3 (CF-)EHTs remained which generated a force higher than 0.2 mN.

#### 2.4.2 Electrical pacing

In multiple (CF-)EHT experiments, the (CF-)EHTs were electrically stimulated (electrical pacing) at the last day of culture, to measure the contractility of the (CF-)EHTs at a standardised beating frequency, the protocol for which had been previously established in-house (Hirt et al., 2014). To electrically pace the (CF-)EHTs, the medium of the (CF-)EHTs on the second to last day of culture was replaced with 2 ml (fresh) medium, instead of the regular 1.5 ml. On the last day of culture, the (CF-)EHTs were shortly lifted out of their 24-well plate, custom made carbon electrodes were placed into the 24-well plate and the (CF-)EHTs were mounted onto the electrodes. The (CF-)EHT plate with electrodes was then equilibrated in an incubator (37 °C, 7% CO<sub>2</sub>, 40% O<sub>2</sub>, 95% humidity) for at least half an hour up to 1 hour, after which the contractility of the (CF-)EHTs was measured under electrical pacing, at 2.5 V and with a biphasic pulse duration of 4 ms per phase, at various frequencies, ranging from 1 Hz to 3 Hz. The pacing was controlled by a S88X Dual Output Square stimulator (Grass/Natus Neurology Incorporated).

#### 2.4.3 Harvesting

At the respective last day of culture, (CF-)EHTs were harvested. To harvest the (CF-)EHTs, they were either snap frozen in liquid N<sub>2</sub>, or they were fixed for histological analysis. To snap freeze the (CF-)EHTs, they were cut in half with a scalpel, gently removed from the posts, placed in separate 2 ml centrifuge tubes and placed in a liquid N<sub>2</sub> container for 1 minute, after which the (CF-)EHT pieces were kept for long-term storage at -80 °C. To fix the (CF-)EHTs, they remained attached to their mounting posts, were washed in DPBS and fixed in 4% formaldehyde (Roti-Histofix) at 4 °C overnight. The (CF-)EHTs were then gently removed from the posts and placed in 2 ml centrifuge tubes containing 1 ml DPBS + sodium azide (Sigma-Aldrich), after which the fixed (CF-)EHTs were stored at 4 °C.

## 2.5 Molecular analysis

### 2.5.1 Gene expression

#### 2.5.1.1 RNA isolation

RNA isolation from either 2D cultured cells or from harvested (CF-)EHT halves was performed with either the RNeasy Mini kit (QIAGEN) or with TRIzol (Life Technologies).

When using the RNeasy Mini kit, 2D cultured cells in 6-well, 12-well or 24-well cell culture plates were detached from the plate and lysed in the same step by adding 350 µl RLT buffer (QIAGEN) + 1% 2-mercaptoethanol (Sigma-Aldrich) per well and gently pipetting it. To isolate RNA from (CF-)EHT halves, the tissue was first disrupted and homogenized. This was achieved by adding a steel bead to a 2 ml microtube containing both the (CF-)EHT half and the RLT buffer + 1% 2-mercaptoethanol. Set at 30 Hz for 2 minutes, the TissueLyser (QIAGEN) was used to disrupt and homogenize the (CF-)EHT half. RNA was extracted from the lysate, either from the 2D cultured cells or the (CF-)EHT half, according to the manufacturer's instructions of the RNeasy Mini kit.

When isolating RNA from 2D cultured cells using TRIzol, the cells were again detached from the wells and lysed in the same step, by adding 1 ml TRIzol per well and gently pipetting it. The (CF-)EHT halves were disrupted and homogenized in the same manner as previously described. After the 2D cultured cells or (CF-)EHT halves had been lysed, 200 µl chloroform (J.T. Baker) was added and the lysate was thoroughly mixed. The lysate and chloroform mixture was then incubated at room temperature for 2 minutes and centrifuged at 4 °C, 1200 rpm, for 15 minutes. The centrifugation led to a separation of the mixture into multiple phases, including an aqueous phase containing the RNA. This phase was carefully transferred to a new 1.5 ml microtube, the RNA was precipitated 1:1 with isopropanol, washed in 70% ethanol and resuspended in 20 µl RNase-free water.

The amount of RNA present in the RNase-free water was quantified with a Nanodrop 1000 Spectrophotometer (Thermo Fisher Scientific). The RNA suspension was either stored at -80 °C or directly reverse transcribed into cDNA.

#### 2.5.1.2 Reverse transcription

When possible, 500 ng of RNA was reverse transcribed into cDNA. If less than 500 ng was available, the maximum available amount of RNA was reverse transcribed into cDNA. The RNA was reverse transcribed with the High-Capacity cDNA Reverse Transcription kit (Applied Biosystems). The reaction mix was independent of the amount of RNA (Table 8). The reaction mix was placed in a GeneAMP PCR System 9700 thermocycler (Thermo Fisher Scientific). The thermocycling conditions are listed in Table 9.

Table 8: Reaction mix for reverse transcription of RNA to cDNA

Component	Quantity for 1 reaction
RNA	500 ng
10x RT buffer	2.5 µl
10x Random primer	2.5 µl
25x dNTPs (100 mM)	1 µl
MultiScribe reverse transcriptase (50 U/µl)	1 µl
Nuclease-free water	Top up to 25 µl

Table 9: Thermocycling conditions for reverse transcription of RNA to cDNA

Temperature	Time
25 °C	10 minutes
37 °C	120 minutes
85 °C	5 minutes
4 °C	Indefinitely

The cDNA was either stored at -20 °C or directly used for quantitative real-time PCR.

#### 2.5.1.3 Quantitative real-time PCR

When 500 ng RNA was reverse transcribed into cDNA, the cDNA was diluted 10 times in nuclease-free water to prepare for quantitative real-time PCR (qPCR). When less than 500 ng RNA was reverse transcribed into cDNA, the dilution was adapted accordingly.

A primer mix was prepared for each primer by diluting 10 µl forward primer and 10 µl reverse primer in 80 µl nuclease-free water. These primer mixes were used for the final qPCR reaction mixes (Table 10).

Table 10: qPCR reaction mix for 1 primer

Component	Quantity for 1 reaction
Nuclease-free water	5.5 µl
EvaGreen master mix (Solis BioDyne)	2 µl
10 µM Primer mix	0.5 µl

Each well of a 384-well qPCR plate was filled with 8 µl qPCR reaction mix and 2 µl diluted cDNA. The plate was then closed with an adhesive plastic cover. The plate was centrifuged at 2000 rpm for 1 minute. The qPCR was performed on an ABI PRISM 7900HT Sequence Detection System (Thermo Fisher Scientific) or a QuantStudio 5 (Thermo Fisher Scientific). The thermocycling conditions are listed in Table 11.

The gene expression relative to control was calculated with the average of the relative expression of the control condition, compared to the relative expression of the other conditions.

Table 11: Thermocycling conditions for quantitative real-time PCR

Cycles	Temperature	Time
1	50 °C	2 minutes
1	95 °C	10 minutes
40	95 °C	15 seconds
	60 °C	1 minute
1	95 °C	15 seconds
1; 0.075 °C/sec ramp rate	60 °C	1 minute
	95 °C	15 seconds

Different primers were used for the qPCRs performed in this work (Table 12).

Table 12: Primer list for quantitative real-time PCR

Gene	Sequence (5'-3')	Size (bp)
<i>ACTA2</i>	Fw: TGGAAAAGATCTGGCACCCT Rv: GGCATAGAGAGACAGCACCG	188
<i>CCN2</i>	Fw: TGTGCATTCTCCAGCCATCA Rv: GCCACAAGCTGTCCAGTCTA	137
<i>COL1A1</i>	Fw: TGGGATTCCCTGGACCTAAAG Rv: GGGAGACCCTGGAATCCG	199
<i>COL1A2</i>	Fw: CAGCCGGAGATAGAGGACCA Rv: CAGCAAAGTTCCACCGAGA	135
<i>COL3A1</i>	Fw: GGACACAGAGGCTTCGATGG Rv: CTCGAGCACCGTCATTACCC	190
<i>DDR2</i>	Fw: TTTTGGGTTGGGGAAACGC Rv: TCCTCAAAAACAGCTGGCCT	203
<i>GATA4</i>	Fw: TTCCAGCAACTCCAGCAACG Rv: GCTGCTGTGCCCCGTAGTGAG	97
<i>GUSB</i>	Fw: ACGATTGCAGGGTTTCACCA Rv: CACTCTCGTCGGTGAAGTGT	171
<i>NKX2.5</i>	Fw: CCAAGGACCCTAGAGCCGAA Rv: CCACCGACACGTCTCACTC	162
<i>POSTN</i>	Fw: GAGGCTTGGGACAACTTGGA Rv: ACAGTGACAACCCATTAGGA	200
<i>RUNX1</i>	Fw: TGAGAAATGCTACCGCAGCC Rv: TCCCTCTTCCACTTCGACCG	81
<i>TAGLN</i>	Fw: GAAGGCGGCTGAGGACTATG Rv: TGCTCCTGCGCTTTCTTCAT	183
<i>TBX18</i>	Fw: CTTCAACAACCGTCACTGCCTA Rv: GGCTTCAAACCCATTCTGTT	115
<i>TCF21</i>	Fw: ACACCAAGCTCTCCAAGCTG Rv: CCATAAAGGGCCACGTCAGG	132
<i>TNC</i>	Fw: AGTGGGACAGCAGGTGACTC Rv: CTATCCCAACATTCCCCGCTT	992

<i>VIM</i>	Fw: GCAGGAGATGCTTCAGA Rv: GCAGCTCCTGGATTCCTCT	167
<i>WT1</i>	Fw: CGCCCTACAGCAGTGACAAT Rv: GCGTTGTGTGGTTATCGCTC	129

### 2.5.2 Collagen quantification

The amount of collagen (in mg/l) present in cell suspensions or medium was quantified with the Total Collagen Assay kit (QuickZyme Biosciences), which is able to detect hydroxyproline, a modified amino acid mainly present in collagen. To prepare the samples, 50-250  $\mu$ l of the samples was transferred into specialised screw-capped tubes and diluted 1:1 with 12 M HCl, after which the samples were incubated at 95 °C for 20 hours. Once the samples had cooled down to room temperature, the samples were centrifuged at 13000 rpm for 10 minutes. The supernatant was aspirated into a clean microtube and diluted 2:1 with water.

To prepare the standard, 50  $\mu$ l of the collagen stock (12000  $\mu$ g/ml in 0.02 M acetic acid) was transferred into specialised screw-capped tubes and diluted 1:1 with 12 M HCl, after which the diluted stock was incubated at 95 °C for 20 hours. Once the diluted stock had cooled down to room temperature, it was centrifuged at 13000 rpm for 10 minutes. The supernatant was used to prepare 8 dilutions of the stock, the standard, according to Table 13.

Table 13: Pipetting scheme for the 8 stock dilutions for the standard.

Standard label	Sample from	4 M HCl	Water	Collagen concentration ( $\mu$ g/ml)
<b>S1</b>	80 $\mu$ l diluted collagen stock	40 $\mu$ l	40 $\mu$ l	300
<b>S2</b>	100 $\mu$ l from S1	50 $\mu$ l	-	200
<b>S3</b>	90 $\mu$ l from S2	90 $\mu$ l	-	100
<b>S4</b>	90 $\mu$ l from S3	90 $\mu$ l	-	50
<b>S5</b>	90 $\mu$ l from S4	90 $\mu$ l	-	25
<b>S6</b>	90 $\mu$ l from S5	90 $\mu$ l	-	12.5
<b>S7</b>	90 $\mu$ l from S6	90 $\mu$ l	-	6.25
<b>S8</b>	-	90 $\mu$ l	-	0

For the assay, 35  $\mu$ l of each stock dilution was pipetted into 8 connecting wells of a 96-well assay plate. 35  $\mu$ l of each sample was pipetted into a well of the same 96-well assay plate. 75  $\mu$ l assay buffer was added into each well and thoroughly mixed. The 96-well assay plate was closed and incubated while shaking at room temperature for 20 minutes. A detection reagent mix of detection reagent A and detection reagent B was prepared at a 2:3 ratio. 75  $\mu$ l of the detection reagent mix was added to each well. The 96-well assay plate was closed and the detection reagent was mixed in the wells by shaking. The 96-well assay plate was incubated at 60 °C for 1 hour, after which it was cooled on ice for maximally 5 minutes. The absorption of the 96-well assay plate was photometrically read at 570 nm with a Safire<sup>2</sup> Multi Detection Plate Reader (Tecan). The absorption data was then analysed, using the standard, to determine the collagen concentration.

### 2.5.3 Protein expression

To determine protein expression in 2D cultured cardiac fibroblasts or CF-EHT halves, samples were prepared for Western blots, which were kindly performed by Grit Höppner (IEPT, UKE, Hamburg). 2D cultured cells were detached from the wells and lysed in the same step, by dissolving them in 50 µl Krnias buffer + 2 mM DTT + 1x Laemmli buffer + 1.2% 2-mercaptoethanol. CF-EHT halves needed to be disrupted and homogenized using the TissueLyser as previously described. To reduce the viscosity of the lysate, the lysate was transferred into a 1.5 ml microtube and incubated at 95 °C for 5 minutes.

A 10% SDS-PAGE gel was installed in an electrophoresis chamber (Bio-Rad), which was filled with 1x electrophoresis buffer. 10-12 µl of the lysate was loaded onto the gel, framed by 8 µl of protein size standard on either side of the gel. The electrophoresis was conducted at 80 V for 10-15 minutes, until the bands had moved into a straight line in the stacking gel. The voltage was then increased to 120 V until the lowermost bands had reached the end of the separating gel. The proteins were then blot-transferred from the gel onto a nitrocellulose membrane (0.45 µm) at 350 mA for 2 hours in 1x transfer buffer. The bands were inspected by staining the blot with Ponceau S solution (Sigma-Aldrich) for 5 minutes. After the blot was washed, it was blocked for 1 hour in TBS + 0.1% Tween 20 (TBST, Sigma-Aldrich) + 5% milk powder (Roth). The blot could now be cut to allow for staining with multiple primary antibodies, by incubating each part of the blot with 1 primary antibody at 4 °C overnight. In this work, blots were stained for periostin (Invitrogen), αSMA (Dako) and α-tubulin (Cell Signaling) or lamin A/C (Santa Cruz), all diluted in TBST. After incubating the blot with either an anti-mouse or anti-rabbit IgG peroxidase-conjugated secondary antibody, diluted in TBST + 5% milk powder, at room temperature for 1 hour, the protein bands were visualised with the Pierce ECL Western Blotting Substrate (Thermo Fisher Scientific) on the Bio-Rad ChemiDoc Touch Imaging System (Bio-Rad Laboratories). The protein abundance of α-tubulin or lamin A/C was quantified for standardization of protein loading, unless otherwise specified.

### 2.5.4 Flow cytometry

Flow cytometry was used to analyse the expression of cell surface markers and/or intracellular markers.

#### 2.5.4.1 Cell surface markers

When using flow cytometry to analyse cell surface markers,  $0.5-1 \times 10^6$  living cells were first blocked for 15 minutes at 4 °C in 1 ml FBS. The cell suspension was distributed over 2 fluorescence-activated cell sorting (FACS) tubes; 1 stained sample and 1 isotype control sample. All cells were washed with DPBS and centrifuged at 1000 rpm for 2 minutes. For direct labelling of the cell surface markers, the stained sample was resuspended in 100 µl antibody solution (antibody diluted in FACS buffer) and incubated for 45 minutes on ice. The isotype control sample was resuspended in 100 µl isotype control solution (isotype control staining diluted in FACS buffer) or in 100 µl FACS buffer, depending on the staining. All samples were washed twice, after which the samples were resuspended in 250 µl DPBS for analysis. For indirect labelling, the stained sample was incubated overnight in the first antibody solution and the isotype control sample was incubated overnight in FACS buffer, after which all samples were washed twice and incubated with the second antibody solution for 1 hour. After removal of unbound antibodies by washing twice, the cells were resuspended in DPBS for analysis. Flow cytometry was

conducted with a Canto II flow cytometer (BD Biosciences). FACSDiva 9 (BD Biosciences) software was used to analyse the obtained data.

The cell surface marker SSEA-3 (antibody from BD Pharmingen) was used as a marker for the pluripotency of hiPSCs.

#### *2.5.4.2 Intracellular markers*

When using flow cytometry to analyse intracellular markers, the cells needed to be permeabilised to allow the antibodies to enter the cell and bind to intracellular markers. Before the cells could be permeabilised, they needed to be fixed in 4% formaldehyde for 20 minutes, after which the cells were permeabilised overnight in permeabilization buffer (FACS buffer, 0.5% saponin (Merck) and 0.05% sodium azide). The cell suspension was then split into 2 FACS tubes; 1 stained sample and 1 isotype control sample. All cells were washed with DPBS and centrifuged at 1000 rpm for 2 minutes. For direct labelling of the intracellular markers, the stained sample was resuspended in 100 µl antibody solution (antibody diluted in permeabilization buffer) and incubated for 45 minutes on ice. The isotype control sample was resuspended in 100 µl isotype control solution (isotype control staining diluted in permeabilization buffer) or in 100 µl permeabilization buffer, depending on the staining. All samples were washed twice, after which the samples were resuspended in 250 µl DPBS for analysis. For indirect labelling, the stained sample was incubated overnight in the first antibody solution and the isotype control sample was incubated overnight in permeabilization buffer, after which all samples were washed twice and incubated with the second antibody solution for 1 hour. The expression of the specific intracellular marker was then measured with the FACSCanto II flow cytometer. FACS Diva 9 was used to analyse the obtained data.

Cardiac troponin T (cTnT, Miltenyi Biotec) was measured as a marker of cardiomyocytes and was used to determine the purity of the cells obtained with each cardiomyocyte differentiation run. Only cardiomyocytes with a purity of >60% were used.

#### *2.5.4.3 Cell surface marker and an intracellular marker*

When flow cytometry was used to analyse cells for both cell surface markers and intracellular markers, the above-described protocols needed to be combined.

The cells surface markers needed to be stained first, as described above, by blocking-incubation of the cells, followed by staining the cell surface markers either directly or indirectly. The cells were then permeabilised and stained again, directly or indirectly, for intracellular markers. The expression of cell surface markers and intracellular markers was then measured with a FACSCanto II flow cytometer. Flowing Software 2 (Turku Bioscience Centre) was used to analyse the obtained data.

By staining samples for the cell surface marker DDR2 (Thermo Fisher) and the intracellular marker  $\alpha$ SMA, the amount of  $\alpha$ SMA<sup>+</sup> cells as a percentage of DDR2<sup>+</sup> cells could be used as the percentage of cardiac fibroblasts which were in an activated state. For the dual staining of DDR2 and  $\alpha$ SMA, the cells were fixed prior to the staining.

All flow cytometry analyses were performed in the FACS Core Facility, UKE.

## 2.6 Nanoindentation

The stiffness of CF-EHTs was measured with nanoindentation. To prepare the CF-EHTs for nanoindentation measurements, the CF-EHTs were first fixed in 4% formaldehyde, as previously described. 4% agarose in DPBS was left to settle overnight at 60 °C. The fixed CF-EHTs were embedded in 4% agarose, which was left to polymerize at room temperature for 1 hour. A small, polymerized agarose cube containing the CF-EHT was excised with a scalpel. The agarose was then carefully removed, until the surface of the CF-EHT was reached. The CF-EHT in agarose was then mounted on a stage, after which the stiffness of the CF-EHTs was measured with the Chiaro Nanoindenter (Optics11 Life). Nanoindentation measurements were kindly performed by Dr. Sandra Hemkemeyer (ICCLM, UKE, Hamburg).

## 2.7 Statistics

Statistical analyses of the results were conducted with GraphPad Prism 5. When possible ( $n \geq 3$ ), data are presented as mean  $\pm$  SEM. Statistical differences between groups were calculated by one or two-way analysis of variance (ANOVA) plus Bonferroni's multiple comparisons test when appropriate. A P-value of less than 0.05 was considered to be statistically significant.



### 3. Results

#### 3.1 Results I: Development of an *in vitro* fibrosis model

##### 3.1.1 Fibroblast differentiation

The first step in establishing an *in vitro* 3D EHT based fibrosis model was the optimization of a differentiation protocol for cardiac fibroblasts, which were to be used in this model.

In the department of Experimental Pharmacology and Toxicology, led by Professor Thomas Eschenhagen, Dr. Tessa Werner and Dr. Bangfen Pan had previously established an unpublished cardiac fibroblast differentiation protocol based on EB formation, here referred to as the EB protocol. It was suspected and confirmed during this work that the fibroblasts differentiated using this EB protocol were in a considerably activated state at baseline. For the fibrosis model created in this work, it was important to establish a quiescent baseline, to allow for a high dynamic range of regulation. It was therefore desirable to employ quiescent cardiac fibroblasts. A previously published protocol for the differentiation of quiescent cardiac fibroblasts was thus adapted (H. Zhang et al., 2019), here referred to as the quiescent protocol. A hybrid protocol, a combination of the EB protocol and the quiescent protocol, was additionally developed and evaluated. In the hybrid protocol, hiPSCs were pushed into the mesoderm stage according to the EB protocol, after which the cells were pushed into proepicardial cells and subsequently towards cardiac fibroblasts following the quiescent protocol. The hybrid protocol was developed to reduce differentiation time, as according to this protocol the differentiation from hiPSCs into cardiac fibroblasts took 18 days, whereas this differentiation took 20 days according to the quiescent protocol and 24 days according to the EB protocol. The hybrid protocol was further developed to investigate whether this protocol would yield higher cell numbers and/or more quiescent cells than the quiescent protocol. The 3 protocols were analysed for suitability for the *in vitro* EHT based fibrosis model.

For readability of the figures in which these analyses are portrayed, the cells differentiated with any of the cardiac fibroblast differentiation protocols are referred to as cardiac fibroblasts (CFs).

It was investigated which protocol generated the most quiescent cells after dissociation, by comparing mRNA abundance of the fibroblast activation markers collagen1a1, periostin and ACTA2 relative to the housekeeping gene GUSB (Figure 10; for the mRNA abundance analyses of transgelin and CCN2, see supplement section 10.1.1). A higher abundance of collagen1a1 and ACTA2 mRNA was present in primary foreskin fibroblasts and cells differentiated with the EB protocol compared to cells differentiated with either other protocol. This suggested that the other 2 protocols either indeed generated more quiescent fibroblasts or did not generate well-defined fibroblasts.

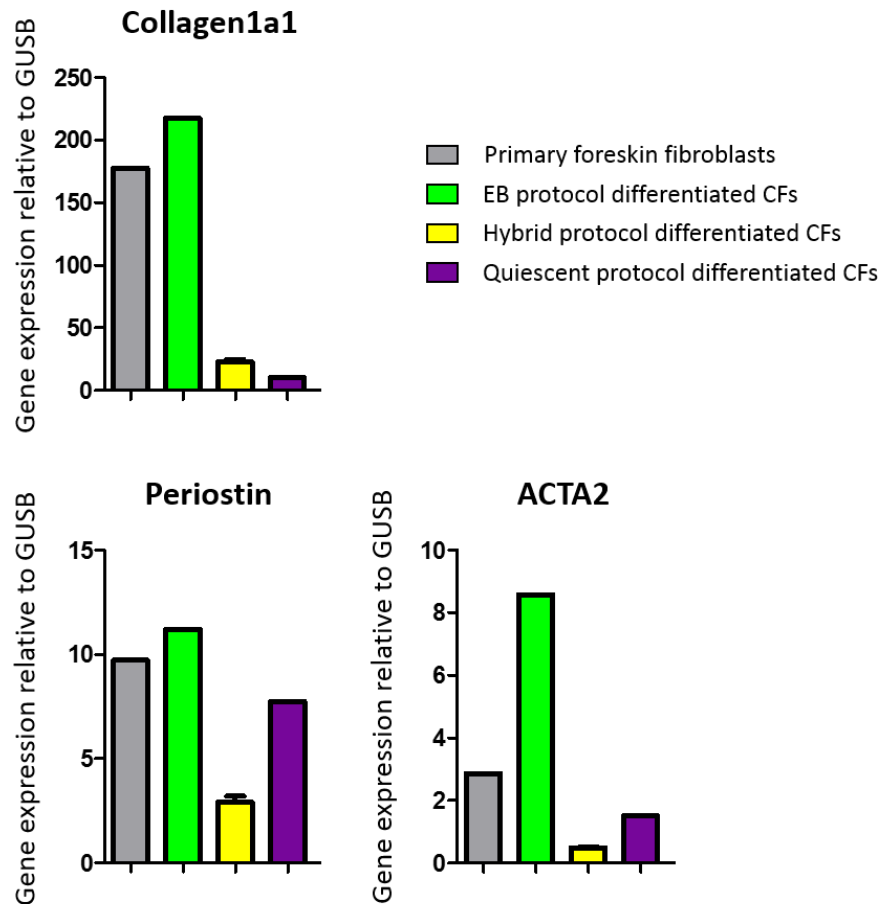


Figure 10: The mRNA abundance relative to GUSB of the fibroblast activation markers collagen1a1, periostin and ACTA2 in primary foreskin fibroblasts and CFs differentiated with the EB protocol, the hybrid protocol or the quiescent protocol. CFs were harvested on the last day of the respective differentiation protocol. When possible ( $n \geq 3$ ), data are presented as mean  $\pm$  SEM,  $n=1-4$  per condition.

An in-depth characterization of the development of the cells undergoing the hybrid protocol and the quiescent protocol, to establish whether the differentiated cells were indeed cardiac fibroblasts, was thus conducted. Markers expressed at various stages of cardiac fibroblast development were analysed in samples taken at different time points during the differentiation processes (Figure 11). Collagen1a1 and connective tissue growth factor (CTGF), encoded by *CCN2*, were used as fibroblast activation markers. *TCF21* was analysed as a marker for mesenchyme derived cells, which represent the majority of cardiac fibroblasts. T-box transcription factor 18 (*TBX18*) and Wilms' tumour protein 1 (*WT1*) were analysed as fibroblast markers, as they are typically expressed by epicardial fibroblast progenitors (Fu et al., 2020). For the mRNA abundance analyses of GATA4 and NKX2.5, see supplement section 10.1.1.

In samples taken from either the hybrid protocol differentiation run or the quiescent protocol differentiation run, the presence of collagen1a1 and *CCN2* mRNA increased over time, followed by a substantial decrease on the last day of differentiation. This again suggested the differentiation of quiescent fibroblasts. *TCF21* and *TBX18* mRNA was more abundant in the cells obtained on the last day of the hybrid protocol differentiation run compared to in hiPSCs or primary foreskin fibroblasts (for *TCF21* 20.6 and 17.6 times more, respectively, and for *TBX18* 5.2 and 2 times more, respectively). In the cells obtained on the last day of the quiescent protocol differentiation run compared to hiPSCs or primary foreskin fibroblasts, *TCF21* mRNA was 17.4 and 14.8 times more abundant, respectively, and *TBX18* was 8.1 and 3.2 times more abundant, respectively. These results strongly suggested that the

cells differentiated with both the hybrid protocol and the quiescent protocol were indeed fibroblasts. A higher abundance of WT1 mRNA in the cells obtained on the last day of the hybrid protocol differentiation run compared to hiPSCs or primary foreskin fibroblasts (54.8 and 1.8 times more, respectively) also strongly suggested that the cells differentiated with this protocol were fibroblasts. WT1 mRNA was 4.5 times more abundant in primary foreskin fibroblasts than in the cells obtained on the last day of the quiescent protocol differentiation run, but WT1 mRNA was 6.9 times more abundant in the cells obtained on the last day of the quiescent protocol differentiation run than in hiPSCs. This still suggested that the cells differentiated with this protocol were fibroblasts. In this experiment, the mRNA abundance of GATA4 and NKX2.5 was higher in the hiPSCs than in the CFs. However, as will be discussed later (Figure 29), the mRNA abundance of GATA4 was substantially higher in 3 runs of CFs differentiated with the quiescent protocol than in hiPSCs, which strongly suggested a cardiac lineage of the differentiated fibroblasts.

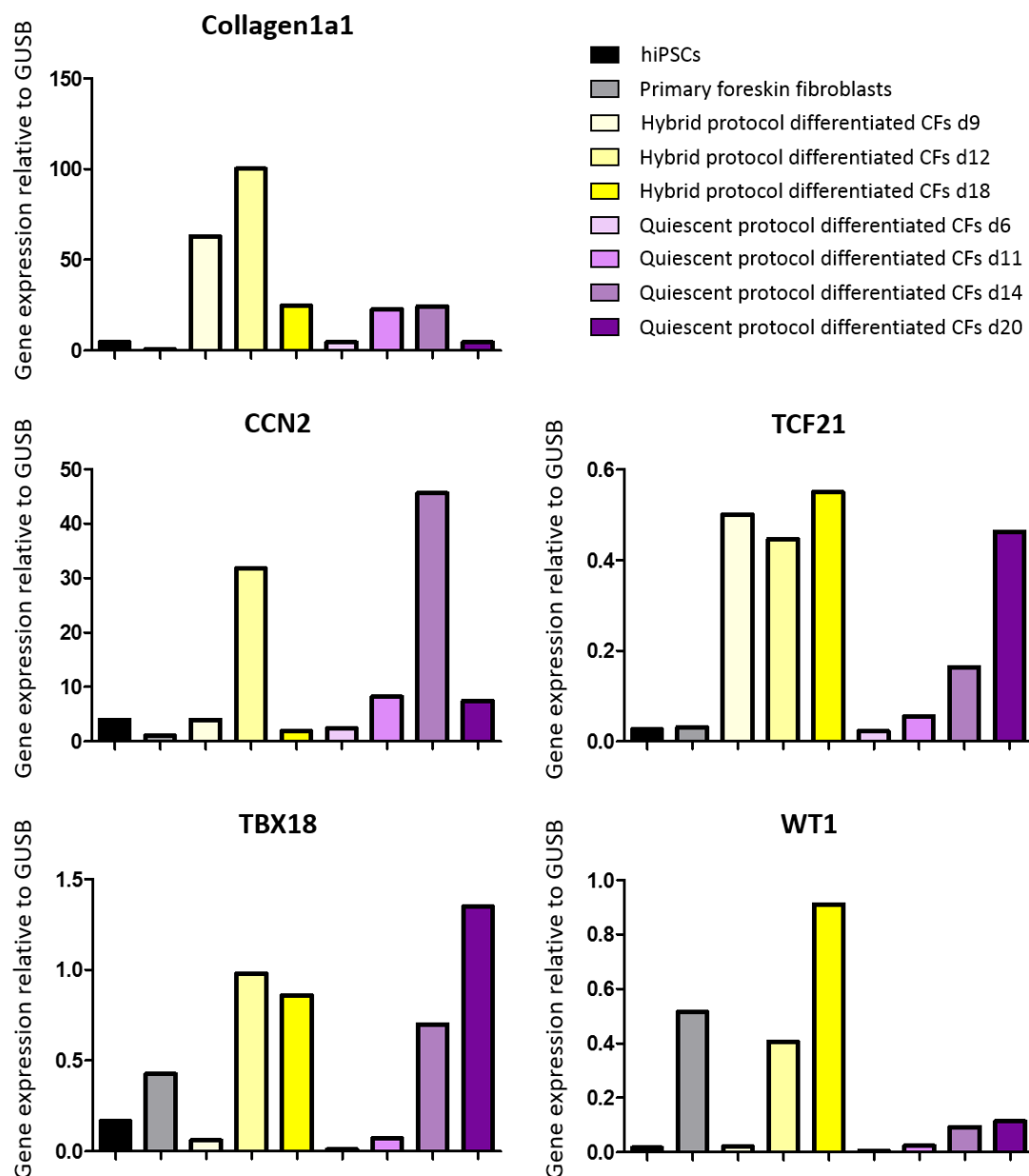


Figure 11: The mRNA abundance relative to GUSB of different markers present during and at the end of the development of CFs. The mRNA abundance of collagen1a1, CCN2, TCF21, TBX18 and WT1 are presented. The mRNA abundance was analysed

*in hiPSCs, primary foreskin fibroblasts and in cells sampled at different days of differentiation for both the hybrid protocol and the quiescent protocol. For the hybrid protocol differentiation, cells were sampled on day 9, day 12 and on the last day of differentiation, day 18. For the quiescent protocol differentiation, cells were sampled on day 6, day 11, day 14 and on the last day of differentiation, day 20, n=1 per condition.*

Aside from mRNA presence in the cells during and after differentiation, the morphology of the cells was an important factor in determining the generated cell type. To analyse the morphology, microscope images were taken at different days during an EB protocol, a hybrid protocol and a quiescent protocol differentiation run (Table 14).


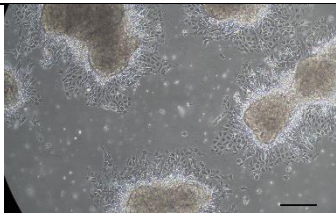
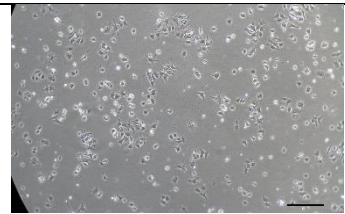
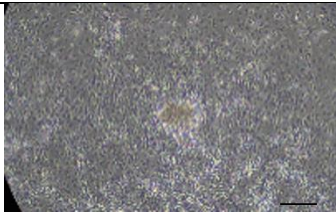
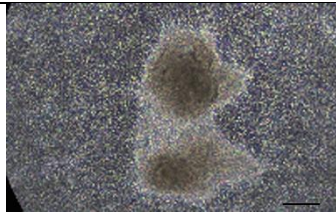
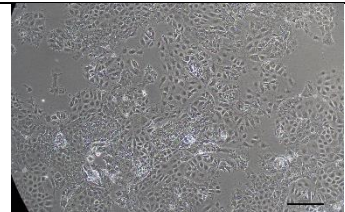
During the first few days of differentiation, EBs were clearly visible in the images of the cells undergoing the EB protocol. On day 15 the EBs were dissociated into single cells, and from then on, the EBs were no longer visible in the microscope images.

Cardiac progenitor cells (CPCs) display a spheroid morphology, which could be observed in cells undergoing the quiescent protocol on day 6.

On day 12, the cells undergoing the hybrid protocol and the quiescent protocol displayed the flattened, slightly circular morphology of epicardial cells, referred to as ‘cobblestone morphology’ (Jiang et al., 2021; Velecela et al., 2019). This morphology was not observed in the cells undergoing the EB protocol.

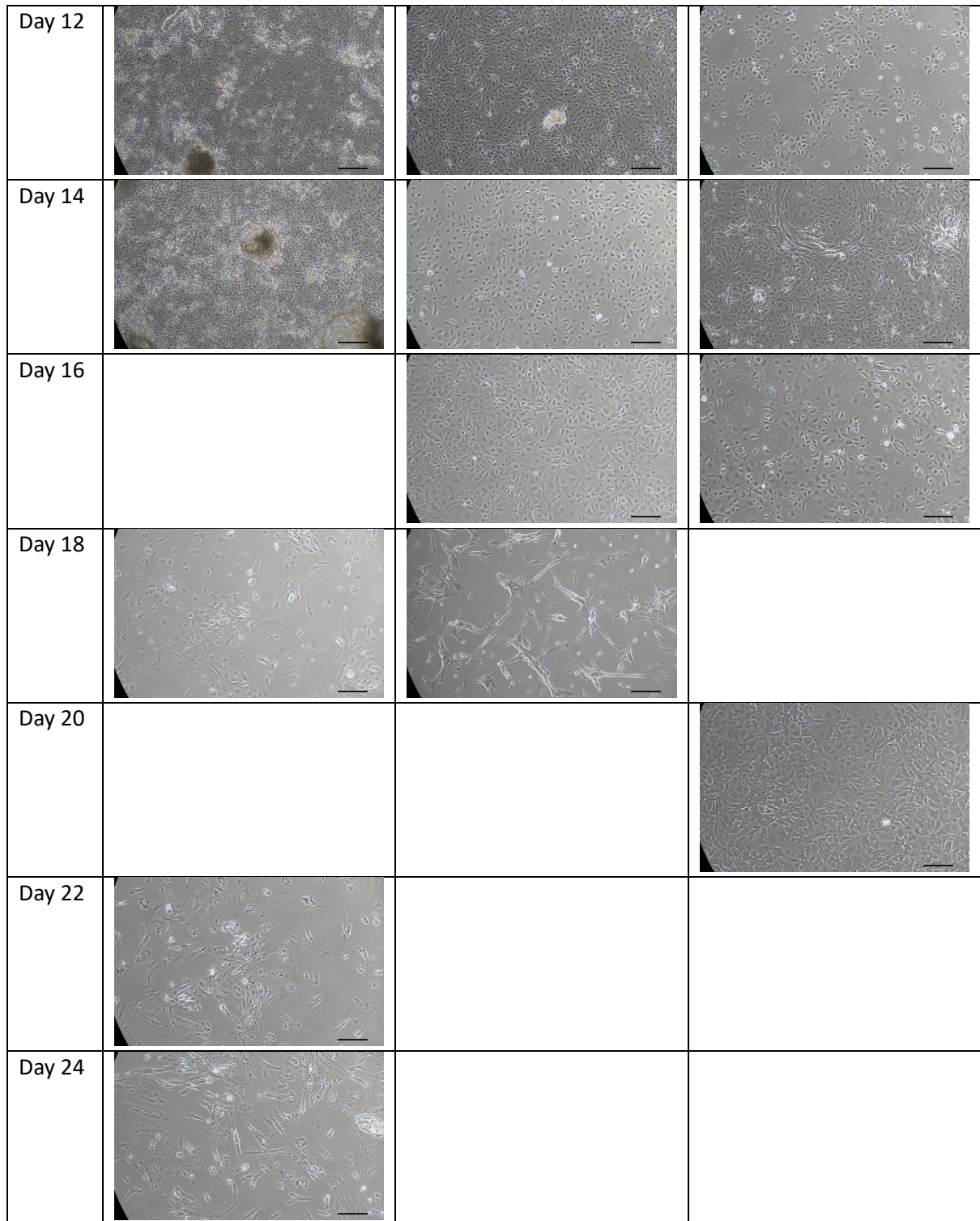
Over time, the cells undergoing any of the differentiation protocols became more elongated, compatible with the typical morphology of fibroblasts. On the last day of differentiation, the cells which had undergone either the EB protocol or the hybrid protocol, appeared to exhibit more contractile stress fibres, which argued for their differentiation into activated fibroblasts; myofibroblasts.

*Table 14: Microscope images at 10x magnification, which show the morphology of cells undergoing either the EB protocol, the hybrid protocol or the quiescent protocol, at different days during differentiation, starting from day 3 until the respective end of culture. A representative image is shown from n=4. Scale bar is 200  $\mu$ m.*

	EB protocol	Hybrid protocol	Quiescent protocol
Day 3			
Day 6			
Day 8 or 9			



# Results I: Development of an *in vitro* fibrosis model - 47



To optimize both the hybrid and the quiescent protocol for following and future experiments, the coating of the cell culture vessels on which the cells were seeded during the differentiation was investigated. Cell culture vessels regularly need to be coated to allow for cell attachment. In the original publication of the quiescent protocol, the cells were plated on Matrigel (MG) coated cell culture vessels. MG is an extract of the mouse Engelbreth-Holm-Swarm tumour, which is rich in basement membrane. The use of Geltrex (GTX), a basement membrane extract, coated cell culture vessels was more common in the department where this work was conducted than the use of MG coated cell

culture vessels. Both GTX and MG contain laminin and collagen IV. Differences attributable to the 2 coatings in the morphology of the cells which undergo the hybrid protocol, were analysed with microscope images at different time points during the differentiation (see supplement section 10.1.1).

There was no difference in morphology either during differentiation or on the last day of differentiation between the cells differentiated on MG coated T75 cell culture flasks and the cells differentiated on GTX coated T75 cell culture flasks. As GTX was the more common coating, it was decided to use GTX coated T75 cell culture flasks in the following differentiations.

The published protocol for quiescent fibroblast differentiation described the cultivation of hiPSCs in Essential E8 medium prior to the start of the differentiation. However, the cultivation of hiPSCs in FTDA medium was more common in the department in which this work was conducted. Therefore, the difference in morphology of the cells which underwent the quiescent fibroblast differentiation protocol in which the hiPSCs were cultivated in either Essential E8 or FTDA medium prior to the start of differentiation was evaluated at different time points of differentiation (see supplement section 10.1.1).

From day 12 on, the cells which were previously cultivated in Essential E8 medium had a higher confluency compared to the cells previously cultivated in FTDA medium. On day 20, the cells which were previously cultivated in FTDA medium displayed a slightly more elongated morphology compared to the cells previously cultivated in Essential E8 medium, which could be considered a more typical fibroblast morphology. In light of the slightly more fibroblast-like morphology and as cultivation of hiPSCs in FTDA medium rather than Essential E8 medium was more common, the respective hiPSCs were cultivated in FTDA medium prior to the start of differentiation for all following differentiations.

Aside from the mRNA marker presence in the cells and morphology of the cells undergoing each protocol, the yield of each protocol, defined as the amount of cells which could be differentiated from 1 million hiPSCs, was another important characterization factor. Each protocol was conducted with UKEi001-A/ERC001 (in short ERC001) hiPSCs and the yield of each protocol was calculated for these differentiation runs (Figure 12, top). The quiescent protocol was carried out with different hiPSC lines (including episomal line A18945, in short A18945 and UKEi003-C/ERC018, in short ERC018) and the yield was calculated for each of these hiPSC lines as well (Figure 12, bottom).

The EB protocol provided a yield of around 0.2 million differentiated cells from 1 million ERC001 hiPSCs. The hybrid protocol provided a yield of around 2.2 million differentiated cells from 1 million ERC001 hiPSCs. The yield of the quiescent protocol was dependent on the hiPSC line. From 1 million ERC001 hiPSCs, 57.8 million cells could be differentiated with the quiescent protocol. Regardless of the hiPSC line, the yield of the quiescent protocol did not undercut 42 million differentiated cells from 1 million hiPSCs, with a recorded high of 623 million differentiated cells from 1 million hiPSCs.

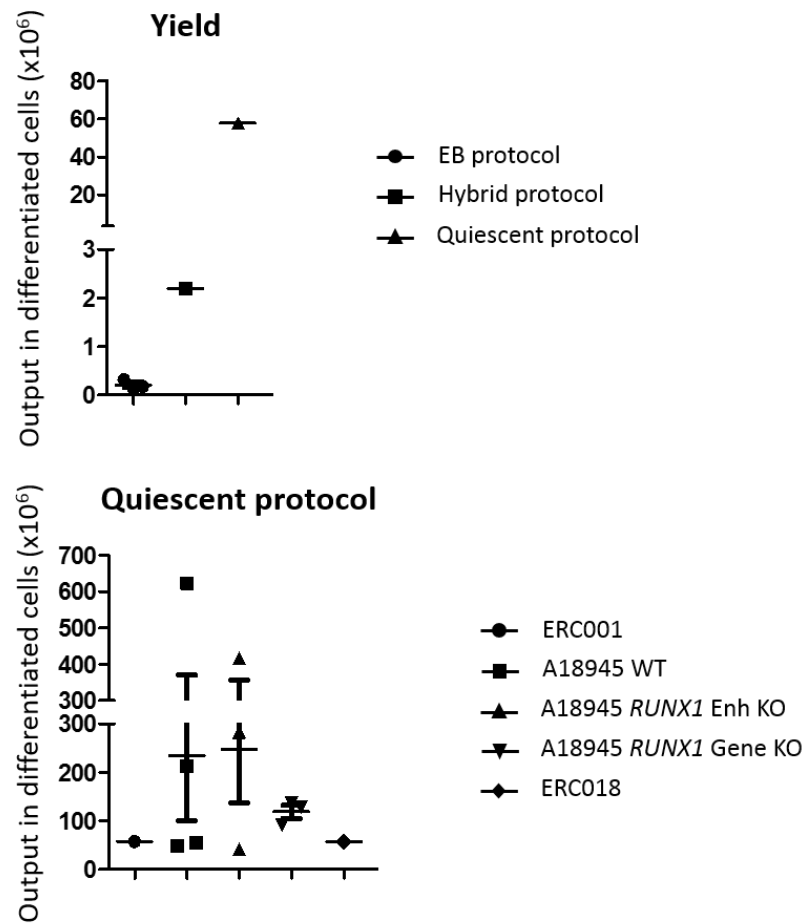


Figure 12: The yield of the differentiation protocols in millions of cells, where the yield was defined as the amount of cells which could be differentiated from 1 million hiPSCs. Top, the yield of the 3 protocols from ERC001 hiPSCs. Bottom, the yield of the quiescent fibroblast differentiation protocol for different hiPSC lines. When possible, data are presented as mean  $\pm$  SEM,  $n=1-4$  per condition.

As mRNA of the fibroblast activation markers collagen1a1, periostin and ACTA2 was more abundant in cells differentiated with the EB protocol compared to cells differentiated with either the hybrid protocol or the quiescent fibroblasts protocol (Figure 10) and owing to the low yield of the EB protocol (Figure 12), it was decided to forego the EB protocol for the differentiation of cardiac fibroblasts.

Messenger RNA of the cardiac fibroblast marker TCF21 (Figure 11) was similarly abundant in cells differentiated with either the quiescent protocol or the hybrid protocol. Messenger RNA of the fibroblast marker TBX18 was 1.8 times more abundant in the cells differentiated with the quiescent protocol compared to the hybrid protocol. Messenger RNA of TBX18 was still 5.2 times more abundant in the differentiated cells obtained with the hybrid protocol compared to hiPSCs. Conversely, mRNA of the fibroblast marker WT1 was 8 times more abundant in the cells differentiated with the hybrid protocol compared to the quiescent protocol. Messenger RNA of WT1 was still 6.9 times more abundant in the cells differentiated with the quiescent protocol compared to hiPSCs. Combined with the lower mRNA presence of collagen1a1 in the cells differentiated with the quiescent protocol compared to the hybrid protocol (Figure 10) and the substantially higher yield of differentiated cells with the quiescent protocol compared to the hybrid protocol (Figure 12) the decision was made to continue differentiating cardiac fibroblasts following the quiescent protocol.

Substantially more mRNA of the fibroblast markers WT1, TBX18 and TCF21 was present in the cells differentiated with either the quiescent protocol or the hybrid protocol compared to in hiPSCs (Figure 11). These results combined with the cell morphology (Table 14) strongly suggested that cells differentiated with the hybrid protocol or the quiescent protocol were indeed fibroblasts. Substantially more mRNA of the early cardiac development marker GATA4 was present in cells differentiated with the quiescent protocol compared to in hiPSCs, as will be discussed later (Figure 29). This strongly suggested the cardiac lineage of these cells. These cells will therefore be referred to cardiac fibroblasts for the remainder of this work.

### 3.1.2 Serum concentration

Undefined serum components can activate (cardiac) fibroblasts and stimulate collagen synthesis, interfering with a quiescent baseline. The standard culture medium for EHT contains 10% (horse) serum. To analyse the effect of serum on the activation of fibroblasts, 2D cultured primary foreskin fibroblasts were cultured with medium containing different percentages of serum. The mRNA abundance was analysed for fibroblasts cultured in medium containing 10% vs 0% serum (Figure 13), 10% vs 0.5% serum (Figure 14), or 0% vs 0.5% serum (Figure 15). In each experiment, the different serum groups were further divided into 3 subgroups, a control group, an inhibited group treated with 5.4  $\mu$ M of the TGF- $\beta$ 1 receptor inhibitor SB-431542 and an activated group treated with 48 ng/ml TGF- $\beta$ 1.

As expected, mRNA abundance of collagen1a1 and ACTA2 at basal level was several fold lower in the fibroblasts cultured in 0% serum containing medium compared to in the fibroblasts cultured in 10% serum containing medium, whereas the mRNA abundance in the TGF- $\beta$ 1 treated fibroblasts was similar under both serum conditions (Figure 13; for the mRNA abundance analysis of collagen3a1 and TNC, see supplement section 10.1.2). This led to a 7.7 higher ratio between TGF- $\beta$ 1 treated fibroblasts and SB-431542 treated fibroblasts for collagen1a1 and a 3.2 higher ratio for ACTA2 in fibroblasts cultured in 0% serum containing medium than in fibroblasts cultured in 10% serum containing medium. In other words, the dynamic range of regulation of mRNA abundance was considerably higher, when the fibroblasts were cultured in 0% serum containing medium than in 10% serum containing medium. Messenger RNA of the activation marker periostin was comparably expressed in fibroblasts cultured in either 10% or 0% serum containing medium. Unexpectedly, collagen3a1 and TNC mRNA was slightly more abundant in the fibroblasts cultured in 0% serum containing medium.



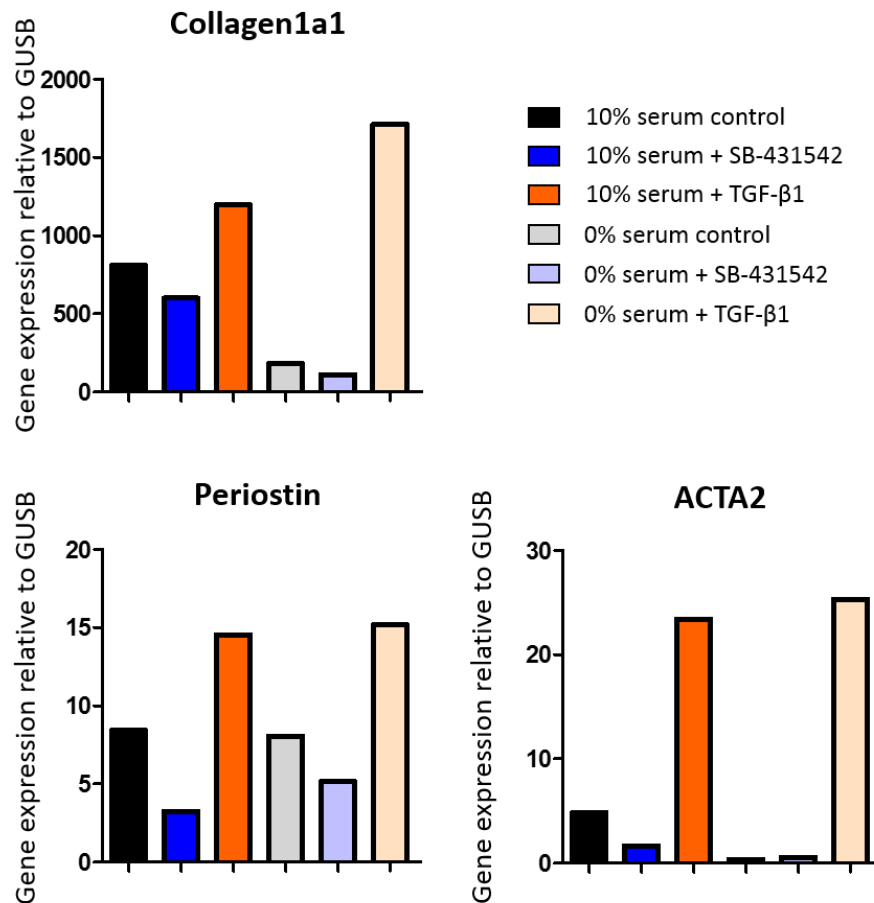


Figure 13: The mRNA abundance relative to GUSB of multiple fibroblast activation markers in 2D cultured primary foreskin fibroblasts: collagen1a1, periostin and ACTA2. All fibroblasts were cultured in 10% serum containing medium until day 6, after which half of the fibroblasts were cultured in medium containing 0% serum. Additionally, the fibroblasts were assigned different exposure conditions, and either kept as control, treated with 5.4  $\mu$ M SB-431542 or treated with 48 ng/ml TGF- $\beta$ 1 for 5 days. Data are presented as mean,  $n=2$  per group.

Long term cell culture without serum is challenging. As problems with cellular integrity of both cardiomyocytes and cardiac fibroblasts in later EHT culture was anticipated, the experiments were repeated with 0.5% serum rather than 0% serum. The mRNA abundance of collagen1a1, periostin and CCN2 was analysed in fibroblasts cultured in 10% serum containing medium compared to fibroblasts cultured in 0.5% serum containing medium (Figure 14; for the mRNA abundance analysis of collagen1a2, see supplement section 10.1.2). Messenger RNA of these activation markers was more abundant in the fibroblasts cultured in 10% serum containing medium for each respective subgroup (control fibroblasts compared to control fibroblasts, etc). The fold difference between the inhibited fibroblasts and activated fibroblasts was smaller in the fibroblasts cultured in 10% serum containing medium, than in the fibroblasts cultured in 0.5% serum containing medium. With regards to the collagen1a1 mRNA abundance the fold difference was 5.45 vs 20.05, for periostin mRNA abundance the fold difference was 7.43 vs 13.76 and for CCN2 mRNA abundance the fold difference was 14.04 vs 22.46.

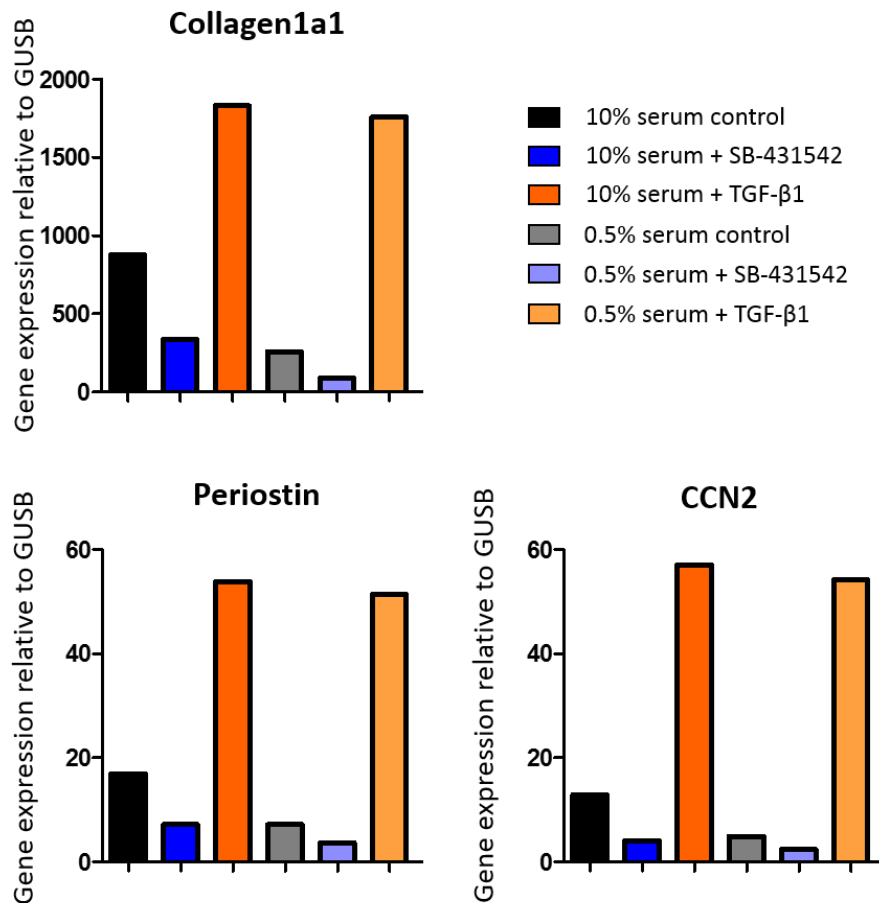


Figure 14: The mRNA abundance relative to GUSB of multiple fibroblast activation markers in 2D cultured primary foreskin fibroblasts: collagen1a1, periostin and CCN2. All fibroblasts were cultured in 10% serum containing medium until day 4, after which half of the fibroblasts were cultured in medium containing only 0.5% serum. Additionally, the fibroblasts were assigned different exposure conditions, and either kept as control, treated with 5.4  $\mu$ M SB-431542 or treated with 48 ng/ml TGF- $\beta$ 1 for 3 days,  $n=1$  per condition.

To directly compare the activations states of fibroblasts cultured with 0% or 0.5% serum, respectively, the mRNA abundance of collagen1a1, periostin and CCN2 was analysed in fibroblasts cultured under these conditions (Figure 15; for the mRNA abundance analysis of collagen1a2, see supplement section 10.1.2). As expected, per subgroup, the mRNA abundance of most of the fibrosis markers was similar, when comparing the fibroblasts cultured in 0% serum containing medium to the fibroblasts cultured in 0.5% serum containing medium. The lowest expression was found in the inhibited fibroblasts. Each subgroup of the 0.5% serum containing medium exposed fibroblasts unexpectedly expressed the same amount of periostin mRNA.

This experiment suggested 0.5% serum culture as a compromise suitable to maintain cardiomyocyte integrity and low fibroblast activation in parallel.

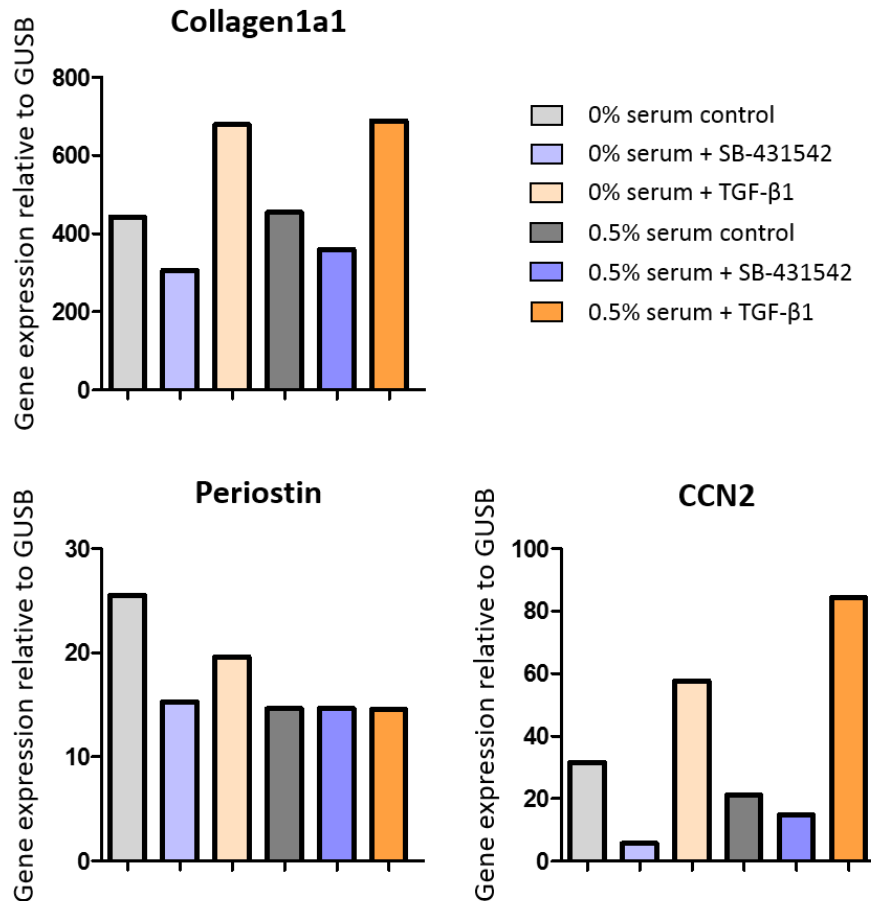


Figure 15: The mRNA abundance relative to GUSB of multiple fibroblast activation markers in 2D cultured primary foreskin fibroblasts: collagen1a1, periostin and CCN2. From day 0, half of the fibroblasts were cultured in medium containing 0% serum, the other half of the fibroblasts were cultured in medium containing 0.5% serum. Additionally, the fibroblasts were assigned to different conditions, and either kept as control, treated with 5.4  $\mu$ M SB-431542 or treated with 48 ng/ml TGF- $\beta$ 1 for 3 days,  $n=1$  per condition.

The collagen concentration in fibroblasts and in used cell culture medium was analysed for all subgroups of fibroblasts cultured in either 10% serum containing medium or 0.5% serum containing medium. Due to the detection threshold of the collagen assay, certain values were measured as below 0 ( $\mu$ g/ml). Though these values should be seen as 0, to illustrate differences between the conditions better, the values are displayed as measured (see supplement section 10.1.2).

A higher collagen concentration was detected in fibroblasts cultured in 10% serum containing medium than in fibroblast cultured in 0.5% serum containing medium, for each subgroup. The collagen concentration was significantly higher in the medium aspirated from fibroblasts cultured in 10% serum containing medium, when comparing medium from both control groups and both activated groups. The collagen concentration was also significantly higher in the medium from the activated group than in the medium from the inhibited group for fibroblasts cultured in 10% serum containing medium. The difference in collagen concentration was not significant when comparing medium from both inhibited groups or when comparing medium from the inhibited group and medium from the activated group in the medium aspirated from fibroblasts cultured in 0.5% serum containing medium. As expected, a higher collagen concentration was present in fresh 10% serum containing medium than in fresh 0.5% serum containing medium.

From these 2D culture-related results, it could be concluded that the fibroblasts cultured in both 0% and 0.5% serum containing medium presented less mRNA of different fibrosis markers than fibroblasts cultured in 10% serum containing medium, but there were no major differences in the mRNA abundance in fibroblasts cultured in 0% or 0.5% serum containing medium. To maintain viability of the cardiomyocytes in EHT and to obtain a more quiescent baseline, it was decided to use 0.5% serum in the culture media.

The next step was to investigate the effect of 0.5% serum containing medium in CF-EHTs, composed of 90% hiPSC-derived cardiomyocytes and 10% hiPSC-derived cardiac fibroblasts. CF-EHTs were either continuously cultured in 10% serum; the control group, or serum was depleted from the culture medium to 0.5% either on day 3 or day 14. Different parameters of the contractility of the CF-EHTs were analysed.

The force and frequency of the contractions of the CF-EHTs were analysed as functional parameters. The resting length of the CF-EHTs was analysed as a measure of remodelling. The relaxation velocity and 80% relaxation time of the CF-EHTs were analysed for a possible relaxation deficit, as this could render relaxation time and velocity important readouts for matrix stiffness of potential translational relevance. Significant differences (\* $p < 0.05$ , \*\* $p < 0.005$ , \*\*\* $p < 0.001$ ) between CF-EHTs are depicted in the analysis with asterisks. Black asterisks indicate that the CF-EHTs were significantly different from the control CF-EHTs. The development over time of the force and frequency are depicted here (Figure 16). For the development over time of the resting length, relaxation velocity and 80% relaxation time, see supplement section 10.1.2.

CF-EHTs in which the serum was depleted contracted with a lower force than control CF-EHTs, but with a higher frequency. The CF-EHTs in which the serum was depleted unexpectedly had a shorter resting length than the control CF-EHTs, but as expected, the CF-EHTs in which the serum was depleted had a tendency towards a shorter 80% relaxation time. The relaxation velocity of the CF-EHTs was comparable.

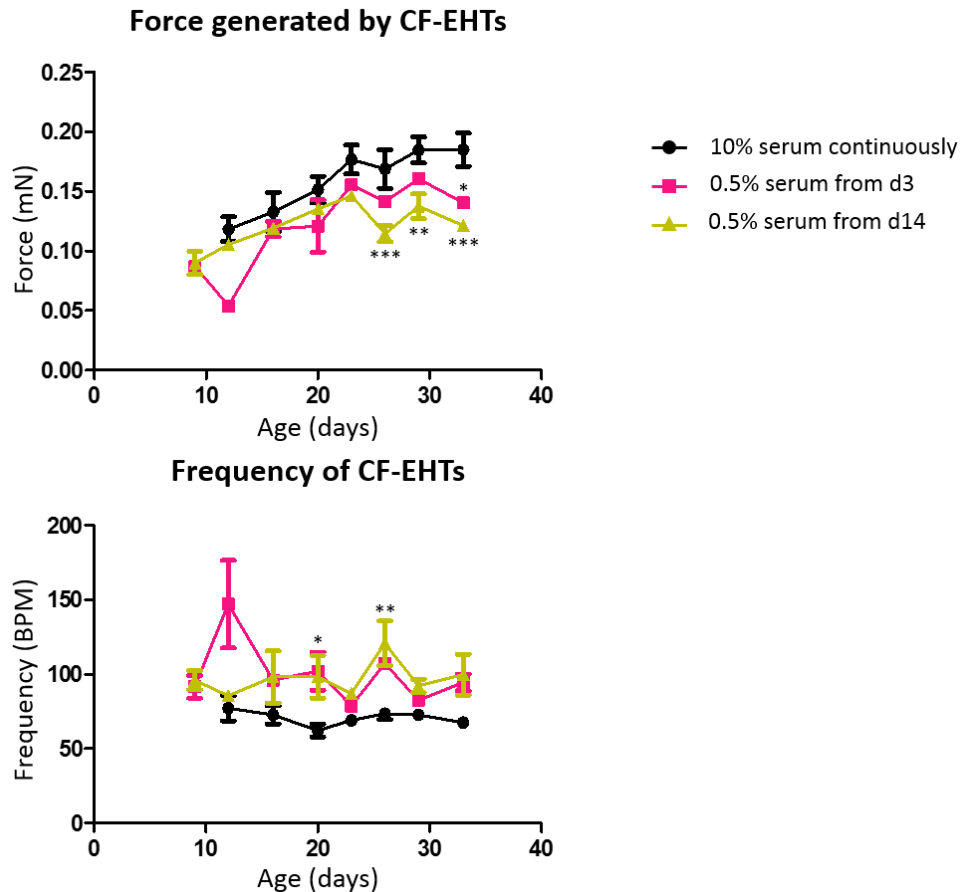


Figure 16: Contractility analyses of CF-EHTs. The development of the generated force and the beating frequency of the CF-EHTs are presented over time. The CF-EHTs were either continuously cultured in medium containing 10% serum or switched to medium containing 0.5% serum on either day 3 or day 14, CF-EHTs were harvested on day 33. Data are presented as mean  $\pm$  SEM, \* $p < 0.05$ , \*\* $p < 0.005$ , \*\*\* $p < 0.001$  by two-way ANOVA plus Bonferroni's post-test for multiple comparisons, only biologically meaningful comparisons are shown,  $n = 4$  per group.

In summary, these experiments argued that 2D cultured primary fibroblasts displayed a strong activation pattern when they were cultured in 10% serum containing medium, as suggested by the high prevalence of mRNA of multiple fibroblast activation markers and high collagen content (Figure 13, Figure 14 and supplement section 10.1.2).

Though the force generated by the CF-EHTs in which serum was depleted from the culture medium was lower than the force generated by CF-EHTs continuously cultured in 10% serum containing medium, the CF-EHTs in which serum was depleted were still viable and contracting at the end of the culture period. A longer 80% relaxation time, as measured in the CF-EHTs continuously cultured in 10% serum containing medium, was a possible sign of a more fibrotic tissue (supplement section 10.1.2). It was therefore decided to transition to 0.5% serum containing medium early on in the culture period of CF-EHTs, preferably on day 3.

### 3.1.3 CF percentage

The suitable percentage of cardiac fibroblasts which were to be incorporated into the EHTs had to be determined. To determine this, (CF-)EHTs were cast containing either 0%, 5%, 10%, 15% or 20% hiPSC-derived cardiac fibroblasts, based on previous experience. Aside from the previously mentioned

parameters of contractility, the width of the (CF-)EHTs was included in the contractility analysis as an added measure of remodelling (Figure 17, the beating frequency analysis can be found in supplement section 10.1.3). Significant differences between (CF-)EHTs are depicted in all following contractility analyses included in this work, as follows:

\* Black asterisk: the (CF-)EHTs are significantly different from the control (CF-)EHTs, or the control (CF-)EHTs significantly differ from all other conditions, depending on the location of the asterisks.

\* Coloured asterisk: the (CF-)EHTs are significantly different from the (CF-)EHTs depicted in the colour of the asterisks.

[ Black bracket: the (CF-)EHTs included in the bracket are significantly different with respect to the control (CF-)EHTs for multiple days in a row.

[ Coloured bracket: the (CF-)EHTs (in the colour of the bracket) significantly differ from other (CF-)EHTs (in the colour of the asterisk) for multiple days in a row.

The CF-EHTs containing 5% CFs stopped contracting after day 16 and could not be stimulated to contract under electrical pacing.

The force generated by all (CF-)EHTs decreased after 16 days, likely attributable to the long-term culture in 0.5% serum containing medium. The force generated by the CF-EHTs containing 5% or 10% serum was comparable to the EHTs containing no CFs, whereas the force generated by the CF-EHTs containing more than 10% CFs was lower than the EHTs containing no CFs. These findings suggested that in CF-EHTs containing more than 10% CFs, the contractility of the cardiomyocytes in the tissues was disturbed.

The width of the CF-EHTs composed of 5%, 10% or 20% cardiac fibroblasts decreased significantly more than the width of the EHTs, throughout the entire culture period, suggesting an influence of cardiac fibroblasts on the structural remodelling of the CF-EHTs.

There was a trend towards a longer resting length of EHTs containing no CFs compared to the CF-EHTs, but this difference was only significant on day 14.

There was a clear difference in relaxation velocity of CF-EHTs from the different conditions. Compared to the EHTs containing no CFs, the relaxation velocity was significantly lower in the CF-EHTs containing CFs. The 80% relaxation time was longer in the CF-EHTs with the highest percentages of cardiac fibroblasts present, suggesting a CF percentage dependent relaxation deficiency.

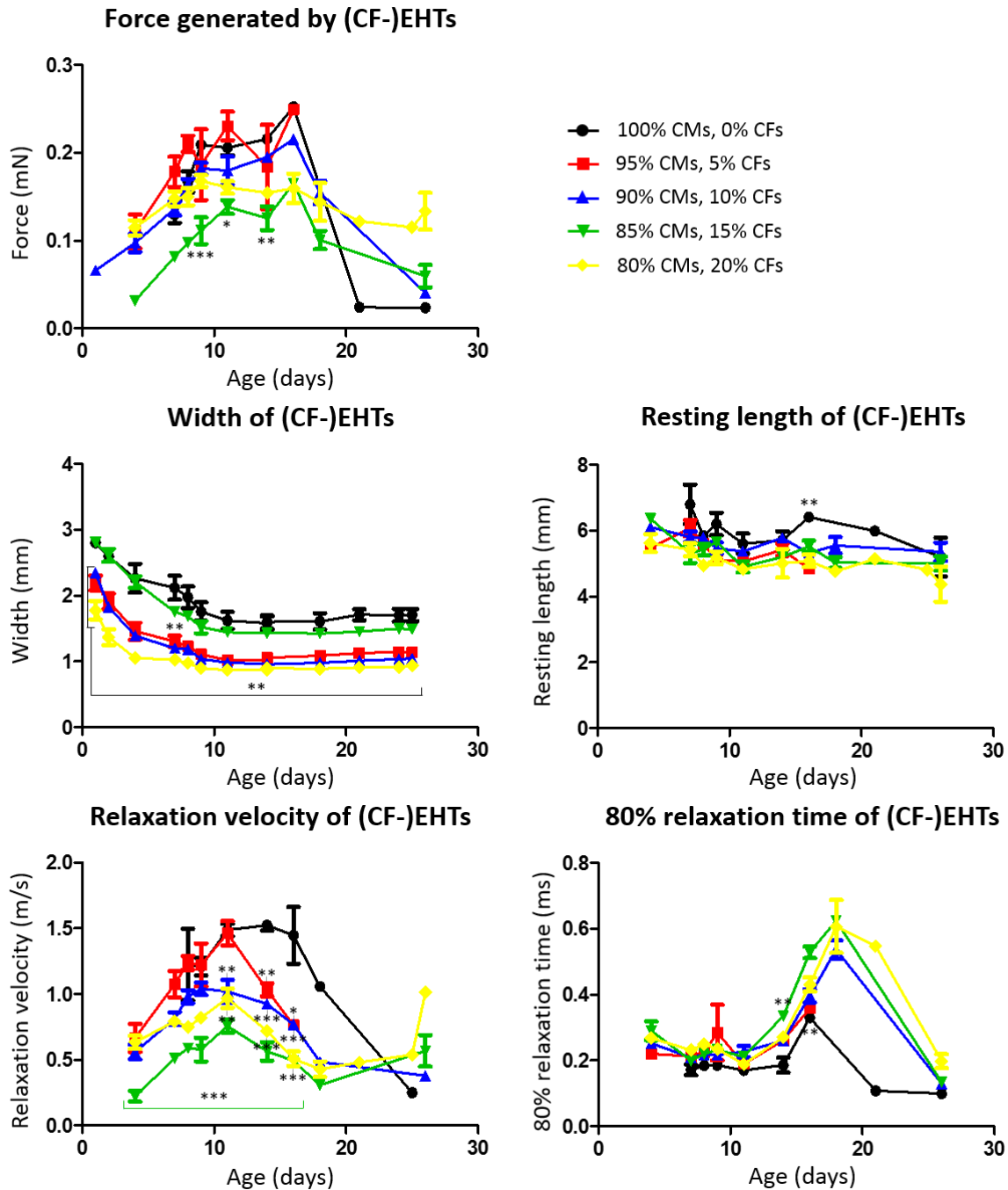
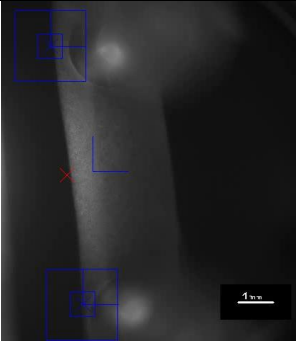
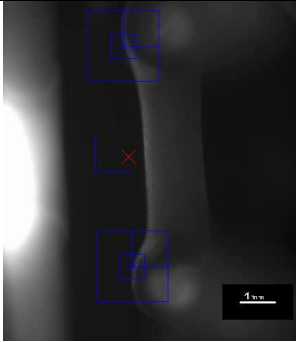
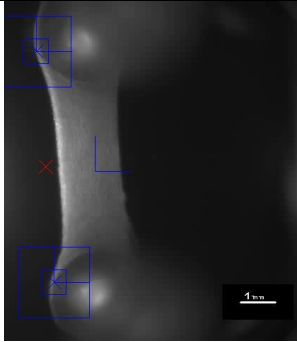
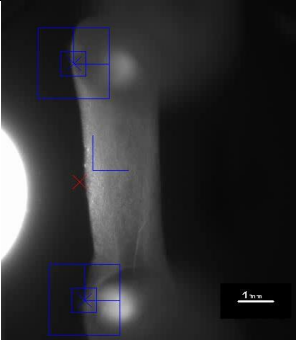
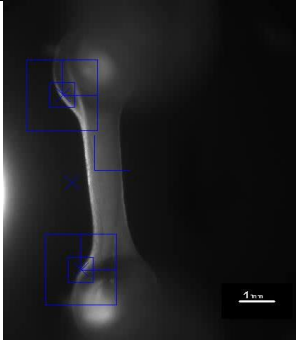
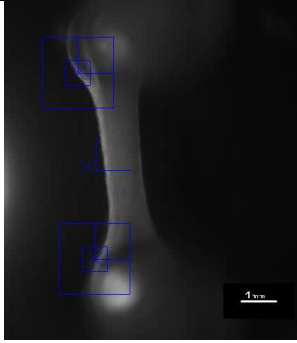
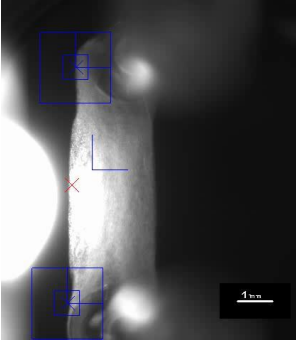
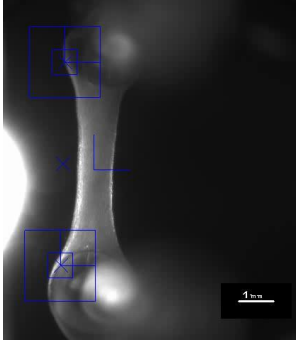
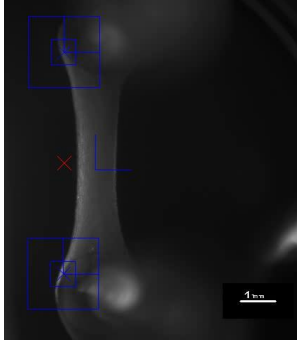
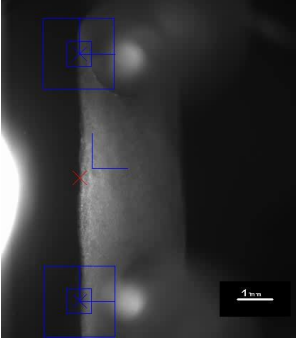
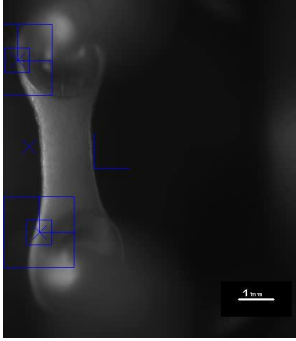
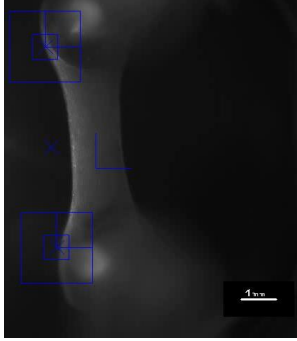


Figure 17: Contractility analyses of (CF-)EHTs containing 0%, 5%, 10%, 15% or 20% hiPSC-derived cardiac fibroblasts. The development of the generated force, width, resting length, relaxation velocity and 80% relaxation time of the (CF-)EHTs are presented over time. The (CF-)EHTs were cultured in 10% serum containing medium until day 4, after which they were cultured in 0.5% serum containing medium. On the last day of culture, day 25, the contractility of the CF-EHTs was analysed under pacing, the results of which are presented as the fictional analysis on day 26 here. Data are presented as mean  $\pm$  SEM, \* $p < 0.05$ , \*\* $p < 0.005$ , \*\*\* $p < 0.001$  by two-way ANOVA, only biologically meaningful comparisons are shown,  $n = 4$  per group.

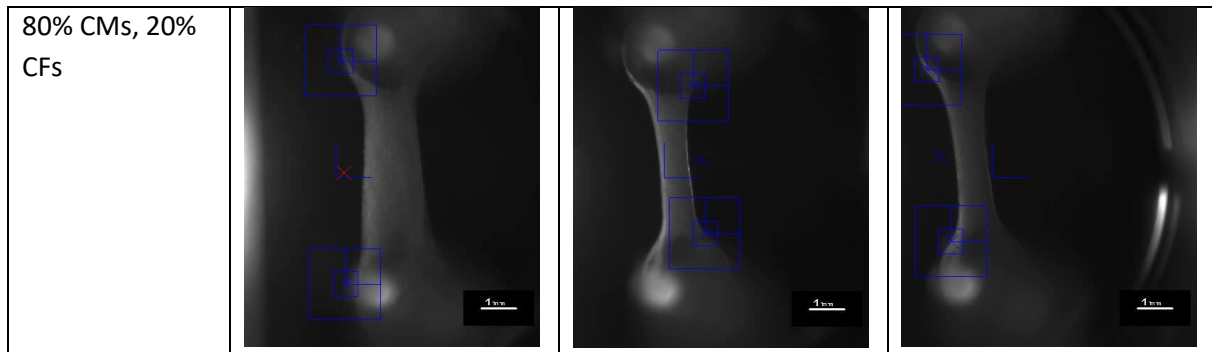
To further analyse the remodelling of the (CF-)EHTs over time, images were taken during the contractility measurements of the (CF-)EHTs (Table 15). The respective percentages of cardiomyocytes and cardiac fibroblasts are stated in the 1<sup>st</sup> column. In the 2<sup>nd</sup> column, images taken on day 1 (casting day was counted as day 0) are depicted, to show the starting shape of the (CF-)EHTs. In the 3<sup>rd</sup> column images taken on day 14 are depicted. Day 14 was the last day of contraction for the majority of the (CF-)EHTs. In the 4<sup>th</sup> column images taken on day 26, the last day of culture, are depicted.

Table 15 illustrates that the higher the percentage of cardiac fibroblasts present in the (CF-)EHTs, the thinner the (CF-)EHTs get over time. In other words, the higher the percentage of cardiac fibroblasts present in the (CF-)EHTs, the more the (CF-)EHTs remodel over time.

Table 15: Microscope images which show the shape of the (CF-)EHTs over time. Images were taken 1 day after casting, 14 days after casting and 26 days after casting (day of harvesting). Representative from n=4. Scale bar is 1 mm.

	Day 1	Day 14	Day 26
100% CMs, 0% CFs			
95% CMs, 5% CFs			
90% CMs, 10% CFs			
85% CMs, 15% CFs			





To assess how and to which extent the addition of cardiac fibroblasts to (CF-)EHT translates to one of the most important routine readouts after EHT culture, mRNA abundance of marker genes, qPCR analysis of the fibroblast activation markers collagen1a1, periostin, transgelin, CCN2, ACTA2 and collagen1a2, relative to GUSB was carried out from respective different tissues (see supplement section 10.1.3). The mRNA abundance analysis confirmed a positive correlation between fibroblast percentage and fibroblast activation markers.

The (CF-)EHTs contained 100% or 90% hiPSC-derived cardiomyocytes, with a purity of 93%, as assessed by content of troponin positive cells in flow cytometry. This means that 7% of the cells after differentiation were not cardiomyocytes, but rather an undefined other cell type. It could have been possible that (a part of) these cells were fibroblasts-like cells, which could have contributed to the presence of mRNA of the analysed fibrosis markers. However, from the abundance of especially collagen1a1 and periostin, it was concluded that the addition of fibroblasts to the CF-EHTs was necessary for fibrosis to occur in the (CF-)EHTs, as the baseline mRNA expression of these markers was very low, and mRNA of these markers was substantially more expressed the more cardiac fibroblasts were present in the (CF-)EHTs.

A high ACTA2 expression baseline was observed, which is common in developing cardiomyocytes (Kwong et al., 2019; Woodcock-Mitchell et al., 1988).

These mRNA abundance analyses furthermore suggested that the cardiac fibroblasts survived in the CF-EHTs during the culture time.

For the *in vitro* fibrosis model to physiologically represent ventricular tissue, it was desired to use a ratio of cardiomyocytes:cardiac fibroblasts as close to the physiological ratio as possible. The human ventricle consists of roughly 30% cardiomyocytes and 20% cardiac fibroblasts (Bergmann et al., 2015). If we were to calculate these percentages as if cardiomyocytes and cardiac fibroblasts were the only cell types present in the human ventricle, this would constitute:

$$\frac{30}{30+20} = 60\% \text{ cardiomyocytes}$$

$$\frac{20}{30+20} = 40\% \text{ cardiac fibroblasts}$$

However, the analysis of the different percentages of cardiac fibroblasts in the (CF-)EHTs had provided evidence that the (CF-)EHTs with a low percentage of cardiac fibroblasts present in the tissue generated a higher force than the CF-EHTs with a high percentage of cardiac fibroblasts (Figure 17). Furthermore, CF-EHTs with less cardiac fibroblasts did not become as thin as the CF-EHTs with more cardiac fibroblasts (Figure 17 and Table 15). Exaggerated CF-EHT thinning is known to increase the chance of

CF-EHT rupture before the end of the culture period. Lastly, the more cardiac fibroblasts were present in the (CF-)EHTs, the higher the mRNA abundance of fibrosis markers was at baseline (supplement section 10.1.3), which was undesirable up to an extent.

Combining these results with the desire to represent close to physiological conditions, a ratio of 9:1 cardiomyocytes:cardiac fibroblasts was used for the *in vitro* fibrosis model.

#### 3.1.4 2D fibroblast activation

After basal conditions of the model had successfully been established, the next step was to evaluate suitable activation conditions. This was first investigated in hiPSC-derived cardiac fibroblasts in standard 2D culture. A control condition was compared to a cardiac fibroblast inhibition condition, where the cardiac fibroblasts were exposed to the TGF- $\beta$ 1 receptor inhibitor SB-431542, and to multiple activation conditions, to determine the most effective way to activate the cardiac fibroblasts. The activation conditions were treatment with TGF- $\beta$ 1; the platelet derived growth factor that is composed of 2 A subunits (PDGF-AA), which is a mitogen for cardiac fibroblasts; a combination of TGF- $\beta$ 1 and PDGF-AA; angiotensin II, which is known to have pro-fibrotic effects in human cardiac fibroblasts (Bertaud et al., 2023; Kim et al., 2013); or a combination of phenylephrine and endothelin 1 which upregulated CTGF in rat cardiomyocytes and may therefore indirectly promote fibrosis (Kemp et al., 2004). The mRNA abundance relative to GUSB of the fibroblast activation markers collagen1a1, ACTA2 and CCN2 was analysed for all conditions (Figure 18; for the mRNA abundance analyses of collagen1a2, periostin and transgelin see supplement section 10.1.4).

For all 3 fibroblast activation markers a significantly lower mRNA abundance was present in the inhibited CFs compared to the control CFs. A significantly higher expression of all 3 fibroblast activation markers was evident in the cardiac fibroblasts treated with either TGF- $\beta$ 1 or TGF- $\beta$ 1 + PDGF-AA, when comparing these CFs to either the control CFs or the inhibited CFs. No significant differences in the mRNA abundance of any of the fibroblast activation markers were present when comparing any of the other activated CFs to the control CFs. There were no significant differences between the TGF- $\beta$ 1 treated CFs and the TGF- $\beta$ 1 + PDGF-AA treated CFs.

The mRNA abundance analysis of collagen1a2 and transgelin displayed the same pattern, though the differences between the differently treated CFs were less pronounced. An unexpected, but not significantly higher abundance of periostin mRNA was present in the SB-431542 treated CFs (supplement section 10.1.4).

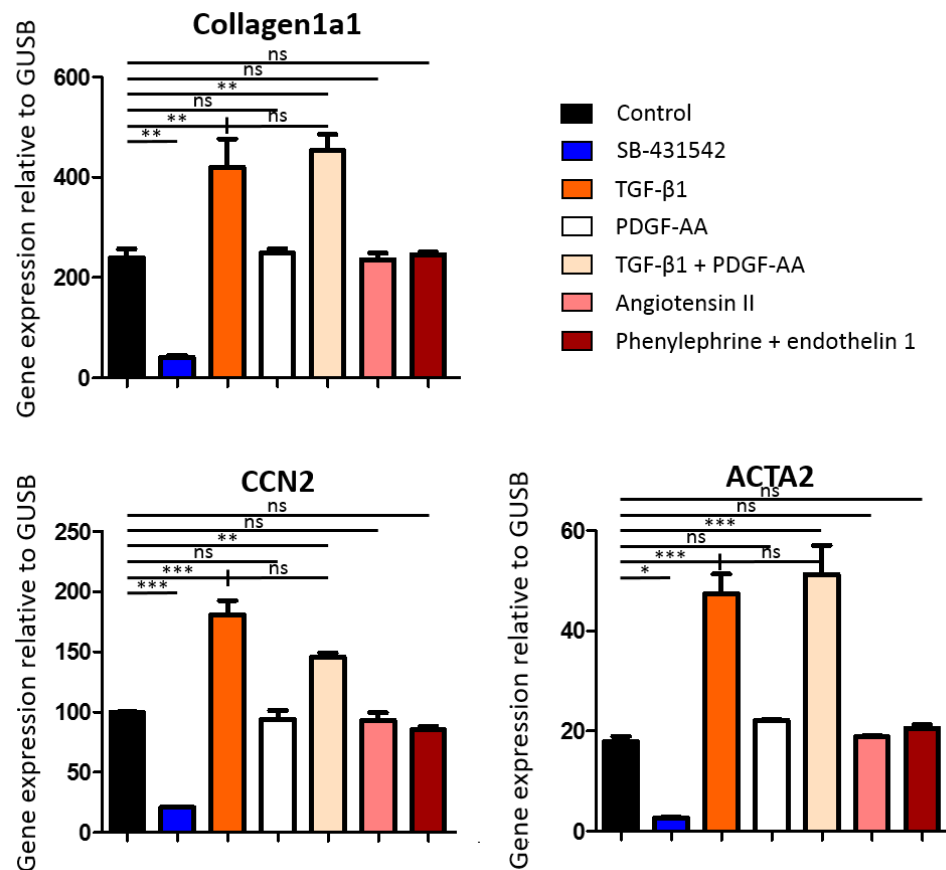


Figure 18: The mRNA abundance relative to GUSB of multiple fibroblast activation markers in 2D cultured hiPSC-derived cardiac fibroblasts: collagen1a1, CCN2 and ACTA2. The 2D cultured cardiac fibroblasts were either assigned to a control group, an inhibited group treated with SB-431542 or an activation group, treated with either TGF-β1, PDGF-AA, TGF-β1 + PDGF-AA, angiotensin II or phenylephrine + endothelin 1. The fibroblasts were cultured in 0.5% serum containing medium from day 0, assigned to their respective conditions on day 4 and kept on these conditions until they were harvested on day 11. Data are presented as mean ± SEM. ns: not significant, \* $p < 0.05$ , \*\* $p < 0.005$ , \*\*\* $p < 0.001$  by one-way ANOVA plus Bonferroni's post-test for multiple comparisons, only meaningful comparisons are shown,  $n = 3$  per group.

In the 2D culture of cardiac fibroblasts, the highest activation state (defined as the highest mRNA abundance of cardiac fibroblast markers) was present in the CFs exposed to either TGF-β1 or TGF-β1 + PDGF-AA. Treatment with SB-431542 led to significantly lower mRNA abundance of these markers in CFs compared to both the control CFs and the activated CFs.

### 3.1.5 3D fibroblast activation

Both the activation and inhibition of cardiac fibroblasts were successful in 2D culture. The next step was to investigate the effect of the activation and inhibition of hiPSC-derived cardiac fibroblasts in 3D culture. Though in 2D culture no differences were observed with regard to the mRNA abundance of fibrosis markers between TGF-β1 treated cardiac fibroblasts and TGF-β1 + PDGF-AA treated cardiac fibroblasts, the effect both of these conditions on the contractility of CF-EHTs was investigated. An inhibited group and control group were included in this experiment (Figure 19, for the analysis of the beating frequency and the resting length, see supplement section 10.1.5).

The control CF-EHTs and the SB-431542 treated CF-EHTs generated a higher force than CF-EHTs from either activated group.

As expected, the relaxation velocity of the SB-431542 treated CF-EHTs was significantly higher than the relaxation velocity of the control CF-EHT, whereas the relaxation velocity of the activated CF-EHTs tended to be lower than the control CF-EHTs. This was considered an indirect sign of increased fibrosis formation in the activated CF-EHTs.

Conversely, at the end of the culture time, the SB-431542 treated CF-EHTs had a significantly shorter 80% relaxation time than the control CF-EHTs. Unexpectedly however, the activated CF-EHTs also had a significantly shorter 80% relaxation time than the control CF-EHTs.

The 80% relaxation time was the only contractile parameter showing a clear difference between the TGF- $\beta$ 1 treated CF-EHTs and the TGF- $\beta$ 1 + PDGF-AA treated CF-EHTs, for the first 18 days of culture. During this time, the TGF- $\beta$ 1 + PDGF-AA treated CF-EHTs presented a significantly higher 80% relaxation time than the TGF- $\beta$ 1 treated CF-EHTs. The contractility analysis of CF-EHTs from these 2 groups was similar with regard to all other parameters.

The control CF-EHTs and the SB-431542 treated CF-EHTs contracted with a higher frequency than CF-EHTs from either activated group, but the resting length of all CF-EHTs was comparable (supplement section 10.1.5).

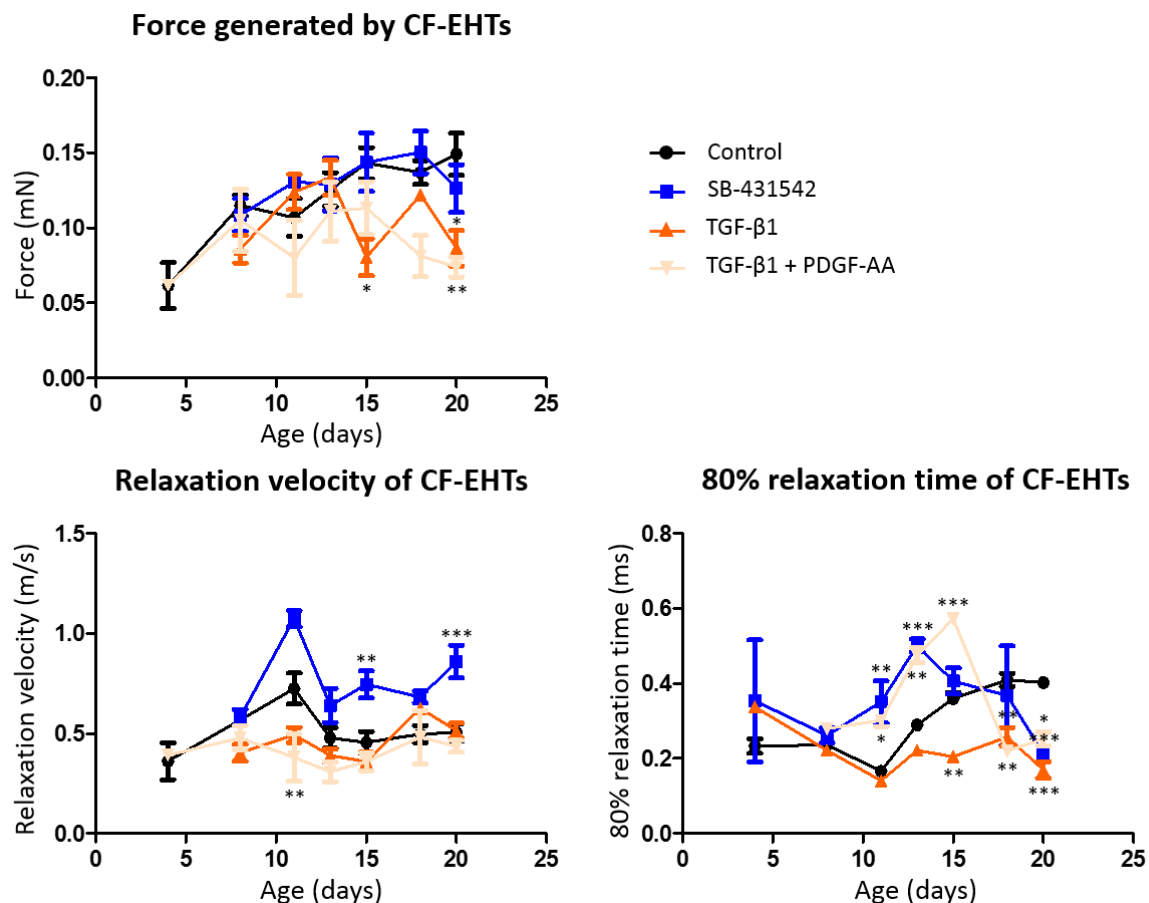


Figure 19: Contractility analyses of CF-EHTs assigned to either a control group, an inhibited group, treated with 1  $\mu$ M SB-431542 for 7 days and 5  $\mu$ M for the remainder of the culture period, or to 1 of 2 activated groups, treated with either 15 ng/ml TGF- $\beta$ 1 or 15 ng/ml TGF- $\beta$ 1 + 10 ng/ml PDGF-AA. The development of the generated force, relaxation velocity and 80% relaxation time of the CF-EHTs are presented over time. The CF-EHTs were cultured in 10% serum containing medium until day 4, after which the CF-EHTs were cultured in 0.5% serum containing medium, assigned to their respective groups on day 8 and kept on these conditions until the last day of culture, day 21. Data are presented as mean  $\pm$  SEM, \* $p$ <0.05, \*\* $p$ <0.005, \*\*\* $p$ <0.001 by two-way ANOVA, only biologically meaningful comparisons are shown,  $n$ =4-5 per group.

To further quantify a possible pro-fibrotic effect of the different interventions, the mRNA abundance of the fibrosis markers collagen1a1, periostin, transgelin, CCN2, ACTA2 and collagen1a2 was assessed (see supplement section 10.1.5).

Unexpectedly, contrarily to the similar experiment with 2D cultured cardiac fibroblasts, in this 3D experiment, none of the fibrosis markers was more abundant in the activated CF-EHTs, compared to the inhibited CF-EHTs. On the contrary, a higher mRNA abundance was recorded in the inhibited CF-EHTs compared to the control CF-EHTs. We reasoned that this could have been a consequence of a too early initiation of the treatment. The timing of the treatment therefore had to be further optimized, which is discussed in a later part of this work. The differences in mRNA abundance between the TGF- $\beta$ 1 treated CF-EHTs and the TGF- $\beta$ 1 + PDGF-AA treated CF-EHTs were not significant.

Regardless of the treatment the CF-EHTs received, they contracted regularly and generated force until the end of culture, implying that the cardiomyocytes were not detrimentally affected by any of the treatments. The differences between the CF-EHTs treated with either TGF- $\beta$ 1 or TGF- $\beta$ 1 + PDGF-AA were negligible, thus the 'TGF- $\beta$ 1 + PDGF-AA' condition was perceived as redundant. Based on these results it was decided to continue the following experiments with the CF-EHTs divided into 3 groups, a control group, an inhibited group treated with SB-431542 and an activated group, treated with TGF- $\beta$ 1. Based on the previously verified effects of serum on the activation of cardiac fibroblasts, it was decided to also include an activated condition for the *in vitro* fibrosis model which would be exposed to 10% serum containing medium, called 'high serum'. In light of the mRNA abundance results (supplement section 10.1.5), the protocol needed further refinement, which was conducted later.

### 3.1.6 SB-431542 treatment

To assess if high baseline fibroblast activation was responsible for the lack of differences between control and activation conditions in previous CF-EHT experiments, an inhibition group treated with the TGF- $\beta$ 1 receptor inhibitor SB-431542 was evaluated. Thus, a suitable concentration of SB-431542 had to be determined. CF-EHTs were treated with either no SB-431542 (control), 1  $\mu$ M, 5  $\mu$ M, or 10  $\mu$ M SB-431542, based on previous experience and published research, starting at d0 of culture, which was the day of CF-EHT casting (Inman, Nicolás, & Hill, 2002). Contractility was regularly analysed (Figure 20, for the analysis of the beating frequency, resting length and relaxation velocity, see supplement section 10.1.6).

A similar force was generated by the control CF-EHTs and the 1  $\mu$ M SB-431542 treated CF-EHTs, but the CF-EHTs treated with higher concentrations of SB-431542 generated a lower force, indicating a detrimental effect of SB-431542 on the cardiomyocytes.

The width of the CF-EHTs decreased significantly less in the CF-EHTs treated with 10  $\mu$ M SB-431542 than in the control CF-EHTs. The width of the CF-EHTs treated with a lower concentration of SB-431542 decreased slower than the control CF-EHTs, though at the end of culture, the width of the CF-EHTs was similar.

A tendency towards a longer 80% relaxation time was observed in the control CF-EHTs compared to the SB-431542 treated CF-EHTs.

Considerable variability was observed in the beating frequency of the SB-431542 treated CF-EHTs. The resting length of the SB-431542 treated CF-EHTs was comparable to the control CF-EHTs, regardless of

the concentration of SB-431542. The CF-EHTs treated with 1  $\mu\text{M}$  SB-431542 had a significantly higher relaxation velocity than the control CF-EHTs and the CF-EHTs treated with higher concentration of SB-431542 (supplement section 10.1.6).

These results indirectly suggested a SB-431542 dependent inhibition on fibrosis formation in the CF-EHTs and on the remodelling of the CF-EHTs.

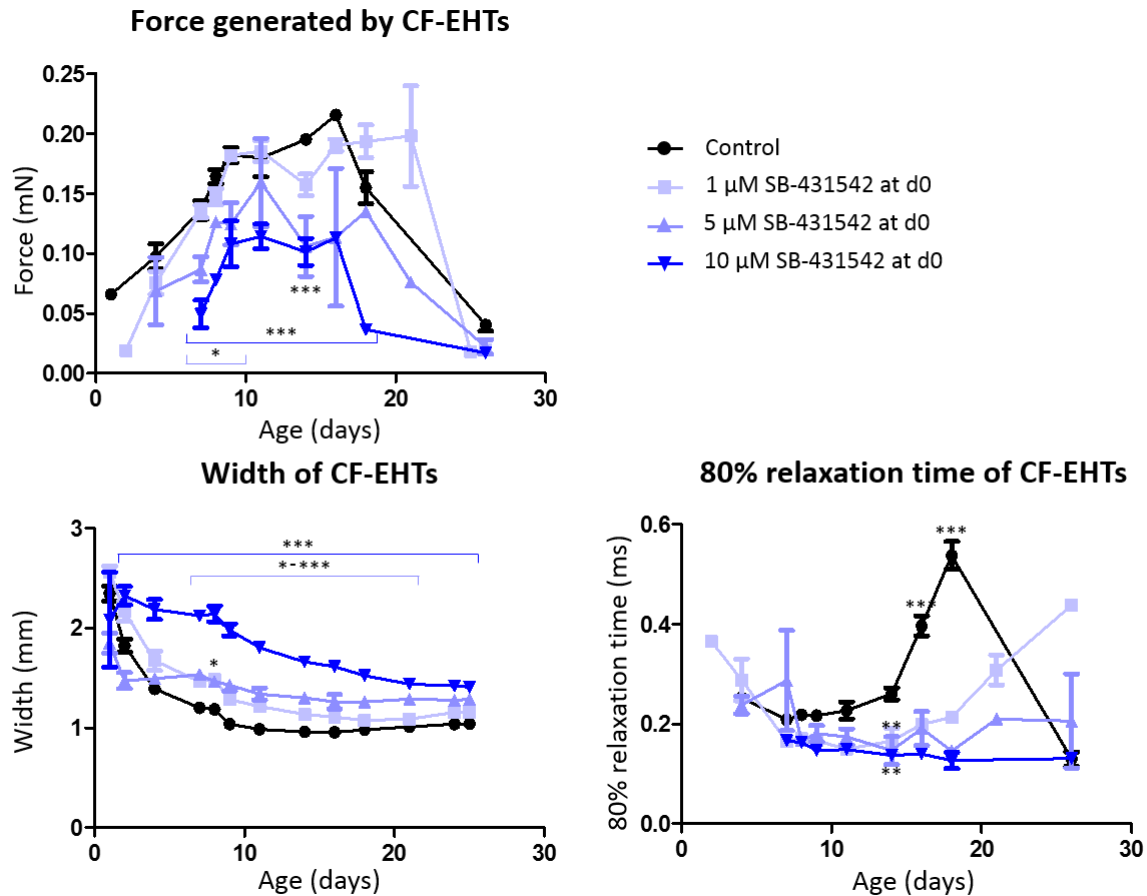


Figure 20: Contractility analyses of CF-EHTs treated with either no SB-431542 (control), 1  $\mu\text{M}$ , 5  $\mu\text{M}$ , or 10  $\mu\text{M}$  SB-431542 from day 0. The CF-EHTs were cultured in 10% serum containing medium until day 4, after which the CF-EHTs were cultured in 0.5% serum containing medium. The development of the generated force, width and 80% relaxation time of the CF-EHTs are presented over time. On the last day of culture, day 25, the contractility of the CF-EHTs was analysed under pacing, the results of which are presented as the fictional analysis on day 26 here. Data are presented as mean  $\pm$  SEM, \* $p < 0.05$ , \*\* $p < 0.005$ , \*\*\* $p < 0.001$  by two-way ANOVA, only biologically meaningful comparisons are shown,  $n = 4-11$  per group.

From this contractility analysis, it was concluded that treatment with 1  $\mu\text{M}$  SB-431542 did not have a major impact on the contractility of the CF-EHTs, whereas treatment with 10  $\mu\text{M}$  SB-431542 did, especially on the force and the width of the CF-EHTs.

To analyse the expected anti-fibrotic effect of the different concentrations of SB-431542, the mRNA abundance relative to GUSB of the fibrosis markers collagen1a1, periostin, transgelin, CCN2, ACTA2 and collagen1a2 was analysed (see supplement section 10.1.6).

Unexpectedly, the mRNA abundance of most fibrosis markers was higher in the CF-EHTs treated with SB-431542, regardless of the concentration, compared to the control CF-EHTs. Only the mRNA abundance of periostin was clearly lower in the CF-EHTs treated with SB-431542 compared to the

control CF-EHTs. These unexpected results were attributed to the timing of the treatment start, day 0, which was further investigated, as is discussed later in this work.

To determine whether the effect of SB-431542 on the contractility of the CF-EHTs could be attributed to inhibiting effects of the SB-431542 on the cardiac fibroblasts or to an influence of SB-431542 on the cardiomyocytes, EHTs (containing no cardiac fibroblasts) underwent the same treatment. They were therefore treated with either no SB-431542 (control), 1  $\mu$ M, 5  $\mu$ M or 10  $\mu$ M SB-431542. Their contractility was regularly analysed (see supplement section 10.1.6).

The EHTs treated with 5  $\mu$ M SB-431542 stopped contracting after day 14. The EHTs treated with either 1  $\mu$ M or 10  $\mu$ M SB-431542 stopped contracting after day 18. From day 16, only 1 control EHT spontaneously contracted. In light of this, the protocol needed to be further optimized, which was conducted later. The control EHTs tended to generate a higher force than any of the SB-431542 treated EHTs. Furthermore, the control EHTs tended to retain a longer resting length and longer 80% relaxation time. The width of the EHTs, when looking at the overall development over time, decreased significantly less in the EHTs treated with SB-431542 than in the control EHTs. This data pointed towards an inhibiting effect of SB-431542 on the cardiomyocytes within the EHTs.

When comparing the width of the control CF-EHTs to the width of the control EHTs, the change in width of the control CF-EHTs over time was larger than the change in width of the control EHTs over time. On day 1, the control CF-EHTs had an average width of 2.35 mm and they remodelled to an average width of 1.04 mm on day 26; a 56% change (Figure 20). On day 1, the control EHTs had an average width of 2.80 mm and they remodelled to an average width of 1.71 mm on day 26; a 39% change (supplement section 10.1.6). This data pointed to an effect the presence of cardiac fibroblasts has on CF-EHT, especially with regards to the remodelling of the tissue.

Both the CF-EHTs and the EHTs treated with 10  $\mu$ M SB-431542 contracted with a lower force and a lower frequency than the CF-EHTs and EHTs treated with a lower concentration of SB-431542. The CF-EHTs and EHTs treated with 10  $\mu$ M SB-431542 also revealed the least amount of remodelling. The treatment with 1  $\mu$ M SB-431542 had negligible effect on the contractility of the CF-EHTs and the EHTs. As an optimum between inhibition of remodelling on the one hand and (unwanted) inhibition of contractility, it was decided that in the optimized fibrosis model, the inhibited group would be treated with 5  $\mu$ M SB-431542. SB-431542 treated (CF-)EHTs generated less force than (CF-)EHTs not treated with SB-431542. To mitigate this negative effect of the SB-431542 treatment, the timing of the SB-431542 treatment was further optimized, as will be discussed later.

### 3.1.7 TGF- $\beta$ 1 treatment

On the other end of the activation spectrum, the TGF- $\beta$ 1 treated activated group had to be further optimized. To determine the optimal concentration, CF-EHTs were treated with either no TGF- $\beta$ 1 (control), 20 ng/ml or 48 ng/ml TGF- $\beta$ 1 (Figure 21, for the contractility analysis of the resting length, relaxation velocity and 80% relaxation time, see supplement section 10.1.7).

The treatment with TGF- $\beta$ 1 had no effect on the force of the CF-EHTs, but TGF- $\beta$ 1 treated CF-EHTs displayed a trend of contracting with a lower frequency than the control CF-EHTs. An unexpected tendency towards a larger width was displayed in the TGF- $\beta$ 1 treated CF-EHTs compared to the control CF-EHTs.



The resting length of the CF-EHTs was relatively similar in all conditions and approximately constant over time, though at the end of the culture time, the 20 ng/ml TGF- $\beta$ 1 treated CF-EHTs displayed a significantly shorter resting length than the control CF-EHTs. A similar relaxation velocity and 80% relaxation time of the CF-EHTs was observed, regardless of the treatment with TGF- $\beta$ 1 (supplement section 10.1.7).

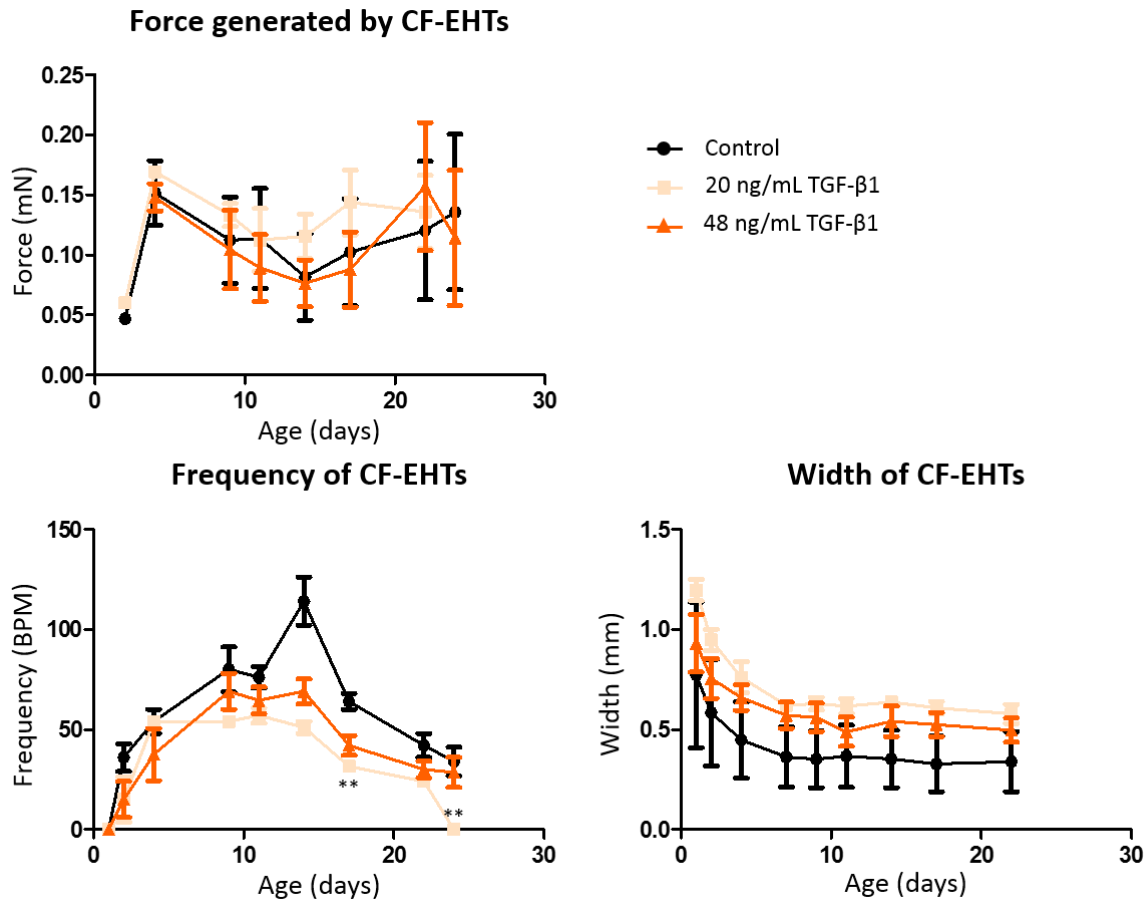


Figure 21: Contractility analyses of CF-EHTs treated with either no TGF- $\beta$ 1 (control), 20 ng/ml or 48 ng/ml TGF- $\beta$ 1 from day 0. The CF-EHTs were cultured in 10% serum containing medium until day 4, after which they were cultured in 0.5% serum containing medium. The development of the generated force, beating frequency and width of the CF-EHTs are presented over time. The CF-EHTs were harvested on day 24. Data are presented as mean  $\pm$  SEM, \* $p$ <0.05, \*\* $p$ <0.005 by two-way ANOVA, only biologically meaningful comparisons are shown,  $n$ =4 per group.

To analyse the pro-fibrotic effect of the different concentrations of TGF- $\beta$ 1 on the CF-EHTs, the mRNA abundance relative to GUSB of the fibrosis markers collagen1a1, periostin, transgelin, CCN2, ACTA2 and collagen1a2 was measured (see supplement section 10.1.7).

Again unexpectedly, the mRNA abundance of all measured fibrosis markers was lower in the TGF- $\beta$ 1 treated CF-EHTs, regardless of the concentration, compared to the control CF-EHTs. Similar to the unexpected mRNA abundance of the SB-431542 treated CF-EHTs, these results were attributed to the timing of the treatment start, day 0, which was further investigated.

Though no major effects on the contractility of the CF-EHTs could be attributed to treatment with TGF- $\beta$ 1, the effect of TGF- $\beta$ 1 treatment on the cardiomyocytes in the CF-EHTs was additionally investigated. Therefore, EHTs (containing no cardiac fibroblasts) underwent the same treatment. EHTs were treated with either no TGF- $\beta$ 1 (control), 20 ng/ml or 48 ng/ml TGF- $\beta$ 1 and contractility was regularly analysed



(supplement section 10.1.7). After day 4, 2 of the 4 EHTs treated with 20 ng/ml TGF- $\beta$ 1 ruptured. The TGF- $\beta$ 1 treated EHTs contracted with a lower beating frequency and tended towards exhibiting a longer 80% relaxation time than the control EHTs, but no further differences were detected.

No major effects of TGF- $\beta$ 1 treatment were present in the contractility of either the CF-EHTs (Figure 21) or the EHTs (supplement section 10.1.7). The largest visible effect was that both the CF-EHTs and the EHTs treated with TGF- $\beta$ 1 contracted with a lower frequency than the untreated (CF-)EHTs. It was therefore decided to use a lower concentration of TGF- $\beta$ 1 (10 ng/ml) in the final fibrosis model. Lower concentrations are more commonly used for the activation of cardiac fibroblasts (Cho et al., 2018).

### 3.1.8 Timing of treatment

As previously mentioned, a possible explanation for the unexpected mRNA abundance results from the CF-EHT activation experiment (supplement section 10.1.5), the SB-431542 concentration experiments (supplement section 10.1.6) and the TGF- $\beta$ 1 concentration experiments (supplement section 10.1.7) and for the premature contraction stop of the SB-431542 treated EHTs, could have been a too early initiation of the respective treatment. The cells might not have recovered from the thawing procedure and adapted to their new culture environment prior to the start of the treatment, or they might have compensated the consequences of the treatment by the end of the culture. It was therefore relevant to evaluate the ideal timing for the treatment.

It was analysed whether starting with a lower concentration of the respective treatment and increasing the concentration later would be beneficial for the development of the contractility of the CF-EHTs or whether the treatment should only be initiated at a later time point (supplement section 10.1.8 and Figure 22).

To start, CF-EHTs were treated with 1  $\mu$ M SB-431542 from the day of casting for 1 week, after which the concentration was increased to 5  $\mu$ M SB-431542. The contractility of these CF-EHTs was compared to the contractility of control CF-EHTs which did not receive any treatment, and of activated CF-EHTs which were treated with 10 ng/ml TGF $\beta$ 1 continuously from the day of casting. The contractility analysis of this experiment can be found in supplement section 10.1.8. The control CF-EHTs and the TGF- $\beta$ 1 treated CF-EHTs stopped contracting after day 22. In this experiment the SB-431542 treated CF-EHTs generated significantly more force than the control CF-EHTs. Furthermore, the SB-431542 treated CF-EHTs displayed a significantly higher relaxation velocity and a shorter 80% relaxation time than the control CF-EHTs, which indirectly pointed towards inhibition of fibrosis development in the SB-431542 treated CF-EHTs. The TGF- $\beta$ 1 treated CF-EHTs generated a force similar to the control CF-EHTs and displayed a similar relaxation velocity. Unexpectedly, the 80% relaxation time at the end of the experiment was shorter in the TGF- $\beta$ 1 treated CF-EHTs than in the control CF-EHTs.

From the contractility analysis, it appeared that SB-431542 treated CF-EHTs generated a higher force than control CF-EHTs when the concentration of SB-431542 was increased at a later time point (supplement section 10.1.8), which was not observed when the CF-EHTs were treated with a higher concentration of SB-431542 from the start (Figure 20).

It was furthermore analysed whether starting the treatment of the CF-EHTs at a later time point would be beneficial. Thus, both CF-EHTs and EHTs were treated with different concentrations of SB-431542: no SB-431542 (control), 1  $\mu$ M, 5  $\mu$ M, or 10  $\mu$ M SB-431542, with the treatment starting on day 8

(supplement section 10.1.8), instead of the previous initiation on day 0 (Figure 20). Both the CF-EHTs and the EHTs treated with SB-431542 generated less force than control (CF-)EHTs and the width of the SB-431542 treated (CF-)EHTs was smaller than the width of the control (CF-)EHTs. The other examined parameters displayed some variability. There was a tendency towards a longer 80% relaxation time of the control (CF-)EHTs than the SB-431542 treated (CF-)EHTs. While the larger width and shorter 80% relaxation time were in line with an inhibiting effect of the SB-431542 on the (CF-)EHTs, the negative effect of the treatment on the generated force called for more optimization.

With regards to contractility analysis, there did not appear to be major differences between starting the treatment with SB-431542 on day 0 or on day 8. Once the treatment was started, the addition of SB-431542 seemed to have a negative effect on the force generated by the CF-EHTs. However, when the treatment was initiated later, CF-EHTs were able to reach a higher force baseline compared to when treatment was initiated on day 0. Additionally, the CF-EHTs which were treated with SB-431542 from day 8 contracted with a frequency more similar to the control CF-EHTs than the CF-EHTs which were treated with SB-431542 from day 0.

To characterize the expected anti-fibrotic effect of the different concentrations of SB-431542 when the treatment was started on day 8, the mRNA abundance relative to GUSB of the fibrosis markers collagen1a1, periostin, transgelin, CCN2, ACTA2 and collagen1a2 was measured (supplement section 10.1.8). Contrary to the mRNA abundance of the CF-EHTs treated with SB-431542 from day 0 (supplement section 10.1.6), only the mRNA abundance of the fibroblast activation marker ACTA2 was higher in the control CF-EHTs than in any of the CF-EHTs treated with SB-431542 from day 8. The mRNA abundance of the other fibrosis markers was lower in at least 2 of the SB-431542 treated CF-EHT groups than in the control group, as expected. Therefore, the mRNA abundance analysis of the CF-EHTs which were treated with SB-431542 from day 8 matched expectations better than the mRNA analysis from the CF-EHTs treated with SB-431542 from day 0.

From the contractility analysis it was clear that the timing of the treatment was not yet optimized, as the addition of SB-431542 on day 8 led to a decrease in the generated force. To further optimize the ideal timing to start treatment of the CF-EHTs, CF-EHTs were treated with SB-431542 or TGF- $\beta$ 1 from either day 3 or day 15 and the contractility of these CF-EHTs was regularly analysed (Figure 22, for the analysis of the beating frequency, see supplement section 10.1.8). In this experiment it was directly investigated whether starting with a low concentration of SB-431542 and increasing this concentration later would have a more beneficial effect on the development of the contractility of the CF-EHTs than starting the SB-431542 treatment later. Therefore, the CF-EHTs treated with SB-431542 from day 3 were first treated with 1  $\mu$ M SB-431542 and this concentration was increased to 5  $\mu$ M SB-431542 on day 10. The CF-EHTs treated with SB-431542 from day 15 were immediately treated with 5  $\mu$ M SB-431542. The TGF- $\beta$ 1 CF-EHTs were treated with 10 ng/ml starting either on day 3 or day 15.

All inhibited CF-EHTs contracted with a higher force than the control CF-EHTs, whereas the activated CF-EHTs contracted with a similar force as the control CF-EHTs. Compared to the CF-EHTs treated with SB-431542 from day 3, the CF-EHTs treated with TGF- $\beta$ 1 from day 3 exhibited a shorter resting length. The SB-431542 treated CF-EHTs exhibited a significantly higher relaxation velocity than the control CF-EHTs and the TGF- $\beta$ 1 treated CF-EHTs. Compared to the control CF-EHTs, the CF-EHTs which were treated with SB-431542 from day 3 exhibited a significantly shorter 80% relaxation time on the last day of culture. On this same day, the CF-EHTs which were treated with TGF- $\beta$ 1 from day 15 exhibited a significantly longer 80% relaxation time than the CF-EHTs which were treated with TGF- $\beta$ 1 from day 3.

and the CF-EHTs which were treated with SB-431542 from day 15. All CF-EHTs contracted with a similar frequency (supplement section 10.1.8).

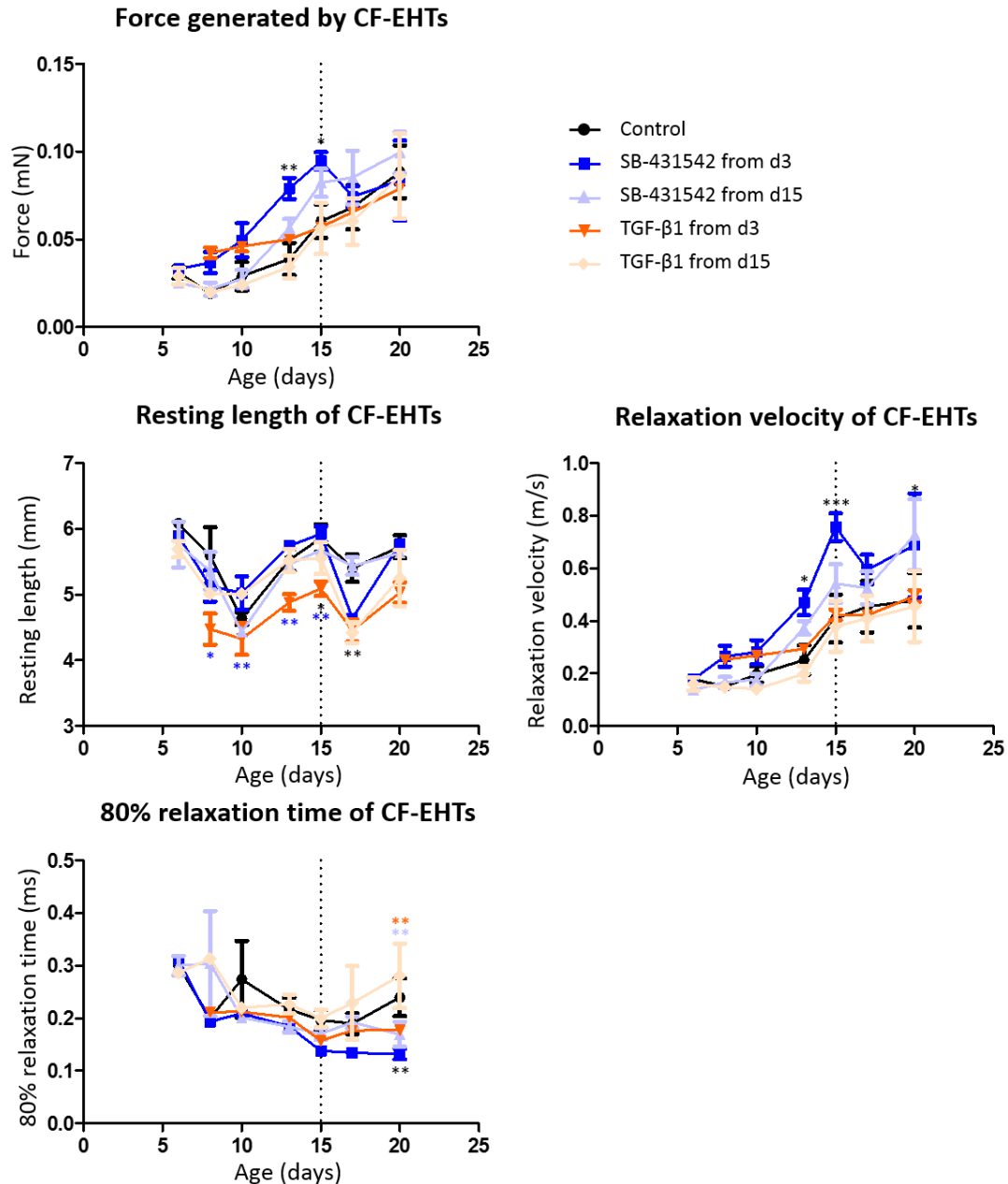


Figure 22: Contractility analyses of CF-EHTs assigned to either a control group, 1 of 2 inhibited groups, or 1 of 2 activated groups. The CF-EHTs were harvested on day 21. The CF-EHTs from 1 inhibited group were treated with 1  $\mu$ M SB-431542 from day 3 and 5  $\mu$ M SB-431542 from day 10 until they were harvested. The CF-EHTs from the other inhibited group were treated with 5  $\mu$ M SB-431542 from day 15 until they were harvested. The CF-EHTs from 1 activated group were treated with 10 ng/ml TGF- $\beta$ 1 from day 3 until they were harvested. The CF-EHTs from the other activated group were treated with 10 ng/ml TGF- $\beta$ 1 from day 15 until they were harvested. The CF-EHTs were cultured in 10% serum containing medium until day 3, after which they were cultured in 0.5% serum containing medium. The development of the generated force, resting length, relaxation velocity and 80% relaxation time of the CF-EHTs are presented over time. On the second to last day of culture, day 20, the contractility of the CF-EHTs was analysed under pacing. Data are presented as mean  $\pm$  SEM, \* $p$ <0.05, \*\* $p$ <0.005, \*\*\* $p$ <0.001 by two-way ANOVA plus Bonferroni's post-test for multiple comparisons, only biologically meaningful comparisons are shown,  $n$ =4-6 per group.

A longer resting length, higher relaxation velocity and shorter relaxation time, as visible in the contractility analysis of the SB-431542 treated CF-EHTs, could be attributed to anti-fibrotic effects of

SB-431542. No negative impact on the force generated by the CF-EHTs was detected as a result of any of the conditions.

To analyse the pro- or anti-fibrotic effects of the different treatments and the different time points, the mRNA abundance relative to GUSB of the fibrosis markers collagen1a1, periostin and transgelin was assessed (Figure 23; for the mRNA abundance analyses of collagen1a2, ACTA2 and CCN2, see supplement section 10.1.8). Messenger RNA of collagen1a1 and periostin was most abundant in activated CF-EHTs and least abundant in inhibited CF-EHTs. When the treatment was initiated on day 15, the difference between the activated condition and the inhibited condition was the most pronounced, though not significant. The transgelin mRNA abundance was unexpectedly highest in the CF-EHTs treated with SB-431542 from day 3 on. These CF-EHTs presented a significantly higher abundance compared to the CF-EHTs treated with SB-431542 from day 15. Transgelin mRNA was more abundant in the CF-EHTs treated with TGF- $\beta$ 1 from day 15 on than in the CF-EHTs treated with TGF- $\beta$ 1 from day 3 on.

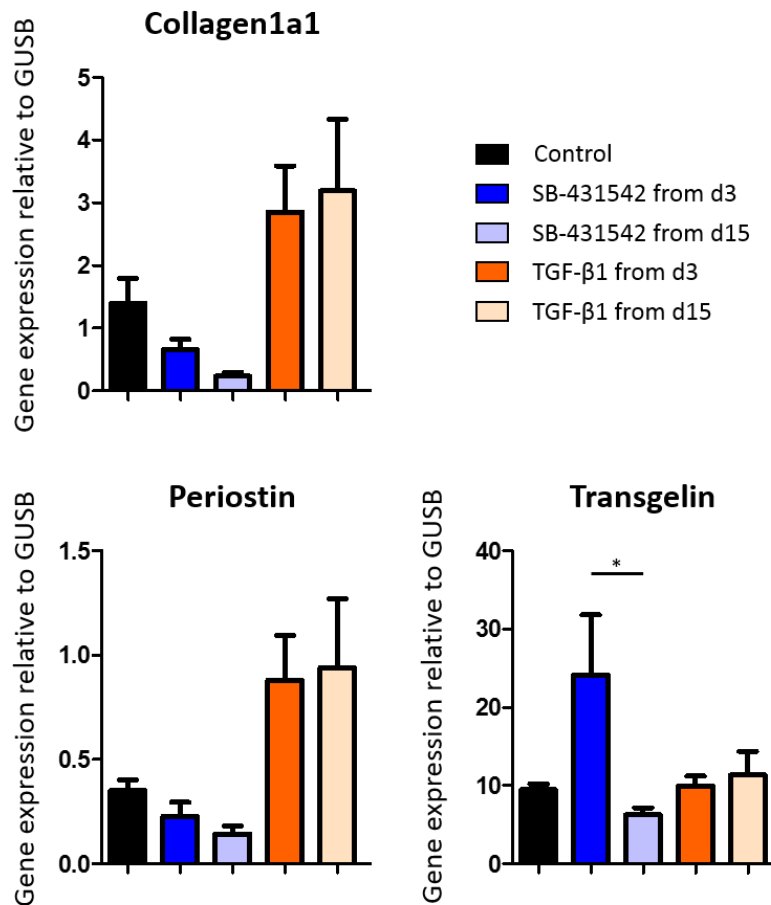


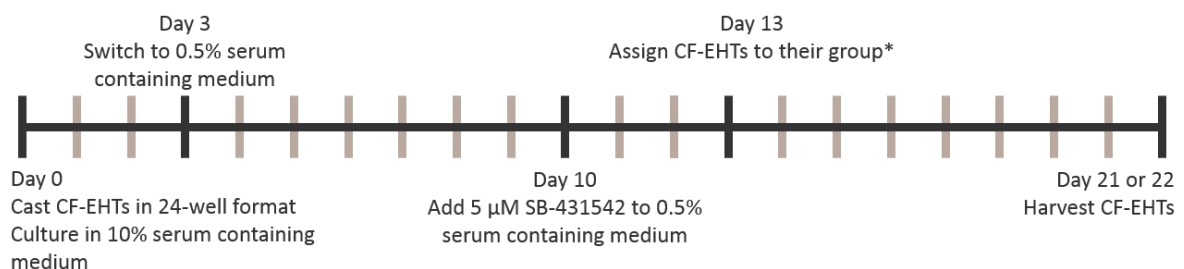
Figure 23: The mRNA abundance relative to GUSB of multiple fibroblast activation markers in CF-EHTs: collagen1a1, periostin and transgelin. The CF-EHTs were assigned to either a control group, 1 of 2 inhibited groups, or 1 of 2 activated groups. The CF-EHTs were harvested on day 21. The CF-EHTs from 1 inhibited group were treated with 1  $\mu$ M SB-431542 from day 3 and 5  $\mu$ M SB-431542 from day 10 until they were harvested. The CF-EHTs from the other inhibited group were treated with 5  $\mu$ M SB-431542 from day 15 until they were harvested. The CF-EHTs from 1 activated group were treated with 10 ng/ml TGF- $\beta$ 1 from day 3 until they were harvested. The CF-EHTs from the other activated group were treated with 10 ng/ml TGF- $\beta$ 1 from day 15 until they were harvested. The CF-EHTs were cultured in 10% serum containing medium until day 3, after which the CF-EHTs were cultured in 0.5% serum containing medium. Data are presented as mean  $\pm$  SEM. \* $p$ <0.05 by one-way ANOVA plus Bonferroni's post-test for multiple comparisons,  $n$ =3-4 per group.

From these experiments it was concluded that the force and beating frequency of the CF-EHTs was less affected when the treatment was initiated at a later time point, whereas the effect of the treatment on the mRNA abundance of the CF-EHTs and on relaxation parameters was more pronounced and closer to what was expected. It was therefore decided to start the treatment of the CF-EHTs at a later time point; day 13.

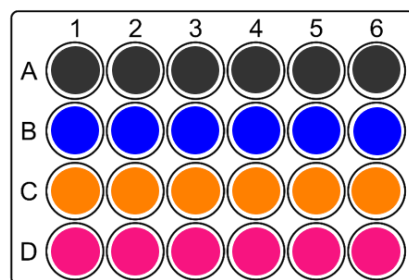
### 3.1.9 The *in vitro* fibrosis model

After the different aspects of the desired *in vitro* fibrosis model that had required optimization were evaluated, a definitive protocol for the model could be established (Figure 24).

The optimized *in vitro* fibrosis model was based on 3 weeks of CF-EHT culture. The CF-EHTs were composed of hiPSC-CMs and hiPSC-derived (quiescent) cardiac fibroblasts, which were cast together in a 9:1 ratio. To acquire a quiescent baseline, the CF-EHTs were transitioned from 10% serum containing medium to 0.5% serum containing medium early in culture, on day 3. Additionally, 5  $\mu$ M SB-431542 was added to the 0.5% serum containing medium on day 10. From day 13 the CF-EHTs were assigned to a group, and they were cultured according to their respective group until they were harvested on day 21 or 22. The different groups the CF-EHTs could be assigned to, were a control group where the CF-EHTs were cultured in 0.5% serum containing medium, an inhibited group where the CF-EHTs were cultured in 0.5% serum containing medium + 5  $\mu$ M SB-431542, or 1 of 2 activated groups, 1 in which the CF-EHTs were cultured in 0.5% serum containing medium + 10 ng/ml TGF- $\beta$ 1, and 1 in which the CF-EHTs were cultured in 10% serum containing medium.



\* Groups:



- Control, 0.5% serum containing medium
- Inhibited, 0.5% serum containing medium + 5  $\mu$ M SB-431542
- Activated, 0.5% serum containing medium + 10 ng/mL TGF- $\beta$ 1
- Activated, 10% serum containing medium

Figure 24: Protocol for the *in vitro* fibrosis model. Top, the timeline, based on 3 weeks of CF-EHT culture. The CF-EHTs were cultured in 10% serum containing medium for 3 days, after which they were cultured in 0.5% serum containing medium for 7 days. On day 10, 5  $\mu$ M SB-431542 was added to the 0.5% serum containing medium for 3 days for all CF-EHTs to achieve quiescent baseline conditions. After this (at day 13), the CF-EHTs were assigned to different groups. The CF-EHTs were cultured according to their respective group for 8 or 9 days, after which they were harvested. Bottom, the different groups the CF-EHTs could be assigned to; a control group cultured in 0.5% serum containing medium, an inhibited group treated with 5  $\mu$ M SB-431542, and 2 activated groups: 1 treated with 10 ng/ml TGF- $\beta$ 1, the other exposed to 10% serum containing medium.

To investigate the suitability of this *in vitro* fibrosis model, CF-EHTs composed of cardiomyocytes and cardiac fibroblasts differentiated from 3 different healthy donor hiPSC lines underwent this protocol. These hiPSC lines were the A18945 hiPSC line and the established control hiPSC lines ERC001 and ERC018. In this section, the combined results of the 3 cell lines will be discussed. For detailed results of CF-EHTs undergoing the *in vitro* EHT based fibrosis protocol for each separate cell line, including the development over time of different contractility parameters, see supplement section 10.1.9.

The resting length (RL), relaxation velocity (RV) and 80% relaxation time (RT) of the spontaneous contractions of the CF-EHTs on the last day of culture were analysed relative to the batch average (Figure 25), as possible important signs of fibrosis. The resting length was considered an indicator of remodelling; the relaxation velocity and 80% relaxation time were considered as possible indicators of a relaxation deficit. A relaxation deficit in CF-EHTs could argue for an increase in the matrix stiffness as a response to the respective treatment.

The inhibited CF-EHTs exhibited a significantly longer resting length compared to all other CF-EHTs. The control CF-EHTs had a significantly longer resting length than the high serum activated CF-EHTs. Both the control CF-EHTs and the inhibited CF-EHTs exhibited a significantly higher relaxation velocity than the high serum activated CF-EHTs. The high serum activated CF-EHTs displayed a significantly longer 80% relaxation time than all other CF-EHTs.

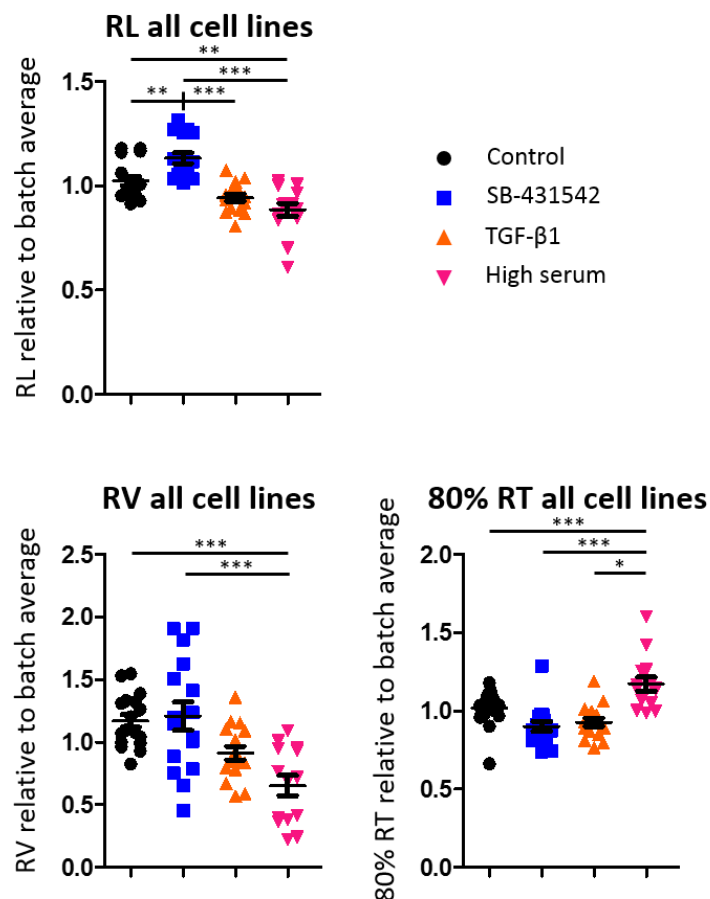


Figure 25: Combined contractility analyses of A18945, ERC001 and ERC018 CF-EHTs. The CF-EHTs were assigned to either a control group, an inhibited group, or 1 of 2 activated groups, and treated as previously described. The resting length, relaxation velocity and 80% relaxation time of the spontaneous contractions of the CF-EHTs on the last day of culture, day 21 or day 22, relative to the batch average are presented. Data are presented as mean  $\pm$  SEM. \* $p < 0.05$ , \*\* $p < 0.005$ , \*\*\* $p < 0.001$  by one-way ANOVA plus Bonferroni's post-test for multiple comparisons,  $n = 14-17$  per group.

When examining the combined contractility analyses from the A18945, ERC001 and ERC018 CF-EHTs, the findings affirm the suitability of the fibrosis model. The inhibited CF-EHTs displayed a longer resting length, higher relaxation velocity and shorter relaxation time compared to the control CF-EHTs and the activated CF-EHTs, especially compared to the high serum activated CF-EHTs. The control CF-EHTs displayed a longer resting length, higher relaxation velocity and shorter relaxation time compared to the activated CF-EHTs, especially to the high serum activated CF-EHTs. These findings indirectly affirm that the inhibited CF-EHTs show the least signs of fibrosis, followed by the control CF-EHTs. The activated CF-EHTs, especially the high serum activated CF-EHTs, show the most signs of fibrosis.

To further quantify a possible pro-fibrotic effect of the different interventions, the mRNA abundance of the fibrosis markers collagen1a1, periostin and transgelin in both the A18945 and ERC001 CF-EHTs relative to the respective control CF-EHTs, was combined for analysis (Figure 26; for the combined mRNA abundance analysis of collagen1a2, CCN2 and ACTA2, see supplement section 10.1.9.4).

A higher mRNA abundance of all analysed fibrosis markers in the activated CF-EHTs compared to the inhibited CF-EHTs was observed. For collagen1a1, periostin and transgelin, these differences were significant. Messenger RNA of these genes was significantly more abundant in high serum activated CF-EHTs compared to control CF-EHTs. Periostin mRNA was also significantly more abundant in TGF- $\beta$ 1 activated CF-EHTs compared to control CF-EHTs. Transgelin mRNA was significantly more abundant in high serum activated CF-EHTs than in TGF- $\beta$ 1 activated CF-EHTs. In the mRNA abundance analysis of collagen1a2, CCN2 and ACTA2, the same trends were observed.

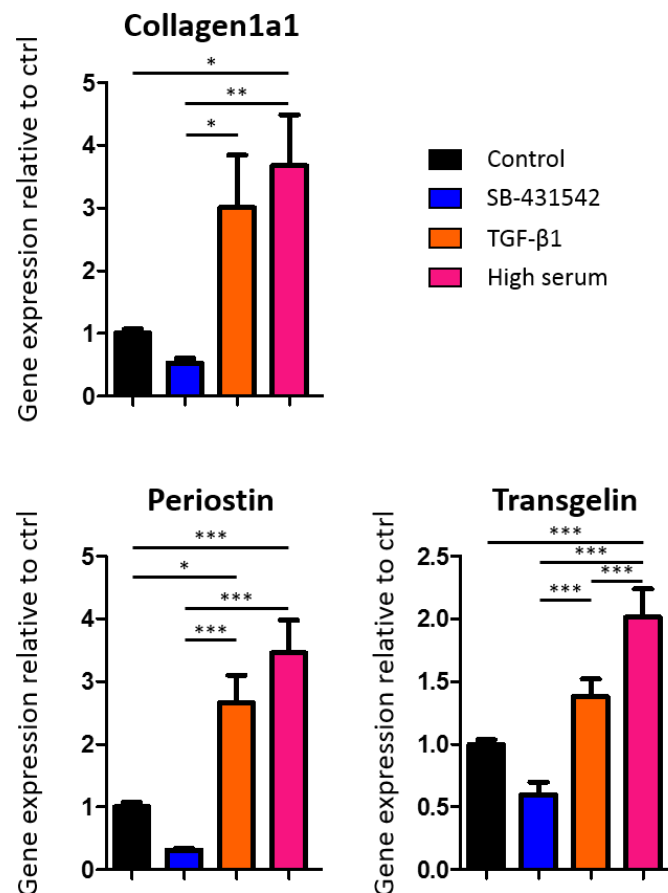


Figure 26: Combined mRNA abundance analyses relative to GUSB and control CF-EHTs of multiple fibroblast activation markers in A18945 and ERC001 CF-EHTs: collagen1a1, periostin and transgelin. The CF-EHTs were assigned to either a control group,

*an inhibited group, or 1 of 2 activated groups, and treated as previously described. The CF-EHTs were harvested on day 21 or day 22. Data are presented as mean  $\pm$  SEM. \* $p < 0.05$ , \*\* $p < 0.005$ , \*\*\* $p < 0.001$  by one-way ANOVA plus Bonferroni's post-test for multiple comparisons,  $n = 6-8$  per group.*

In summary, when the contractility analyses of the 3 hiPSC lines were combined (Figure 25) it became obvious that the activated CF-EHTs exhibited a shorter resting length than the control and inhibited CF-EHTs, which could be a sign of attenuated remodelling. The activated CF-EHTs moreover exhibited a lower relaxation velocity and higher 80% relaxation time compared to the inhibited CF-EHTs. These observations argue for a relaxation deficit in these CF-EHTs, which was exploited in later experiments.

In the mRNA abundance analysis results (Figure 26) all fibroblast activation markers were more abundant in the activated CF-EHTs compared to the control and inhibited CF-EHTs.

These findings suggested that in the developed protocol for the *in vitro* EHT based fibrosis model, the activated CF-EHTs indeed presented a number of indirect signs of increased fibrosis, affirming the suitability of the model.



### 3.2 Results II: Implementation of the *in vitro* fibrosis model

A functional *in vitro* EHT based fibrosis model had been developed, in which the activated tissues exhibited a relaxation deficit and higher abundance of multiple fibroblast activation markers compared to the inhibited tissues. The fibrosis model was therefore considered sufficiently developed to be implemented, to study the effect of genetic interventions on the formation of fibrosis in this model. The genetic interventions that were studied were the knockout of the pro-fibrotic enhancer sequence *enh35232*, a *RUNX1*-related enhancer, and the knockout of the *RUNX1* gene. For this purpose, WT A18945 hiPSCs, A18945 hiPSCs with *enh35232* deleted and A18945 hiPSCs with *RUNX1* deleted were kindly provided by Dr. Thomas Moore-Morris and Dr. Alenca Harrington (Institute for Regenerative Medicine & Biotherapy, Montpellier, France). The enhancer sequence data, including the location of the *enh35232* deletion in the A18945 hiPSC line, can be found in the supplements (section 10.1.15).

#### 3.2.1 Quality control

The quality of the WT hiPSCs, the *enh35232* (Enh) KO hiPSCs and the *RUNX1* (Gene) KO hiPSCs was evaluated with regard to the karyotype, sterility and pluripotency of the hiPSCs.

##### 3.2.1.1 Karyotype

Visible karyograms of the WT hiPSCs, the Enh KO hiPSCs and the Gene KO hiPSCs in metaphase were produced by Giemsa-banding at the Institute of Human Genetics (UKE, Hamburg). A resolution of 350-500 bands per haploid set were investigated. All hiPSCs showed a normal, female karyotype (46, XX), with no visible aberrations (Figure 27 and supplement section 10.1.10.1).



Figure 27: Cytogenetic analysis by Giemsa-banding produced a visible karyogram of wild-type A18945 hiPSCs, which showed a normal, female karyotype (46, XX), with no visible aberrations.

### 3.2.1.2 Mycoplasma

The hiPSCs of each genotype were evaluated for mycoplasma presence by PCR amplification of mycoplasma DNA prior to expansion. No evidence for the presence of mycoplasma was found in the culture medium of the hiPSCs.

### 3.2.1.2 Pluripotency

The pluripotency of the hiPSCs was evaluated by measuring the percentage of hiPSCs positive for the cell surface marker SSEA-3 via flow cytometry. 99.68% of WT hiPSCs expressed SSEA-3 (Figure 28).

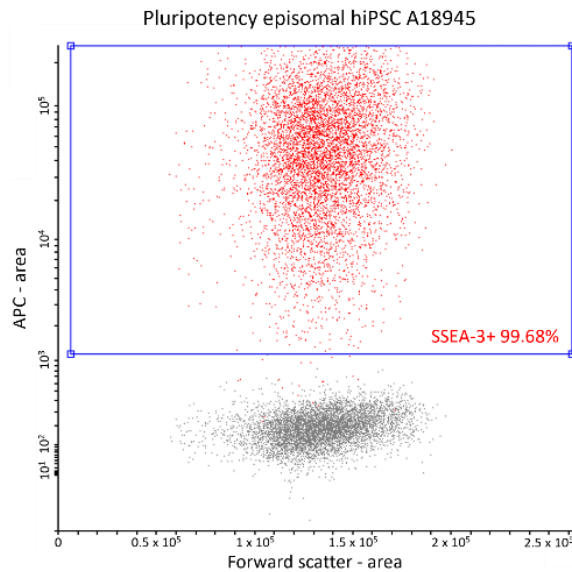


Figure 28: SSEA-3 expression in WT hiPSCs. Unstained isotype control WT hiPSCs (grey) were used to determine the gating. 99.68% of stained WT hiPSCs (red) sufficiently expressed SSEA-3.

### 3.2.1.3 Cardiac fibroblast differentiation

After 3 differentiation runs of each of the different hiPSC genotypes to produce cardiac fibroblasts, the presence of fibrosis markers and cardiac markers in the differentiated cells was assessed to determine the success of the differentiation runs. Messenger RNA abundance in the differentiated CFs was compared to the abundance in hiPSCs, primary foreskin fibroblasts, primary cardiac fibroblasts and hiPSC-derived cardiomyocytes. The mRNA abundance of GATA binding protein 4 (*GATA4*) as an early cardiac development marker, TCF21 as a marker for mesenchyme derived cells and both discoidin domain receptor tyrosine kinase 2 (*DDR2*) and vimentin (*VIM*) as fibroblast markers, all relative to the expression of *GUSB*, were analysed (Figure 29).

*GATA4* mRNA was most abundant in hiPSC-derived cardiomyocytes, followed by the primary cardiac fibroblasts. *GATA4* was least expressed in hiPSCs and primary foreskin fibroblasts. *GATA4* mRNA was less abundant in the hiPSC-derived CFs, especially in the hiPSC-derived Gene KO CFs, than in the primary cardiac fibroblasts. However, *GATA4* mRNA was still 5.56 times and 100 times more abundant in the hiPSC-derived Gene KO CFs than in the hiPSCs and primary foreskin fibroblasts, respectively. Though TCF21 was 4.95 times more abundant in primary cardiac fibroblasts than in hiPSC-derived Enh KO CFs, it was 43.25 times and 4.33 times more abundant in hiPSC-derived Enh KO CFs than in the

hiPSCs and primary foreskin fibroblasts, respectively. DDR2 mRNA was 7.43 times more abundant in primary cardiac fibroblasts than in hiPSC-derived Gene KO CFs, but it was 14.84 times and 1.76 times more abundant in hiPSC-derived Gene KO CFs compared to hiPSCs and hiPSC-derived cardiomyocytes, respectively. Vimentin was similarly expressed in primary foreskin fibroblasts and hiPSC-derived CFs.

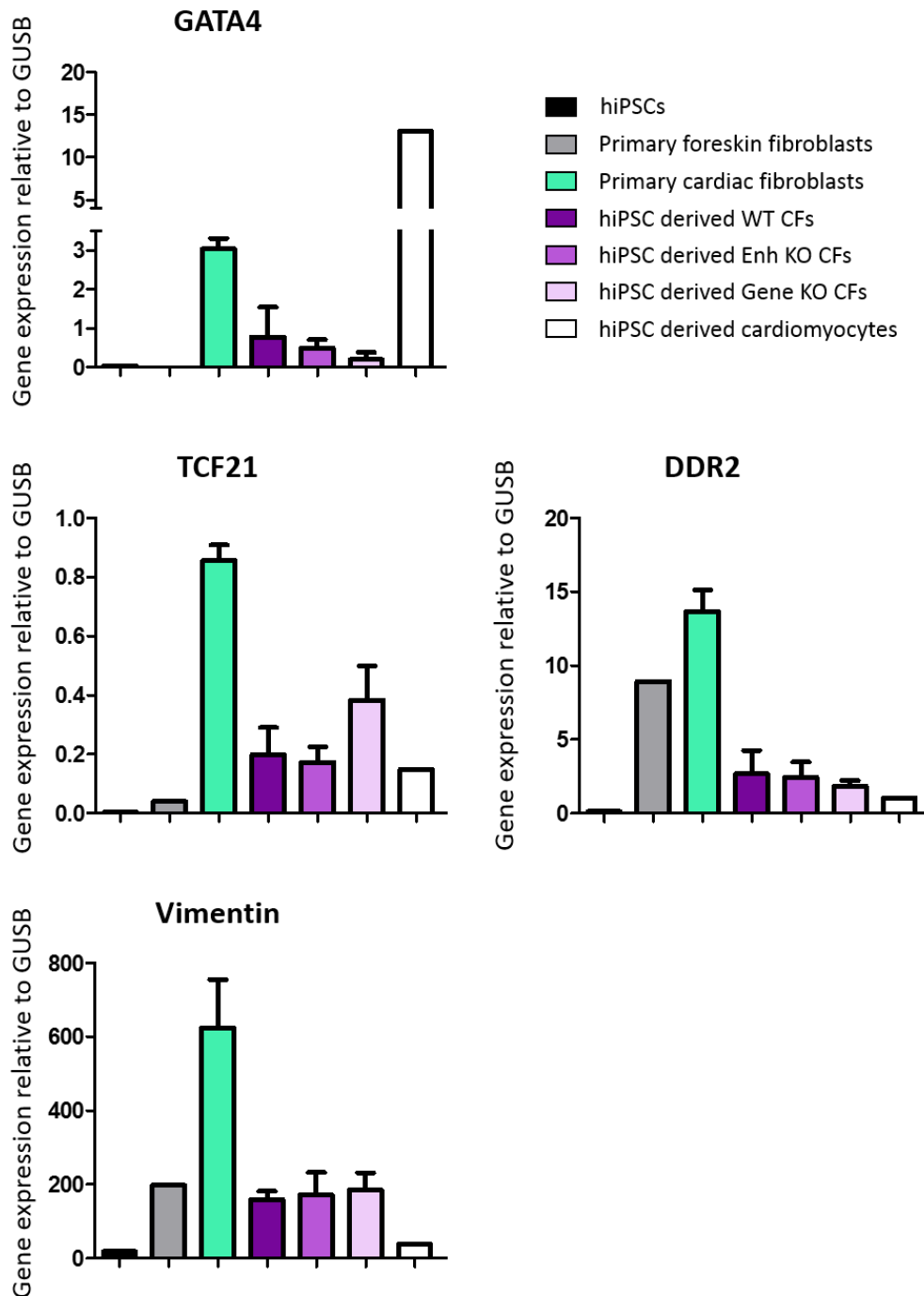


Figure 29: The mRNA abundance relative to GUSB of GATA4, TCF21, DDR2 and vimentin (VIM) in hiPSCs, primary foreskin fibroblasts, primary cardiac fibroblasts, hiPSC-derived WT CFs, hiPSC-derived Enh KO CFs, hiPSC-derived Gene KO CFs and hiPSC-derived cardiomyocytes. When possible, data are presented as mean  $\pm$  SEM,  $n=1$  or 3.

Compared to hiPSCs and primary foreskin fibroblasts, GATA4 and TCF21 were more abundant in the hiPSC-derived CFs, which suggested a cardiac lineage and cardiac fibroblast-like expression pattern, respectively. Compared to hiPSCs and cardiomyocytes, DDR2 and vimentin were more abundantly

expressed in the hiPSC-derived CFs, which argued for a successful fibroblast differentiation. Based on these results, it was determined that WT hiPSCs, Enh KO hiPSCs and Gene KO hiPSCs could successfully be differentiated into cardiac fibroblasts.

In addition to the mRNA abundance of the fibroblast marker DDR2, the percentage of hiPSC-derived CFs positive for the cell surface marker DDR2 was also evaluated via flow cytometry (Figure 30, for dot plots of DDR2 stained CFs vs isotype control CFs of each genotype, see supplement section 10.1.10.2). In the hiPSC-derived WT CFs, 57-76% of the differentiated cells expressed DDR2, depending on the differentiation run. In the hiPSC-derived Enh KO CFs, 56-83% of the differentiated cells expressed DDR2, depending on the differentiation run. In the hiPSC-derived Gene KO CFs, 68-82% of the differentiated cells expressed DDR2, depending on the differentiation run.

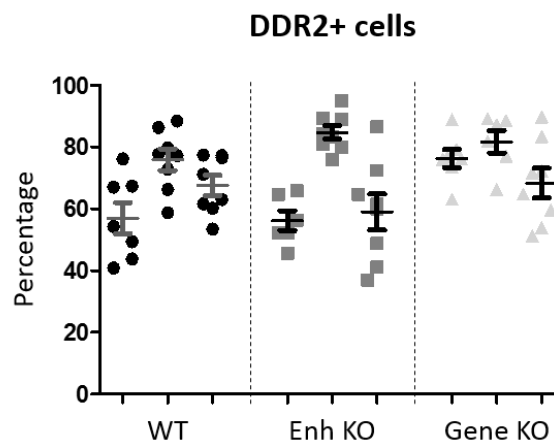


Figure 30: The average percentage of A18945 hiPSC-derived CFs positive for DDR2, for each genotype, for 3 different differentiation runs per genotype. Data are presented as mean  $\pm$  SEM,  $n=7-9$  technical replicates per differentiation run.

As DDR2 is not expressed by all cardiac fibroblasts (Bursac & J. Kim, 2014), a minimum of 56% DDR2<sup>+</sup> cells was considered a successful cardiac fibroblast differentiation.

It was also investigated whether the *enh35232* KO or the *RUNX1* KO affected the ability of hiPSCs to differentiate into viable cardiomyocytes. Human iPSC-derived Enh KO cardiomyocytes were differentiated with a purity (defined as the percentage of cTnT<sup>+</sup> cells) of 70%. Human iPSC-derived Gene KO cardiomyocytes were differentiated with a purity of 91%. The contractility of CF-EHTs composed of 10% WT cardiac fibroblasts and 90% cardiomyocytes, derived from either WT hiPSCs, Enh KO hiPSCs or Gene KO hiPSCs, was analysed (supplement section 10.1.10.3). CF-EHTs from all groups contracted throughout the entire culture time with no difference in generated force, arguing for the unimpaired differentiation of the cardiomyocytes, regardless of the genotype.

In light of the promising quality control results; the normal karyogram of the hiPSCs (Figure 27), high pluripotency of the hiPSCs (Figure 28), the mRNA abundance of marker genes in the differentiated CFs being similar to the abundance in primary cardiac fibroblasts (Figure 29) and the high expression of DDR2 in the differentiated CFs (Figure 30), experiments could commence to investigate the effect of the KOs on the ability of the CFs to become activated.

### 3.2.2 Effects of an *enh35232* or *RUNX1* knockout in 2D culture

To investigate whether the knockout of either the *RUNX1*-related enhancer *enh35232* or of the *RUNX1* gene influenced the ability of the CFs to become activated, CFs first underwent a shortened 2D version of the fibrosis model, as requested by partners of the consortium. The 2D analysis has also been used for RNA sequencing analysis, which is not included in this work, but will be published in future. In the 2D version, a quiescent baseline was again first established in all CFs by serum depletion of the culture medium and treatment with SB-431542. Afterwards, the CFs were assigned to either a control group, an inhibited group, treated with 5  $\mu$ M SB-431542, or 1 of 2 activated groups. The CFs from 1 activated group were treated with 10 ng/ml TGF- $\beta$ 1, the CFs from the other activated group were exposed to 10% serum containing medium.

#### 3.2.2.1 The mRNA abundance

##### *RUNX1* mRNA abundance after activation

To investigate whether the genomic deletion of either *enh35232* or *RUNX1* had an effect on the expression of *RUNX1* in the CFs, the *RUNX1* mRNA abundance in inhibited CFs was compared to the *RUNX1* mRNA abundance in TGF- $\beta$ 1 activated CFs, for each genotype (Figure 31).

The quiescent baseline expression of *RUNX1* was similar in WT CFs and Enh KO CFs. A trend towards a higher mRNA abundance in activated WT CFs compared to activated Enh KO CFs was observed, but this was not significant. Activated WT CFs had a significantly higher *RUNX1* mRNA abundance than inhibited WT CFs. Though activated Enh KO CFs seemed to express more *RUNX1* than inhibited Enh KO CFs, this difference was not significant. Both inhibited and activated Gene KO CFs did not express *RUNX1*.

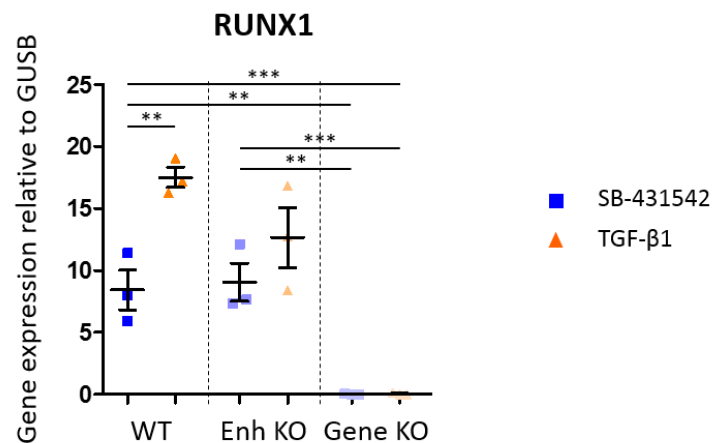


Figure 31: The mRNA abundance relative to GUSB of *RUNX1* in WT CFs, Enh KO CFs and Gene KO CFs. The CFs were assigned to either an inhibited group, treated with 5  $\mu$ M SB-431542, or an activated group, treated with 10 ng/ml TGF- $\beta$ 1. All CFs were cultured in 10% serum containing medium until day 3, after which they were cultured in 0.5% serum containing medium + 5  $\mu$ M SB-431542 until day 7, when they were assigned to their respective group. The CFs were treated according to their group until day 10, when they were harvested. Data are presented as mean  $\pm$  SEM. \*\* $p$ <0.005, \*\*\* $p$ <0.001 by two-way ANOVA plus Bonferroni's post-test for multiple comparisons, only biologically meaningful comparisons are shown,  $n$ =3 per group.

#### Fibrosis markers

To quantify pro-fibrotic effects of the activation of the CFs which underwent the 2D version of the fibrosis model, the mRNA abundance in the WT CFs, Enh KO CFs and Gene KO CFs of the fibrosis markers collagen1a1, periostin and transgelin, relative to the mRNA abundance of GUSB and the WT control

CFs, was assessed (Figure 32; for the mRNA abundance analysis of collagen1a2, CCN2 and ACTA2, see supplement section 10.1.11.1).

Most of the fibrosis markers were more abundant in activated CFs than in control CFs and inhibited CFs, and the lowest amount of mRNA was often detected in inhibited CFs. Significant differences were present between inhibited WT CFs and activated WT CFs in the mRNA abundance of collagen1a1 and periostin. The difference was significant between inhibited Enh KO CFs and activated Enh KO CFs in periostin and transgelin mRNA abundance. Inhibited CFs expressed significantly less periostin than their control counterparts in WT CFs and Enh KO CFs. No significant differences were present between the separate groups in the Gene KO CFs.

When comparing WT CFs to Enh KO CFs, significant differences were only found with regards to transgelin mRNA abundance: the activated Enh KO CFs unexpectedly expressed significantly more transgelin mRNA than the activated WT CFs. When comparing WT CFs to Gene KO CFs, significant differences were only found with regards to periostin expression, where both the control and the activated WT CFs expressed significantly more periostin mRNA than the control and activated Gene KO CFs. However, a striking trend towards a lower mRNA abundance of the fibrosis markers in all Gene KO conditions compared to the WT conditions can be observed, whereas the Enh KO conditions share a similar activation and inhibition pattern as the WT conditions.

All probed fibrosis markers were significantly less abundant in the activated Gene KO CFs than in the activated Enh KO CFs. The control Gene KO CFs expressed significantly less periostin and transgelin mRNA than the control Enh KO CFs.

Similar results were observed with regard to the mRNA abundance of collagen1a2, CCN2 and ACTA2, with a trend towards a lower abundance in the inhibited CFs for all genotypes and a lower baseline abundance in the Gene KO CFs (supplement section 10.1.11.1).

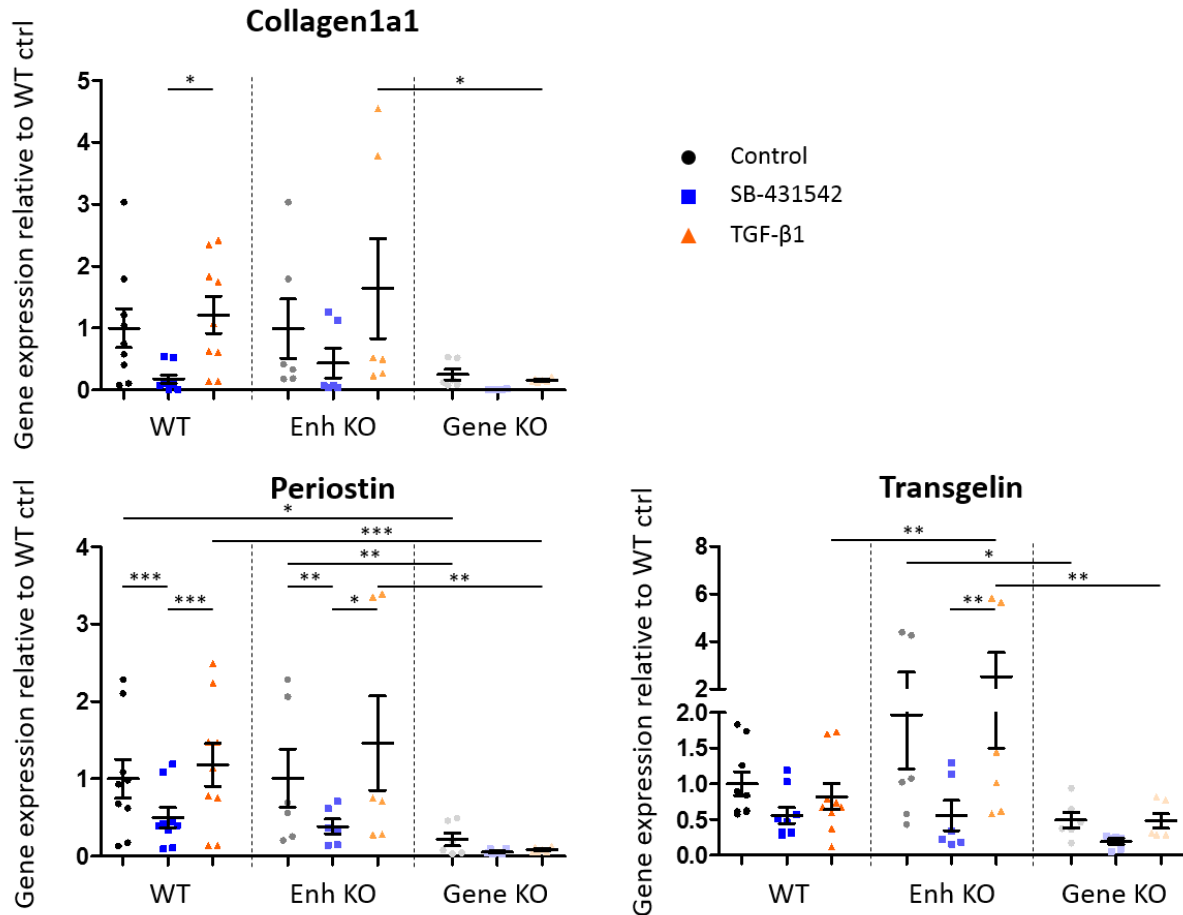


Figure 32: The mRNA abundance relative to GUSB and WT control of the fibrosis markers collagen1a1, periostin and transgelin in WT CFs, Enh KO CFs and Gene KO CFs. The CFs were assigned to either a control group, an inhibited group, treated with 5  $\mu$ M SB-431542, or an activated group treated with 10 ng/ml TGF- $\beta$ 1. All CFs were cultured in 10% serum containing medium until day 3, after which they were cultured in 0.5% serum containing medium + 5  $\mu$ M SB-431542 until day 7, when they were assigned to their respective groups. The CFs were treated according to their group until day 10, when they were harvested. Data are presented as mean  $\pm$  SEM. \* $p$ <0.05, \*\* $p$ <0.005, \*\*\* $p$ <0.001 by two-way ANOVA plus Bonferroni's post-test for multiple comparisons, only biologically meaningful comparisons are shown,  $n$ =6-9 per group.

This mRNA abundance analysis argued that the 2D version of the fibrosis model was also functional, as fibrosis markers were more abundant in the activated CFs than in the other CF groups. However, more research was necessary to compare the different genotypes. So far, a strong trend could be observed which argued that the Gene KO CFs expressed less fibrosis markers than either the WT CFs or the Enh KO CFs, but the data did not argue for a pronounced effect of the Enh KO.

### 3.2.2.2 Protein expression

For further in-depth analysis of the 2D version of the fibrosis model, the expression of the fibroblast activation marker proteins periostin and  $\alpha$ SMA in the CFs was analysed. Though the expression of the housekeeping protein  $\alpha$ -tubulin was also used to account for the loading difference of the samples, quantification was conducted relative to Ponceau S staining. The protein expression is also depicted relative to the expression of the WT control CFs (Figure 33 and Figure 34). In this experiment, a high serum activated group was included.

No significant differences were observed in the abundance of either periostin or  $\alpha$ SMA, either between the differently treated CFs or the different genotypes, in light of a high variability. For the periostin expression in the Gene KO CFs, a trend towards a higher expression in activated CFs than in control or inhibited CFs was observed. This same trend was observed in the  $\alpha$ SMA expression in the Enh KO CFs, but not in the expression in the WT CFs.

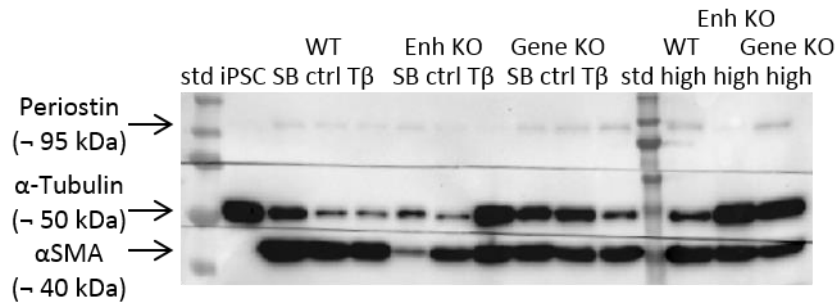


Figure 33: Western blot analysis. The band for periostin was visible at 95 kDa, for  $\alpha$ -tubulin at 50 kDa and for  $\alpha$ SMA at 40 kDa. Lane 1: protein size standard (std). Lane 2: hiPSCs. Lane 3, 4 and 5: WT CFs, in order: inhibited (SB), control and TGF- $\beta$ 1 (T $\beta$ ) activated. Lane 6, 7 and 8: Enh KO CFs, in order: inhibited, control and TGF- $\beta$ 1 activated. Lane 9, 10 and 11: Gene KO CFs, in order: inhibited, control and TGF- $\beta$ 1 activated. Lane 12: protein size standard. Lane 13: high serum activated WT CFs. Lane 14: high serum activated Enh KO CFs. Lane 15: high serum activated Gene KO CFs.

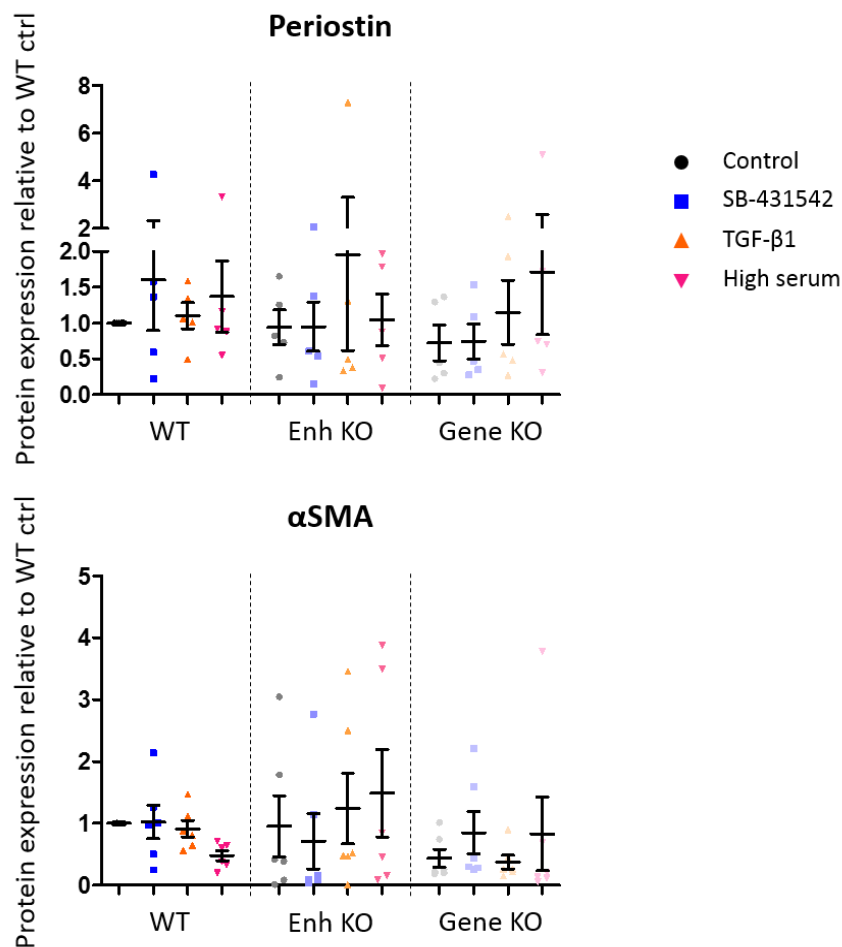


Figure 34: Protein quantification of periostin and  $\alpha$ SMA by Western blot, relative to Ponceau S staining and WT control. The CFs were assigned to either a control group, an inhibited group, treated with 5  $\mu$ M SB-431542, or 1 of 2 activated groups. The CFs from 1 activated group were treated with 10 ng/ml TGF- $\beta$ 1, the CFs from the other activated group were exposed to 10%



serum containing medium. All CFs were cultured in 10% serum containing medium until day 3, after which they were cultured in 0.5% serum containing medium + 5  $\mu$ M SB-431542 until day 6, when they were assigned to their respective groups. The CFs were treated according to their group until day 10, when they were harvested. Data are presented as mean  $\pm$  SEM. \* $p$ <0.05, \*\* $p$ <0.005, \*\*\* $p$ <0.001 by two-way ANOVA plus Bonferroni's post-test for multiple comparisons,  $n$ =5 per group.

### 3.2.2.3 Flow cytometry

To further quantify the effect of the 2D version of the fibrosis model on the activation of cardiac fibroblasts, the expression of the intracellular marker  $\alpha$ SMA was analysed (Figure 35, for histograms of SB-431542 treated CFs vs TGF- $\beta$ 1 treated CFs of each genotype, see supplement section 10.1.11.2). To ensure that only cardiac fibroblasts were analysed rather than cells of poorly defined cell types, the CFs were stained for both DDR2 and  $\alpha$ SMA, and the  $\alpha$ SMA expression was solely measured in DDR2<sup>+</sup> cells via flow cytometry.

In this analysis the only significant difference was the higher percentage of  $\alpha$ SMA<sup>+</sup> CFs in the activated high serum Enh KO CFs compared to the activated high serum Gene KO CFs. A trend was visible of an elevated percentage of  $\alpha$ SMA<sup>+</sup> CFs in the activated Enh KO CFs compared to in the control and inhibited Enh KO CFs, but this trend was not observed in the WT CFs or the Gene KO CFs.

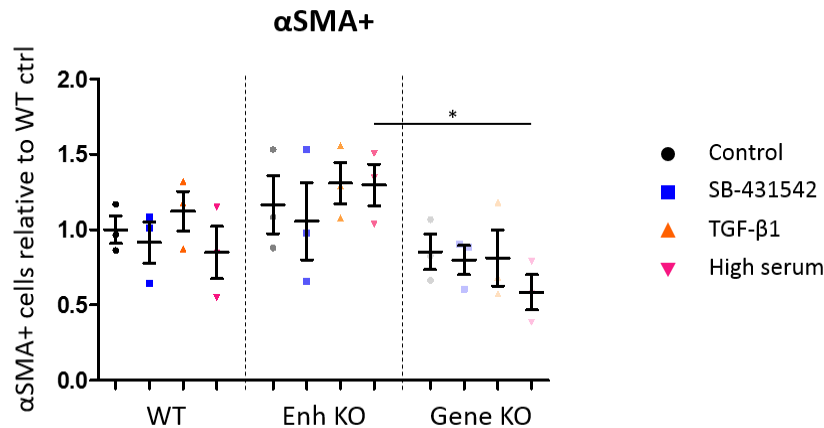


Figure 35: The average percentage of  $\alpha$ SMA<sup>+</sup> cells (of DDR2<sup>+</sup> cells) per treated group, per genotype, of 3 different differentiation runs. The CFs were assigned to either a control group, an inhibited group, treated with 5  $\mu$ M SB-431542, or 1 of 2 activated groups. The CFs from 1 activated group were treated with 10 ng/ml TGF- $\beta$ 1, the CFs from the other activated group were exposed to 10% serum containing medium. All CFs were cultured in 10% serum containing medium until day 3, after which they were cultured in 0.5% serum containing medium + 5  $\mu$ M SB-431542 until day 6, when they were assigned to their respective groups. The CFs were treated according to their group until day 10, when they were harvested. Data are presented as mean  $\pm$  SEM. \* $p$ <0.05 by two-way ANOVA plus Bonferroni's post-test for multiple comparisons, only biologically meaningful comparisons are shown,  $n$ =6, as each dot represents the average of 2 samples of 1 differentiation run.

From the results of the 2D experiments, it was concluded that while the 2D version of the fibrosis model worked as expected on an mRNA abundance level (Figure 32), with a higher mRNA abundance found in activated CFs, these effects were not observed when analysing the protein expression via Western blot analysis (Figure 34) or antibody staining and subsequent flow cytometry (Figure 35). Gene KO CFs displayed a lower expression of fibrosis markers than Enh KO CFs, but no further clear differences between the genotypes were visible.

### 3.2.3 Effects of an *enh35232* or *RUNX1* knockout in 3D culture

The simplified 2D version of the fibrosis model yielded preliminary results in clear which differences between the genotypes were not observed. To expand on these preliminary results, multiple batches

of A18945 CF-EHTs underwent the *in vitro* 3D EHT based fibrosis model. It was investigated whether differences between the genotypes were more prominent in CF-EHTs which underwent this *in vitro* 3D EHT based fibrosis model.

### 3.2.3.1 Contractility of A18945 CF-EHTs

The contractility of A18945 CF-EHTs composed of 90% hiPSC-derived WT cardiomyocytes and 10% hiPSC-derived cardiac fibroblasts, either WT, Enh KO or Gene KO, which were cultured according to the *in vitro* EHT based fibrosis model, was analysed. The contractility of CF-EHTs from 4 different batches, containing cardiomyocytes and CFs from 3 different differentiation runs, were combined. The purity of the cardiomyocytes ranged from 63-95%, as determined by cTnT expression. Considering the differences in cardiomyocyte purity, the contractility data could not be combined directly. Instead, for each analysis time point, batch and parameter, the average of that specific analysis was calculated. The contractility parameters of each individual CF-EHT in this respective analysis were then normalized and related to this average, after which the analyses from the 4 different batches were combined. As determined in the *in vitro* EHT based 3D fibrosis model optimization stage, the CF-EHTs were assigned to 1 of 4 groups, a control group, an inhibited group, treated with 5  $\mu$ M SB-431542, or 1 of 2 activated groups. The CF-EHTs from 1 activated group were treated with 10 ng/ml TGF- $\beta$ 1, the CF-EHTs from the other activated group were exposed to 10% serum containing medium. From the previous analysis of CF-EHTs which had undergone the *in vitro* 3D EHT based fibrosis model protocol, it had been determined that activation with high serum had a more pronounced impact on the contractility of the CF-EHTs than activation with TGF- $\beta$ 1 (Figure 25). For readability of the contractility analysis, only the data of the most inhibited CF-EHTs and the most activated CF-EHTs (high serum) are displayed (Figure 36). A more in-depth analysis of the resting length, relaxation velocity and 80% relaxation time of all CF-EHTs, including the control CF-EHTs and the TGF- $\beta$ 1 activated CF-EHTs, on the last day of culture, together with the analysis of the beating frequency of the CF-EHTs, can be found in the supplements (section 10.1.10.1).

No differences with regards to the force were present, neither between the inhibited CF-EHTs and the activated CF-EHTs, nor between the different genotypes.

The inhibited CF-EHTs, regardless of genotype, possessed a significantly longer resting length than their activated counterparts, which suggested more active remodelling in the activated CF-EHTs.

On the last day of culture, the activated WT and Enh KO CF-EHTs had a significantly lower relaxation velocity than their inhibited counterparts. A significant difference between the relaxation velocity of the activated Gene KO CF-EHTs and the inhibited Gene KO CF-EHTs was present on day 20, but this difference was no longer significant on the last day of culture.

At the end of the culture time, the activated WT and Enh KO CF-EHTs had a significantly longer 80% relaxation time than the inhibited WT and Enh KO CF-EHTs, respectively. The activated Gene KO CF-EHTs only showed a slightly longer 80% relaxation time than the inhibited Gene KO CF-EHTs. Additionally, the inhibited WT CF-EHTs had a significantly shorter 80% relaxation time than the inhibited Gene KO CF-EHTs, and the activated WT CF-EHTs had a significantly longer 80% relaxation time than the activated Gene KO CF-EHTs.

The activated Enh KO and Gene KO CF-EHTs contracted with a significantly higher beating frequency than their inhibited counterparts. The activated WT CF-EHTs displayed the same tendency (supplement section 10.1.12.1).

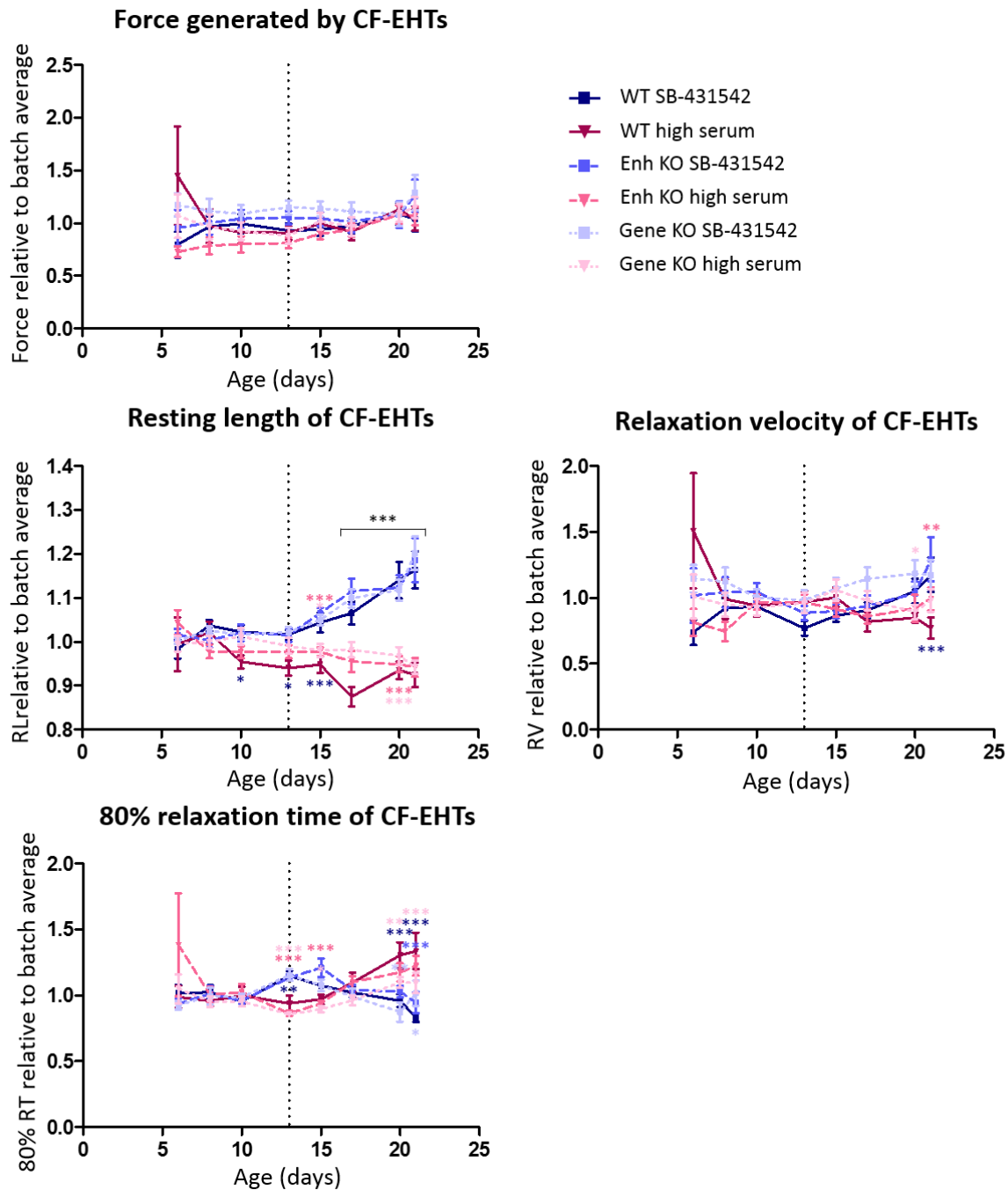


Figure 36: Contractility analysis of WT, Enh KO and Gene KO CF-EHTs, assigned to either an inhibited group, treated with 5  $\mu$ M SB-431542, or an activated group, exposed to 10% serum containing medium, and treated as previously described. The CF-EHTs were harvested on day 21. The development of the generated force, resting length, relaxation velocity and 80% relaxation time of the CF-EHTs are presented over time, relative to batch average. Data are presented as mean  $\pm$  SEM, \* $p < 0.05$ , \*\* $p < 0.005$ , \*\*\* $p < 0.001$  by two-way ANOVA plus Bonferroni's post-test for multiple comparisons, only biologically meaningful comparisons are shown,  $n = 20-25$  per group, from 4 different batches.

As expected, multiple parameters of the contractility analysis indicated signs of elevated fibrosis in the activated CF-EHTs compared to the inhibited CF-EHTs, especially the shorter resting length, a sign of

more remodelling, and the lower relaxation velocity in combination with a longer 80% relaxation time, both arguing for a relaxation deficit. The differences between the activated and inhibited CF-EHTs with regard to the relaxation velocity and 80% relaxation time were significant in both the WT CF-EHTs and the Enh KO CF-EHTs, but not in the Gene KO CF-EHTs.

The only difference in the contractility of the WT CF-EHTs compared to the Enh KO CF-EHTs was the lower beating frequency of the activated WT CF-EHTs. The activated WT CF-EHTs also contracted with a lower frequency than the activated Gene KO CF-EHTs, but more importantly, the 80% relaxation time of the WT CF-EHTs differed significantly from the 80% relaxation time of the Gene KO CF-EHTs. The 80% relaxation time was longer in the activated WT CF-EHTs than in the activated Gene KO CF-EHTs and it was shorter in the inhibited WT CF-EHTs than in the inhibited Gene KO CF-EHTs. These findings suggested a higher dynamic range, and therefore a larger effect of activation, in the WT CF-EHTs than in the Gene KO CF-EHTs. This indicated a possible attenuation of fibrosis development in the Gene KO CF-EHTs.

### *3.2.3.2 The mRNA abundance of A18945 CF-EHTs*

To further quantify a possible pro-fibrotic effect of the different interventions and differences between the genotypes, the mRNA abundance of the fibrosis markers collagen1a1, periostin and transgelin, relative to the mRNA abundance of GUSB and of WT control CF-EHTs, was assessed (Figure 37; for the mRNA abundance analysis of collagen1a2, CCN2 and ACTA2, see supplement section 10.1.12.2).

The fibrosis markers collagen1a1, periostin and transgelin showed a clear difference in mRNA abundance when comparing the inhibited CF-EHTs to the activated CF-EHTs, for each genotype. Except for the abundance of periostin mRNA in the Enh KO CF-EHTs, for each of these markers and in each genotype, the inhibited CF-EHTs presented the least amount of mRNA, followed by the control CF-EHTs, and the highest abundance was measured in the activated CF-EHTs.

A trend towards a higher mRNA abundance in the control WT CF-EHTs compared to in the control Enh KO CF-EHTs, with an even lower presence of mRNA in the control Gene KO CF-EHTs was observed for each fibrosis marker.

Similar trends were displayed in the mRNA abundance of collagen1a2 and CCN2, but not in the abundance of ACTA2 (supplement section 10.1.12.2).

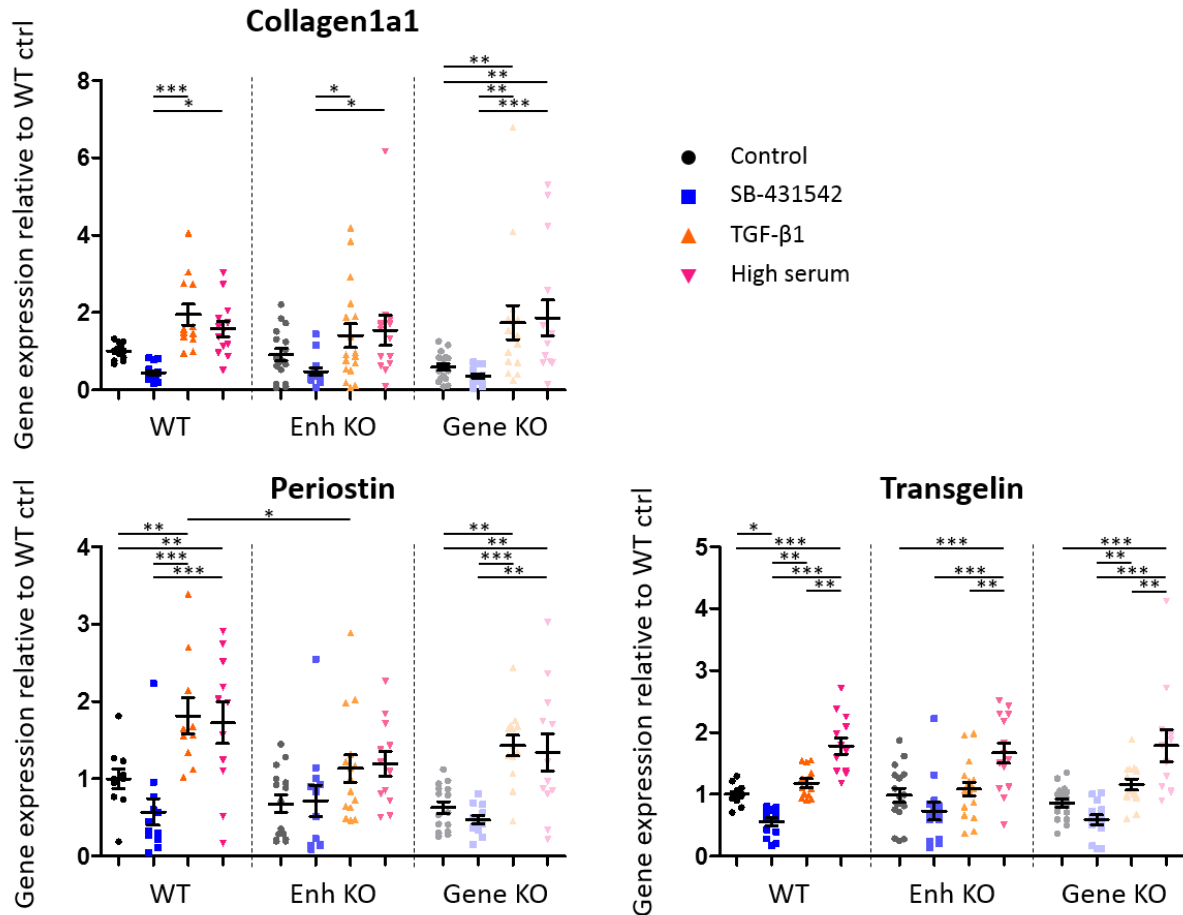


Figure 37: The mRNA abundance relative to *GUSB* and WT control of the fibrosis markers collagen1a1, periostin and transgelin in WT, Enh KO and Gene KO CF-EHTs. The CF-EHTs were assigned to either a control group, an inhibited group, or 1 of 2 activated groups, and treated as previously described. The CF-EHTs were harvested on day 21. Data are presented as mean  $\pm$  SEM, \* $p$ <0.05, \*\* $p$ <0.005, \*\*\* $p$ <0.001 by two-way ANOVA plus Bonferroni's post-test for multiple comparisons, only biologically meaningful comparisons are shown,  $n$ =12-17 per group, from 4 different batches.

This mRNA abundance analysis again argued for the suitability of the *in vitro* 3D EHT based fibrosis model, as most of the fibrosis markers were more abundant in the activated CF-EHTs than in the inhibited CF-EHTs. Clear, consistent differences between the genotypes were however not observed. More in-depth analysis of the CF-EHTs was therefore required.

### 3.2.3.3 Protein expression of A18945 CF-EHTs

An additional method to quantify a possible pro-fibrotic effect of the different interventions and to observe possible differences between the genotypes, was the protein level analysis of periostin (Figure 39) and  $\alpha$ SMA (Figure 40) in the CF-EHTs. The protein abundance of both periostin and  $\alpha$ SMA was quantified relative to the housekeeping protein lamin A/C (Figure 38) and the average batch expression.

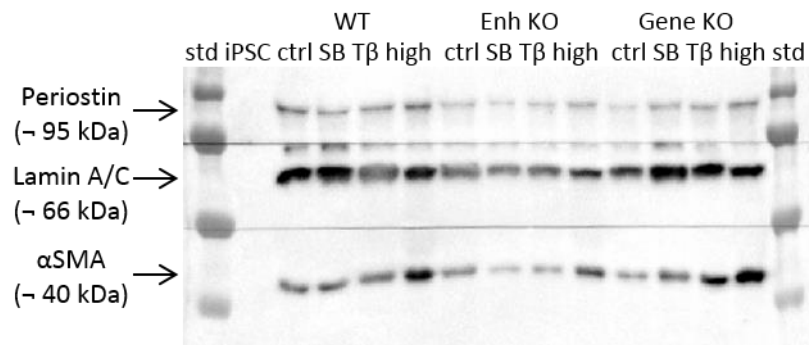


Figure 38: Western blot analysis. The periostin band was visible at 95 kDa, lamin A/C at 66 kDa and αSMA at 40 kDa. Lane 1: protein size standard. Lane 2: hiPSCs. Lane 3 to 6: WT CF-EHTs, in order: control, inhibited, TGF-β1 activated and high serum activated. Lane 7 to 10: Enh KO CF-EHTs, in order: control, inhibited, TGF-β1 activated and high serum activated. Lane 11 to 14: Gene KO CF-EHTs, in order: control, inhibited, TGF-β1 activated and high serum activated. Lane 15: protein size standard.

When analysing the periostin expression in all batches of CF-EHTs relative to batch average (Figure 39), significantly more periostin was expressed in the TGF-β1 activated CF-EHTs than in the inhibited CF-EHTs, for each genotype. Though this difference was not significant in each separate batch, the same trend was observed, regardless of the purity of the cardiomyocytes used in the CF-EHTs. Despite some differences between the genotypes in individual batches, when examining all batches together, no significant differences were found between the genotypes. There was a trend of a lower baseline protein expression in the control Enh KO and Gene KO CF-EHTs compared to the control WT CF-EHTs.

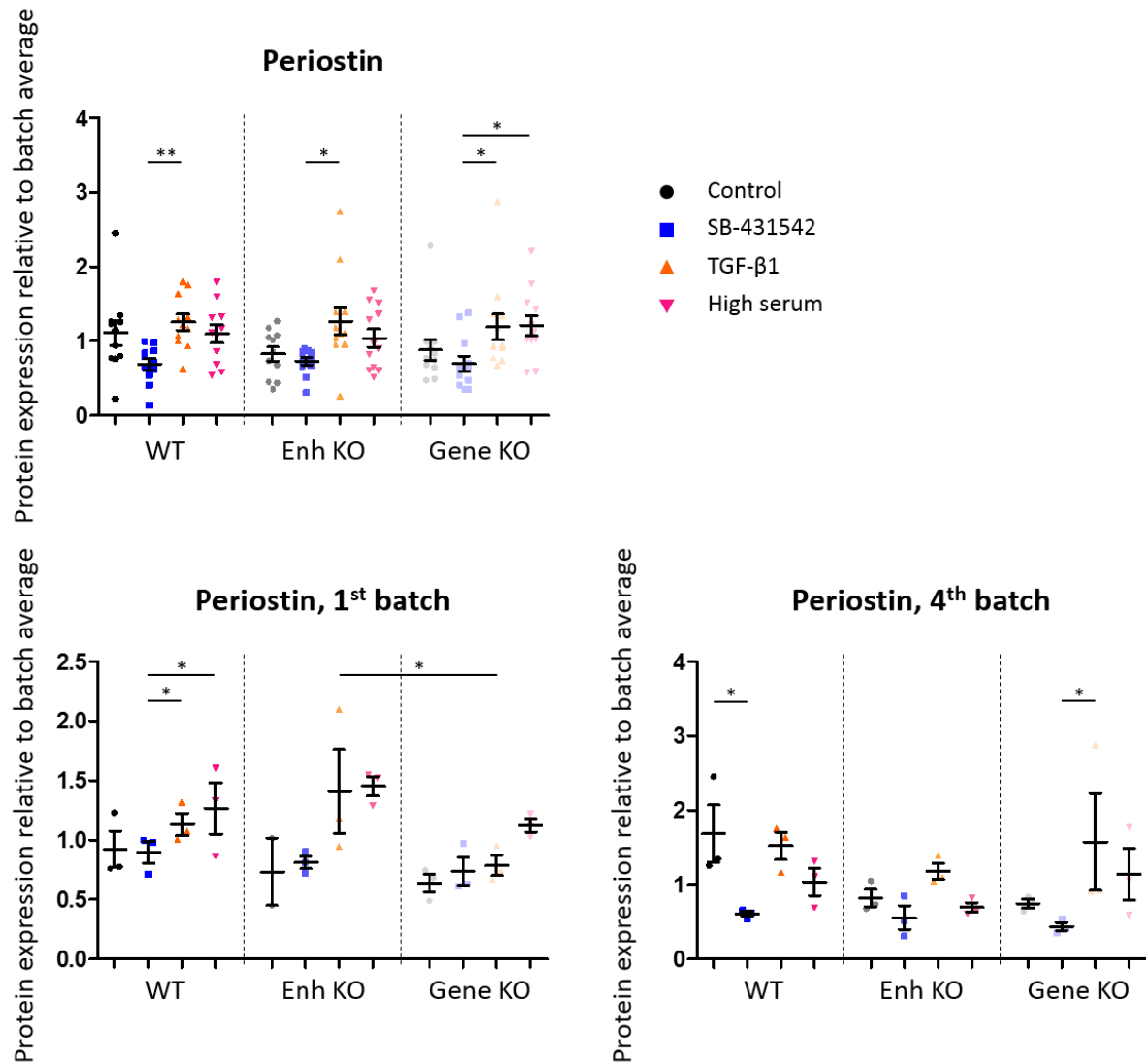


Figure 39: Quantification of periostin by Western blot, relative to lamin A/C and batch average, in WT, Enh KO and Gene KO CF-EHTs. Top, periostin expression in all batches of CF-EHTs. N=11-12 from 4 batches. Bottom left, periostin expression in the 1<sup>st</sup> batch of CF-EHTs. The purity of the cardiomyocytes in the 1<sup>st</sup> batch of CF-EHTs was 95%. N=3. Bottom right, periostin expression in the 4<sup>th</sup> batch of CF-EHTs. The purity of the cardiomyocytes in the 4<sup>th</sup> batch of CF-EHTs was 63%. N=3. All CF-EHTs were assigned to either a control group, an inhibited group, or 1 of 2 activated groups, and treated as previously described. The CF-EHTs were harvested on day 21. Data are presented as mean  $\pm$  SEM, \* $p$ <0.05, \*\* $p$ <0.005, \*\*\* $p$ <0.001 by two-way ANOVA plus Bonferroni's post-test for multiple comparisons, only biologically meaningful comparisons are shown.

When analysing the  $\alpha$ SMA expression in all batches of CF-EHTs relative to batch average (Figure 40), significantly more  $\alpha$ SMA was expressed in the high serum activated CF-EHTs than in the inhibited CF-EHTs, for each genotype. A similar trend was noticed when comparing the TGF- $\beta$ 1 activated CF-EHTs to the inhibited CF-EHTs, but this difference was not significant in any genotype. The same trend was observed in each separate batch of CF-EHTs, regardless of the purity of the cardiomyocytes in the respective batch. Unexpectedly, in the combined analysis of all batches, the high serum activated Gene KO CF-EHTs expressed more  $\alpha$ SMA protein than the high serum activated WT or Enh KO CF-EHTs.

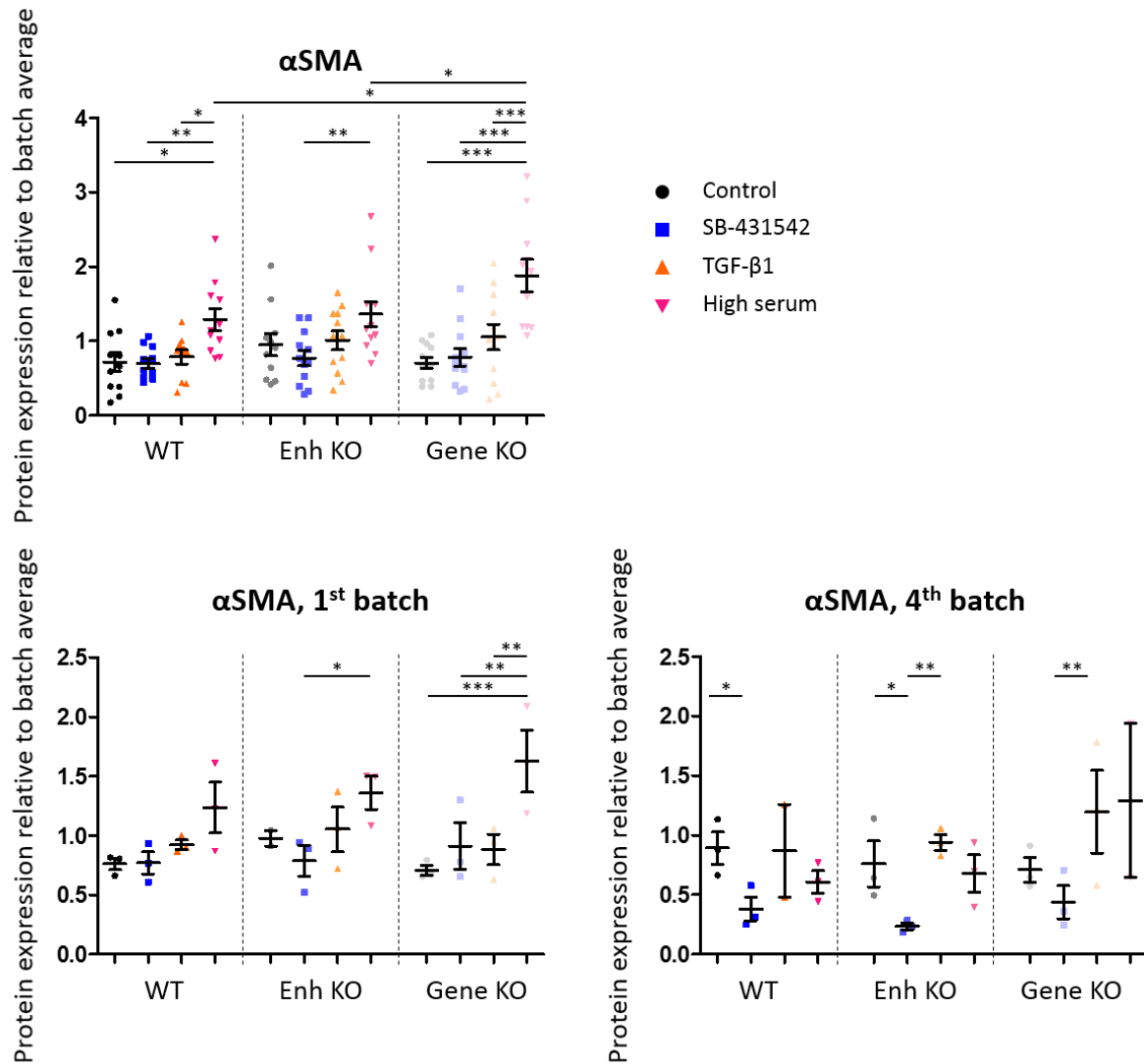


Figure 40: Quantification of  $\alpha$ SMA by Western blot, relative to lamin A/C and batch average, in WT, Enh KO and Gene KO CF-EHTs. Top,  $\alpha$ SMA expression in all batches of CF-EHTs.  $N=11-12$  from 4 batches. Bottom left,  $\alpha$ SMA expression in the 1<sup>st</sup> batch of CF-EHTs. The purity of the cardiomyocytes in the 1<sup>st</sup> batch of CF-EHTs was 95%.  $N=3$ . Bottom right, the expression of  $\alpha$ SMA in the 4<sup>th</sup> batch of CF-EHTs. The purity of the cardiomyocytes in the 4<sup>th</sup> batch of CF-EHTs was 63%.  $N=3$ . All CF-EHTs were assigned to either a control group, an inhibited group, or 1 of 2 activated groups, and treated as previously described. The CF-EHTs were harvested on day 21. Data are presented as mean  $\pm$  SEM, \* $p<0.05$ , \*\* $p<0.005$ , \*\*\* $p<0.001$  by two-way ANOVA plus Bonferroni's post-test for multiple comparisons, only biologically meaningful comparisons are shown.

Similar to the findings in the mRNA abundance analysis, the protein expression analysis argued for the suitability of the *in vitro* EHT based 3D fibrosis model, as both periostin and  $\alpha$ SMA were more abundant in the activated CF-EHTs than in the inhibited CF-EHTs. Clear, consistent, differences between the genotypes, however, were again not observed. Additional analysis of the CF-EHTs was therefore still required.

#### 3.2.3.4 Stiffness of A18945 CF-EHTs

One of the important characteristics of fibrosis is the increased deposition of extracellular matrix in the tissue. The accumulation of ECM is associated with increased tissue stiffness (Weber, 1997). The stiffness of CF-EHTs can be measured with nanoindentation. To quantify resistance by nanoindentation, a microneedle which is coupled to a cantilever and a force transducer is used to probe the tissue, here



the CF-EHTs. The stiffness of the CF-EHTs was measured in multiple locations. The average of the different measurements per CF-EHT was plotted together, relative to the length of each individual CF-EHT, to account for modulation of tissue compaction by contractile state and to account for the substantial differences in CF-EHT size (Figure 41). When these measurements were performed, it was not yet clear that the differences between inhibited CF-EHTs and activated CF-EHTs were considerably more striking than differences between control CF-EHTs and activated CF-EHTs. To be able to accurately investigate the effect of CF-EHT activation on the stiffness of the CF-EHTs in future research, the SB-431542 treated CF-EHTs should be included in the analysis.

For each genotype, a trend was observed of a higher stiffness of the activated CF-EHTs, compared to the control CF-EHTs, and of a higher stiffness of the WT CF-EHTs compared to either the Enh KO CF-EHTs or the Gene KO CF-EHTs, for each group of CF-EHTs. However, none of these differences were significant.

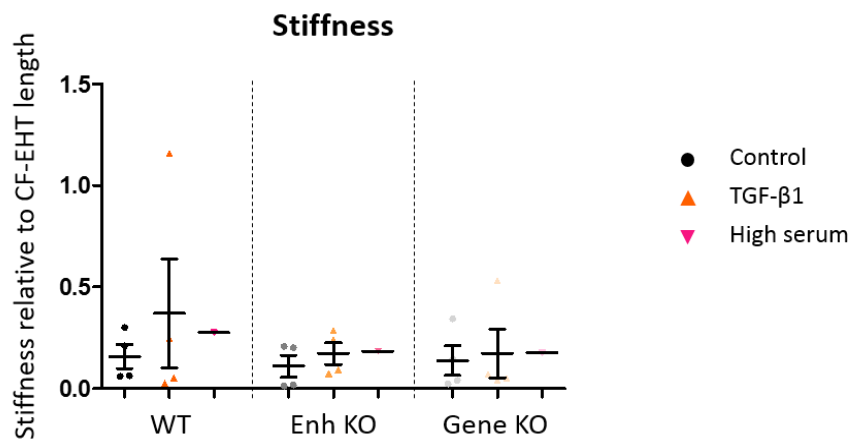


Figure 41: Stiffness of WT, Enh KO and Gene KO CF-EHTs as measured by nanoindentation. All CF-EHTs were assigned to either a control group or 1 of 2 activated groups, and treated as previously described. The CF-EHTs were harvested on day 21. When possible, data are presented as mean  $\pm$  SEM, no significant differences were present between the control CF-EHTs and the TGF- $\beta$ 1 activated CF-EHTs by two-way ANOVA.  $N=4$ , from 2 batches, for the control and the TGF- $\beta$ 1 activated CF-EHTs,  $n=1$  for the high serum activated CF-EHTs.

So far, no clear differences between the different genotypes had been observed in the mRNA abundance analysis (Figure 37), the protein level analysis (Figure 39 and Figure 40) or the stiffness analysis (Figure 41). Therefore, an experiment was conducted with CF-EHTs composed of 75% WT cardiomyocytes and 25% WT, Enh KO or Gene KO cardiac fibroblasts (75/25 CF-EHTs), to potentially increase the possible effect of the genotype in the CF-EHTs. The contractility and mRNA abundance of these CF-EHTs were analysed (supplement section 10.1.13).

The 75/25 Gene KO CF-EHTs generated a significantly higher force than either the 75/25 WT CF-EHTs or the 75/25 Enh KO CF-EHTs. The resting length of the activated 75/25 Gene KO CF-EHTs did not differ from the resting length of the inhibited 75/25 Gene KO CF-EHTs, whereas it had differed in the 90/10 Gene KO CF-EHTs. On the other hand, the relaxation velocity of the inhibited 75/25 Gene KO CF-EHTs was significantly higher than the relaxation velocity of the activated 75/25 Gene KO CF-EHTs from day 15 until day 21, a difference which was only significant on day 20 in the 90/10 Gene KO CF-EHTs. Differences between the WT CF-EHTs and the Enh KO CF-EHTs or between the inhibited and the activated CF-EHTs of either genotype, were not exaggerated in the 75/25 CF-EHTs compared to the 90/10 CF-EHTs.

Similar trends were displayed in the mRNA abundance analysis of the 75/25 CF-EHTs compared to the analysis of the 90/10 CF-EHTs, with attenuated expression of the fibrosis markers observed in the inhibited CF-EHTs and elevated expression of the fibrosis markers observed in the activated CF-EHTs.

In the mRNA abundance analysis of the 75/25 CF-EHTs, a trend towards a lower mRNA abundance of the fibrosis markers in Enh KO CF-EHTs from each condition than in their counterparts in the WT CF-EHTs was observed, and an even lower mRNA abundance was present in the Gene KO CF-EHTs from each condition than in their counterparts in the Enh KO CF-EHTs. This observation argued for attenuated fibrosis in the Enh KO CF-EHTs and the Gene KO CF-EHTs compared to the WT CF-EHTs, both at baseline and under activated conditions. This trend was not observed in the 90/10 CF-EHTs.

### 3.2.4 Effects of an *enh35232* or *RUNX1* knockout in ERC001

To provide a more in-depth analysis of the *RUNX1*-related enhancer KO *enh35232* and the *RUNX1* gene KO, similar regions were knocked out in another hiPSC line, the control hiPSC line ERC001. For this purpose, ERC001 hiPSCs with either one of the genetic deletions were kindly provided by Dr. Thomas Moore-Morris and Dr. Alenca Harrington (Institute for Regenerative Medicine & Biotherapy, Montpellier, France). The enhancer sequence data, including the location of the *enh35232* deletion in the ERC001 hiPSC line, can be found in the supplements (section 10.1.15).

#### 3.2.4.1 CF Quality control

After ERC001 hiPSCs of each of the genotypes were differentiated into CFs, the percentage of hiPSC-derived CFs positive for the cell surface marker DDR2 was evaluated via flow cytometry as a quality control (Figure 42, for dot plots of DDR2 stained CFs vs isotype control CFs of each genotype, see supplement section 10.1.14.1). In the hiPSC-derived WT CFs, 70% of the differentiated cells expressed DDR2. In the hiPSC-derived Enh KO CFs, 86% of the differentiated cells expressed DDR2. In the hiPSC-derived Gene KO CFs, 82% of the differentiated cells expressed DDR2.

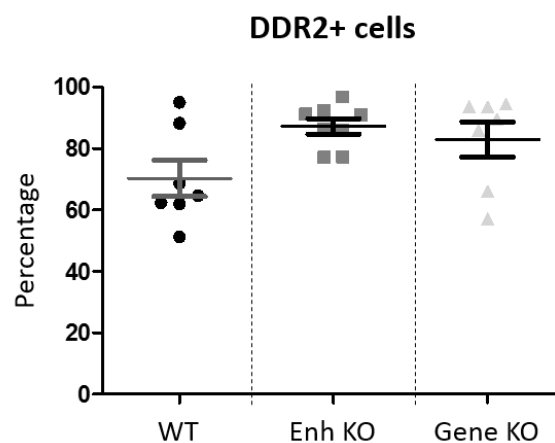


Figure 42: The average percentage of ERC001 hiPSC-derived CFs positive for DDR2, for each genotype, data are presented as mean  $\pm$  SEM,  $n=7-8$  technical replicates from 1 differentiation run.

As DDR2 is not expressed by all cardiac fibroblasts (Bursac & J. Kim, 2014), a minimum of 70% DDR2<sup>+</sup> cells was considered a remarkably successful cardiac fibroblast differentiation.

### 3.2.4.2 2D culture

To investigate whether the knockout of either the *RUNX1*-related enhancer *enh35232* or of the *RUNX1* gene influenced the activation of the ERC001 CFs, they underwent a shortened 2D version of the fibrosis model.

#### Protein expression

The protein expression of periostin and  $\alpha$ SMA in the CFs was analysed by Western blot. The expression of the housekeeping protein  $\alpha$ -tubulin was also analysed, but to account for the loading difference of the samples, quantification was conducted relative to Ponceau S staining. The protein expression was additionally normalized to the expression in the WT control CFs (Figure 43 and Figure 44).

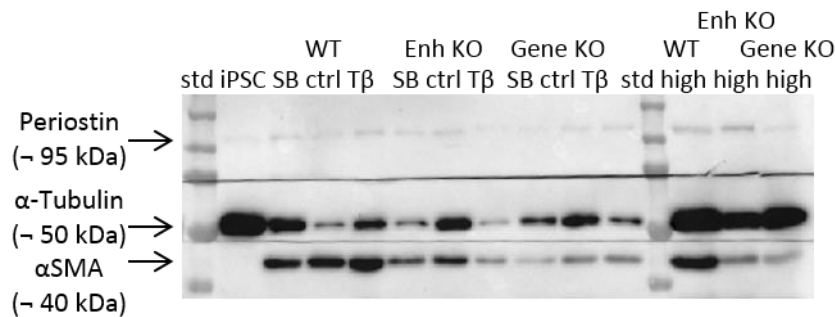


Figure 43: Western blot analysis. The periostin band was visible at 95 kDa,  $\alpha$ -tubulin at 50 kDa and  $\alpha$ SMA at 40 kDa. Lane 1: protein size standard. Lane 2: hiPSCs. Lane 3, 4 and 5: WT CFs, in order: inhibited, control and TGF- $\beta$ 1 activated. Lane 6, 7 and 8: Enh KO CFs, in order: inhibited, control and TGF- $\beta$ 1 activated. Lane 9, 10 and 11: Gene KO CFs, in order: inhibited, control and TGF- $\beta$ 1 activated. Lane 12: protein size standard. Lane 13: high serum activated WT CFs. Lane 14: high serum activated Enh KO CFs. Lane 15: high serum activated Gene KO CFs.

While this experiment was not repeated ( $n=1$ ), a trend towards a higher expression of periostin was visible in at least 1 of the activated groups of CFs compared to the inhibited CFs, for each genotype. A higher expression of  $\alpha$ SMA was also observed in the TGF- $\beta$ 1 activated CFs compared to the control CFs for both the WT CFs and the Gene KO CFs, but not for the Enh KO CFs. A lower baseline of both periostin and  $\alpha$ SMA expression was observed in the Enh KO CFs and the Gene KO CFs, compared to the WT CFs.

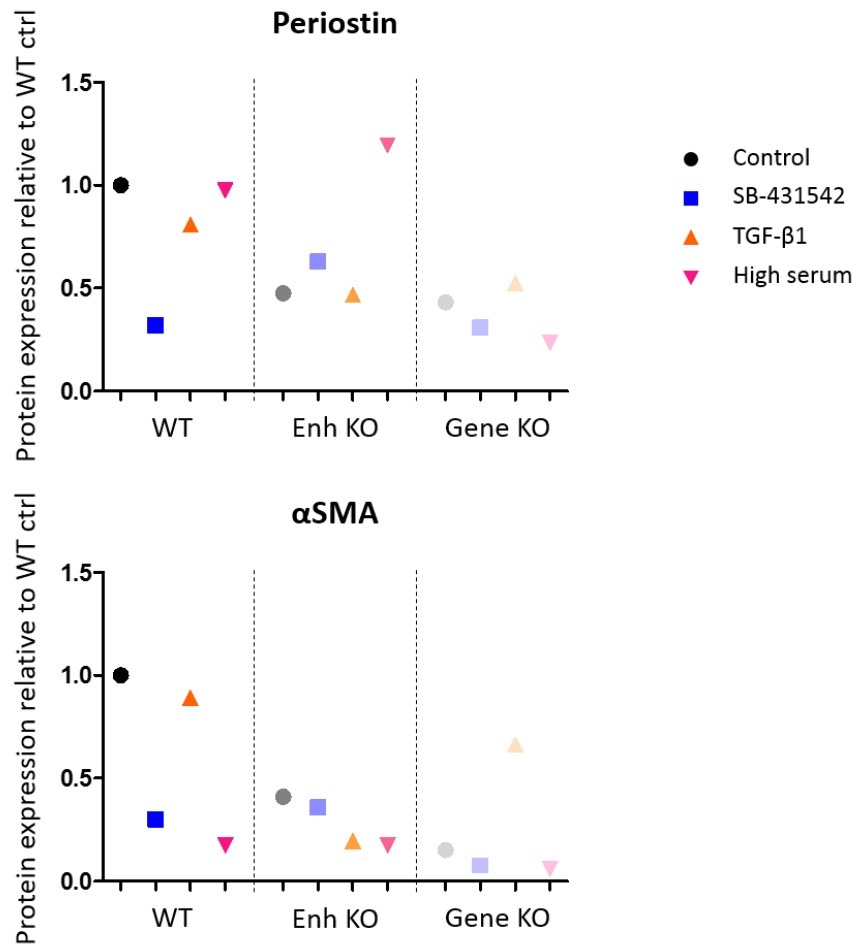


Figure 44: Protein quantification of periostin and  $\alpha$ SMA by Western blot, relative to Ponceau S and WT control. The ERC001 CFs were assigned to either a control group, an inhibited group, treated with 5  $\mu$ M SB-431542, or 1 of 2 activated groups. The CFs from 1 activated group were treated with 10 ng/ml TGF- $\beta$ 1, the CFs from the other activated group were exposed to 10% serum containing medium. All CFs were cultured in 10% serum containing medium until day 3, after which they were cultured in 0.5% serum containing medium + 5  $\mu$ M SB-431542 until day 6, when they were assigned to their respective groups. The CFs were treated according to their group until day 10, when they were harvested. N=1 per group.

No further clear conclusions could be derived from this experiment, likely attributable to the fact that it was not repeated. Due to the seemingly better predictive value of the previous 3D experiments, CF-EHT experiments were conducted rather than repeating the 2D experiment.

#### Flow cytometry

To further quantify the activation of cardiac fibroblasts in the 2D culture model, the expression of the intracellular marker  $\alpha$ SMA was analysed via flow cytometry. To ensure that mostly cardiac fibroblasts were analysed rather than poorly defined cells, the CFs were stained for both DDR2 and  $\alpha$ SMA and the  $\alpha$ SMA expression was only quantified in DDR2<sup>+</sup> cells (Figure 45, for histograms of SB-431542 treated CFs vs TGF- $\beta$ 1 treated CFs of each genotype, see supplement section 10.1.14.2).

For each genotype, a trend to a higher percentage of  $\alpha$ SMA<sup>+</sup> CFs was observed in at least 1 of the activated groups of CFs compared to the inhibited CFs. The Gene KO CFs exhibited a trend to a lower baseline percentage of  $\alpha$ SMA<sup>+</sup> cells, compared to the WT CFs and the Enh KO CFs.

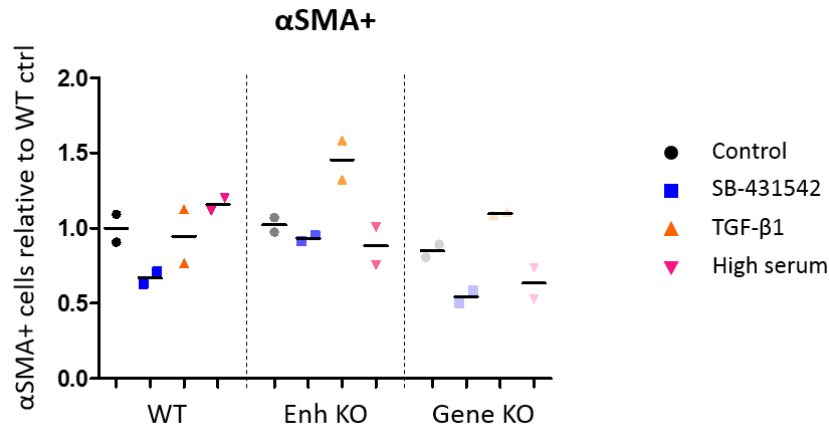


Figure 45: The average percentage of  $\alpha$ SMA<sup>+</sup> cells (of DDR2<sup>+</sup> cells) per treated group, per genotype. The CFs were assigned to either a control group, an inhibited group, treated with 5  $\mu$ M SB-431542, or 1 of 2 activated groups. The CFs from 1 activated group were treated with 10 ng/ml TGF- $\beta$ 1, the CFs from the other activated group were exposed to 10% serum containing medium. All CFs were cultured in 10% serum containing medium until day 3, after which they were cultured in 0.5% serum containing medium + 5  $\mu$ M SB-431542 until day 6, after which they were assigned to their respective groups. The CFs were treated according to their group until day 10, when they were harvested. Data are presented as mean,  $n=2$ .

The 2D experiments showed promising results with regards to signs of increased activation, suggested by an increased protein level of periostin and  $\alpha$ SMA (Figure 44) and by a higher percentage of  $\alpha$ SMA<sup>+</sup> CFs (Figure 45), in the activated CFs. Moreover, the Enh KO CFs and the Gene KO CFs displayed a lower protein expression baseline than the WT CFs.

#### 3.2.4.3 Contractility of ERC001 CF-EHTs

Considering the encouraging 2D experiments, it was investigated whether in the EHT based *in vitro* 3D fibrosis model an even more prominent effect on either the fibrosis formation in the CF-EHTs or on the differences between the genotypes could be detected.

Therefore, the contractility of CF-EHTs composed of 90% ERC001 hiPSC-derived WT cardiomyocytes and 10% ERC001 hiPSC-derived cardiac fibroblasts, either WT, Enh KO or Gene KO, which were cultured according to the established fibrosis model, was analysed (Figure 46).

For readability of the contractility analysis, only the data of the inhibited CF-EHTs and the high serum activated CF-EHTs are displayed. Nevertheless, the contractility of the control CF-EHTs and the TGF- $\beta$ 1 activated CF-EHTs was measured and analysed as well. The resting length, relaxation velocity and 80% relaxation time of all CF-EHTs, including the control CF-EHTs and the TGF- $\beta$ 1 activated CF-EHTs, on the last day of culture, together with the analysis of the beating frequency, can be found in the supplements (section 10.1.12.3).

All inhibited CF-EHTs generated significantly more force than their activated counterparts. The activated WT CF-EHTs generated significantly less force than the activated Enh KO and Gene KO CF-EHTs.

Regardless of the genotype, the inhibited CF-EHTs had a longer resting length than their activated counterparts at the end of the culture time. The activated WT CF-EHTs had a significantly shorter resting length than either the activated Enh KO or Gene KO CF-EHTs.

All inhibited CF-EHTs had a higher relaxation velocity than their activated counterparts. The activated WT CF-EHTs had a significantly lower relaxation velocity than either the activated Enh KO or Gene KO CF-EHTs.

The inhibited WT and Enh KO CF-EHTs had a significantly shorter 80% relaxation time than their activated counterparts. There was no difference in the 80% relaxation time of the inhibited Gene KO CF-EHTs compared to the activated Gene KO CF-EHTs. The activated WT CF-EHTs had a significantly longer 80% relaxation time than either the activated Enh KO or Gene KO CF-EHTs.

The activated CF-EHTs had a tendency towards contracting with a higher frequency than their inhibited counterparts, though this finding was only significant for the Gene KO CF-EHTs (supplement section 10.1.14.3).

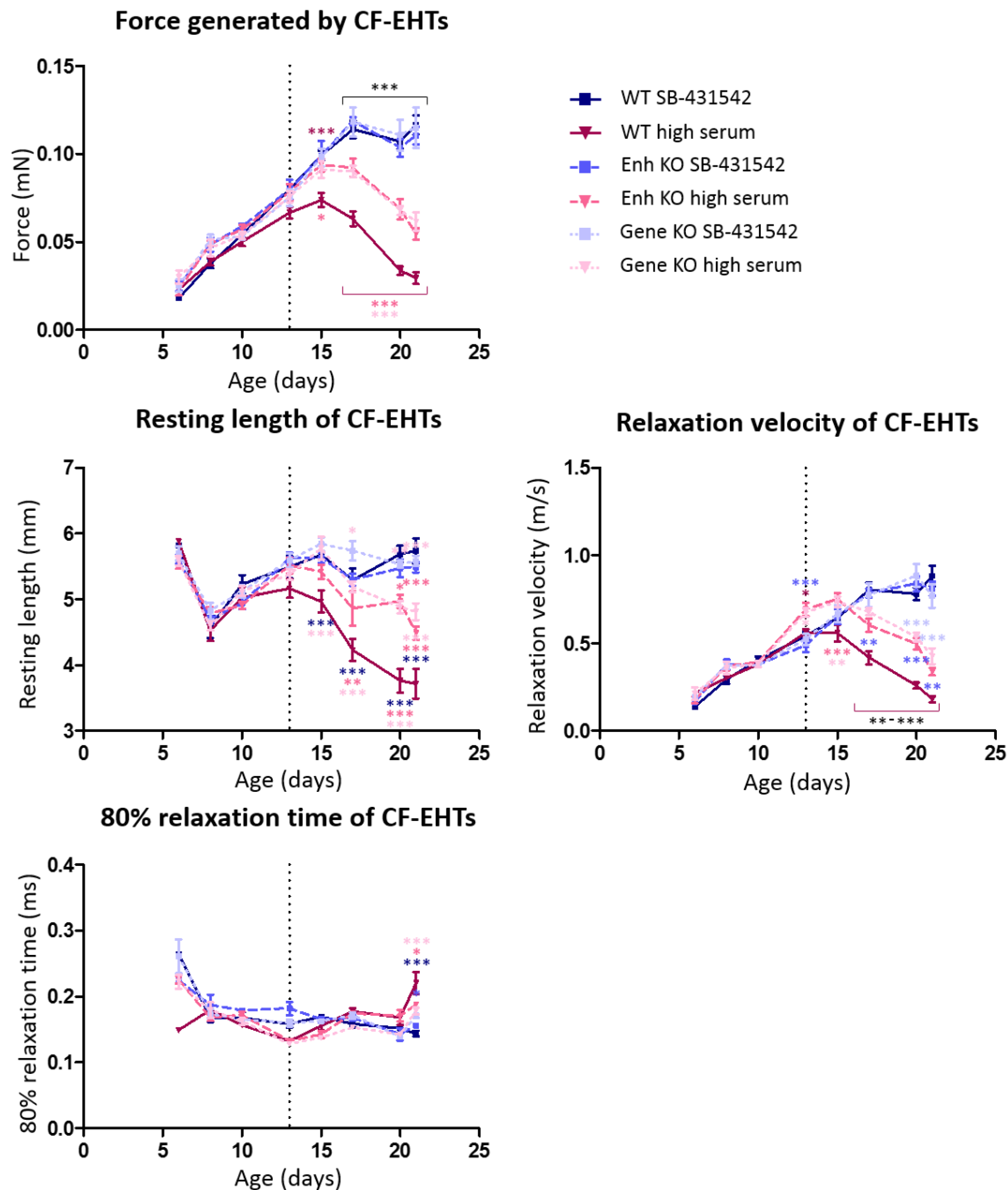


Figure 46: Contractility analysis of ERC001 WT, Enh KO and Gene KO CF-EHTs, assigned to either an inhibited group, treated with 5  $\mu$ M SB-431542, or an activated group, exposed to 10% serum containing medium, and treated as previously described.

*The CF-EHTs were harvested on day 21. The development of the generated force, resting length, relaxation velocity and 80% relaxation time of the CF-EHTs are presented over time. Data are presented as mean  $\pm$  SEM, \* $p < 0.05$ , \*\* $p < 0.005$ , \*\*\* $p < 0.001$  by two-way ANOVA plus Bonferroni's post-test for multiple comparisons, only biologically meaningful comparisons are shown,  $n = 6$  per group.*

This contractility analysis not only argued for the suitability of the *in vitro* fibrosis model, but also revealed significant differences between the genotypes. The activated Enh KO and Gene KO CF-EHTs had a significantly longer resting length, higher relaxation velocity and shorter 80% relaxation time than the activated WT CF-EHTs, which argued for attenuated fibrosis in the activated Enh KO and Gene KO CF-EHTs compared to the activated WT CF-EHTs.

The CF-EHTs of all genotypes were further analysed to determine whether this difference between the genotypes was present only in the contractility of the CF-EHTs, or whether a difference would also be present in different molecular analyses.

#### 3.2.4.4 The mRNA abundance of ERC001 CF-EHTs

To analyse possible pro-fibrotic effects of the different interventions and possible differences between the genotypes, the mRNA abundance of the fibrosis markers collagen1a1, periostin and transgelin, relative to the mRNA abundance of GUSB and the WT control CF-EHTs, was assessed in the ERC001 CF-EHTs (Figure 47; for the mRNA abundance analysis of collagen1a2, CCN2 and ACTA2 see supplement section 10.1.14.4).

The fibrosis markers collagen1a1, periostin and transgelin showed a clear difference in mRNA abundance when comparing the inhibited CF-EHTs to the activated CF-EHTs, regardless of the genotype. For each of these fibrosis markers, in all genotypes, the lowest amount of mRNA was present in the inhibited CF-EHTs, followed by the control CF-EHTs, and the highest mRNA abundance was present in the activated CF-EHTs.

The mRNA abundance of all fibrosis markers significantly differed between the conditions in the WT CF-EHTs. In contrast to that, mRNA levels only significantly differed between the conditions in the Enh KO and Gene KO CF-EHTs for periostin and transgelin.

Differences between the genotypes were primarily detected in the mRNA abundance of collagen1a1 and periostin. For each of these fibrosis markers, both the TGF- $\beta$ 1 activated WT CF-EHTs and the high serum activated WT CF-EHTs displayed a significantly higher abundance of mRNA, compared to the TGF- $\beta$ 1 activated Enh KO and Gene KO CF-EHTs and the high serum activated Enh KO and Gene KO CF-EHTs, respectively.

Similar trends were displayed in the mRNA abundance of collagen1a2, CCN2 and ACTA2 (supplement section 10.1.14.4).

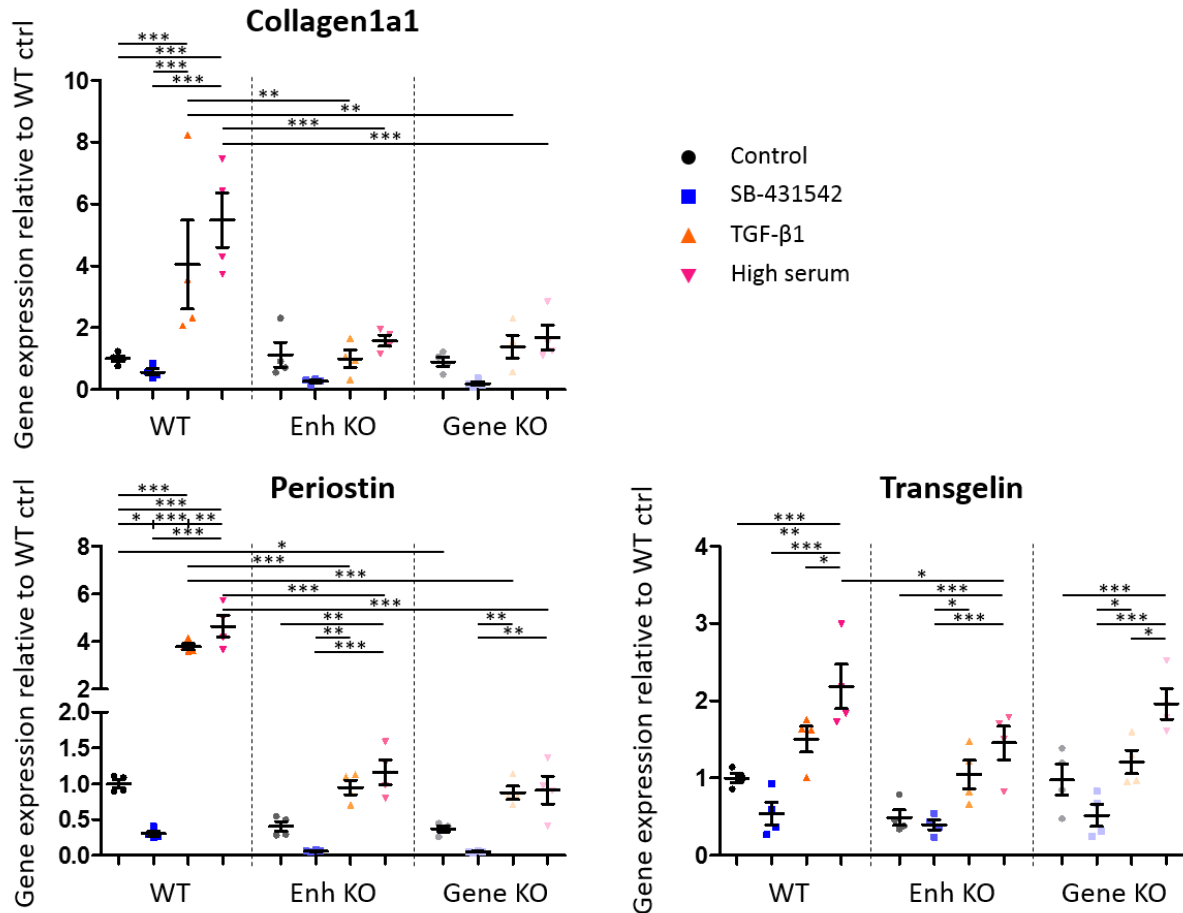


Figure 47: The mRNA abundance relative to GUSB and WT control of the fibrosis markers collagen1a1, periostin and transgelin in ERC001 WT, Enh KO and Gene KO CF-EHTs. The CF-EHTs were assigned to either a control group, an inhibited group, or 1 of 2 activated groups, and treated as previously described. The CF-EHTs were harvested on day 21. Data are presented as mean  $\pm$  SEM, \* $p < 0.05$ , \*\* $p < 0.005$ , \*\*\* $p < 0.001$  by two-way ANOVA plus Bonferroni's post-test for multiple comparisons, only biologically meaningful comparisons are shown,  $n = 4$  per group.

Whereas in the mRNA abundance analysis of the A18945 CF-EHTs differences between the genotypes were sporadic, in the mRNA abundance analysis of the ERC001 CF-EHTs, differences between the genotypes were more frequent and more consistent, as the expression of multiple fibrosis markers was significantly higher in the WT CF-EHTs. Furthermore, where activated WT CF-EHTs often expressed significantly more mRNA of the fibrosis markers than the inhibited WT CF-EHTs, a significant difference between the activated and inhibited CF-EHTs was not always present in the Enh KO or the Gene KO CF-EHTs.

These findings argued for attenuated fibrosis in the activated Enh KO and Gene KO CF-EHTs, compared to the activated WT CF-EHTs. Differences between the Enh KO CF-EHTs and the Gene KO CF-EHTs were not detected.

#### 3.2.4.5 Protein expression of ERC001 CF-EHTs

To again quantify a possible pro-fibrotic effect of the different treatments and to further analyse possible differences between the genotypes, periostin and  $\alpha$ SMA protein abundance were quantified in the ERC001 CF-EHTs. Both periostin and  $\alpha$ SMA were quantified relative to the band size of the housekeeping protein lamin A/C (Figure 48) and the average batch abundance.



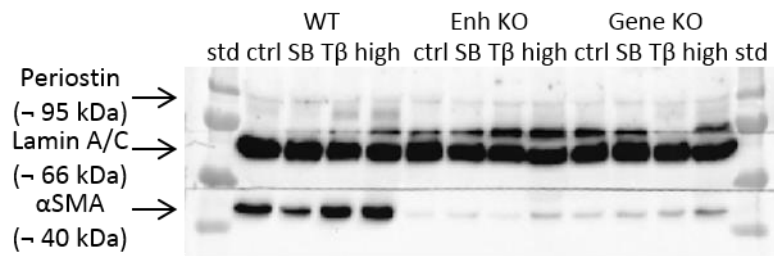


Figure 48: Western blot analysis. Periostin was visible at 95 kDa, lamin A/C at 66 kDa and αSMA at 40 kDa. Lane 1: protein size standard. Lane 2 to 5: WT CF-EHTs, in order: control, inhibited, TGF-β1 activated and high serum activated. Lane 6 to 9: Enh KO CF-EHTs, in order: control, inhibited, TGF-β1 activated and high serum activated. Lane 10 to 13: Gene KO CF-EHTs, in order: control, inhibited, TGF-β1 activated and high serum activated. Lane 14: protein size standard.

Both periostin and αSMA abundance (Figure 49) demonstrated a significant difference when comparing the inhibited WT CF-EHTs to the activated WT CF-EHTs. The inhibited WT CF-EHTs also expressed significantly less αSMA protein than the control WT CF-EHTs. The periostin expression in the Enh KO CF-EHTs and the Gene KO CF-EHTs displayed a similar trend, but the difference was only significant between the inhibited Gene KO CF-EHTs and the high serum activated Gene KO CF-EHTs. The expression of αSMA in the Enh KO CF-EHTs and the Gene KO CF-EHTs was similar in all the CF-EHTs, regardless of the treatment.

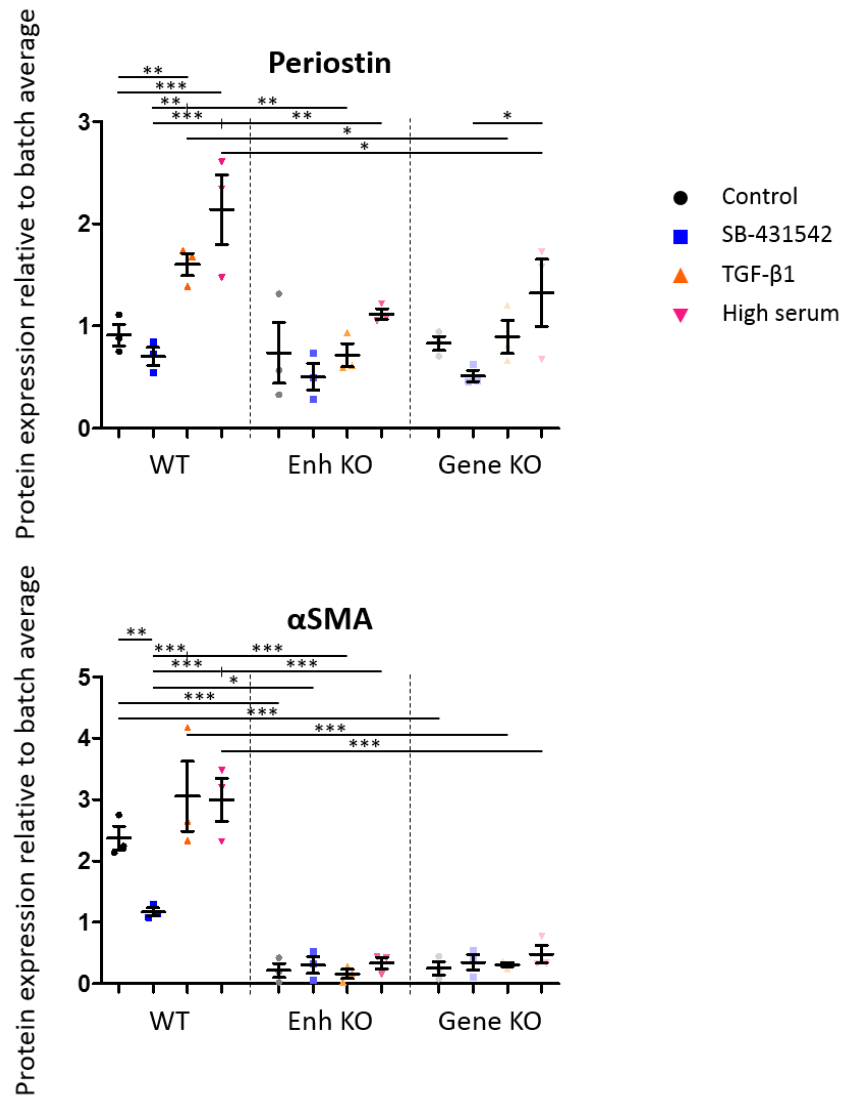


Figure 49: Protein quantification of periostin and  $\alpha$ SMA by Western blot, relative to lamin A/C and batch average, in WT, Enh KO and Gene KO CF-EHTs. The CF-EHTs were assigned to either a control group, an inhibited group, or 1 of 2 activated groups, and treated as previously described. The CF-EHTs were harvested on day 21. Data are presented as mean  $\pm$  SEM, \* $p$ <0.05, \*\* $p$ <0.005, \*\*\* $p$ <0.001 by two-way ANOVA plus Bonferroni's post-test for multiple comparisons, only biologically meaningful comparisons are shown,  $n$ =3 per group.

Similar to the findings in the mRNA abundance analysis, a striking difference in the protein levels of periostin and  $\alpha$ SMA was present between the WT CF-EHTs and the Enh KO and Gene KO CF-EHTs. Secondly, while activated WT CF-EHTs expressed significantly more periostin and  $\alpha$ SMA than inhibited WT CF-EHTs, this higher protein level was not present for  $\alpha$ SMA in activated Enh KO or Gene KO CF-EHTs.

These findings again argued for attenuated fibrosis in the activated Enh KO and Gene KO CF-EHTs, compared to the activated WT CF-EHTs.

## 4. Discussion

The aim of this work was to develop an EHT based *in vitro* 3D fibrosis model and study mechanisms of cardiac fibrosis with a special emphasis on a recently identified putative pro-fibrotic enhancer. The model comprised a co-culture of hiPSC-derived cardiomyocytes and hiPSC-derived cardiac fibroblasts at a 9:1 ratio, cast together to form CF-EHTs. A high dynamic range of regulation was an important requirement of this model, which was obtained by optimizing a quiescent baseline on the one hand and pro-fibrotic treatment conditions on the other hand. In light of this high dynamic range of regulation, the developed model was suitable to study the effect of genetic interventions on fibrosis formation. To quantify fibrosis formation, among others, contractility parameters and the mRNA abundance of fibrosis markers in the CF-EHTs were assessed. The model was used to study both the consequences of a genetic deletion of the *RUNX1*-related enhancer sequence *enh35232* and the effect of a knockout of the *RUNX1* gene in cardiac fibroblasts. The fibrosis formation in the respective knockout CF-EHTs subjected to pro-fibrotic treatment conditions was compared to fibrosis formation in CF-EHTs composed of WT cardiac fibroblasts.

### 4.1 Fibrosis model development

In the first part of this study, optimal conditions for the *in vitro* 3D EHT based fibrosis model were determined.

#### 4.1.1 Quiescent baseline

##### 4.1.1.1 Quiescent cardiac fibroblasts

To allow for a high dynamic range of regulation, a quiescent baseline of the model was necessary, starting with the differentiation of quiescent cardiac fibroblasts.

Cardiac fibroblasts were first derived from hiPSCs according to a previously established in-house protocol (Pan, 2022; Werner, 2018). The obtained cardiac fibroblasts displayed contractile stress fibres and a high mRNA abundance of collagen1a1, periostin and ACTA2, suggesting an activated phenotype at baseline. To obtain a more quiescent baseline for the fibrosis model, the suitability of a novel differentiation protocol for hiPSC-derived quiescent cardiac fibroblasts which had recently been published, was investigated (H. Zhang et al., 2019). The cells obtained with the quiescent protocol indeed expressed less mRNA of the fibroblast activation markers collagen1a1, periostin and ACTA2 (Figure 10). The lack of specific, ubiquitous markers for cardiac fibroblasts (Bursac & J. Kim, 2014) renders it difficult to ascertain with certainty whether the cells differentiated with the quiescent cardiac fibroblast differentiation protocol, were indeed cardiac fibroblasts rather than non-cardiac fibroblasts or even poorly defined cell-types. In the original published protocol, the obtained cells were defined as cardiac fibroblasts as they were positive for the early cardiac development related markers GATA4 and TBX20, the epicardial marker TCF21 and for markers highly expressed in cardiac fibroblasts, but also in other fibroblasts; collagen1a1, DDR2, vimentin and periostin (H. Zhang et al., 2019). In a similar fashion, compared to the mRNA abundance in hiPSCs and primary foreskin fibroblasts, the cells differentiated according to the quiescent protocol in this work expressed more mRNA of the markers TCF21, collagen1a1 (Figure 11), GATA4, DDR2 and vimentin (Figure 29). Additionally, compared to hiPSCs, the differentiated cells expressed more mRNA of the fibroblast markers TBX18 and WT1 (Figure

11), and at least 56% of the differentiated cells were sufficiently positive for DDR2, as measured with flow cytometry (Figure 30 and Figure 42). Considering the genotype analysis and the amount of DDR2<sup>+</sup> cells, we felt confident to say that the majority of the cells differentiated with the quiescent cardiac fibroblast differentiation protocol, indeed displayed a cardiac fibroblast phenotype.

ACTA2 and transgelin were investigated as fibrosis markers. However, these markers are also highly expressed in smooth muscle cells (H. Zhang et al., 2019). Though activated CFs closely resemble a smooth muscle cell phenotype (Beauchamp et al., 2020; Tomasek et al., 2002), it was also possible that a part of the mRNA abundance of these genes would be attributable to partial differentiation of the hiPSCs towards smooth muscle cells, rather than cardiac fibroblasts. The phenotypes could have been further differentiated by studying the expression of, e.g., myosin heavy chain 11 (encoded by *MYH11*), a smooth muscle cell marker (Babij et al., 1991; Ruan et al., 2021) which is rarely expressed in (myo)fibroblasts (Desmoulibre et al., 1996; Eddy et al., 1988).

The previously published quiescent cardiac fibroblast differentiation protocol was adapted for suitability for the laboratory in which this work was performed, first by culturing the hiPSCs in FTDA medium instead of Essential E8 medium prior to the differentiation. Both media have proven to enable robust maintenance and proliferation of hiPSCs in an undifferentiated state (G. Chen et al., 2011; Frank et al., 2012). As FTDA was more affordable than Essential E8 and more commonly used, the transition was important to increase the approachability of the quiescent fibroblast differentiation protocol. The protocol was further amended by seeding the cells on GTX coated cell culture vessels rather than MG coated ones during differentiation. Though GTX and MG are similar, GTX may be more consistent in composition (Gargotti et al., 2018) and was again more commonly used. No differences in morphology were observed in cells undergoing the cardiac fibroblast differentiation protocol, depending on hiPSCs cultivation either in FTDA or Essential E8 prior to the start of the differentiation, or on seeding on GTX or MG coated cell culture vessels (supplement section 10.1.1).

#### 4.1.1.2 Serum depletion

To further optimize the quiescence of the cardiac fibroblasts during culture in the CF-EHTs, the possibility to deplete serum from the culture medium was investigated, as culturing fibroblasts in high serum conditions can lead to transdifferentiation into myofibroblasts (Swaney et al., 2005). In line with the literature, also in our hands fibroblasts cultured in 10% serum containing medium more abundantly expressed the fibrosis markers collagen1a1, periostin and CCN2, compared to fibroblasts cultured in either 0% or 0.5% serum containing medium (Figure 13 and Figure 14). As serum deprivation has been associated with cardiomyocyte apoptosis (Sheng et al., 1997), it was investigated whether CF-EHTs could be maintained in 0.5% serum containing medium for long term culture, rather than 0% serum containing medium.

CF-EHTs continuously cultured in 10% serum containing medium generated a higher force than CF-EHTs cultured in medium in which the serum was depleted. However, the force generated by CF-EHTs cultured in 0.5% serum containing medium from day 3 on only decreased on day 33, arguing for the suitability of 0.5% serum containing medium for CF-EHT culture for at least 4 weeks (Figure 16). Hence, it was decided that experiments on CF-EHTs cultured in 0.5% serum containing medium would be performed within 21 or 22 days, to avoid a reduction in force as a result of a potential loss of cardiomyocytes or cardiomyocyte damage in the CF-EHTs.

#### 4.1.1.3 SB-431542 treatment

Even when serum was depleted, CF-EHTs still exhibited signs of fibroblast activation (mRNA analysis in supplement section 10.1.3). A possible explanation for this observation was the mechanical stretch exerted on the cardiac fibroblasts during culture between the 2 flexible posts, as mechanical stretch can cause fibroblast activation (Walker et al., 2020). To counteract the high baseline activation, further quiescence of the CF-EHTs was desired. For practical reasons, the matrix and geometry of the CF-EHTs were however not altered.

From the 2D fibroblast activation experiments, the conclusion was drawn that treatment with the TGF- $\beta$ 1 receptor inhibitor SB-431542 led to a continuous quiescence of the CFs, indicated by attenuated expression of the fibrosis markers collagen1a1, CCN2 and ACTA2 (Figure 18). SB-431542 is a competitive inhibitor most specific for the TGF- $\beta$ 1R1 kinase ALK5, for which it has a half maximal inhibitory concentration of 0.75  $\mu$ M (SB-431542 [301836-41-9], 2023). ALK5 is part of the Smad-dependent pathway in which TGF- $\beta$ 1 can induce the expression of  $\alpha$ SMA, which promotes the transdifferentiation of cardiac fibroblasts into myofibroblasts (Desmouliere et al., 1996; H.-H. Hu et al., 2018). Inhibition of ALK5 led to attenuated  $\alpha$ SMA expression and transdifferentiation of cardiac fibroblasts into myofibroblasts (X. Yang et al., 2014). Owing to these observations SB-431542 is frequently used in cardiac fibroblast research to inhibit activation (Law & Carver, 2013), or even to reverse fibroblast activation (Hall et al., 2023).

As SB-431542, used in a final concentration between 1  $\mu$ M and 10  $\mu$ M, was dissolved in DMSO, between 0.01% and 0.1% (v/v) DMSO was also added to the culture medium. DMSO has been reported to be toxic for skin fibroblasts at concentrations of 0.5% to 3%, but safe at concentrations of 0.1% and lower. The proliferation of skin fibroblasts even increased when they were treated with 0.01-0.1% DMSO (Singh et al., 2017). DMSO can also be toxic for cardiomyocytes, though the reported toxic concentration is highly variable. The toxicity threshold was reported to be as low as  $\geq 0.1\%$  (A. Sharma et al., 2018), but other reports have indicated that concentrations of DMSO up to 0.3% did not affect cell death or electrophysiological parameters in hiPSC-derived CMs (Hyun et al., 2017; M. Yang et al., 2019). A reduced contractile force and an enhanced contraction frequency have been reported in hiPSC-derived CMs at DMSO concentrations of  $>0.1\%$  (Himmel, 2013). In 3D maturing cardiac models, DMSO has altered miRNA and epigenetic landscape, even at 0.1% DMSO (Verheijen et al., 2019). In cardiomyoblasts, no cytotoxic effects of DMSO were detected at a concentration of  $\leq 0.5\%$  (Sangweni et al., 2021).

Treatment with 10  $\mu$ M SB-431542 and accordingly 0.1% DMSO starting from day 0 led to a lower generated force in both CF-EHTs and EHTs, compared to untreated control CF-EHTs and EHTs, respectively. A similar trend indicating a lower generated force was observed in CF-EHTs and EHTs treated with only 5  $\mu$ M SB-431542 (Figure 20 and supplement section 10.1.6). Treatment with 10  $\mu$ M SB-431542 starting from day 8 caused a slight, but not significant, decrease in the force generated by CF-EHTs, whereas treatment with 5  $\mu$ M SB-431542 starting from day 8 had a negligible effect on the force generated by the CF-EHTs (supplement section 10.1.8). Treatment with 1  $\mu$ M SB-431542 had no effect on the force generated by the (CF-)EHTs, regardless of when the treatment started (Figure 20 and supplement sections 10.1.6 and 10.1.8). The effect of the treatment with 10  $\mu$ M SB-431542 on the generated force may in part be attributable to cytotoxicity caused by the 0.1% DMSO concentration, though previous experiments with DMSO had not argued for significant toxicity. Instead, DMSO treated EHTs generated more force than control EHTs (Rhoden et al., 2021). Similarly, CF-EHTs generated more

force when they were treated with 1  $\mu$ M SB-431542 from day 3 onwards and 5  $\mu$ M SB-431542 from day 10 onwards, or 5  $\mu$ M SB-431542 from day 15 onwards, compared to untreated control CF-EHTs (Figure 22).

In the final fibrosis model, all CF-EHTs, regardless of the group they were assigned to, were treated with 5  $\mu$ M SB-431542 from day 10 to day 13, meaning all CF-EHTs were exposed to 0.05% DMSO for 72 hours. The quiescent CF-EHTs were then continuously exposed to 0.05% DMSO for another 8 to 9 days. In the first batch of A18945 CF-EHTs, the quiescent CF-EHTs generated less force than the control CF-EHTs (supplement section 10.1.9.1). However, when looking at the analysis of ERC001 and ERC018 CF-EHTs, the quiescent CF-EHTs generated a force comparable to the force generated by the control CF-EHTs (supplement sections 10.1.9.2 and 10.1.9.3). ERC018 CF-EHTs treated with SB-431542 contracted with a higher frequency than the control CF-EHTs (supplement section 10.1.9.3), whereas A18945 and ERC001 CF-EHTs treated with SB-431542 contracted at a similar frequency as the control CF-EHTs (supplement section 10.1.9.1 and 10.1.9.2). These findings suggested that the contractility of the CF-EHTs was not affected by possible toxic effects caused by long term exposure to 0.05% DMSO.

The SB-431542 treated CF-EHTs did exhibit a longer resting length, higher relaxation velocity and shorter 80% relaxation time than either the activated CF-EHTs or the control CF-EHTs, which were all signs of attenuated fibrosis formation in the SB-431542 treated CF-EHTs. In other words, the SB-431542 treated CF-EHTs were more quiescent than either the activated or the control CF-EHTs.

In summary, a quiescent baseline was established as a starting point for the fibrosis model, to allow for a high dynamic range of activation. The quiescent baseline was obtained by differentiating explicitly quiescent cardiac fibroblasts, depleting the serum concentration in the culture medium from 10% to 0.5% and additional pre-treatment with the TGF- $\beta$ 1 receptor inhibitor SB-431542.

#### 4.1.2 Fibroblast activation

On the other end of the dynamic range the cardiac fibroblasts needed to be activated to generate a fibrosis model in which a possible attenuating effect on fibrosis development could be detected with sufficient sensitivity. Multiple methods of activation were investigated in 2D cultured cardiac fibroblasts, including treatment with PDGF-AA, angiotensin II and a combination of phenylephrine and endothelin 1 (Figure 18). Though these treatments had been previously reported to activate fibroblasts (Broekmans et al., 2020; Fullerton & Funder, 1994; Kemp et al., 2004; L. Wang et al., 2017), we did not observe an induction of the fibrosis markers collagen1a1, CCN2 or ACTA2. We did however observe significantly elevated levels of these fibrosis markers after treatment with TGF- $\beta$ 1 (Figure 18), a classical inductor of fibroblast activation and transdifferentiation into myofibroblasts (Bracco Gartner et al., 2019, 2022; Cho et al., 2018; Cumberland et al., 2023; Iseoka et al., 2021; Lee et al., 2019; Mastikhina et al., 2020; Sadeghi et al., 2017).

Another effective method of fibroblast activation was exposing the fibroblasts to high serum concentrations. As previously stated, it was decided to deplete serum from the culture medium, as serum components can lead to the transdifferentiation of cardiac fibroblasts into myofibroblasts (Swaney et al., 2005; Tao et al., 2016). Though it remains to be fully defined which serum components exactly lead to the activation of fibroblasts, there are multiple compounds present in serum related to

the activation of cardiac fibroblasts (Booz & Baker, 1995). Serum comprises multiple growth factors, such as PDGF, TGF- $\beta$ 1 and VEGF (Czarkowska-Paczek et al., 2006; Schuler et al., 1999), which could contribute to fibroblast activation (M. Zeisberg et al., 2000). Retinol is reported to be attributable to fibroblast activation and is also present in serum (Y. Chen et al., 1997). Moreover, multiple cytokines and chemokines can lead to fibroblast activation (Wei et al., 2021), of which several can be present in serum, such as TNF- $\alpha$  and IL-1 (Di Iorio et al., 2003; Mussi et al., 1997). Other cytokines present in serum which have been related to fibroblast activity include IL-13 and IL-33 (Y. Sun et al., 2021; Wijnenbeek et al., 2018; Wulff et al., 2019). Furthermore, serum can contain ACE2, angiotensin II and aldosterone (Rieder et al., 2020), which, as previously mentioned, can contribute to fibrosis formation by induction of TGF- $\beta$ 1 (Bertaud et al., 2023; Brilla et al., 1994; Fullerton & Funder, 1994; Lijnen & Petrov, 2000). It is additionally likely that serum contains other fibroblast inducing compounds. One pathway in which these compounds could lead to fibroblast activation, is the serum response factor, a transcription factor (Chai & Tarnawski, 2002; Misra et al., 1991) linked to TGF- $\beta$ 1 induced fibroblast activation, including the formation of stress fibres (Angelini et al., 2015; Olsson et al., 2023; Sisson et al., 2015).

In light of the different ways serum can stimulate fibrosis formation, in addition to TGF- $\beta$ 1 treatment, a second activation group was included, in which the CF-EHTs were exposed to 10% serum containing medium. Indeed, a higher abundance of mRNA of the fibrosis markers collagen1a1, periostin and transgelin was detectable in CF-EHTs exposed to 10% serum containing medium compared to control CF-EHTs exposed to 0.5% serum containing medium (Figure 26).

When comparing the effect of TGF- $\beta$ 1 activation to the effect of high serum activation on the CF-EHTs, the contractility of the CF-EHTs was more affected by exposure to 10% serum containing medium than by treatment with TGF- $\beta$ 1. CF-EHTs exposed to high serum had a significantly shorter resting length, lower relaxation velocity and longer 80% relaxation time than quiescent CF-EHTs. Though the same trends were observed in CF-EHTs treated with TGF- $\beta$ 1 compared to quiescent CF-EHTs, the only significant difference was the resting length of the CF-EHTs. The CF-EHTs exposed to 10% serum containing medium had a significantly longer 80% relaxation time than the CF-EHTs treated with TGF- $\beta$ 1 (Figure 25). Messenger RNA of multiple fibrosis markers was also more abundant in CF-EHTs exposed to high serum than in CF-EHTs treated with TGF- $\beta$ 1, with a significant difference in the mRNA abundance of transgelin (Figure 26).

These results suggested that the combination of components present in the high serum conditions activated the cardiac fibroblasts in the CF-EHTs more than direct activation by TGF- $\beta$ 1. Direct activation by TGF- $\beta$ 1 treatment can activate cardiac fibroblasts through a Smad-dependent or independent pathway (H.-H. Hu et al., 2018; Humeres et al., 2022; Papakrivopoulou et al., 2004; M. Tang et al., 2007; Wojciechowski et al., 2017). As mentioned, serum activation has also been linked to TGF- $\beta$ 1 induced fibroblast activation, which was possibly responsible for part of the serum-associated activation in this work (Angelini et al., 2015; Olsson et al., 2023; Rieder et al., 2020; Sisson et al., 2015).

#### 4.1.3 Fibrosis model validation

##### 4.1.3.1 Contractility

We established an *in vitro* 3D EHT based fibrosis model with a control condition, an inhibited condition continuously treated with SB-431542 and 2 activated conditions; treated with TGF- $\beta$ 1 or exposed to



10% serum containing medium. A thorough evaluation of this model was performed with CF-EHTs composed of CMs and CFs derived from 3 different hiPSC lines.

One of the characteristics of cardiac fibrosis is increased remodelling of the ECM (Schimmel et al., 2022), which here was observed as shortening of the resting length of the activated CF-EHTs, both over time and compared to quiescent CF-EHTs. The resting length of both the TGF- $\beta$ 1 activated CF-EHTs and the high serum activated CF-EHTs was shorter than the resting length of the quiescent CF-EHTs (Figure 25).

Increased ECM deposition, or scar formation, can cause impaired electrical conduction of the heart (de Bakker et al., 1993; Hinderer & Schenke-Layland, 2019; Miragoli et al., 2006) and increased remodelling of the ECM can lead to impaired relaxation of the heart tissue (Schimmel et al., 2022). Indeed, a relaxation deficit was observed in the activated CF-EHTs, evident as both a lower relaxation velocity and a longer 80% relaxation time. In accordance with increased remodelling, the relaxation deficit could have been caused by a higher stiffness of the CF-EHTs as a result of increased ECM deposition, similar to the effect of an increased ECM deposition in the heart (Zile et al., 2015). Though cardiac fibroblasts are non-excitabile, i.e. cannot generate an AP, cardiac fibroblasts and cardiomyocytes are able to electrically couple to propagate the AP through the heart (Quinn et al., 2014). Though the exact mechanism behind the coupling and its biological relevance is not entirely resolved (Mahoney et al., 2016; Y. Wang et al., 2023), coupling is observed to partially occur via gap junctions and the formation of nanotubes (Rog-Zielinska et al., 2016). The action potential needed to excite cardiomyocytes is also conducted through cardiac fibroblasts. In part, electrical signals to conduct the AP may be transmitted through nanotubes, as calcium signals can be propagated through these nanotubes from CMs to CFs and vice versa (He et al., 2011). Activated cardiac fibroblasts have a more stretched morphology than quiescent cardiac fibroblasts. Stretched cardiac fibroblasts in turn are hyperpolarized compared to quiescent cardiac fibroblasts (Kamkin et al., 2003; Rog-Zielinska et al., 2016). Hyperpolarization of the cardiac fibroblasts, when coupled to cardiomyocytes, could potentially lead to a delay in the conduction of the action potential, as it would take longer to depolarize these cardiac fibroblasts, which could provide a further explanation behind the relaxation deficit.

Different signs of fibrosis formation in the activated A18945 and ERC001 CF-EHTs were observed in the contractility analysis. For example, the quiescent CF-EHTs had a significantly longer resting length at the end of the culture time than the activated CF-EHTs. Furthermore, the high serum activated CF-EHTs had a significantly lower relaxation velocity and longer 80% relaxation time than the quiescent CF-EHTs (Figure 25).

The generally shorter resting length, lower relaxation velocity and longer relaxation time of CF-EHTs from activated groups were thus indicators on a contractility level, which argued for a more fibrotic phenotype in these CF-EHTs and moreover indicated the suitability of the developed *in vitro* 3D EHT based fibrosis model.

#### 4.1.3.2 mRNA abundance

Messenger RNA of the fibrosis markers collagen1a1, periostin and transgelin was more abundant in the activated A18945 and ERC001 CF-EHTs than in their quiescent counterparts (Figure 26). One outcome did not fit to the others and the concept: Messenger mRNA of ACTA2 was unexpectedly most abundant in the quiescent A18945 CF-EHTs (supplement section 10.1.9.1). However, in the other cell line,



ERC001, ACTA2 mRNA was significantly more abundant in high serum activated CF-EHTs than in quiescent CF-EHTs (supplement section 10.1.9.2). Though of particular importance, as only ACTA2 of the 5 analysed fibrosis markers was not more abundant in the activated CF-EHTs in only 1 of the 2 cell lines, these findings together still suggested that the activated CF-EHTs, especially the high serum activated CF-EHTs, were more fibrotic than the quiescent CF-EHTs, confirming the suitability of the developed 3D EHT based *in vitro* fibrosis model at mRNA abundance level.

#### 4.2 Assessment of potential anti-fibrotic genetic interventions in the fibrosis model

The fibrosis model was implemented to investigate the effect of the genetic deletion of the *RUNX1*-related enhancer sequence *enh35232* and the knockout of *RUNX1* in cardiac fibroblasts. Both knockouts were implemented in 2 different hiPSC lines each: the A18945 hiPSC line and the ERC001 hiPSC line. In the A18945 hiPSC line, DNA sequences were targeted by the CRISPR guide RNAs, which encompassed a 250 bp DNA sequence including a substantial portion of *enh35232* (in the conventional direction of DNA from 5' to 3' end of its backbone). In the ERC001 hiPSC line, a different DNA sequence located 3' of the sequence deleted in the A18945 line was targeted. This targeting strategy led to a deletion of 100 bp of the enhancer sequence at the 3' end in ERC001 hiPSCs. The sequence data, including both *enh35232* knockouts, can be found in the supplements (section 10.1.15). A significant deletion of any part of an enhancer sequence can influence the activity of the enhancer, hence the partial KO in the ERC001 line could also have had an influence on the fibrosis formation in the CF-EHTs.

##### 4.2.1 2D cultured cardiac fibroblasts

The effect of the knockouts was first investigated in a simplified 2D version of the fibrosis model.

###### 4.2.1.1 mRNA abundance

The mRNA analysis of the A18945 CFs revealed a higher abundance of collagen1a1, periostin and transgelin mRNA in the TGF- $\beta$ 1 activated CFs compared to the quiescent CFs, regardless of the genotype. A trend indicating a lower abundance of the fibrosis markers in all conditions of the Gene KO CFs compared to the WT and Enh KO CFs was visible, suggesting attenuated activation of the Gene KO cardiac fibroblasts. No consistent differences were visible between the WT CFs and the Enh KO CFs (Figure 32).

###### 4.2.1.2 Protein analysis

In the protein analysis of the 2D cultured A18945 CFs, we observed a tendency towards a higher level of periostin in activated compared to quiescent Enh KO CFs and Gene KO CFs, but not in the WT CFs. A high variability was present in the periostin expression in the quiescent WT CFs (Figure 34). In the 2D cultured ERC001 CFs, activated CFs tended to express more periostin than quiescent CFs, regardless of the genotype (Figure 44).

With regard to the other assessed activation marker,  $\alpha$ SMA, comparing conditions in the A18945 CFs, more  $\alpha$ SMA was only present in the activated Enh KO CFs compared to the quiescent Enh KO CFs (Figure 34), but not in any other comparison between conditions in any genotype. In the other cell line, ERC001

CFs, the situation was different. Here, a higher level of  $\alpha$ SMA was observed in the TGF- $\beta$ 1 activated CFs compared to the quiescent CFs in both the WT CFs and the Gene KO CFs, but not in the Enh KO CFs (Figure 44).

For both cell lines, control Enh KO and Gene KO CFs tended to express less periostin and  $\alpha$ SMA than control WT CFs, with the lowest level of protein in the control Gene KO CFs. These results might point towards an attenuated activation of both the Enh KO cardiac fibroblasts and the Gene KO cardiac fibroblasts compared to the WT cardiac fibroblasts.

#### 4.2.1.3 Flow cytometry

The percentage of  $\alpha$ SMA<sup>+</sup> CFs (of DDR2<sup>+</sup> CFs, to ensure that the analysed cells were predominantly CFs) was measured via flow cytometry. A higher amount of  $\alpha$ SMA<sup>+</sup> DDR2<sup>+</sup> CFs was present in the TGF- $\beta$ 1 activated CFs compared to the quiescent CFs, for all genotypes, WT, Enh KO and Gene KO, in both A18945 and ERC001 CFs (Figure 35 and Figure 45). In the mRNA abundance and the protein expression analyses, the measured baseline expression was highest in the WT CFs, compared to the Enh KO and Gene KO CFs. In the flow cytometry results however, a higher proportion of  $\alpha$ SMA<sup>+</sup> CFs was present in the A18945 Enh KO CFs compared to the A18945 WT CFs. Nevertheless, the baseline proportion of  $\alpha$ SMA<sup>+</sup> CFs was lower in the Gene KO CFs than in the WT CFs in both the A18945 and ERC001 CFs.

Though trends indicated a lower baseline activation in the mRNA abundance analysis and the protein expression analysis for both the Enh KO CFs and the Gene KO CFs compared to the WT CFs, this tendency was not observed in the  $\alpha$ SMA analysis by flow cytometry. It seems that the simplified 2D version of the 3D EHT based fibrosis model was not sensitive enough to detect consistent differences in the activation of the cardiac fibroblasts which could be ascribed to the different genotypes. Cardiac fibroblasts cultured on (stiff) 2D surfaces are known to become more activated than cardiac fibroblasts in a 3D culture (Htwe et al., 2015; Solon et al., 2007). Undesired activation of the cardiac fibroblasts attributable to the culture conditions could have influenced the results.

### 4.2.2 The 3D EHT based fibrosis model

#### 4.2.2.1 Contractility

To expand on the preliminary results from the simplified 2D version of the fibrosis model, multiple batches of A18945 CF-EHTs and 1 batch of ERC001 CF-EHTs underwent the fully developed *in vitro* EHT based 3D fibrosis model protocol.

When examining the contractility analyses of the 2 cell lines (Figure 36 and Figure 46), it is important to note that the values for the A18945 CF-EHT analyses represent the combined contractility data of 4 batches relative to the batch average, whereas the values for the ERC001 CF-EHT analysis represent a single batch.

No difference in force was observed between the activated A18945 CF-EHTs and the inhibited CF-EHTs, whereas the activated ERC001 CF-EHTs generated significantly less force than the quiescent ERC001 CF-EHTs. A significantly lower generated force by fibrotic tissue in a cardiac fibrosis-on-a-chip model has previously been reported (Mastikhina et al., 2020).

As previously described, a shorter resting length, lower relaxation velocity and longer 80% relaxation time were indirect signs of fibrosis formation in the CF-EHTs. A reduced relaxation velocity after treatment with TGF- $\beta$ 1 has more often been observed in cardiac fibrosis models (Iseoka et al., 2021) and similarly a relaxation deficit has previously been linked to cardiac fibrosis formation (Czubryt, 2012; Hinderer & Schenke-Layland, 2019; Murtha et al., 2017).

Similar to in the model validation experiments, in the activated CF-EHTs a shorter resting length, lower relaxation velocity and longer 80% relaxation time were observed, compared to the quiescent CF-EHTs. This indicated elevated fibrosis, in both the A18945 and the ERC001 CF-EHTs (Figure 36 and Figure 46). These results were significant in both cell lines in the WT and the Enh KO CF-EHTs. A similar trend (but without significant differences) towards these elevated signs of fibrosis was observed in the activated A18945 Gene KO CF-EHTs compared to the quiescent A18945 Gene KO CF-EHTs. However, no difference was detected with regard to the 80% relaxation time of the activated ERC001 Gene KO CF-EHTs compared to the quiescent ERC001 Gene KO CF-EHTs. This argued for attenuated fibrosis in the activated Gene KO CF-EHTs compared to the activated WT and Enh KO CF-EHTs, for both the A18945 CF-EHTs and the ERC001 CF-EHTs.

Further signs that argued for attenuated fibrosis in the activated Gene KO CF-EHTs included a significantly shorter 80% relaxation time in the activated Gene KO CF-EHTs than in the activated WT CF-EHTs in both A18945 and ERC001 CF-EHTs. Additionally, both activated Enh KO and Gene KO ERC001 CF-EHTs had a longer resting length and higher relaxation velocity than activated WT ERC001 CF-EHTs. These signs argued that the cardiac fibroblasts in the Enh KO and Gene KO CF-EHTs might have been less activated than the cardiac fibroblasts in the WT CF-EHTs.

(CF-)EHTs were cast between 2 flexible posts. Contraction of the (CF-)EHTs deflected these posts. This deflection was quantified and converted into the force generated by the CF-EHTs (Hansen et al., 2010). As previously stated, fibrosis can cause an increase in the stiffness of the CF-EHTs (Zile et al., 2015). The stiffness of a material is defined as the resistance of that material to deformation after applied force (Clayton, 2011). Hence, in stiffer CF-EHTs, more force is required to move the flexible posts (and deform the tissue) than in more pliable CF-EHTs. Conversely, with a similar force exertion, the posts would deflect less in stiffer CF-EHTs than in more pliable CF-EHTs. This could explain the progressive drop in force that was observed in the activated ERC001 CF-EHTs, regardless of the genotype. Here, the cardiomyocytes embedded in the stiffer, activated ERC001 CF-EHTs might have generated a similar force as those within the more pliable, quiescent CF-EHTs, but this force generation might not have been accurately converted into a deflection of the posts and therefore not been accessible to adequate quantification. Additionally, a post deflection in the activated, shorter, CF-EHTs fractionally similar to a post deflection in the quiescent, longer, CF-EHTs would be measured as a lower generated force in the activated CF-EHTs than in the quiescent CF-EHTs, as the absolute post deflection would have been shorter.

Nevertheless, these contractility results indicated that the ERC001 cell line seemed more sensitive to genetic interventions than the A18945 cell line, as certain significant differences between the genotypes were observed in the contractility analysis of the ERC001 CF-EHTs, which were not observed in the contractility analysis of the A18945 CF-EHTs.

#### 4.2.2.2 mRNA abundance

The mRNA analysis of both the A18945 CF-EHTs and ERC001 CF-EHTs displayed a higher mRNA abundance of the fibrosis markers collagen1a1, periostin and transgelin in the activated CF-EHTs compared to the quiescent CF-EHTs, regardless of genotype (Figure 37 and Figure 47). In the A18945 mRNA abundance analysis, differences between the genotypes were not consistent. However, in the ERC001 CF-EHTs, the mRNA abundance of collagen1a1, periostin, collagen1a2 and ACTA2 was significantly lower in the activated Enh KO and the Gene KO CF-EHTs compared to the activated WT CF-EHTs (Figure 47 and supplement section 10.1.14.4). These results indicated that in the Enh KO cardiac fibroblasts and the Gene KO cardiac fibroblasts activation might have been attenuated. In the ERC001 CF-EHTs, significant differences between the mRNA abundance in activated CF-EHTs and quiescent CF-EHTs were observed for collagen1a1 and ACTA2 in the WT CF-EHTs, while these differences in mRNA abundance were not significant in the Enh KO CF-EHTs or the Gene KO CF-EHTs, again arguing for attenuated fibrosis formation in the Enh KO CF-EHTs and the Gene KO CF-EHTs.

Similar to what was observed in the contractility analysis, the ERC001 CF-EHTs seemed more sensitive to the genetic intervention than the A18945 CF-EHTs.

#### 4.2.2.3 Protein expression

In accordance with the mRNA abundance analysis, a higher expression of periostin was observed in the activated CF-EHTs compared to the quiescent CF-EHTs, for each genotype, in both the A18945 CF-EHTs and the ERC001 CF-EHTs (Figure 39 and Figure 49). A higher expression of  $\alpha$ SMA was also observed in the activated A18945 CF-EHTs compared to the quiescent CF-EHTs for each genotype (Figure 40). The highest abundance was recorded in the high serum activated Gene KO CF-EHTs. In contrast to this, the protein expression analysis of the ERC001 CF-EHTs displayed a significantly lower periostin and  $\alpha$ SMA expression in the activated Enh and Gene KO CF-EHTs compared to the activated WT CF-EHTs (Figure 49). This again suggested a more pronounced response to the genetic interventions in the ERC001 CF-EHTs.

#### 4.2.2.4 Stiffness

Increased ECM deposition, especially of collagen, is a characteristic of cardiac fibrosis, which has been linked to an increase in myocardial stiffness (Zile et al., 2015). In this work, nanoindentation was employed to analyse the stiffness of the CF-EHTs. The resting length of A18945 CF-EHTs varied per batch, attributable to the respective different cardiomyocyte purity of the 4 batches. Activation of cardiac fibroblasts led to extensive remodelling, reflected in this fibrosis model as a decrease in the width and resting length of the CF-EHTs. Shorter CF-EHTs were expected to be stiffer than longer CF-EHTs, as a function of their more compact structure and higher cell density. To account for the variation in the resting length of the CF-EHTs, the stiffness of the CF-EHTs was analysed normalised to their resting length. For each genotype, the activated CF-EHTs had a tendency toward a higher stiffness relative to their length than the control CF-EHTs (Figure 41). A trend indicating that the difference in stiffness between the activated and control WT CF-EHTs was larger than the difference in stiffness between the activated and control CF-EHTs for either the Enh KO CF-EHTs or the Gene KO CF-EHTs was additionally observed, suggesting a possible attenuation of ECM deposition in the Enh KO and Gene KO CF-EHTs.

In the analysis of the 3D EHT based fibrosis model, differences between the genotypes were more pronounced than in the simplified 2D version. Both the Enh KO CF-EHTs and the Gene KO CF-EHTs showed attenuated signs of fibrosis at baseline and after activation compared to the WT CF-EHTs, though these signs were more pronounced and more significant in the ERC001 CF-EHTs.

As previously reported, in the A18945 hiPSC line a substantial portion of the *enh35232* sequence was deleted, whereas in the ERC001 cell line only 100 bp of the enhancer sequence was deleted. Prediction of how a sequence deletion of any part of an enhancer can influence the activity of the enhancer is difficult, hence the partial KO in the ERC001 line could have influenced the fibrosis formation in the CF-EHTs. An important difference between cell lines should be mentioned. While the A18945 hiPSC line had not been previously used for EHT generation, the ERC001 hiPSC line had been extensively used as a control line for EHT generation. ERC001 had been assessed in a cohort with 40 other healthy donor hiPSC lines and found to be most robust in proliferation and cardiomyocyte differentiation (Eschenhagen, 2015; Schulze, 2019). EHTs cast with ERC001 hiPSC-derived cardiomyocytes had the most robust force development and were sufficiently sensitive to drug interventions. It was therefore possible that the ERC001 hiPSC line was more suitable for interventions in EHT models than the A18945 hiPSC line and could have detected the effects of the genetic deletions with higher sensitivity and specificity.

A further possible inconsistency of the data affects ACTA2 expression. Messenger RNA abundance analysis often displayed a higher mRNA abundance of multiple fibrosis markers in activated CFs and CF-EHTs compared to quiescent CFs and CF-EHTs, but not of the fibrosis marker ACTA2. The cardiac fibroblasts were differentiated according to a protocol which focussed on a low expression of ACTA2, to avoid baseline activation and further differentiation into smooth muscle cells. Thus, this protocol yielded cells with a low percentage of  $\alpha$ SMA<sup>+</sup> cells, which remained comparably low even after TGF- $\beta$ 1 activation (H. Zhang et al., 2019), similar to what we observed. This low propensity of  $\alpha$ SMA expression after activation could have limited the suitability of these hiPSC-derived CFs for the model developed in this work.

#### 4.3 Global outlook

Though previous versions of the fibrin based EHT model this work was based on had already been established in 1997 (Eschenhagen et al., 1997), the model has primarily been used as a monoculture of cardiomyocytes. After chicken cardiomyocytes in a collagen matrix had been used, the model was further developed, and later based on neonatal rat heart cells (Hansen et al., 2010) and subsequently hiPSC-derived cardiomyocytes (Eder et al., 2016). To model cardiac fibrosis, co-cultures of cardiomyocytes and cardiac fibroblasts have been established with especially primary rodent cardiomyocytes and cardiac fibroblasts (Fullerton & Funder, 1994; Y. Li et al., 2017; Saini et al., 2015; van Spreeuwel et al., 2017). A co-culture of hiPSC-derived cardiomyocytes and other cell types in the fibrin based EHT, including hiPSC-derived cardiac fibroblasts differentiated via mesoderm induction, was previously established in our laboratory (Werner, 2018). Differentiation of hiPSCs into epicardial

progenitor cells, which could potentially further differentiate into cardiac fibroblasts, has been possible since 2014 (Witty et al., 2014). Protocols for differentiation of hiPSCs into well characterized cardiac fibroblasts were published in 2019, either via second heart field progenitors (J. Zhang et al., 2019) or via epicardial cells, focussing on the differentiation of quiescent cardiac fibroblasts by addition of SB-431542 (H. Zhang et al., 2019).

To develop EHT with a co-culture of cardiomyocytes and cardiac fibroblasts, multiple factors needed to be optimized. These included, but were not limited to, the medium in which the CF-EHTs were cultured, so as to maintain viability of the cardiomyocytes, but to not activate the cardiac fibroblasts at baseline. A balance was achieved by depleting the serum in the culture medium from 10% to 0.5%. The duration of culture time had to be optimized, to prevent detrimental effects of the low serum percentage on the cardiomyocytes in the tissue, but to still allow enough time for an effect of the different treatments on the CF-EHTs to develop. We decided on a culture time of 3 weeks, including 8 days of treatment. The stiffness of the fibrin matrix was also an important characteristic, as fibroblasts become more activated on stiffer substrates. Fibroblasts have been reported to develop stress fibres when they were cultured on surfaces with a stiffness of 3 kPa or more (Yeung et al., 2005). At the concentrations of fibrinogen and thrombin used for the casting of the CF-EHTs, the fibrin was expected to have a stiffness of more than 4 kPa (Duong et al., 2009). However, in fibrin blocks devoid of any cells, kindly provided by Kinga Wrona, a stiffness of only 0.77 kPa was measured via nanoindentation by Dr. Sandra Hemkemeyer. The human heart is reported to have a stiffness of over 10 kPa (Gaetani et al., 2020; Majkut et al., 2013). Given these uncertainties and the well-developed nature of the standard EHT, we thus aimed to maintain fibroblast quiescence at the previously established matrix stiffness. However, by increasing the concentration of thrombin and/or fibrinogen in the mastermix of the CF-EHTs, the model could have been tailored to have a higher Young's modulus to mimic physiological conditions. Cardiac fibroblasts cultured in a gelatin methacryloyl hydrogel with a stiffness of around 22 kPa, which more closely mimicked the Young's modulus of the human heart, were unexpectedly not reported to be more activated than cardiac fibroblasts cultured in a gelatin methacryloyl hydrogel with a stiffness of around 4 kPa. Hence, the matrix stiffness could potentially be further optimized to mimic physiological conditions.

The appropriate percentage of cardiac fibroblasts to be incorporated in the EHTs also had to be determined. To physiologically represent the human ventricle as if composed of only cardiomyocytes and cardiac fibroblasts, a ratio of 60:40 would have been the most physiological ratio. However, in our model CF-EHTs consisting of 15% or more CFs generated a lower force than CF-EHTs composed of 10% CFs or less (Figure 17). Furthermore, exaggerated remodelling was detected when more CFs were present in the CF-EHTs (Figure 17 and Table 15). Previous studies have used both higher ratios of CMs:CFs to more closely reflect physiological conditions, such as 4:1 with hiPSC-derived CMs:primary human CFs (Beauchamp et al., 2020), 10:3 primary rat CMs:primary rat CFs (Y. Li et al., 2017) and similar ratios, 8.5:1.5 for hiPSC-derived CMs:hiPSC-derived CFs (Aalders et al., 2024), 9:1 for hiPSC-derived CMs:primary human CFs (Cofiño-Fabres et al., 2024) and 10:1 for hiPSC-derived CMs:hiPSC-derived CFs (Stempien et al., 2024). Though a ratio of 9:1 resembles physiological conditions less closely, this ratio does have an established basis in literature. Considering this, in combination with the contractility analysis findings, a ratio of 9:1 cardiomyocytes:cardiac fibroblasts was considered a suitable compromise and an appropriate ratio for the EHT based *in vitro* fibrosis model.

To develop a fibrosis model with a high dynamic range of regulation, it was necessary to acquire quiescent baseline conditions. The cardiac fibroblasts differentiated according to a protocol previously established in the laboratory in which this work was performed, were found to be considerably activated already at baseline. We therefore decided to focus on establishing a protocol for the differentiation of quiescent cardiac fibroblasts, which was partially achieved by addition of the TGF- $\beta$ 1 receptor inhibitor SB-431542. Baseline quiescence of the fibroblasts used in our model was acquired by a combination of continued exposure to SB-431542 and a depletion of serum in the culture medium. In other cardiac fibrosis models, quiescence was maintained by reproducing the physiological mechanical stiffness of the heart (Bracco Gartner et al., 2019; Sadeghi et al., 2017), by simulating the mechanical stiffness, exposing the tissue to pirfenidone and using quiescent fibroblasts (Bracco Gartner et al., 2022), solely by the use of quiescent fibroblasts (Iseoka et al., 2021), or the quiescence was not taken into account (Mastikhina et al., 2020; Richards et al., 2020; Szepes et al., 2020). Though the use of SB-431542 to potentially maintain cardiac fibroblast quiescence has been investigated before (Cumberland et al., 2023), a fibrosis model which used SB-431542 to control quiescence of the cardiac fibroblasts was not previously developed. Though adjusting the mechanical stiffness as close to physiological conditions as possible is preferable for any *in vitro* fibrosis model, (additional) exposure of the CF-EHTs to SB-431542 and depletion of serum from the culture medium to maintain quiescence further decreased baseline activation and increased flexibility, as SB-431542 concentration can be adjusted, the compound can be removed from the culture medium, and serum can be added to the culture medium.

As previously mentioned, TGF- $\beta$ 1 exposure is a standard tool for fibrosis induction *in vitro* (Bracco Gartner et al., 2019, 2022; Cho et al., 2018; Cumberland et al., 2023; Iseoka et al., 2021; Lee et al., 2019; Mastikhina et al., 2020; Sadeghi et al., 2017). Further known fibroblast activators include PDGF-AA, angiotensin II and a combination of phenylephrine and endothelin 1 (Broekmans et al., 2020; Fullerton & Funder, 1994; Kemp et al., 2004; L. Wang et al., 2017). CFs have also been activated with aldosterone, both *in vivo* in rats and *in vitro* (Lijnen & Petrov, 2000; Neumann et al., 2002). Increasing the amount of fibroblasts in the tissue has also been found to increase fibrosis formation (van Spreeuwel et al., 2017), similar to the addition of pericytes (Szepes et al., 2020). In animal models, cardiac fibrosis induction is regularly achieved with TAC surgery (W.-W. Zhang et al., 2017) or prolonged treatment with noradrenaline (Richards et al., 2020), isoprenaline (T.-L. Sun et al., 2021) or adrenaline (El-Marasy et al., 2020). Though it is known that *in vitro* exposure to animal or human serum can activate cardiac fibroblasts (Swaney et al., 2005), serum in the culture medium has not been systematically used as a mode of cardiac fibroblast activation in cardiac fibrosis models.

Irrespective of how cardiac fibrosis was stimulated in other studies, readouts to quantify fibrosis induction included analysis of contraction parameters such as force, relaxation time and peak duration, analysing the mRNA expression of the markers collagen1a1, collagen3a1, periostin, CCN2, ACTA2, MMP2 and fibronectin, quantifying the stiffness of the tissue and quantifying cell proliferation either by cell proliferation assays or staining for EdU incorporated during proliferation. Collagen deposition was visualised in other models via second harmonic generation microscopy or by staining for collagen, for example with picrosirius red or by immunohistochemistry or immunofluorescence. Other histological analyses included staining for  $\alpha$ SMA and periostin (Bracco Gartner et al., 2019, 2022; Cumberland et al., 2023; Iseoka et al., 2021; Lee et al., 2019; Mastikhina et al., 2020; Neumann et al., 2002; Sadeghi et al., 2017; Szepes et al., 2020; van Spreeuwel et al., 2017). In the model developed in this work, fibrosis was mainly indirectly quantified by analysing contraction parameters such as force,

resting length, relaxation velocity and 80% relaxation time, analysing the mRNA expression of the fibrosis markers collagen1a1, periostin, transgelin, CCN2 and ACTA2, analysing the protein expression of periostin and  $\alpha$ SMA and quantifying the stiffness of the model. Each of these readouts individually suggested increased fibrosis induction in the model after stimulation. This was further corroborated from the combined readouts, as they suggested that activation of fibroblasts in our model, either via treatment with TGF- $\beta$ 1 or with high serum, led to fibrosis induction.

A collaborative second harmonic generation (SHG) study was initiated in this work to directly visualise collagen deposition in the CF-EHTs. Unfortunately, collagen could not be successfully visualized in these experiments. Collagen is a so-called non-centrosymmetric structure, meaning that there is no centre point around which the organization of collagen fibres is symmetric. When illuminated with a laser, non-centrosymmetric structures produce a signal which can pass through an SHG filter to the detector. Myosin is another non-centrosymmetric structure in the CF-EHTs which can be visualised via SHG (Esquibel et al., 2020). In the frame of this work, 'standard' SHG images were produced, in which it was not possible to distinguish the deposited collagen from myosin structures. We therefore aimed to improve the SHG imaging method to visualise only collagen, by rotating the polarization direction of the light emitted from the laser. The signal emitted by myosin is dependent on the polarization direction of the light, whereas the signal emitted by collagen is independent of the polarization direction (Kumar et al., 2015; Tiaho et al., 2007). Attributable to the rotating polarization direction, the intensity of the signal emitted by the myosin decreased, while the intensity of the signal emitted by collagen remained unchanged. However, the myosin was still visible in the images. To block the signal emitted from the myosin, it was planned to incorporate a low band width filter. Unfortunately, this was unsuccessful, and we were unable to visualise solely collagen deposition via SHG. As we had focussed on SHG to directly visualize collagen deposition in the CF-EHTs, more standard methods, such as staining for collagen by immunohistochemistry or immunofluorescence, remained underexploited. Thus, including a readout to directly quantify collagen deposition in the model is an important characterization method to include in future research with the model. Alternatively, collagen deposition in the CF-EHTs could be visualised with polarized light microscopy (Cristoforetti et al., 2023).

Activation of enhancer sequences can elevate the transcriptional activity of the target gene. By genetically deleting enhancer sequences, downregulation of pathologically upregulated genes could potentially be achieved (H. Li et al., 2021). Downregulation of genes associated with fibrosis formation could therefore lead to attenuated fibrosis induction. In activated cardiac fibroblasts obtained from TAC-treated mice, the *Meox1* gene has been found to be substantially upregulated. By targeting *Meox1* enhancers via bromodomain and extra-terminal (BET) inhibition, enhancer-to-promoter signaling could be reversed. TAC-treated mice which were further treated with a BET inhibitor displayed a left ventricular ejection fraction similar to Sham treated mice, portraying the importance of targeting gene enhancers (Alexanian et al., 2021).

The *RUNX1* gene has previously been associated with fibrosis formation, as *RUNX1* was overexpressed in pulmonary, renal, hepatic and cardiac fibrosis, and adverse cardiac remodelling was blunted in *Runx1* deficient mice following injury (Dubey et al., 2022; Z. Guo et al., 2023; McCarroll et al., 2018; Ni et al., 2021). Moreover, deletion of *RUNX1* inhibited the formation of renal fibrosis (Zhou et al., 2018). The 3D EHT based *in vitro* fibrosis model was developed to investigate whether the knockout of the *RUNX1*-related enhancer sequence *enh35232* or of the *RUNX1* gene attenuated fibrosis formation in the model. Subtle signs of attenuation of fibrosis induction were indeed found in both activated Enh KO CF-



EHTs and activated Gene KO CF-EHTs, compared to activated WT CF-EHTs. These signs included an attenuated relaxation deficit and lower mRNA abundance of different fibrosis markers. These signs were partially absent in A18945 CF-EHTs, but consistently present in ERC001 CF-EHTs, though at lower experiment numbers. The deletion of *enh35232* and *RUNX1* thus seemed to be subtle interventions to attenuate fibrosis formation. Of note, CF-EHTs were in culture for 3 weeks, and they were subjected to pro-fibrotic conditions for 8 days, whereas in humans it might take decades for fibrosis to form in the heart (Kurose, 2021). It is thus highly likely that the relatively brief time period in which fibrosis formation was induced in the CF-EHTs contributed to the subtlety of the observed signs of attenuated fibrosis formation.

More drastic interventions to limit fibrosis formation have been studied, such as the genetic ablation of collagen1a2-expressing cells in zebrafish. Zebrafish are known to retain the potential for proliferation of cardiomyocytes after injury, in contrast to most adult mammals. This proliferation was impaired after the ablation of collagen1a2 expressing cells, suggesting that a fibrotic effect or at least the respective fibroblast sub-type was necessary for heart regeneration (Sánchez-Iranzo et al., 2018). Implementation of chimeric antigen receptor (CAR) T cells targeted against fibroblast activation protein (FAP), expressed by activated fibroblasts, has been studied in mice suffering from MI. After CAR T cells bind to the FAP expressed on activated fibroblasts, the CAR T cells induce apoptosis in the activated fibroblasts. Restored cardiac function and a reduction of fibrosis were promising results (Aghajanian et al., 2019; Rurik et al., 2022). However, safety concerns remain: CAR T cells can remain in the body for months, up to years (Barnes, 2022). When a repeated injury would occur while the CAR T cells are still viable, they would again attack the activated fibroblasts. Activated fibroblasts are crucial directly after injury to maintain tissue integrity at the injury site and prevent rupture. Thus, clinical application of CAR T cells to target activated fibroblasts is currently limited. Consequently, the use of CAR T cells is currently only FDA approved for cancer treatment (Stern & Stern, 2021). These examples demonstrate why more subtle approaches can be beneficial over drastic interventions. Though the knockout of the *enh35232* seemed to be a very subtle approach, it did provide valuable insight into the mechanisms of cardiac fibrosis.

In preliminary results on mice with the *enh35232* KO, provided by one of our partners, Dr. Thomas Moore-Morris, the atria were significantly dilated in KO mice compared to WT mice 6 weeks after TAC surgery. Considerably less collagen deposition in KO mice than in WT mice was observed, as quantified by staining for type 1 collagen. These preliminary results seem consistent, as attenuated collagen deposition after injury can compromise tissue integrity, which can lead to cardiac wall dilation. The survival rate was considerably lower in KO mice. As an initial fibrotic response after injury is crucial for injury repair, the decreased survival rate suggests that the initial fibrotic response was blunted in *enh35232* deficient mice. These preliminary results indicated that in mice models, as expected, the deletion of *enh35232* had a larger impact than the subtle effect in CF-EHTs.

*Runx1* gene deficient animals have been studied more intensively (Riddell et al., 2020). Mice with a homozygous deletion of *Runx1* lack necessary haematopoiesis and are therefore not able to survive past embryonic day 11.5-12.5 (Q. Wang et al., 1996). However, encouraging results have been observed in mice with a cardiomyocyte specific *Runx1* KO subjected to MI. The adverse remodelling observed in control mice after MI, was not observed in the KO mice. While in control mice the ventricular wall thinned and dilated, in KO mice, the thickness of the ventricular wall was maintained. The contractile function in KO mice was maintained as well (McCarroll et al., 2018). In another mouse model with a

cardiomyocyte specific *Runx1* KO subjected to MI, a preserved contractile function following MI was again observed (Martin et al., 2022). In rats, the expression of *Runx1* was silenced directly after MI via the expression of miR-101. In rats in which the *Runx1* expression was silenced, the cardiac function was improved, the infarct size was smaller and there were less collagen fibres present, compared to rats with a normal *Runx1* expression (X. Li et al., 2019).

In these studies, again a genetic deletion of *Runx1* (in cardiomyocytes) had a more significant effect on the animals after MI, compared to the subtle effect we observed in KO CF-EHTs subjected to pro-fibrotic conditions. As previously mentioned, the CF-EHTs were subjected to these pro-fibrotic conditions for 8 days, whereas in animal experiments the fibrosis formation after interventions is often studied after multiple weeks (Gabisonia et al., 2019; McCarroll et al., 2018; Tao et al., 2016; Yuan et al., 2019), which is an advantage of employing animal models for the study of a genetic deletion. As another advantage of animal models, in contrast to CF-EHTs, all cell types which play a role in the development of MI are considered. For example, the inflammatory response, in which macrophages are recruited to the injury site after MI (Huebener et al., 2008; Humeres & Frangogiannis, 2019; Prabhu & Frangogiannis, 2016) can be studied in animal models, but could not be studied in CF-EHTs, as macrophages were not included in the CF-EHT model. However, as previously mentioned, major disadvantages of animal models are the associated ethical considerations (Kiani et al., 2022), which are not relevant in CF-EHT models. Other advantage of using CF-EHTs include the high reproducibility of the CF-EHTs and the possibility to perform studies with high numbers. While the use of animal models is associated with high costs, *in vitro* experiments are often more cost-effective (Fernandes & Pedroso, 2017; Kiani et al., 2022).

A possibility to study the genetic deletion in specifically cardiac fibroblasts, besides 2D culture, is by developing engineered fibroblast tissue, EFTs. The activation baseline in EFTs is expected to be lower than in 2D cultured CFs, as the CFs would not be cultured on a stiff substrate (Htwe et al., 2015; Solon et al., 2007), hence one would expect a larger impact of the genetic deletion in EFTs than we observed in the 2D cultured CFs. In this work, the emphasis was placed on developing a cardiac fibrosis model with a direct readout related to contractility and therefore cardiomyocytes were considered a vital part of the model. However, the study of the *enh35232* KO in EFTs could provide additional interesting insights into cardiac fibroblast activation. Another option to study the effect of the genetic deletion on the activation of specifically the cardiac fibroblasts in the CF-EHTs more precisely, relied on sorting the cardiac fibroblasts and the cardiomyocytes after harvesting. (CF-)EHTs can be dissociated by papain (Pan, 2022), after which the cells can be sorted via flow cytometry (Telford, 2023). This was attempted in this work, by fluorescently labelling the cardiomyocytes and cardiac fibroblasts via lentivirus transduction, with a dKathuska and Venus fluorochrome label, respectively. However, after dissolution and sorting, cell integrity was often compromised and the mRNA content in the cell suspension could not safely be considered as cell type specific. Optimizing a sorting process to sort cardiomyocytes and cardiac fibroblasts after CF-EHT culture could benefit the readout options of the CF-EHT fibrosis model for future research.

#### 4.4 Conclusion and future perspectives

In conclusion, an *in vitro* 3D EHT based fibrosis model was developed, with a high dynamic range of regulation partially attributable to a quiescent baseline. In this model, fibrosis was formed after activation either by treatment with TGF- $\beta$ 1 or by exposure to a high serum concentration in the culture

medium. The fibrosis indicators which were quantified comprised a shorter resting length, lower relaxation velocity and longer 80% relaxation time, mRNA abundance of the fibrosis markers collagen1a1, periostin, transgelin, collagen1a2 and CCN2, abundance of periostin and  $\alpha$ SMA protein and an increased CF-EHT stiffness.

Genetic interventions had a subtle effect on signs of fibrosis in the newly developed model. The genetic deletion of either the *RUNX1*-related enhancer sequence *enh35232* or of the *RUNX1* gene, led to attenuated signs of fibrosis particularly in the ERC001 CF-EHTs. Though the observed changes were subject to large variability and mainly limited to contractility and partially mRNA abundance, it could still be concluded that *enh35232* and *RUNX1* may play a role in fibrosis formation.

For further characterization of the model, additional direct quantification of fibrosis formation, such as collagen deposition, would be necessary, especially as the genetic intervention only had a subtle effect. Proliferation and cell survival of both the cardiomyocytes and the cardiac fibroblasts over time are further parameters which still need to be investigated. As activated cardiac fibroblasts have been found to cause slower action potential conduction and prolonged action potential duration (Y. Li et al., 2017), measuring the action potential in the CF-EHTs could also be an interesting parameter to investigate differences between the genotypes.

In summary, the EHT based fibrosis model developed in this work is functional, reliable, reproducible and will be used for future research. Differences between the investigated genotypes however, appeared to be surprisingly minute, albeit detectable. Thus, implementation of further readouts with higher sensitivity should be additionally conducted to enable robust detection of subtle differences in fibrosis development.

## 5. Summary – Zusammenfassung

### Summary

More than 60 million people worldwide are affected by heart failure, often caused by myocardial infarction (MI). After an injury such as MI, cardiac fibrosis is a required response to stably repair the injury site, creating a scar to prevent wall rupture. However, adverse cardiac fibrosis, which can for example occur on account of chronic inflammation following a large injury site or which can be a consequence of chronic pressure overload in hypertension, can contribute to heart failure. During cardiac fibrosis formation, cardiac fibroblasts residing in the heart become activated, transdifferentiate into myofibroblasts and produce increased amounts of extracellular matrix. Many mechanisms contributing to cardiac fibrosis and the activation of cardiac fibroblasts are known. The cytokine TGF- $\beta$ 1, mainly secreted by recruited macrophages, is involved in the main activation pathways and induces  $\alpha$ SMA expression, a hallmark of transdifferentiation of cardiac fibroblasts into myofibroblasts. However, many of the mechanisms behind the formation of cardiac fibrosis remain unclear.

In the first part of this work, a 3D engineered heart tissue (EHT) based *in vitro* fibrosis model with a high dynamic range of regulation was developed to study mechanisms of cardiac fibrosis. The model is a fibrin-based tissue co-culture of both hiPSC-derived cardiomyocytes and hiPSC-derived cardiac fibroblasts cast together in a 9:1 ratio, to form CF-EHTs. A high dynamic range of regulation was attributable to a quiescent baseline versus pro-fibrotic treatment conditions. To ensure a quiescent baseline, a protocol for the differentiation of quiescent cardiac fibroblasts was established. The cardiac fibroblast phenotype was characterized by the high mRNA abundance of multiple fibroblast markers, including DDR2, vimentin and GATA4, and the typical elongated morphology. Fibroblast quiescence was furthermore maintained by the depletion of serum from the culture medium from 10% to 0.5% on day 3 of culture, as serum components could activate cardiac fibroblasts, and by the exposure of all CF-EHTs to the TGF- $\beta$ 1 receptor inhibitor SB-431542 from day 10 to day 13 of culture.

On the other end of the activation spectrum, 2 pro-fibrotic conditions were established: either treatment of CF-EHTs with TGF- $\beta$ 1, or exposure to 10% serum containing medium. On day 13 of culture, the CF-EHTs were assigned to 1 of 4 groups: a control group, a quiescent group with continuous SB-431542 exposure, or 1 of the 2 activated groups. At the end of the culture time, day 21 or day 22, CF-EHTs from the activated groups regularly exhibited a shorter resting length, a lower relaxation velocity and longer 80% relaxation time, i.e. a relaxation deficit, compared to CF-EHTs from the quiescent group. Furthermore, the activated CF-EHTs displayed a higher mRNA abundance of the fibrosis markers collagen1a1, periostin, CCN2 and transgelin compared to either the control CF-EHTs or the quiescent CF-EHTs. These results indicated the successful development of a 3D EHT based *in vitro* fibrosis model.

In the second part of this work, the effect of the genetic deletion (KO) of either the *RUNX1*-related enhancer sequence *enh35232* or of the *RUNX1* gene in hiPSC-derived cardiac fibroblasts was studied in 2 different cell lines. The resulting KO CF-EHTs, especially those based on the cell line ERC001, showed attenuated signs of fibrosis compared to WT CF-EHTs, when subjected to pro-fibrotic treatment conditions. Compared to the activated WT CF-EHTs, the activated KO CF-EHTs had a longer resting length and the regular relaxation deficit under pro-fibrotic conditions was attenuated. Additionally, the activated KO CF-EHTs exhibited a lower mRNA abundance of the fibrosis markers collagen1a1, periostin and ACTA2 and a lower expression of periostin and  $\alpha$ SMA protein. These results indicated that both *enh35232* and *RUNX1* have a role in fibrosis formation and emphasized the suitability of the *in vitro* 3D EHT based fibrosis model for the study of genetic interventions.

---

Zusammenfassung

---

Weltweit leiden über 60 Millionen Menschen an Herzinsuffizienz, am häufigsten verursacht durch einen Herzinfarkt. Nach einem Herzinfarkt ist die Ausbildung einer fibrotischen Narbe eine erforderliche Reaktion, um die Verletzungsstelle zu stabilisieren. Obwohl an sich physiologisch, kann die fibrotische Reaktion pathologisch werden und zu Herzinsuffizienz und einem Relaxationsdefizit beitragen. Im Rahmen der kardialen Fibrose werden gewebständige Fibroblasten aktiviert, sie transdifferenzieren zu Myofibroblasten und produzieren mehr extrazelluläre Matrix. Obwohl zahlreiche Mechanismen der kardialen Fibrose bekannt sind, sind viele Mechanismen noch unklar.

Im ersten Teil dieser Dissertation wurde ein auf künstlichem Herzgewebe (*engineered heart tissue*, EHT) basiertes *in vitro*-Fibrose-Modell mit einer hohen dynamischen Regulationsbreite etabliert, um daran Mechanismen der kardialen Fibrose studieren zu können. Das Modell beruht auf einer Co-Kultur von aus humanen induzierten pluripotenten Stammzellen (hiPSCs) abgeleiteten Kardiomyozyten und hiPSCs-abgeleiteten kardialen Fibroblasten in einem 9:1-Verhältnis, woraus CF-EHTs generiert werden. Ein hoher Dynamikumfang der Regulierung wurde angestrebt, um eine hohe Sensitivität und Spezifität zu gewährleisten und wurde erreicht durch Erzielung von wenig aktivierten Grundbedingungen auf der einen Seite und pro-fibrotischen Behandlungsbedingungen auf der anderen Seite. Zum Erreichen der nicht-aktivierten Grundbedingungen wurden zunächst nicht-aktivierte kardiale Fibroblasten differenziert. Zur Phänotypisierung der differenzierten Fibroblasten wurden die Expression geeigneter Marker wie DDR2, Vimentin und GATA4 auf mRNA-Ebene und die typische Morphologie herangezogen. Der niedrige Aktivierungsstatus der hiPSC-Fibroblasten wurde durch einen verminderten Serumgehalt im Kulturmedium sichergestellt, da Serumkomponenten Fibroblasten aktivieren können. Die Serumkonzentration wurde hierzu von 10% auf 0.5% am Tag 3 der Kultur reduziert. Zusätzlich wurden alle CF-EHTs mit dem TGF- $\beta$ 1-Rezeptor-Inhibitor SB-431542 von Tag 10 bis Tag 13 der Kultur behandelt.

Am anderen Ende des Aktivierungsspektrums standen zwei pro-fibrotische Behandlungen, bei denen die CF-EHTs entweder mit TGF- $\beta$ 1 behandelt wurden, oder 10% Serum im Kulturmedium ausgesetzt wurden. Am Tag 13 wurden die CF-EHTs in 4 Gruppen eingeteilt, eine Kontrollgruppe, eine inaktivierte Gruppe mit SB-431542 oder eine der zwei aktivierten Gruppen. Am Ende der Kultur, am Tag 21 oder Tag 22, zeigten die pro-fibrotisch behandelten CF-EHTs eine kürzere Ausgangslänge, niedrigere Relaxationsgeschwindigkeit und längere 80%-Relaxationszeit, in der Summe also ein Relaxationsdefizit, im Vergleich zu CF-EHTs der inaktivierten Gruppe. Darüber hinaus zeigten die aktivierten CF-EHTs eine höhere mRNA-Menge der Fibrosemarker collagen1a1, periostin, CCN2 und transgelin im Vergleich zu den Kontroll-CF-EHTs und den inaktivierten CF-EHTs. Zusammengefasst sprachen die Ergebnisse des ersten Teils der Arbeit für eine erfolgreiche Entwicklung auf EHT basierten *in vitro*-Fibrose-Modells.

Im zweiten Teil dieser Dissertation wurden die Konsequenzen einer genetischen Ablation (KO) der RUNX1-bezogenen Enhancer-Sequenz *enh35232* oder des *RUNX1*-Gens in kardialen hiPSC-Fibroblasten auf die Fibroseentwicklung im Modell in zwei verschiedenen Zelllinien untersucht. Die aktivierten KO-CF-EHTs, insbesondere die ERC001 KO-CF-EHTs, zeigten abgeschwächte Zeichen von Fibrose gegenüber aktivierten Wildtyp- (WT-) CF-EHTs. Zum Beispiel, im Vergleich zu aktivierten WT-CF-EHTs zeigten die aktivierten KO-CF-EHTs eine längere Ausgangslänge und abgeschwächtes Relaxationsdefizit. Zusätzlich wiesen die aktivierten KO-CF-EHTs eine geringere mRNA-Menge der Fibrosemarker collagen1a1, periostin und ACTA2 auf. Diese Ergebnisse deuten darauf hin, dass *enh35232* und *RUNX1* eine Rolle in der Entwicklung kardialer Fibrose spielen könnten und dass das hier etablierte *in vitro*-Fibrose-Modell geeignet ist, die Konsequenzen genetischer Eingriffe auf die Fibroseentwicklung zu untersuchen.

## 6. List of abbreviations

2D	Two-dimensional
3D	Three-dimensional
4C	Circularized chromosome conformation capture
$\alpha$ SMA	$\alpha$ -Smooth muscle actin
$\mu$ M	Micromolar
<b>A</b>	
ACE	Angiotensin-converting enzyme
ACTA2	$\alpha$ -Smooth muscle actin
ALK5	Activin receptor-like kinase 5
AML	Acute myeloid leukaemia
Ang I	Angiotensin I
Ang II	Angiotensin II
AP	Action potential
APS	Ammonium persulfate
AT1	Angiotensin receptor 1
ATAC-seq	Assay for transposase-accessible chromatin with high-throughput sequencing
ATP	Adenosine triphosphate
<b>B</b>	
BET	Bromodomain and extra-terminal
bFGF	Basic fibroblast growth factor
BMP	Bone morphogenetic protein
bp	Base pair
bpm	Beats per minute
BSA	Bovine serum albumin
<b>C</b>	
CAR	Chimeric antigen receptor
Cas9	CRISPR associated protein 9
CBF	Core binding factor
CBF $\alpha$	Core binding factor $\alpha$ subunit
CBF $\beta$	Core binding factor $\beta$ subunit
CCN2	Cellular communication network 2
cDNA	Complementary DNA
CF	Cardiac fibroblast
CF-EHT	Cardiomyocyte-cardiac fibroblast EHT
ChIP-seq	Chromatin immunoprecipitation sequencing
CM	Cardiomyocyte
CNIC	Centro Nacional de Investigaciones Cardiovasculares
COL1A1	Collagen1a1
COL1A2	Collagen1a2
COL3A1	Collagen3a1
CPC	Cardiac progenitor cell
CRISPR	Clustered regularly interspaced short palindromic repeats
CTGF	Connective tissue growth factor
CTMV	Consulting Team Machine Vision
cTnT	Cardiac troponin T
Ctrl	Control

## D

d	Day
DDR2	Discoidin domain receptor tyrosine kinase 2
DDRs	Discoidin domain receptors
DMEM	Dulbecco's Modified Eagle Medium
DMSO	Dimethyl sulfoxide
DNA	Deoxyribonucleic acid
dNTP	Deoxynucleoside triphosphate
DPBS	Dulbecco's Phosphate Buffered Saline
DTT	1,4-Dithiothreitol

## E

EB	Embryoid body
ECM	Extracellular matrix
EDTA	Ethylenediaminetetraacetic acid
EFT	Engineered fibroblast tissue
EHT	Engineered heart tissue
Enh KO CF-EHT	CF-EHT composed of WT CMs and <i>enh35232</i> knockout CFs
ERK	Extracellular signal-related kinase
ESC	Embryonic stem cell

## F

FACS	Fluorescence-activated cell sorting
FAP	Fibroblast activation protein
FBS	Foetal bovine serum
FSP1	Fibroblast specific protein 1
FTDA	bFGF, TGF $\beta$ 1, dorsomorphin and activin A-based hiPSC culture medium
Fw	Forward

## G

GATA4	GATA binding protein 4
Gene KO CF-EHT	CF-EHT composed of WT CMs and <i>RUNX1</i> gene knockout CFs
GSK3 $\beta$	Glycogen synthase kinase 3 $\beta$
GTX	Geltrex
GUSB	Glucuronidase beta

## H

H3K4me1	H3 lysine 4 mono-methylation
HBSS	Hanks' Balanced Salt Solution
HCl	Hydrochloric acid
HEPES	4-(2-hydroxyethyl)-1-piperazineethanesulfonic acid
HFpEF	Heart failure with a preserved ejection fraction
HFrEF	Heart failure with a reduced ejection fraction
Hi-C	High-throughput chromosome conformation capture
hiPSC	Human induced pluripotent stem cell
hiPSC-CM	hiPSC-derived cardiomyocyte
HSA	Human serum albumin

## I

ICCLM	Institute of Clinical Chemistry and Laboratory Medicine
IEPT	Institute of Experimental Pharmacology and Toxicology
IGF	Institut de Génomique Fonctionnelle

IHG	Institute of Human Genetics
IL	Interleukin
iPSC	Induced pluripotent stem cell
IRCCS	Istituti di Ricovero e Cura a Carattere Scientifico
<b>J</b>	
JNK	c-Jun N-terminal kinase
<b>K</b>	
kb	Kilobase
kDa	Kilodalton
KO	Knockout
<b>M</b>	
M	Molar
MAPK	Mitogen-activated protein kinase
MDS	Multi-dimensional scaling
MG	Matrigel
MI	Myocardial infarction
miRNA	Micro RNA
mM	Millimolar
mN	Millinewton
mRNA	Messenger RNA
MYH11	Myosin heavy chain 11
<b>N</b>	
NaCl	Sodium chloride
NCX	Na <sup>+</sup> /Ca <sup>2+</sup> antiporters
NKX2.5	NK2 Homeobox 5
<b>P</b>	
PCR	Polymerase chain reaction
PDGF-AA	Platelet derived growth factor that is composed of 2 A subunits
PDGFR $\alpha$	Platelet-derived growth factor receptor $\alpha$
PE-Cy5	Phycoerythrin-Cyanine 5
POSTN	Periostin
PTFE	Polytetrafluoroethylene
<b>Q</b>	
qPCR	Quantitative real-time PCR
<b>R</b>	
RAAS	Renin-angiotensin-aldosterone system
RL	Resting length
RNA	Ribonucleic acid
ROS	Reactive oxygen species
rpm	Revolutions per minute
RPMI	Roswell park memorial institute
RT	Relaxation time
RUNX1	Runt-related transcription factor 1
RV	Relaxation velocity
Rv	Reverse



**S**

SB	SB-431542
SDS	Sodium dodecyl sulfate
SEM	Standard error of the mean
SERCA2	Sarcoplasmic/endoplasmic reticulum $\text{Ca}^{2+}$ ATPase 2
SHG	Second harmonic generation
SR	Sarcoplasmic reticulum
SSEA-3	Stage-specific embryonic antigen 3

**T**

TAC	Transverse aortic constriction
TAE	Tris acetate EDTA
TAGLN	Transgelin
TBS	Tris-buffered saline
TBST	TBS + 0.1% Tween 20
TBX18	T-box transcription factor 18
TCF21	Transcription factor 21
TGF- $\beta$	Transforming growth factor- $\beta$
TGF- $\beta$ 1RI	TGF- $\beta$ 1 receptor I
TGF- $\beta$ 1RII	TGF- $\beta$ 1 receptor II
Thy1	Thymus cell antigen 1
TNC	Tenascin C
T $\beta$	TGF- $\beta$ 1

**U**

U	Unit
UKE	University Medical Center Hamburg-Eppendorf

**V**

V	Volt
v/v	Volume by volume
VEGF	Vascular endothelial growth factor
VIM	Vimentin

**W**

w/v	Weight by volume
WB	Western blot
WT CF-EHT	CF-EHT composed of WT CMs and WT CFs
WT	Wild type
WT1	Wilms' tumour protein 1

## 7. References

- Aalders, J., Léger, L., Van der Meeren, L., Sinha, S., Skirtach, A. G., De Backer, J., & van Hengel, J. (2024). Three-dimensional co-culturing of stem cell-derived cardiomyocytes and cardiac fibroblasts reveals a role for both cell types in Marfan-related cardiomyopathy. *Matrix Biology*, 126, 14–24. <https://doi.org/https://doi.org/10.1016/j.matbio.2024.01.003>
- Aghajanian, H., Kimura, T., Rurik, J. G., Hancock, A. S., Leibowitz, M. S., Li, L., Scholler, J., Monslow, J., Lo, A., Han, W., Wang, T., Bedi, K., Morley, M. P., Linares Saldana, R. A., Bolar, N. A., McDaid, K., Assenmacher, C.-A., Smith, C. L., Wirth, D., ... Epstein, J. A. (2019). Targeting cardiac fibrosis with engineered T cells. *Nature*, 573(7774), 430–433. <https://doi.org/10.1038/s41586-019-1546-z>
- Ahmed, M. S., Øie, E., Vinge, L. E., Yndestad, A., Øystein Andersen, G., Andersson, Y., Attramadal, T., & Attramadal, H. (2004). Connective tissue growth factor—a novel mediator of angiotensin II-stimulated cardiac fibroblast activation in heart failure in rats. *Journal of Molecular and Cellular Cardiology*, 36(3), 393–404. <https://doi.org/https://doi.org/10.1016/j.yjmcc.2003.12.004>
- Alberts B, Johnson A, Lewis J, et al. (2002). *Molecular Biology of the Cell* (4th ed.). New York: Garland Science. <https://www.ncbi.nlm.nih.gov/books/NBK26887/>
- Alex, L., Tuleta, I., Hanna, A., & Frangogiannis, N. G. (2023). Diabetes Induces Cardiac Fibroblast Activation, Promoting a Matrix-Preserving Nonmyofibroblast Phenotype, Without Stimulating Pericyte to Fibroblast Conversion. *Journal of the American Heart Association*, 12(6), e027463. <https://doi.org/10.1161/JAHA.122.027463>
- Alexanian, M., Przytycki, P. F., Micheletti, R., Padmanabhan, A., Ye, L., Travers, J. G., Gonzalez-Teran, B., Silva, A. C., Duan, Q., Ranade, S. S., Felix, F., Linares-Saldana, R., Li, L., Lee, C. Y., Sadagopan, N., Pelonero, A., Huang, Y., Andreoletti, G., Jain, R., ... Srivastava, D. (2021). A transcriptional switch governs fibroblast activation in heart disease. *Nature*, 595(7867), 438–443. <https://doi.org/10.1038/s41586-021-03674-1>
- AlQudah, M., Hale, T. M., & Czubryt, M. P. (2020). Targeting the renin-angiotensin-aldosterone system in fibrosis. *Matrix Biology*, 91–92, 92–108. <https://doi.org/https://doi.org/10.1016/j.matbio.2020.04.005>
- Angelini, A., Li, Z., Mericskay, M., Decaux, J. F., & Samuel, J. L. (2015). Regulation of connective tissue growth factor and cardiac fibrosis by an SRF/MicroRNA-133a Axis. *PLoS ONE*, 10(10). <https://doi.org/10.1371/journal.pone.0139858>
- Avissar, Y., Belardo, G. M. M., Choi, J., DeSaix, J., Jurukovski, V., & Rye, C. (2016). Muscle Contraction and Locomotion - Regulatory Proteins. In *General Biology*. OpenStax. [https://bio.libretexts.org/Bookshelves/Introductory\\_and\\_General\\_Biology/Book%3A\\_General\\_Biology\\_\(Boundless\)/38%3A\\_The\\_Musculoskeletal\\_System/38.18%3A\\_Muscle\\_Contraction\\_and\\_Locomotion\\_-\\_Regulatory\\_Proteins#:~:text=If%20present%2C%20calcium%20ions%20bind,actin%20and%20myosin%2C%20triggering%20contraction](https://bio.libretexts.org/Bookshelves/Introductory_and_General_Biology/Book%3A_General_Biology_(Boundless)/38%3A_The_Musculoskeletal_System/38.18%3A_Muscle_Contraction_and_Locomotion_-_Regulatory_Proteins#:~:text=If%20present%2C%20calcium%20ions%20bind,actin%20and%20myosin%2C%20triggering%20contraction)
- Avissar, Y., Choi, J., DeSaix, J., Jurukovski, V., Wise, R., & Rye, C. (2016). The Cardiac Cycle. In *Biology for Majors*. OpenStax.

- [https://bio.libretexts.org/Courses/Lumen\\_Learning/Biology\\_for\\_Majors\\_II\\_\(Lumen\)/21%3A\\_Module\\_18-\\_The\\_Circulatory\\_System/21.11%3A\\_The\\_Cardiac\\_Cycle](https://bio.libretexts.org/Courses/Lumen_Learning/Biology_for_Majors_II_(Lumen)/21%3A_Module_18-_The_Circulatory_System/21.11%3A_The_Cardiac_Cycle)
- Babij, P., Kelly, C., & Periasamy, M. (1991). Characterization of a mammalian smooth muscle myosin heavy-chain gene: Complete nucleotide and protein coding sequence and analysis of the 5' end of the gene. In *Proc. Natl. Acad. Sci. USA* (Vol. 88). <https://www.pnas.org>
- Banjeree, I., Yekkala, K., Borg, T. K., & Baudino, T. A. (2006). Dynamic Interactions between Myocytes, Fibroblasts, and Extracellular Matrix. *Annals of the New York Academy of Sciences*, 1080(1), 76–84. <https://doi.org/https://doi.org/10.1196/annals.1380.007>
- Barnes, K. (2022). CAR T cells remain during long-term cancer remission. *Communications Medicine*, 2(1), 28. <https://doi.org/10.1038/s43856-022-00092-w>
- Barrangou, R., Fremaux, C., Deveau, H., Richards, M., Boyaval, P., Moineau, S., Romero, D. A., & Horvath, P. (2007). CRISPR Provides Acquired Resistance Against Viruses in Prokaryotes. *Science*, 315(5819), 1709–1712. <https://doi.org/10.1126/science.1138140>
- Baudino, T. A., Carver, W., Giles, W., & Borg, T. K. (2006). Cardiac fibroblasts: friend or foe? *American Journal of Physiology-Heart and Circulatory Physiology*, 291(3), H1015–H1026. <https://doi.org/10.1152/ajpheart.00023.2006>
- Beagrie, R. A., & Pompo, A. (2016). Gene activation by metazoan enhancers: Diverse mechanisms stimulate distinct steps of transcription. *BioEssays*, 38(9), 881–893.
- Beauchamp, P., Jackson, C. B., Ozhatil, L. C., Agarkova, I., Galindo, C. L., Sawyer, D. B., Suter, T. M., & Zuppinger, C. (2020). 3D Co-culture of hiPSC-Derived Cardiomyocytes With Cardiac Fibroblasts Improves Tissue-Like Features of Cardiac Spheroids. *Frontiers in Molecular Biosciences*, 7. <https://www.frontiersin.org/articles/10.3389/fmolb.2020.00014>
- Becher, P. M., Lund, L. H., Coats, A. J. S., & Savarese, G. (2022). An update on global epidemiology in heart failure. *European Heart Journal*, 43(32), 3005–3007. <https://doi.org/10.1093/eurheartj/ehac248>
- Bellissimo, D. C., & Speck, N. A. (2017). RUNX1 mutations in inherited and sporadic leukemia. In *Frontiers in Cell and Developmental Biology* (Vol. 5, Issue DEC). Frontiers Media S.A. <https://doi.org/10.3389/fcell.2017.00111>
- Bergmann, O., Zdunek, S., Felker, A., Salehpour, M., Alkass, K., Bernard, S., Sjöström, S. L., Szeewczykowska, M., Jackowska, T., dos Remedios, C., Malm, T., Andrä, M., Jashari, R., Nyengaard, J. R., Possnert, G., Jovinge, S., Druid, H., & Frisén, J. (2015). Dynamics of Cell Generation and Turnover in the Human Heart. *Cell*, 161(7), 1566–1575. <https://doi.org/https://doi.org/10.1016/j.cell.2015.05.026>
- Bertaud, A., Joshkon, A., Heim, X., Bachelier, R., Bardin, N., Leroyer, A. S., & Blot-Chabaud, M. (2023). Signaling Pathways and Potential Therapeutic Strategies in Cardiac Fibrosis. In *International Journal of Molecular Sciences* (Vol. 24, Issue 2). MDPI. <https://doi.org/10.3390/ijms24021756>
- Betts, J. G., Young, K. A., Wise, J. A., Johnson, E., Poe, B., Kruse, D. H., Korol, O., Johnson, J. E., Womble, M., & DeSaix, P. (2022). Heart Anatomy. In *Anatomy and Physiology 2e* (2nd ed.). OpenStax.

- Bian, W., Liao, B., Badie, N., & Bursac, N. (2009). Mesoscopic hydrogel molding to control the 3D geometry of bioartificial muscle tissues. *Nature Protocols*, 4(10), 1522–1534. <https://doi.org/10.1038/nprot.2009.155>
- Blankesteyn, W. M., Essers-Janssen, Y. P. G., Verluyten, M. J. A., Daemen, M. J. A. P., & Smits, J. F. M. (1997). A homologue of *Drosophila* tissue polarity gene frizzled is expressed in migrating myofibroblasts in the infarcted rat heart. *Nature Medicine*, 3(5), 541–544. <https://doi.org/10.1038/nm0597-541>
- Booz, G. W., & Baker, K. M. (1995). Molecular signalling mechanisms controlling growth and function of cardiac fibroblasts. *Cardiovascular Research*, 30(4), 537–543. [https://doi.org/10.1016/S0008-6363\(96\)88507-5](https://doi.org/10.1016/S0008-6363(96)88507-5)
- Borg, T. K., Rubin, K., Carver, W., Samarel, A., & Terracio, L. (1996). The cell biology of the cardiac interstitium. *Trends in Cardiovascular Medicine*, 6(2), 65–70. [https://doi.org/https://doi.org/10.1016/1050-1738\(96\)00005-9](https://doi.org/https://doi.org/10.1016/1050-1738(96)00005-9)
- Bracco Gartner, T. C. L., Crnko, S., Leiteris, L., van Adrichem, I., van Laake, L. W., Bouten, C. V. C., Goumans, M. J., Suyker, W. J. L., Sluijter, J. P. G., & Hjortnaes, J. (2022). Pirfenidone Has Anti-fibrotic Effects in a Tissue-Engineered Model of Human Cardiac Fibrosis. *Frontiers in Cardiovascular Medicine*, 9. <https://doi.org/10.3389/fcvm.2022.854314>
- Bracco Gartner, T. C. L., Deddens, J. C., Mol, E. A., Magin Ferrer, M., van Laake, L. W., Bouten, C. V. C., Khademhosseini, A., Doevendans, P. A., Suyker, W. J. L., Sluijter, J. P. G., & Hjortnaes, J. (2019). Anti-fibrotic Effects of Cardiac Progenitor Cells in a 3D-Model of Human Cardiac Fibrosis. *Frontiers in Cardiovascular Medicine*, 6. <https://doi.org/10.3389/fcvm.2019.00052>
- Bracco Gartner, T. C. L., Wang, Y., Leiteris, L., van Adrichem, I., Marsman, J., Goumans, M. J., Bouten, C. V. C., Sluijter, J. P. G., den Toonder, J. M. J., Suyker, W. J. L., & Hjortnaes, J. (2023). Cyclic strain has antifibrotic effects on the human cardiac fibroblast transcriptome in a human cardiac fibrosis-on-a-chip platform. *Journal of the Mechanical Behavior of Biomedical Materials*, 144, 105980. <https://doi.org/https://doi.org/10.1016/j.jmbbm.2023.105980>
- Breckwoldt, K., Letuffe-Brenière, D., Mannhardt, I., Schulze, T., Ulmer, B., Werner, T., Benzin, A., Klampe, B., Reinsch, M. C., Laufer, S., Shibamiya, A., Prondzynski, M., Mearini, G., Schade, D., Fuchs, S., Neuber, C., Krämer, E., Saleem, U., Schulze, M. L., ... Hansen, A. (2017). Differentiation of cardiomyocytes and generation of human engineered heart tissue. *Nature Protocols*, 12(6), 1177–1197. <https://doi.org/10.1038/nprot.2017.033>
- Brilla, C. G., Zhou, G., Matsubara, L., & Weber, K. T. (1994). Collagen Metabolism in Cultured Adult Rat Cardiac Fibroblasts: Response to Angiotensin II and Aldosterone. *Journal of Molecular and Cellular Cardiology*, 26(7), 809–820. <https://doi.org/https://doi.org/10.1006/jmcc.1994.1098>
- Brodsky, V. Y., Chernyaev, A. L., & Vasilyeva, I. A. (1991). Variability of the cardiomyocyte ploidy in normal human hearts. In *Virchows Archiv B Cell Pathol* (Vol. 61).
- Broekmans, K., Giesen, J., Menges, L., Koesling, D., & Russwurm, M. (2020). Angiotensin II-induced cardiovascular fibrosis is attenuated by NO-sensitive guanylyl cyclase1. *Cells*, 9(11), 1–11. <https://doi.org/10.3390/cells9112436>

- Brønnum, H., & Kalluri, R. (2012). Chapter 29 - Cardiac Fibrosis: Cellular and Molecular Determinants. In J. A. Hill & E. N. Olson (Eds.), *Muscle* (pp. 389–404). Academic Press. <https://doi.org/https://doi.org/10.1016/B978-0-12-381510-1.00029-6>
- Bujak, M., Dobaczewski, M., Chatila, K., Mendoza, L. H., Li, N., Reddy, A., & Frangogiannis, N. G. (2008). Interleukin-1 receptor type I signaling critically regulates infarct healing and cardiac remodeling. *American Journal of Pathology*, 173(1), 57–67. <https://doi.org/10.2353/ajpath.2008.070974>
- Bursac, N., & J. Kim, J. (2014). 30 - Cardiac Fibroblasts and Arrhythmogenesis. In D. P. Zipes & J. Jalife (Eds.), *Cardiac Electrophysiology: From Cell to Bedside (Sixth Edition)* (pp. 297–308). W.B. Saunders. <https://doi.org/https://doi.org/10.1016/B978-1-4557-2856-5.00030-3>
- Caillaud, A., Lévêque, A., Thédrez, A., Girardeau, A., Canac, R., Bray, L., Baudic, M., Barc, J., Gaborit, N., Lamirault, G., Gardie, B., Idriss, S., Rimbert, A., Le May, C., Cariou, B., & Si-Tayeb, K. (2022). FACS-assisted CRISPR-Cas9 genome editing of human induced pluripotent stem cells. *STAR Protocols*, 3(4), 101680. <https://doi.org/https://doi.org/10.1016/j.xpro.2022.101680>
- Cartledge, J. E., Kane, C., Dias, P., Tesfom, M., Clarke, L., Mckee, B., Al Ayoubi, S., Chester, A., Yacoub, M. H., Camelliti, P., & Terracciano, C. M. (2015). Functional crosstalk between cardiac fibroblasts and adult cardiomyocytes by soluble mediators. *Cardiovascular Research*, 105(3), 260–270. <https://doi.org/10.1093/cvr/cvu264>
- Chai, J., & Tarnawski, A. S. (2002). Serum Response Factor: Discovery, Biochemistry, Biological Roles and Implications for Tissue Injury Healing. *Journal of Physiology and Pharmacology*, 53(2), 147–157. [www.jpp.krakow.pl](http://www.jpp.krakow.pl)
- Chen, G., Gulbranson, D. R., Hou, Z., Bolin, J. M., Ruotti, V., Probasco, M. D., Smuga-Otto, K., Howden, S. E., Diol, N. R., Propson, N. E., Wagner, R., Lee, G. O., Antosiewicz-Bourget, J., Teng, J. M. C., & Thomson, J. A. (2011). Chemically defined conditions for human iPSC derivation and culture. *Nature Methods*, 8(5), 424–429. <https://doi.org/10.1038/nmeth.1593>
- Chen, M. J., Yokomizo, T., Zeigler, B. M., Dzierzak, E., & Speck, N. A. (2009). Runx1 is required for the endothelial to haematopoietic cell transition but not thereafter. *Nature*, 457(7231), 887–891. <https://doi.org/10.1038/nature07619>
- Chen, M., Sun, Y., Wang, Q., & Li, Y. (2022). Reduction of Activin Receptor-Like Kinase 4 Expression Ameliorates Myocardial Ischemia/Reperfusion Injury through Inhibiting TGF $\beta$  Signaling Pathway. *Analytical Cellular Pathology*, 2022, 5242323. <https://doi.org/10.1155/2022/5242323>
- Chen, W., & Frangogiannis, N. G. (2013). Fibroblasts in post-infarction inflammation and cardiac repair. In *Biochimica et Biophysica Acta - Molecular Cell Research* (Vol. 1833, Issue 4, pp. 945–953). <https://doi.org/10.1016/j.bbamcr.2012.08.023>
- Chen, Y., Derguini, F., & Buck, J. (1997). Vitamin A in serum is a survival factor for fibroblasts. In *Cell Biology* (Vol. 94). [www.pnas.org](http://www.pnas.org).
- Cho, N., Razipour, S. E., & McCain, M. L. (2018). TGF- $\beta$ 1 dominates extracellular matrix rigidity for inducing differentiation of human cardiac fibroblasts to myofibroblasts. *Experimental Biology and Medicine*, 243(7), 601–612. <https://doi.org/10.1177/1535370218761628>

- Christine, J., Jennifer, M., Jagat, N., & H, M. T. (2010). Assessment of Nonischemic Myocardial Fibrosis. *Journal of the American College of Cardiology*, 56(2), 89–97. <https://doi.org/10.1016/j.jacc.2010.02.047>
- Clayton, C. R. I. (2011). Stiffness at small strain: research and practice. *Géotechnique*, 61(1), 5–37.
- Cofiño-Fabres, C., Boonen, T., Rivera-Arbeláez, J. M., Rijpkema, M., Blauw, L., Rensen, P. C. N., Schwach, V., Ribeiro, M. C., & Passier, R. (2024). Micro-Engineered Heart Tissues On-Chip with Heterotypic Cell Composition Display Self-Organization and Improved Cardiac Function. *Advanced Healthcare Materials*, n/a(n/a), 2303664. <https://doi.org/https://doi.org/10.1002/adhm.202303664>
- Crabos, M., Roth, M., Hahn, A. W. A., & Erne, P. (1994). Characterization of angiotensin II receptors in cultured adult rat cardiac fibroblasts: Coupling to signaling systems and gene expression. *Journal of Clinical Investigation*, 93(6), 2372–2378. <https://doi.org/10.1172/JCI117243>
- CRISPR/Cas9. (2023). <https://crisprtx.com/gene-editing/crispr-cas9>
- Cristoforetti, A., Masè, M., & Ravelli, F. (2023). Model-Based Approach for the Semi-Automatic Analysis of Collagen Birefringence in Polarized Light Microscopy. *Applied Sciences*, 13(5). <https://doi.org/10.3390/app13052916>
- Cumberland, M. J., Euchner, J., Azad, A. J., T N Vo, N., Kirchhof, P., Holmes, A. P., Denning, C., & Gehmlich, K. (2023). Generation of a human iPSC-derived cardiomyocyte/fibroblast engineered heart tissue model. *F1000Research*, 12, 1224. <https://doi.org/10.12688/f1000research.139482.1>
- Czarkowska-Paczek, B., Bartłomiejczyk, I., & Przybylski, J. (2006). The Serum Levels of Growth Factors: PDGF, TGF-Beta and VEGF are increased after strenuous physical exercise. *Journal of Physiology and Pharmacology*, 52(2), 189–197. [www.jpp.krakow.pl](http://www.jpp.krakow.pl)
- Czubryt, M. P. (2012). Common threads in cardiac fibrosis, infarct scar formation, and wound healing. *Fibrogenesis & Tissue Repair*, 5(1), 19. <https://doi.org/10.1186/1755-1536-5-19>
- Czubryt, M. P. (2019). Cardiac fibroblast to myofibroblast phenotype conversion-an unexploited therapeutic target. In *Journal of Cardiovascular Development and Disease* (Vol. 6, Issue 3). MDPI. <https://doi.org/10.3390/JCDD6030028>
- Dargie, H. J., & Byrne, J. (1995). Pathophysiological Aspects of the Renin–Angiotensin–Aldosterone System in Acute Myocardial Infarction. *Journal of Cardiovascular Risk*, 2(5), 389–395. <https://doi.org/10.1177/174182679500200502>
- de Bakker, J. M., van Capelle, F. J., Janse, M. J., Tasseron, S., Vermeulen, J. T., de Jonge, N., & Lahpor, J. R. (1993). Slow conduction in the infarcted human heart. “Zigzag” course of activation. *Circulation*, 88(3), 915–926. <https://doi.org/10.1161/01.CIR.88.3.915>
- de Bruijn, M., & Dzierzak, E. (2017). Runx transcription factors in the development and function of the definitive hematopoietic system. *Blood*, 129(15), 2061–2069. <https://doi.org/10.1182/blood-2016-12-689109>
- Derks, W., & Bergmann, O. (2020). Polyploidy in Cardiomyocytes. *Circulation Research*, 126(4), 552–565. <https://doi.org/10.1161/CIRCRESAHA.119.315408>

- Derynck, R., & Zhang, Y. E. (2003). Smad-dependent and Smad-independent pathways in TGF- $\beta$  family signalling. *Nature*, 425, 577–584. <https://doi.org/10.1038/nature02006>
- Desmoulibre, A., Geinoz, A., Gabbiani, F., & Gabbiani, G. (1996). Transforming Growth Factor- $\beta$  Induces  $\alpha$ -Smooth Muscle Actin Expression in Granulation Tissue Myofibroblasts and in Quiescent and Growing Cultured Fibroblasts. *Arteriosclerosis, Thrombosis, and Vascular Biology*, 16, 1298–1305. <https://doi.org/10.1161/01.ATV.16.10.1298>
- Di Iorio, A., Ferrucci, L., Sparvieri, E., Cherubini, A., Volpato, S., Corsi, A., Bonafè, M., Franceschi, C., Abate, G., & Paganelli, R. (2003). Serum IL-1 $\beta$  levels in health and disease: a population-based study. 'The InCHIANTI study.' *Cytokine*, 22(6), 198–205. [https://doi.org/10.1016/S1043-4666\(03\)00152-2](https://doi.org/10.1016/S1043-4666(03)00152-2)
- Dillinger, S. (2021, February 9). *Complete Guide to Understanding and Using ATAC-Seq*. <https://www.activemotif.com/blog-atac-seq>
- Dobaczewski, M., Chen, W., & Frangogiannis, N. G. (2011). Transforming growth factor (TGF)- $\beta$  signaling in cardiac remodeling. *Journal of Molecular and Cellular Cardiology*, 51(4), 600–606. <https://doi.org/10.1016/j.yjmcc.2010.10.033>
- Doppler, S. A., Carvalho, C., Lahm, H., Deutsch, M. A., Dreßen, M., Puluca, N., Lange, R., & Krane, M. (2017). Cardiac fibroblasts: More than mechanical support. In *Journal of Thoracic Disease* (Vol. 9, pp. S36–S51). AME Publishing Company. <https://doi.org/10.21037/jtd.2017.03.122>
- Doudna, J. A., & Charpentier, E. (2014). The new frontier of genome engineering with CRISPR-Cas9. *Science*, 346(6213), 1258096. <https://doi.org/10.1126/science.1258096>
- Dubey, S., Dubey, P. K., Umeshappa, C. S., Ghebre, Y. T., & Krishnamurthy, P. (2022). Inhibition of RUNX1 blocks the differentiation of lung fibroblasts to myofibroblasts. *Journal of Cellular Physiology*, 237(4), 2169–2182. <https://doi.org/10.1002/jcp.30684>
- Duong, H., Wu, B., & Tawil, B. (2009). Modulation of 3D Fibrin Matrix Stiffness by Intrinsic Fibrinogen-Thrombin Compositions and by Extrinsic Cellular Activity. *Tissue Engineering Part A*, 15(7), 1865–1876.
- Eddy, R. J., Petro, J. A., & Tomasek, J. J. (1988). "Myofibroblast" of Granulation Tissue and Hypertrophic Scar An Immunofluorescence Study. In *American Journal of Pathology* (Vol. 130, Issue 2).
- Eder, A., Vollert, I., Hansen, A., & Eschenhagen, T. (2016). Human engineered heart tissue as a model system for drug testing. *Advanced Drug Delivery Reviews*, 96, 214–224. <https://doi.org/10.1016/j.addr.2015.05.010>
- El-Marasy, S. A., El Awdan, S. A., Hassan, A., & Abdallah, H. M. I. (2020). Cardioprotective effect of thymol against adrenaline-induced myocardial injury in rats. *Heliyon*, 6(7). <https://doi.org/10.1016/j.heliyon.2020.e04431>
- Emmons-Bell, S., Johnson, C., & Roth, G. (2022). Prevalence, incidence and survival of heart failure: A systematic review. In *Heart*. BMJ Publishing Group. <https://doi.org/10.1136/heartjnl-2021-320131>

- Eschenhagen, T. (2015). *Individualized Early Risk Assessment for Heart Diseases (IndivuHeart)*. <https://clinicaltrials.gov/study/NCT02417311>
- Eschenhagen, T. (2018). A new concept of fibroblast dynamics in post-myocardial infarction remodeling. In *Journal of Clinical Investigation* (Vol. 128, Issue 5, pp. 1731–1733). American Society for Clinical Investigation. <https://doi.org/10.1172/JCI121079>
- Eschenhagen, T., Fink, C., Remmers, U., Scholz, H., Wattchow, J., Weil, J., Zimmermann, W., Dohmen, H. H., Schäfer, H., Bishopric, N., Wakatsuki, T., & Elson, E. L. (1997). Three-dimensional reconstitution of embryonic cardiomyocytes in a collagen matrix: a new heart muscle model system. *The FASEB Journal*, 11(8), 683–694. <https://doi.org/https://doi.org/10.1096/fasebj.11.8.9240969>
- Esquibel, C. R., Wendt, K. D., Lee, H. C., Gaire, J., Shoffstall, A., Urdaneta, M. E., Chacko, J. V., Brodnick, S. K., Otto, K. J., Capadona, J. R., Williams, J. C., & Eliceiri, K. W. (2020). Second Harmonic Generation Imaging of Collagen in Chronically Implantable Electrodes in Brain Tissue. *Frontiers in Neuroscience*, 14. <https://doi.org/10.3389/fnins.2020.00095>
- Fernandes, M., & Pedroso, A. (2017). Animal experimentation: A look into ethics, welfare and alternative methods. *Revista Da Associacao Medica Brasileira* (1992), 63, 923–928. <https://doi.org/10.1590/1806-9282.63.11.923>
- Figtree, G. A., Bubb, K. J., Tang, O., Kizana, E., & Gentile, C. (2017). Vascularized Cardiac Spheroids as Novel 3D in vitro Models to Study Cardiac Fibrosis. *Cells Tissues Organs*, 204(3–4), 191–198. <https://doi.org/10.1159/000477436>
- Frangogiannis, N. G. (2021). Cardiac fibrosis. *Cardiovascular Research*, 117(6), 1450–1488. <https://doi.org/10.1093/cvr/cvaa324>
- Frangogiannis, N. G., Michael, L. H., & Entman, M. L. (2000). Myofibroblasts in reperfused myocardial infarcts express the embryonic form of smooth muscle myosin heavy chain (SMemb). In *Cardiovascular Research* (Vol. 48). [www.elsevier.com/locate/cardiores](http://www.elsevier.com/locate/cardiores) [www.elsevier.nl/locate/cardiores](http://www.elsevier.nl/locate/cardiores)
- Frank, S., Zhang, M., Schöler, H. R., & Greber, B. (2012). Small molecule-assisted, line-independent maintenance of human pluripotent stem cells in defined conditions. *PLoS ONE*, 7(7). <https://doi.org/10.1371/journal.pone.0041958>
- Fu, X., Khalil, H., Kanisicak, O., Boyer, J. G., Vagnozzi, R. J., Maliken, B. D., Sargent, M. A., Prasad, V., Valiente-Alandi, I., Blaxall, B. C., & Molkentin, J. D. (2018). Specialized fibroblast differentiated states underlie scar formation in the infarcted mouse heart. *Journal of Clinical Investigation*, 128(5), 2127–2143. <https://doi.org/10.1172/JCI98215>
- Fu, X., Liu, Q., Li, C., Li, Y., & Wang, L. (2020). Cardiac Fibrosis and Cardiac Fibroblast Lineage-Tracing: Recent Advances. In *Frontiers in Physiology* (Vol. 11). Frontiers Media S.A. <https://doi.org/10.3389/fphys.2020.00416>
- Fullerton, M. J., & Funder, J. W. (1994). Aldosterone and cardiac fibrosis: in vitro studies. *Cardiovascular Research*, 28(12), 1863–1867. <https://doi.org/10.1093/cvr/28.12.1863>
- Gabisonia, K., Prosdocimo, G., Aquaro, G. D., Carlucci, L., Zentilin, L., Secco, I., Ali, H., Braga, L., Gorgodze, N., Bernini, F., Burchielli, S., Collesi, C., Zandonà, L., Sinagra, G., Piacenti, M., Zacchigna,



- S., Bussani, R., Recchia, F. A., & Giacca, M. (2019). MicroRNA therapy stimulates uncontrolled cardiac repair after myocardial infarction in pigs. *Nature*, 569(7756), 418–422. <https://doi.org/10.1038/s41586-019-1191-6>
- Gaetani, R., Zizzi, E. A., Deriu, M. A., Morbiducci, U., Pesce, M., & Messina, E. (2020). When Stiffness Matters: Mechanosensing in Heart Development and Disease. In *Frontiers in Cell and Developmental Biology* (Vol. 8). Frontiers Media S.A. <https://doi.org/10.3389/fcell.2020.00334>
- Gargotti, M., Lopez-Gonzalez, U., Byrne, H. J., & Casey, A. (2018). Comparative studies of cellular viability levels on 2D and 3D in vitro culture matrices. *Cytotechnology*, 70(1), 261–273. <https://doi.org/10.1007/s10616-017-0139-7>
- Gaudesius, G., Miragoli, M., Thomas, S. P., & Rohr, Stephan. (2003). Coupling of Cardiac Electrical Activity Over Extended Distances by Fibroblasts of Cardiac Origin. *Circulation Research*, 93(5), 421–428. <https://doi.org/10.1161/01.RES.0000089258.40661.0C>
- Ghisletti, S., Barozzi, I., Mietton, F., Polletti, S., De Santa, F., Venturini, E., Gregory, L., Lonie, L., Chew, A., Wei, C. L., Ragoussis, J., & Natoli, G. (2010). Identification and Characterization of Enhancers Controlling the Inflammatory Gene Expression Program in Macrophages. *Immunity*, 32(3), 317–328. <https://doi.org/10.1016/j.immuni.2010.02.008>
- Gilbert, G., Demydenko, K., Dries, E., Puertas, R. D., Jin, X., Sipido, K., & Llewelyn Roderick, H. (2020). Calcium signaling in cardiomyocyte function. *Cold Spring Harbor Perspectives in Biology*, 12(3). <https://doi.org/10.1101/cshperspect.a035428>
- Goffin, L., Seguin-Estévez, Q., Alvarez, M., Reith, W., & Chizzolini, C. (2010). Transcriptional regulation of matrix metalloproteinase-1 and collagen 1A2 explains the anti-fibrotic effect exerted by proteasome inhibition in human dermal fibroblasts. *Arthritis Research & Therapy*, 12(2), R73. <https://doi.org/10.1186/ar2991>
- Goldsmith, E. C., Bradshaw, A. D., Zile, M. R., & Spinale, F. G. (2014). Myocardial fibroblast-matrix interactions and potential therapeutic targets. In *Journal of Molecular and Cellular Cardiology* (Vol. 70, pp. 92–99). Academic Press. <https://doi.org/10.1016/j.yjmcc.2014.01.008>
- Guo, Y., & Pu, W. T. (2020). Cardiomyocyte Maturation: New Phase in Development. In *Circulation Research* (Vol. 126, Issue 8, pp. 1086–1106). Lippincott Williams and Wilkins. <https://doi.org/10.1161/CIRCRESAHA.119.315862>
- Guo, Z., Liu, X., Zhao, S., Sun, F., Ren, W., & Ma, M. (2023). RUNX1 promotes liver fibrosis progression through regulating TGF- $\beta$  signalling. *International Journal of Experimental Pathology*, 104(4), 188–198. <https://doi.org/https://doi.org/10.1111/iep.12474>
- Hafizi, S., Wharton, J., Morgan, K., Allen, S. P., Chester, A. H., Catravas, J. D., Polak, J. M., & Yacoub, M. H. (1998). Expression of Functional Angiotensin-Converting Enzyme and AT1 Receptors in Cultured Human Cardiac Fibroblasts. *Circulation*, 98(23), 2553–2559. <https://doi.org/10.1161/01.CIR.98.23.2553>
- Hall, C., Law, J. P., Reyat, J. S., Cumberland, M. J., Hang, S., Vo, N. T. N., Raniga, K., Weston, C. J., O’Shea, C., Townend, J. N., Gehmlich, K., Ferro, C. J., Denning, C., & Pavlovic, D. (2023). Chronic activation

- of human cardiac fibroblasts in vitro attenuates the reversibility of the myofibroblast phenotype. *Scientific Reports*, 13(1). <https://doi.org/10.1038/s41598-023-39369-y>
- Hansen, A., Eder, A., Bönstrup, M., Flato, M., Mewe, M., Schaaf, S., Aksehirlioglu, B., Schwörer, A., Uebeler, J., & Eschenhagen, T. (2010). Development of a Drug Screening Platform Based on Engineered Heart Tissue. *Circulation Research*, 107(1), 35–44. <https://doi.org/10.1161/CIRCRESAHA.109.211458>
- He, K., Shi, X., Zhang, X., Dang, S., Ma, X., Liu, F., Xu, M., Lv, Z., Han, D., Fang, X., & Zhang, Y. (2011). Long-distance intercellular connectivity between cardiomyocytes and cardiofibroblasts mediated by membrane nanotubes. *Cardiovascular Research*, 92(1), 39–47. <https://doi.org/10.1093/cvr/cvr189>
- Henriksen, K., & Karsdal, M. A. (2016). Chapter 1 - Type I Collagen. In M. A. Karsdal (Ed.), *Biochemistry of Collagens, Laminins and Elastin* (pp. 1–11). Academic Press. <https://doi.org/https://doi.org/10.1016/B978-0-12-809847-9.00001-5>
- Himmel, H. M. (2013). Drug-induced functional cardiotoxicity screening in stem cell-derived human and mouse cardiomyocytes: Effects of reference compounds. *Journal of Pharmacological and Toxicological Methods*, 68(1), 97–111. <https://doi.org/https://doi.org/10.1016/j.vascn.2013.05.005>
- Hinderer, S., & Schenke-Layland, K. (2019). Cardiac fibrosis – A short review of causes and therapeutic strategies. *Advanced Drug Delivery Reviews*, 146, 77–82. <https://doi.org/https://doi.org/10.1016/j.addr.2019.05.011>
- Hirt, M. N., Boeddinghaus, J., Mitchell, A., Schaaf, S., Börnchen, C., Müller, C., Schulz, H., Hubner, N., Stenzig, J., Stoehr, A., Neuber, C., Eder, A., Luther, P. K., Hansen, A., & Eschenhagen, T. (2014). Functional improvement and maturation of rat and human engineered heart tissue by chronic electrical stimulation. *Journal of Molecular and Cellular Cardiology*, 74, 151–161. <https://doi.org/10.1016/j.yjmcc.2014.05.009>
- Hjelmeland, M. D., Hjelmeland, A. B., Sathornsumetee, S., Reese, E. D., Herbstreith, M. H., Laping, N. J., Friedman, H. S., Bigner, D. D., Wang, X.-F., & Rich, J. N. (2004). SB-431542, a small molecule transforming growth factor-B-receptor antagonist, inhibits human glioma cell line proliferation and motility. *Molecular Cancer Therapeutics*, 3(6), 737–782. <http://aacrjournals.org/mct/article-pdf/3/6/737/1868351/737-745.pdf>
- Hori, M., & Nishida, K. (2009). Oxidative stress and left ventricular remodelling after myocardial infarction. In *Cardiovascular Research* (Vol. 81, Issue 3, pp. 457–464). <https://doi.org/10.1093/cvr/cvn335>
- Horn, M. A., & Trafford, A. W. (2016). Aging and the cardiac collagen matrix: Novel mediators of fibrotic remodelling. *Journal of Molecular and Cellular Cardiology*, 93, 175–185. <https://doi.org/https://doi.org/10.1016/j.yjmcc.2015.11.005>
- Htwe, S. S., Harrington, H., Knox, A., Rose, F., Aylott, J., Haycock, J. W., & Ghaemmaghani, A. M. (2015). Investigating NF-κB signaling in lung fibroblasts in 2D and 3D culture systems. *Respiratory Research*, 16(1), 144. <https://doi.org/10.1186/s12931-015-0302-7>

- Hu, H., Lin, S., Wang, S., & Chen, X. (2020). The Role of Transcription Factor 21 in Epicardial Cell Differentiation and the Development of Coronary Heart Disease. In *Frontiers in Cell and Developmental Biology* (Vol. 8). Frontiers Media S.A. <https://doi.org/10.3389/fcell.2020.00457>
- Hu, H.-H., Chen, D.-Q., Wang, Y.-N., Feng, Y.-L., Cao, G., Vaziri, N. D., & Zhao, Y.-Y. (2018). New insights into TGF- $\beta$ /Smad signaling in tissue fibrosis. *Chemico-Biological Interactions*, 292, 76–83. <https://doi.org/https://doi.org/10.1016/j.cbi.2018.07.008>
- Hudon-David, F., Bouzeghrane, F., Couture, P., & Thibault, G. (2007). Thy-1 expression by cardiac fibroblasts: Lack of association with myofibroblast contractile markers. *Journal of Molecular and Cellular Cardiology*, 42(5), 991–1000. <https://doi.org/10.1016/j.yjmcc.2007.02.009>
- Huebener, P., Abou-Khamis, T., Zymek, P., Bujak, M., Ying, X., Chatila, K., Haudek, S., Thakker, G., & Frangogiannis, N. G. (2008). CD44 Is Critically Involved in Infarct Healing by Regulating the Inflammatory and Fibrotic Response 1. In *The Journal of Immunology* (Vol. 180). [www.jimmunol.org](http://www.jimmunol.org)
- Humeres, C., & Frangogiannis, N. G. (2019). Fibroblasts in the Infarcted, Remodeling, and Failing Heart. In *JACC: Basic to Translational Science* (Vol. 4, Issue 3, pp. 449–467). Elsevier Inc. <https://doi.org/10.1016/j.jacbts.2019.02.006>
- Humeres, C., Shinde, A. V, Hanna, A., Alex, L., Hernández, S. C., Li, R., Chen, B., Conway, S. J., & Frangogiannis, N. G. (2022). Smad7 effects on TGF- $\beta$  and ErbB2 restrain myofibroblast activation and protect from postinfarction heart failure. *The Journal of Clinical Investigation*, 132(3). <https://doi.org/10.1172/JCI146926>
- Hyun, S.-W., Kim, B.-R., Hyun, S.-A., & Seo, J.-W. (2017). The assessment of electrophysiological activity in human-induced pluripotent stem cell-derived cardiomyocytes exposed to dimethyl sulfoxide and ethanol by manual patch clamp and multi-electrode array system. *Journal of Pharmacological and Toxicological Methods*, 87, 93–98. <https://doi.org/https://doi.org/10.1016/j.vascn.2017.03.003>
- Ichikawa, M., Yoshimi, A., Nakagawa, M., Nishimoto, N., Watanabe-Okochi, N., & Kurokawa, M. (2013). A role for RUNX1 in hematopoiesis and myeloid leukemia. *International Journal of Hematology*, 97(6), 726–734. <https://doi.org/10.1007/s12185-013-1347-3>
- Inman, G. J., Nicolás, F. J., Callahan, J. F., Harling, J. D., Gaster, L. M., Reith, A. D., Laping, N. J., & Hill, C. S. (2002). SB-431542 Is a Potent and Specific Inhibitor of Transforming Growth Factor- $\beta$  Superfamily Type I Activin Receptor-Like Kinase (ALK) Receptors ALK4, ALK5, and ALK7. *Molecular Pharmacology*, 62(1), 65. <https://doi.org/10.1124/mol.62.1.65>
- Inman, G. J., Nicolás, F. J., & Hill, C. S. (2002). Nucleocytoplasmic Shuttling of Smads 2, 3, and 4 Permits Sensing of TGF- $\beta$ 1; Receptor Activity. *Molecular Cell*, 10(2), 283–294. [https://doi.org/10.1016/S1097-2765\(02\)00585-3](https://doi.org/10.1016/S1097-2765(02)00585-3)
- Iseoka, H., Miyagawa, S., Sakai, Y., & Sawa, Y. (2021). Cardiac fibrosis models using human induced pluripotent stem cell-derived cardiac tissues allow anti-fibrotic drug screening in vitro. *Stem Cell Research*, 54, 102420. <https://doi.org/https://doi.org/10.1016/j.scr.2021.102420>

- Ishibashi, R., & Taguchi, Y. (2021). Identification of enhancers and promoters in the genome by multidimensional scaling. *Genes*, 12(11). <https://doi.org/10.3390/genes12111671>
- Jiang, H., Song, S., Li, J., Yin, Q., Hu, S., & Nie, Y. (2021). Establishment and characterization of an immortalized epicardial cell line. *Journal of Cellular and Molecular Medicine*, 25(13), 6070–6081. <https://doi.org/https://doi.org/10.1111/jcmm.16496>
- Jones, D. L., Caporarello, N., Meridew, J. A., Choi, K. M., Haak, A. J., Link, P. A., Tan, Q., Ordog, T., Ligresti, G., & Tschumperlin, D. J. (2022). Lung injury epigenetically primes mesenchyme for amplified activation upon re-injury. *BioRxiv*, 2022.03.04.483065. <https://doi.org/10.1101/2022.03.04.483065>
- Kamkin, A., Kiseleva, I., & Isenberg, G. (2003). Activation and inactivation of a non-selective cation conductance by local mechanical deformation of acutely isolated cardiac fibroblasts. *Cardiovascular Research*, 57(3), 793–803. [https://doi.org/10.1016/S0008-6363\(02\)00775-7](https://doi.org/10.1016/S0008-6363(02)00775-7)
- Karasu, N., & Sexton, T. (2021). 4C-Seq: Interrogating Chromatin Looping with Circular Chromosome Conformation Capture. In B. Bodega & C. Lanzuolo (Eds.), *Capturing Chromosome Conformation: Methods and Protocols* (pp. 19–34). Springer US. [https://doi.org/10.1007/978-1-0716-0664-3\\_3](https://doi.org/10.1007/978-1-0716-0664-3_3)
- Keepers, B., Liu, J., & Qian, L. (2020). What's in a cardiomyocyte – And how do we make one through reprogramming? In *Biochimica et Biophysica Acta - Molecular Cell Research* (Vol. 1867, Issue 3). Elsevier B.V. <https://doi.org/10.1016/j.bbamcr.2019.03.011>
- Kemp, T. J., Aggeli, I.-K., Sugden, P. H., & Clerk, A. (2004). Phenylephrine and endothelin-1 upregulate connective tissue growth factor in neonatal rat cardiac myocytes. *Journal of Molecular and Cellular Cardiology*, 37(2), 603–606. <https://doi.org/10.1016/j.yjmcc.2004.04.022>
- Kiani, A. K., Pheby, D., Henahan, G., Brown, R., Sieving, P., Sykora, P., Marks, R., Falsini, B., Capodicasa, N., Miertus, S., Lorusso, L., Dondossola, D., Tartaglia, G. M., Ergoren, M. C., Dundar, M., Michelini, S., Malacarne, D., Bonetti, G., Dautaj, A., ... Bertelli, M. (2022). Ethical considerations regarding animal experimentation. In *Journal of preventive medicine and hygiene* (Vol. 63, Issue 2, pp. E255–E266). NLM (Medline). <https://doi.org/10.15167/2421-4248/jpmh2022.63.2S3.2768>
- Kim, S. S., Jackson-Boeters, L., Darling, M. R., Rieder, M. J., & Hamilton, D. W. (2013). Nifedipine Induces Periostin Expression in Gingival Fibroblasts through TGF-beta. *Journal of Dental Research*, 92(11), 1022–1028. <https://doi.org/10.1177/0022034513503659>
- Koch, F., Fenouil, R., Gut, M., Cauchy, P., Albert, T. K., Zacarias-Cabeza, J., Spicuglia, S., de la Chapelle, A. L., Heidemann, M., Hintermair, C., Eick, D., Gut, I., Ferrier, P., & Andrau, J.-C. (2011). Transcription initiation platforms and GTF recruitment at tissue-specific enhancers and promoters. *Nature Structural & Molecular Biology*, 18(8), 956–963. <https://doi.org/10.1038/nsmb.2085>
- Koitabashi, N., Danner, T., Zaiman, A. L., Pinto, Y. M., Rowell, J., Mankowski, J., Zhang, D., Nakamura, T., Takimoto, E., & Kass, D. A. (2011). Pivotal role of cardiomyocyte TGF-β signaling in the murine pathological response to sustained pressure overload. *Journal of Clinical Investigation*, 121(6), 2301–2312. <https://doi.org/10.1172/JCI44824>

- Kong, M., Lee, J., Yazdi, I. K., Miri, A. K., Lin, Y.-D., Seo, J., Zhang, Y. S., Khademhosseini, A., & Shin, S. R. (2019). Cardiac Fibrotic Remodeling on a Chip with Dynamic Mechanical Stimulation. *Advanced Healthcare Materials*, 8(3), 1801146. <https://doi.org/https://doi.org/10.1002/adhm.201801146>
- Krijger, P. H. L., Geeven, G., Bianchi, V., Hilvering, C. R. E., & de Laat, W. (2020). 4C-seq from beginning to end: A detailed protocol for sample preparation and data analysis. *Methods*, 170, 17–32. <https://doi.org/https://doi.org/10.1016/j.ymeth.2019.07.014>
- Krivega, I., & Dean, A. (2012). Enhancer and promoter interactions—long distance calls. *Current Opinion in Genetics & Development*, 22(2), 79–85. <https://doi.org/https://doi.org/10.1016/j.gde.2011.11.001>
- Kuhn, E. N., & Wu, S. M. (2010). Origin of cardiac progenitor cells in the developing and postnatal heart. In *Journal of Cellular Physiology* (Vol. 225, Issue 2, pp. 321–325). Wiley-Liss Inc. <https://doi.org/10.1002/jcp.22281>
- Kumar, R., Grønhaug, K. M., Romijn, E. I., Finnøy, A., Davies, C. L., Drogset, J. O., & Lilledahl, M. B. (2015). Polarization second harmonic generation microscopy provides quantitative enhanced molecular specificity for tissue diagnostics. *Journal of Biophotonics*, 8(9), 730–739. <https://doi.org/https://doi.org/10.1002/jbio.201400086>
- Kuppe, C., Ramirez Flores, R. O., Li, Z., Hayat, S., Levinson, R. T., Liao, X., Hannani, M. T., Tanevski, J., Wünnemann, F., Nagai, J. S., Halder, M., Schumacher, D., Menzel, S., Schäfer, G., Hoeft, K., Cheng, M., Ziegler, S., Zhang, X., Peisker, F., ... Kramann, R. (2022). Spatial multi-omic map of human myocardial infarction. *Nature*, 608(7924), 766–777. <https://doi.org/10.1038/s41586-022-05060-x>
- Kurose, H. (2021). Cardiac fibrosis and fibroblasts. In *Cells* (Vol. 10, Issue 7). MDPI. <https://doi.org/10.3390/cells10071716>
- Kwong, G., Marquez, H. A., Yang, C., Wong, J. Y., & Kotton, D. N. (2019). Generation of a Purified iPSC-Derived Smooth Muscle-like Population for Cell Sheet Engineering. *Stem Cell Reports*, 13(3), 499–514. <https://doi.org/https://doi.org/10.1016/j.stemcr.2019.07.014>
- Law, B. A., & Carver, W. E. (2013). Activation of Cardiac Fibroblasts by Ethanol Is Blocked by TGF- $\beta$  Inhibition. *Alcoholism: Clinical and Experimental Research*, 37(8), 1286–1294. <https://doi.org/https://doi.org/10.1111/acer.12111>
- Lebeau, B., Zhao, K., Jangal, M., Zhao, T., Guerra, M., Greenwood, C. M. T., & Witcher, M. (2022). Single base-pair resolution analysis of DNA binding motif with MoMotif reveals an oncogenic function of CTCF zinc-finger 1 mutation. *Nucleic Acids Research*, 50(15), 8441–8458. <https://doi.org/10.1093/nar/gkac658>
- Lee, M.-O., Jung, K. B., Jo, S.-J., Hyun, S.-A., Moon, K.-S., Seo, J.-W., Kim, S.-H., & Son, M.-Y. (2019). Modelling cardiac fibrosis using three-dimensional cardiac microtissues derived from human embryonic stem cells. *Journal of Biological Engineering*, 13(1), 15. <https://doi.org/10.1186/s13036-019-0139-6>
- Lettice, L. A., Heaney, S. J. H., Purdie, L. A., Li, L., de Beer, P., Oostra, B. A., Goode, D., Elgar, G., Hill, R. E., & de Graaff, E. (2003). A long-range Shh enhancer regulates expression in the developing limb

- and fin and is associated with preaxial polydactyly. *Human Molecular Genetics*, 12(14), 1725–1735. <https://doi.org/10.1093/hmg/ddg180>
- Levanon, D., Negreanu, V., Bernstein, Y., Bar-Am, I., Avivi, L., & Groner, Y. (1994). AML1, AML2, and AML3, the Human Members of the runt domain Gene-Family: cDNA Structure, Expression, and Chromosomal Localization. *Genomics*, 23(2), 425–432. <https://doi.org/https://doi.org/10.1006/geno.1994.1519>
- Li, D., Sun, J., & Zhong, T. P. (2022). Wnt Signaling in Heart Development and Regeneration. In *Current Cardiology Reports* (Vol. 24, Issue 10, pp. 1425–1438). Springer. <https://doi.org/10.1007/s11886-022-01756-8>
- Li, H., Zhao, C., Li, Z., Yao, K., Zhang, J., Si, W., Liu, X., Jiang, Y., & Zhu, M. (2021). Identification of Potential Pathogenic Super-Enhancers-Driven Genes in Pulmonary Fibrosis. *Frontiers in Genetics*, 12. <https://doi.org/10.3389/fgene.2021.644143>
- Li, M. X., Wang, X. U., & Sykes, B. D. (2005). Structural based insights into the role of troponin in cardiac muscle pathophysiology. *Journal of Muscle Research & Cell Motility*, 559–579. <https://doi.org/https://doi.org/10.1007/s10974-004-5879-2>
- Li, X., Zhang, S., Wa, M., Liu, Z., & Hu, S. (2019). MicroRNA-101 Protects Against Cardiac Remodeling Following Myocardial Infarction via Downregulation of Runt-Related Transcription Factor 1. *Journal of the American Heart Association*, 8(23), e013112. <https://doi.org/10.1161/JAHA.119.013112>
- Li, Y., Asfour, H., & Bursac, N. (2017). Age-dependent functional crosstalk between cardiac fibroblasts and cardiomyocytes in a 3D engineered cardiac tissue. *Acta Biomaterialia*, 55, 120–130. <https://doi.org/https://doi.org/10.1016/j.actbio.2017.04.027>
- Liau, W.-S., Ngoc, P. C. T., & Sanda, T. (2017). Roles of the RUNX1 Enhancer in Normal Hematopoiesis and Leukemogenesis. In Y. Groner, Y. Ito, P. Liu, J. C. Neil, N. A. Speck, & A. van Wijnen (Eds.), *RUNX Proteins in Development and Cancer* (pp. 139–147). Springer Singapore. [https://doi.org/10.1007/978-981-10-3233-2\\_10](https://doi.org/10.1007/978-981-10-3233-2_10)
- Lijnen, P., & Petrov, V. (2000). Induction of Cardiac Fibrosis by Aldosterone. *Journal of Molecular and Cellular Cardiology*, 32(6), 865–879. <https://doi.org/https://doi.org/10.1006/jmcc.2000.1129>
- Lindert, S., Kekenus-Huskey, P. M., Huber, G., Pierce, L., & McCammon, J. A. (2012). Dynamics and calcium association to the N-terminal regulatory domain of human cardiac Troponin C: A multiscale computational study. *Journal of Physical Chemistry B*, 116(29), 8449–8459. <https://doi.org/10.1021/jp212173f>
- Litviňuková, M., Talavera-López, C., Maatz, H., Reichart, D., Worth, C. L., Lindberg, E. L., Kanda, M., Polanski, K., Heinig, M., Lee, M., Nadelmann, E. R., Roberts, K., Tuck, L., Fasouli, E. S., DeLaughter, D. M., McDonough, B., Wakimoto, H., Gorham, J. M., Samari, S., ... Teichmann, S. A. (2020). Cells of the adult human heart. *Nature*, 588(7838), 466–472. <https://doi.org/10.1038/s41586-020-2797-4>
- Liu, L., Zhou, X., Zhang, Q., Li, L., Shang, Y., Wang, Z., Zhong, M., Chen, Y., Zhang, W., & Tang, M. (2022). Activin receptor-like kinase 7 silencing alleviates cardiomyocyte apoptosis, cardiac fibrosis, and

- dysfunction in diabetic rats. *Experimental Biology and Medicine*, 247(16), 1397–1409. <https://doi.org/10.1177/15353702221095049>
- Loomans, H. A., & Andl, C. D. (2016). Activin receptor-like kinases: a diverse family playing an important role in cancer. In *Am J Cancer Res* (Vol. 6, Issue 11). [www.ajcr.us/](http://www.ajcr.us/)
- Lothar, A., Bondareva, O., Saadatmand, A. R., Pollmeier, L., Härdtnr, C., Hilgendorf, I., Weichenhan, D., Eckstein, V., Plass, C., Bode, C., Backs, J., Hein, L., & Gilsbach, R. (2021). Diabetes changes gene expression but not DNA methylation in cardiac cells. *Journal of Molecular and Cellular Cardiology*, 151, 74–87. <https://doi.org/10.1016/j.yjmcc.2020.11.004>
- Ma, T., Qiu, F., Gong, Y., Cao, H., Dai, G., Sun, D., Zhu, D., Lei, H., Liu, Z., & Gao, L. (2023). Therapeutic silencing of lncRNA RMST alleviates cardiac fibrosis and improves heart function after myocardial infarction in mice and swine. *Theranostics*, 13(11), 3826–3843. <https://doi.org/10.7150/thno.82543>
- Mahoney, V. M., Mezzano, V., & Morley, G. E. (2016). A review of the literature on cardiac electrical activity between fibroblasts and myocytes. *Progress in Biophysics and Molecular Biology*, 120(1), 128–133. <https://doi.org/https://doi.org/10.1016/j.pbiomolbio.2015.12.006>
- Majkut, S., Idema, T., Swift, J., Krieger, C., Liu, A., & Discher, D. E. (2013). Heart-specific stiffening in early embryos parallels matrix and myosin expression to optimize beating. *Current Biology*, 23(23), 2434–2439. <https://doi.org/10.1016/j.cub.2013.10.057>
- Martin, T. P., MacDonald, E. A., Bradley, A., Watson, H., Saxena, P., Rog-Zielinska, E. A., Fisher, S., Elbassioni, A. A. M., Almuzaini, O., Booth, C., Campbell, M., Herzyk, P., Blyth, K., Nixon, C., Zentilin, L., Berry, C., Braun, T., Giacca, M., McBride, M. W., ... Loughrey, C. M. (2022). Inhibiting Runx1 protects heart function after myocardial infarction. *BioRxiv*, 2022.02.17.480749. <https://doi.org/10.1101/2022.02.17.480749>
- Mastikhina, O., Moon, B.-U., Williams, K., Hatkar, R., Gustafson, D., Mourad, O., Sun, X., Koo, M., Lam, A. Y. L., Sun, Y., Fish, J. E., Young, E. W. K., & Nunes, S. S. (2020). Human cardiac fibrosis-on-a-chip model recapitulates disease hallmarks and can serve as a platform for drug testing. *Biomaterials*, 233, 119741. <https://doi.org/https://doi.org/10.1016/j.biomaterials.2019.119741>
- Masumoto, H., Ikuno, T., Takeda, M., Fukushima, H., Marui, A., Katayama, S., Shimizu, T., Ikeda, T., Okano, T., Sakata, R., & Yamashita, J. K. (2014). Human iPS cell-engineered cardiac tissue sheets with cardiomyocytes and vascular cells for cardiac regeneration. *Scientific Reports*, 4. <https://doi.org/10.1038/srep06716>
- McCarroll, C. S., He, W., Foote, K., Bradley, A., McGlynn, K., Vidler, F., Nixon, C., Nather, K., Fattah, C., Riddell, A., Bowman, P., Elliott, E. B., Bell, M., Hawksby, C., MacKenzie, S. M., Morrison, L. J., Terry, A., Blyth, K., Smith, G. L., ... Loughrey, C. M. (2018). Runx1 Deficiency Protects Against Adverse Cardiac Remodeling After Myocardial Infarction. *Circulation*, 137(1), 57–70. <https://doi.org/10.1161/CIRCULATIONAHA.117.028911>
- Miko, M., Kyselovic, J., Danisovic, L., Barczy, T., Polak, S., & Varga, I. (2017). Two nuclei inside a single cardiac muscle cell. More questions than answers about the binucleation of cardiomyocytes. *Biologia*, 72(8), 825–830.

- Miragoli, M., Gaudesius, G., & Rohr, S. (2006). Electrotonic Modulation of Cardiac Impulse Conduction by Myofibroblasts. *Circulation Research*, 98(6), 801–810. <https://doi.org/10.1161/01.RES.0000214537.44195.a3>
- Misra, R. P., Rivera, V. M., Wang, J. M., Fan, P.-D., & Greenberg, M. E. (1991). The Serum Response Factor Is Extensively Modified by Phosphorylation Following Its Synthesis in Serum-Stimulated Fibroblasts. *Molecular and Cellular Biology*, 11(9), 4545–4554. <https://doi.org/10.1128/mcb.11.9.4545-4554.1991>
- Mitchell, M. D., Laird, R. E., Brown, R. D., & Long, C. S. (2007). IL-1 $\beta$  stimulates rat cardiac fibroblast migration via MAP kinase pathways. *Am J Physiol Heart Circ Physiol*, 292, 1139–1147. <https://doi.org/10.1152/ajpheart.00881.2005.-The>
- Möllmann, H., Nef, H. M., Kostin, S., von Kalle, C., Pilz, I., Weber, M., Schaper, J., Hamm, C. W., & Elsässer, A. (2006). Bone marrow-derived cells contribute to infarct remodelling. *Cardiovascular Research*, 71(4), 661–671. <https://doi.org/10.1016/j.cardiores.2006.06.013>
- Moore-Morris, T., Cattaneo, P., Guimarães-Camboa, N., Bogomolovas, J., Cedenilla, M., Banerjee, I., Ricote, M., Kisseleva, T., Zhang, L., Gu, Y., Dalton, N. D., Peterson, K. L., Chen, J., Pucéat, M., & Evans, S. M. (2018). Infarct Fibroblasts Do Not Derive From Bone Marrow Lineages. *Circulation Research*, 122(4), 583–590. <https://doi.org/10.1161/CIRCRESAHA.117.311490>
- Moore-Morris, T., Guimarães-Camboa, N., Banerjee, I., Zambon, A. C., Kisseleva, T., Velayoudon, A., Stallcup, W. B., Gu, Y., Dalton, N. D., Cedenilla, M., Gomez-Amaro, R., Zhou, B., Brenner, D. A., Peterson, K. L., Chen, J., & Evans, S. M. (2014). Resident fibroblast lineages mediate pressure overload-induced cardiac fibrosis. *Journal of Clinical Investigation*, 124(7), 2921–2934. <https://doi.org/10.1172/JCI74783>
- Murtha, L. A., Schuliga, M. J., Mabotuwana, N. S., Hardy, S. A., Waters, D. W., Burgess, J. K., Knight, D. A., & Boyle, A. J. (2017). The Processes and Mechanisms of Cardiac and Pulmonary Fibrosis. *Frontiers in Physiology*, 8. <https://www.frontiersin.org/journals/physiology/articles/10.3389/fphys.2017.00777>
- Mussi, A., Bonifati, C., Carducci, M., D'Agosto, G., Pimpinelli, F., D'Urso, D., D'Auria, L., Fazio, M., & Ameglio, F. (1997). Serum TNF-alpha levels correlate with disease severity and are reduced by effective therapy in plaque-type psoriasis. *Journal of Biological Regulators and Homeostatic Agents*, 11(3), 115–118. <http://europepmc.org/abstract/MED/9498161>
- Neumann, S., Huse, K., Semrau, R., Diegeler, A., Gebhardt, R., Buniatian, G. H., & Scholz, G. H. (2002). Aldosterone and d-Glucose Stimulate the Proliferation of Human Cardiac Myofibroblasts In Vitro. *Hypertension*, 39(3), 756–760. <https://doi.org/10.1161/hy0302.105295>
- Ni, T., Huang, X., Pan, S., & Lu, Z. (2021). Dihydrolycorine Attenuates Cardiac Fibrosis and Dysfunction by Downregulating Runx1 following Myocardial Infarction. *Oxidative Medicine and Cellular Longevity*, 2021. <https://doi.org/10.1155/2021/8528239>
- Nielsen, M. J., & Karsdal, M. A. (2016). Chapter 3 - Type III Collagen. In M. A. Karsdal (Ed.), *Biochemistry of Collagens, Laminins and Elastin* (pp. 21–30). Academic Press. <https://doi.org/https://doi.org/10.1016/B978-0-12-809847-9.00003-9>



- Nikolov, A., & Popovski, N. (2022). Extracellular Matrix in Heart Disease: Focus on Circulating Collagen Type I and III Derived Peptides as Biomarkers of Myocardial Fibrosis and Their Potential in the Prognosis of Heart Failure: A Concise Review. In *Metabolites* (Vol. 12, Issue 4). MDPI. <https://doi.org/10.3390/metabo12040297>
- Noseda, M., Peterkin, T., Simões, F. C., Patient, R., & Schneider, M. D. (2011). Cardiopoietic factors extracellular signals for cardiac lineage commitment. In *Circulation Research* (Vol. 108, Issue 1, pp. 129–152). <https://doi.org/10.1161/CIRCRESAHA.110.223792>
- Nottingham, W. T., Jarratt, A., Burgess, M., Speck, C. L., Cheng, J.-F., Prabhakar, S., Rubin, E. M., Li, P.-S., Sloane-Stanley, J., Kong-a-San, J., & de Bruijn, M. F. T. R. (2007). Runx1-mediated hematopoietic stem-cell emergence is controlled by a Gata/Ets/SCL-regulated enhancer. *Blood*, 110(13), 4188–4197. <https://doi.org/10.1182/blood-2007-07-100883>
- O'Hare, M., Amarnani, D., Whitmore, H. A. B., An, M., Marino, C., Ramos, L., Delgado-Tirado, S., Hu, X., Chmielewska, N., Chandrabhas, A., Fitzek, A., Heinrich, F., Steurer, S., Ondruschka, B., Glatzel, M., Krasemann, S., Sepulveda-Falla, D., Lagares, D., Pedron, J., ... Kim, L. A. (2021). Targeting Runt-Related Transcription Factor 1 Prevents Pulmonary Fibrosis and Reduces Expression of Severe Acute Respiratory Syndrome Coronavirus 2 Host Mediators. *The American Journal of Pathology*, 191(7), 1193–1208. <https://doi.org/10.1016/j.ajpath.2021.04.006>
- Okuda, T., Van Deursen, J., & Hiebert, S. W. (1996). AML1, the Target of Multiple Chromosomal Translocations in Human Leukemia, Is Essential for Normal Fetal Liver Hematopoiesis. In *Cell* (Vol. 84).
- Olsson, H., Mattsson, J., Overed-Sayer, C., Stellato, M., Mcelroy, A., Weidner, J., De Baets, G., Monkley, S., Hühn, M., Muthas, D., Bendtsen, C., Escudero-Ibarz, L., Serrano, A., Barrett, I., Kim, C., Ding, M., Johansson, J., Patten, K., Reichert, S., ... Tame, C. (2023). Unbiased Identification of Serum Response Factor as a Central Profibrotic Mechanism in Idiopathic Pulmonary Fibrosis. *American Journal of Respiratory and Critical Care Medicine*. [https://doi.org/https://doi.org/10.1164/ajrccm-conference.2023.207.1\\_MeetingAbstracts.A3954](https://doi.org/https://doi.org/10.1164/ajrccm-conference.2023.207.1_MeetingAbstracts.A3954)
- Palano, G., Jansson, M., Backmark, A., Martinsson, S., Sabirsh, A., Hulténby, K., Åkerblad, P., Granberg, K. L., Jennbacken, K., Müllers, E., & Hansson, E. M. (2020). A high-content, in vitro cardiac fibrosis assay for high-throughput, phenotypic identification of compounds with anti-fibrotic activity. *Journal of Molecular and Cellular Cardiology*, 142, 105–117. <https://doi.org/https://doi.org/10.1016/j.yjmcc.2020.04.002>
- Pan, B. (2022). *Atrial Fibrillation Modelling and Targeted DNA Methylation Editing in Human Engineered Heart Tissue-Based Disease Models* [University of Hamburg]. [https://ediss.sub.uni-hamburg.de/bitstream/ediss/9989/1/Dissertation\\_Bangfen%20Pan.pdf](https://ediss.sub.uni-hamburg.de/bitstream/ediss/9989/1/Dissertation_Bangfen%20Pan.pdf)
- Panigrahi, A., & O'Malley, B. W. (2021). Mechanisms of enhancer action: the known and the unknown. In *Genome Biology* (Vol. 22, Issue 1). BioMed Central Ltd. <https://doi.org/10.1186/s13059-021-02322-1>
- Papakrivopoulou, J., Lindahl, G. E., Bishop, J. E., & Laurent, G. J. (2004). Differential roles of extracellular signal-regulated kinase 1/2 and p38MAPK in mechanical load-induced procollagen  $\alpha 1(I)$  gene

- expression in cardiac fibroblasts. *Cardiovascular Research*, 61(4), 736–744. <https://doi.org/10.1016/j.cardiores.2003.12.018>
- Park, P. J. (2009). ChIP-seq: Advantages and challenges of a maturing technology. In *Nature Reviews Genetics* (Vol. 10, Issue 10, pp. 669–680). <https://doi.org/10.1038/nrg2641>
- Pellman, J., Zhang, J., & Sheikh, F. (2016). Myocyte-fibroblast communication in cardiac fibrosis and arrhythmias: Mechanisms and model systems. In *Journal of Molecular and Cellular Cardiology* (Vol. 94, pp. 22–31). Academic Press. <https://doi.org/10.1016/j.yjmcc.2016.03.005>
- Pennacchio, L. A., Bickmore, W., Dean, A., Nobrega, M. A., & Bejerano, G. (2013). Enhancers: Five essential questions. In *Nature Reviews Genetics* (Vol. 14, Issue 4, pp. 288–295). <https://doi.org/10.1038/nrg3458>
- Post, S. M., Kantarjian, H., & Quintás-Cardama, A. (2015). 28 - Biology of Adult Myelocytic Leukemia and Myelodysplasia. In J. Mendelsohn, J. W. Gray, P. M. Howley, M. A. Israel, & C. B. Thompson (Eds.), *The Molecular Basis of Cancer (Fourth Edition)* (pp. 421–432). W.B. Saunders. <https://doi.org/https://doi.org/10.1016/B978-1-4557-4066-6.00028-7>
- Prabhu, S. D., & Frangogiannis, N. G. (2016). The Biological Basis for Cardiac Repair After Myocardial Infarction. *Circulation Research*, 119(1), 91–112. <https://doi.org/10.1161/CIRCRESAHA.116.303577>
- Querdel, E., Reinsch, M., Castro, L., Köse, D., Bähr, A., Reich, S., Geertz, B., Ulmer, B., Schulze, M., Lemoine, M. D., Krause, T., Lemme, M., Sani, J., Shibamiya, A., Stüdemann, T., Köhne, M., Bibra, C. von, Hornaschewitz, N., Pecha, S., ... Weinberger, F. (2021). Human Engineered Heart Tissue Patches Remuscularize the Injured Heart in a Dose-Dependent Manner. *Circulation*, 143(20), 1991–2006. <https://doi.org/10.1161/CIRCULATIONAHA.120.047904>
- Quinn, T. A., Camelliti, P., Siedlecka, U., Poggioli, T., Loew, L. M., Knöpfel, T., & Kohl, P. (2014). Abstract 11749: Cell-Specific Expression of Voltage-Sensitive Protein Confirms Cardiac Myocyte to Non-Myocyte Electrotonic Coupling in Healed Murine Infarct Border Tissue. *Circulation*, 130(suppl\_2), A11749–A11749. [https://doi.org/10.1161/circ.130.suppl\\_2.11749](https://doi.org/10.1161/circ.130.suppl_2.11749)
- Ragazzini, S., Scocozza, F., Bernava, G., Auricchio, F., Colombo, G., Barbuto, M., Conti, M., Pesce, M., & Garoffolo, G. (2022). Mechanosensor YAP cooperates with TGF-β1 signaling to promote myofibroblast activation and matrix stiffening in a 3D model of human cardiac fibrosis. *Acta Biomaterialia*, 152. <https://doi.org/10.1016/j.actbio.2022.08.063>
- Ran, F. A., Hsu, P. D., Wright, J., Agarwala, V., Scott, D. A., & Zhang, F. (2013). Genome engineering using the CRISPR-Cas9 system. *Nature Protocols*, 8(11), 2281–2308. <https://doi.org/10.1038/nprot.2013.143>
- Raulf, A., Horder, H., Tarnawski, L., Geisen, C., Ottersbach, A., Röhl, W., Jovinge, S., Fleischmann, B. K., & Hesse, M. (2015). Transgenic systems for unequivocal identification of cardiac myocyte nuclei and analysis of cardiomyocyte cell cycle status. *Basic Research in Cardiology*, 110(3), 33. <https://doi.org/10.1007/s00395-015-0489-2>
- Rawles, M. E. (1943). The Heart-Forming Areas of the Early Chick Blastoderm. *Physiological Zoology*, 16(1), 22–43. <https://doi.org/10.1086/physzool.16.1.30151667>

- Raziyeva, K., Kim, Y., Zharkinbekov, Z., Temirkhanova, K., & Saparov, A. (2022). Novel Therapies for the Treatment of Cardiac Fibrosis Following Myocardial Infarction. In *Biomedicines* (Vol. 10, Issue 9). MDPI. <https://doi.org/10.3390/biomedicines10092178>
- Rhoden, A., Friedrich, F. W., Brandt, T., Raabe, J., Schweizer, M., Meisterknecht, J., Wittig, I., Ulmer, B. M., Klampe, B., Uebeler, J., Piasecki, A., Lorenz, K., Eschenhagen, T., Hansen, A., & Cuello, F. (2021). Sulforaphane exposure impairs contractility and mitochondrial function in three-dimensional engineered heart tissue. *Redox Biology*, 41, 101951. <https://doi.org/https://doi.org/10.1016/j.redox.2021.101951>
- Richards, D. J., Li, Y., Kerr, C. M., Yao, J., Beeson, G. C., Coyle, R. C., Chen, X., Jia, J., Damon, B., Wilson, R., Starr Hazard, E., Hardiman, G., Menick, D. R., Beeson, C. C., Yao, H., Ye, T., & Mei, Y. (2020). Human cardiac organoids for the modelling of myocardial infarction and drug cardiotoxicity. *Nature Biomedical Engineering*, 4(4), 446–462. <https://doi.org/10.1038/s41551-020-0539-4>
- Riddell, A., McBride, M., Braun, T., Nicklin, S. A., Cameron, E., Loughrey, C. M., & Martin, T. P. (2020). RUNX1: An emerging therapeutic target for cardiovascular disease. In *Cardiovascular Research* (Vol. 116, Issue 8, pp. 1410–1423). Oxford University Press. <https://doi.org/10.1093/cvr/cvaa034>
- Rieder, M., Wirth, L., Pollmeier, L., Jeserich, M., Goller, I., Baldus, N., Schmid, B., Busch, H.-J., Hofmann, M., Kern, W., Bode, C., Duerschmied, D., & Lother, A. (2020). Serum ACE-2, angiotensin II, and aldosterone levels are unchanged in patients with COVID-19. *American Journal of Hypertension*, 34(3), 278–281.
- Robertson, S. (2023). *What is Fibrosis?* <https://www.news-medical.net/health/What-is-Fibrosis.aspx#:~:text=The%20term%20fibrosis%20describes%20the,occurs%20as%20a%20pathological%20process>
- Roche, P. L., Nagalingam, R. S., Bagchi, R. A., Aroutiounova, N., Belisle, B. M. J., Wigle, J. T., & Czubyrt, M. P. (2016). Role of scleraxis in mechanical stretch-mediated regulation of cardiac myofibroblast phenotype. *Am J Physiol Cell Physiol*, 311, 297–307. <https://doi.org/10.1152/ajpcell.00333.2015>. The
- Rog-Zielinska, E. A., Norris, R. A., Kohl, P., & Markwald, R. (2016). The Living scar - cardiac fibroblasts and the injured heart. In *Trends in Molecular Medicine* (Vol. 22, Issue 2, pp. 99–114). Elsevier Ltd. <https://doi.org/10.1016/j.molmed.2015.12.006>
- Ruan, J., Zhang, L., Hu, D., Qu, X., Yang, F., Chen, F., He, X., Shen, J., Dong, K., Sweet, M., Sanchez, C., Li, D., Shou, W., Zhou, J., & Cai, C.-L. (2021). Novel Myh11 Dual Reporter Mouse Model Provides Definitive Labeling and Identification of Smooth Muscle Cells—Brief Report. *Arteriosclerosis, Thrombosis, and Vascular Biology*, 41(2), 815–821. <https://doi.org/10.1161/ATVBAHA.120.315107>
- Rurik, J. G., Tombácz, I., Yadegari, A., Méndez Fernández, P. O., Shewale, S. V., Li, L., Kimura, T., Soliman, O. Y., Papp, T. E., Tam, Y. K., Mui, B. L., Albelda, S. M., Puré, E., June, C. H., Aghajanian, H., Weissman, D., Parhiz, H., & Epstein, J. A. (2022). CAR T cells produced in vivo to treat cardiac injury. *Science*, 375(6576), 91–96. <https://doi.org/10.1126/science.abm0594>
- Sadeghi, A. H., Shin, S. R., Deddens, J. C., Fratta, G., Mandla, S., Yazdi, I. K., Prakash, G., Antona, S., Demarchi, D., Buijsrogge, M. P., Sluijter, J. P. G., Hjortnaes, J., & Khademhosseini, A. (2017).

- Engineered 3D Cardiac Fibrotic Tissue to Study Fibrotic Remodeling. *Advanced Healthcare Materials*, 6(11), 1601434. <https://doi.org/https://doi.org/10.1002/adhm.201601434>
- Sadoshima, J.-I., & Izumo, S. (1993). Molecular Characterization of Angiotensin II-Induced Hypertrophy of Cardiac Myocytes and Hyperplasia of Cardiac Fibroblasts Critical Role of the AT1 Receptor Subtype WoRDs \* angiotensin II \* AT1 receptor \* immediate-early genes \* mitogenesis \* hypertrophy. In *Circulation Research* (Vol. 73). <http://ahajournals.org>
- Saini, H., Navaei, A., Van Putten, A., & Nikkhah, M. (2015). 3D Cardiac Microtissues Encapsulated with the Co-Culture of Cardiomyocytes and Cardiac Fibroblasts. *Advanced Healthcare Materials*, 4(13), 1961–1971. <https://doi.org/https://doi.org/10.1002/adhm.201500331>
- Sánchez-Iranzo, H., Galardi-Castilla, M., Sanz-Morejón, A., González-Rosa, J. M., Costa, R., Ernst, A., de Aja, J. S., Langa, X., & Mercader, N. (2018). Transient fibrosis resolves via fibroblast inactivation in the regenerating zebrafish heart. *Proceedings of the National Academy of Sciences of the United States of America*, 115(16), 4188–4193. <https://doi.org/10.1073/pnas.1716713115>
- Sangweni, N. F., Dlodla, P. V, Chellan, N., Mabasa, L., Sharma, J. R., & Johnson, R. (2021). The Implication of Low Dose Dimethyl Sulfoxide on Mitochondrial Function and Oxidative Damage in Cultured Cardiac and Cancer Cells. *Molecules*, 26(23). <https://doi.org/10.3390/molecules26237305>
- SB-431542. (2023). MedChemExpress. <https://www.medchemexpress.com/SB-431542.html>
- SB-431542 [301836-41-9]. (2023). <https://www.biotrend.com/-186/sb-431542-301836-41-9-231022773.html#:~:text=SB%2D431542%20is%20a%20TGF,%2C%20apoptosis%2C%20and%20growth%20suppression>
- Schaaf, S., Eder, A., Vollert, I., Stöhr, A., Hansen, A., & Eschenhagen, T. (2014). Generation of Strip-Format Fibrin-Based Engineered Heart Tissue (EHT). In M. Radisic & L. D. Black III (Eds.), *Cardiac Tissue Engineering: Methods and Protocols* (pp. 121–129). Springer New York. [https://doi.org/10.1007/978-1-4939-1047-2\\_11](https://doi.org/10.1007/978-1-4939-1047-2_11)
- Schimmel, K., Ichimura, K., Reddy, S., Haddad, F., & Spiekerkoetter, E. (2022). Cardiac Fibrosis in the Pressure Overloaded Left and Right Ventricle as a Therapeutic Target. In *Frontiers in Cardiovascular Medicine* (Vol. 9). Frontiers Media S.A. <https://doi.org/10.3389/fcvm.2022.886553>
- Schuler, G. D., Moore, T., & Boguski, M. (1999). The Transcriptional Program in the Response of Human Fibroblasts to Serum. *Science*, 283(5398), 83–87. <https://doi.org/DOL:10.1126/science.283.5398.83>
- Schulze, M. L. (2019). *Kardiomyozyten aus humanen induzierten pluripotenten Stammzellen - Untersuchungen zur Reliabilität im 3D-Format und Anwendung als biologischer Schrittmacher*. <https://ediss.sub.uni-hamburg.de/bitstream/ediss/8199/1/Dissertation.pdf>
- Seifert, R. A., Alpers, C. E., & Bowen-Pope, D. F. (1998). Expression of platelet-derived growth factor and its receptors in the developing and adult mouse kidney. *Kidney International*, 54(3), 731–746. <https://doi.org/https://doi.org/10.1046/j.1523-1755.1998.00046.x>
- Sharma, A., McKeithan, W. L., Serrano, R., Kitani, T., BurrIDGE, P. W., del Álamo, J. C., Mercola, M., & Wu, J. C. (2018). Use of human induced pluripotent stem cell-derived cardiomyocytes to assess drug

- cardiotoxicity. *Nature Protocols*, 13(12), 3018–3041. <https://doi.org/10.1038/s41596-018-0076-8>
- Sharma, M., & Bhatt, L. (2022). Emerging Therapeutic Targets for Heart Failure. *Current Cardiology Reports*, 24, 1–18. <https://doi.org/10.1007/s11886-022-01789-z>
- Sheng, Z., Knowlton, K., Chen, J., Hoshijima, M., Brown, J. H., & Chien, K. R. (1997). Cardiotrophin 1 (CT-1) Inhibition of Cardiac Myocyte Apoptosis via a Mitogen-activated Protein Kinase-dependent Pathway: Divergence from Downstream CT-1 Signals for Myocardial Cell Hypertrophy. *Journal of Biological Chemistry*, 272(9), 5783–5791. <https://doi.org/10.1074/jbc.272.9.5783>
- Singh, M., Mckenzie, K., & Ma, X. (2017). Effect of dimethyl sulfoxide on in vitro proliferation of skin fibroblast cells. In *Journal of Biotech Research* (Vol. 8). <https://www.researchgate.net/publication/317268388>
- Sisson, T. H., Ajayi, I. O., Subbotina, N., Dodi, A. E., Rodansky, E. S., Chibucos, L. N., Kim, K. K., Keshamouni, V. G., White, E. S., Zhou, Y., Higgins, P. D. R., Larsen, S. D., Neubig, R. R., & Horowitz, J. C. (2015). Inhibition of myocardin-related transcription factor/serum response factor signaling decreases lung fibrosis and promotes mesenchymal cell apoptosis. *American Journal of Pathology*, 185(4), 969–986. <https://doi.org/10.1016/j.ajpath.2014.12.005>
- Smith, C. L., Baek, S. T., Sung, C. Y., & Tallquist, M. D. (2011). Epicardial-derived cell epithelial-to-mesenchymal transition and fate specification require PDGF receptor signaling. *Circulation Research*, 108(12). <https://doi.org/10.1161/CIRCRESAHA.110.235531>
- Solon, J., Levental, I., Sengupta, K., Georges, P. C., & Janmey, P. A. (2007). Fibroblast adaptation and stiffness matching to soft elastic substrates. *Biophysical Journal*, 93(12), 4453–4461. <https://doi.org/10.1529/biophysj.106.101386>
- Sood, R., Kamikubo, Y., & Liu, P. (2017). Role of RUNX1 in hematological malignancies. *Blood*, 129(15), 2070–2082. <https://doi.org/10.1182/blood-2016-10-687830>
- Stempien, A., Josvai, M., Notbohm, J., Zhang, J., Kamp, T. J., & Crone, W. C. (2024). Influence of Remodeled ECM and Co-culture with iPSC-Derived Cardiac Fibroblasts on the Mechanical Function of Micropatterned iPSC-Derived Cardiomyocytes. *Cardiovascular Engineering and Technology*. <https://doi.org/10.1007/s13239-024-00711-8>
- Sterner, R. C., & Sterner, R. M. (2021). CAR-T cell therapy: current limitations and potential strategies. *Blood Cancer Journal*, 11(4), 69. <https://doi.org/10.1038/s41408-021-00459-7>
- Sun, T.-L., Li, W.-Q., Tong, X.-L., Liu, X.-Y., & Zhou, W.-H. (2021). Xanthohumol attenuates isoprenaline-induced cardiac hypertrophy and fibrosis through regulating PTEN/AKT/mTOR pathway. *European Journal of Pharmacology*, 891, 173690. <https://doi.org/https://doi.org/10.1016/j.ejphar.2020.173690>
- Sun, Y., Lin, J., Luo, Z., Zhang, Y., & Chen, J. (2021). The Serum from Patients with Secondary Frozen Shoulder Following Rotator Cuff Repair Induces Shoulder Capsule Fibrosis and Promotes Macrophage Polarization and Fibroblast Activation. *Journal of Inflammation Research*, 14, 1055–1068. <https://doi.org/10.2147/JIR.S304555>

- Swaney, J. S., Roth, D. M., Olson, E. R., Naugle, J. E., Meszaros, J. G., & Insel, P. A. (2005). Inhibition of cardiac myofibroblast formation and collagen synthesis by activation and overexpression of adenylyl cyclase. *Proceedings of the National Academy of Sciences*, 102(2), 437–442. <https://doi.org/10.1073/pnas.0408704102>
- Szepes, M., Melchert, A., Dahlmann, J., Hegermann, J., Werlein, C., Jonigk, D., Haverich, A., Martin, U., Olmer, R., & Gruh, I. (2020). Dual function of ipsc-derived pericyte-like cells in vascularization and fibrosis-related cardiac tissue remodeling in vitro. *International Journal of Molecular Sciences*, 21(23), 1–20. <https://doi.org/10.3390/ijms21238947>
- Tahirov, T. H., Inoue/Bungo, T., Morii, H., Fujikawa, A., & Osaga, K. (2001). Structural Analyses of DNA Recognition by the AML1/Runx-1 Runt Domain and Its Allosteric Control by CBF. *Cell*, 104, 755–767.
- Takahashi, K., Tanabe, K., Ohnuki, M., Narita, M., Ichisaka, T., Tomoda, K., & Yamanaka, S. (2007). Induction of Pluripotent Stem Cells from Adult Human Fibroblasts by Defined Factors. *Cell*, 131(5), 861–872. <https://doi.org/10.1016/j.cell.2007.11.019>
- Takahashi, K., & Yamanaka, S. (2006). Induction of Pluripotent Stem Cells from Mouse Embryonic and Adult Fibroblast Cultures by Defined Factors. *Cell*, 126(4), 663–676. <https://doi.org/10.1016/j.cell.2006.07.024>
- Tallquist, M. D., & Molkentin, J. D. (2017). Redefining the identity of cardiac fibroblasts. *Nature Reviews Cardiology*.
- Talman, V., & Ruskoaho, H. (2016). Cardiac fibrosis in myocardial infarction—from repair and remodeling to regeneration. In *Cell and Tissue Research* (Vol. 365, Issue 3, pp. 563–581). Springer Verlag. <https://doi.org/10.1007/s00441-016-2431-9>
- Tang, J.-X., Chen, D., Deng, S.-L., Li, J., Li, Y., Fu, Z., Wang, X.-X., Zhang, Y., Chen, S.-R., & Liu, Y.-X. (2018). CRISPR/Cas9-mediated genome editing induces gene knockdown by altering the pre-mRNA splicing in mice. *BMC Biotechnology*, 18(1), 61. <https://doi.org/10.1186/s12896-018-0472-8>
- Tang, M., Zhang, W., Lin, H., Jiang, H., Dai, H., & Zhang, Y. (2007). High glucose promotes the production of collagen types I and III by cardiac fibroblasts through a pathway dependent on extracellular-signal-regulated kinase 1/2. *Molecular and Cellular Biochemistry*, 301(1), 109–114. <https://doi.org/10.1007/s11010-006-9401-6>
- Tang, Y., Nyengaard, J. R., Andersen, J. B., Baandrup, U., & Gundersen, H. J. G. (2009). The application of stereological methods for estimating structural parameters in the human heart. *Anatomical Record*, 292(10), 1630–1647. <https://doi.org/10.1002/ar.20952>
- Tao, L., Bei, Y., Chen, P., Lei, Z., Fu, S., Zhang, H., Xu, J., Che, L., Chen, X., Sluijter, J. P. G., Das, S., Cretoiu, D., Xu, B., Zhong, J., Xiao, J., & Li, X. (2016). Crucial role of miR-433 in regulating cardiac fibrosis. *Theranostics*, 6(12), 2068–2083. <https://doi.org/10.7150/thno.15007>
- Telford, W. G. (2023). Flow cytometry and cell sorting. *Frontiers in Medicine*, 10. <https://www.frontiersin.org/articles/10.3389/fmed.2023.1287884>

- Thomson, J. A., Itskovitz-Eldor, J., Shapiro, S. S., Waknitz, M. A., Swiergiel, J. J., Marshall, V. S., & Jones, J. M. (1998). *Embryonic Stem Cell Lines Derived from Human Blastocysts*. <https://doi.org/10.1126/science.282.5391.1145>
- Tiaho, F., Recher, G., & Rouède, D. (2007). Estimation of helical angles of myosin and collagen by second harmonic generation imaging microscopy. *Optics Express*, 15(19), 12286–12295. <https://doi.org/10.1364/OE.15.012286>
- Tiburcy, M., Meyer, T., Liaw, N. Y., & Zimmermann, W. H. (2020). Generation of Engineered Human Myocardium in a Multi-well Format. *STAR Protocols*, 1(1). <https://doi.org/10.1016/j.xpro.2020.100032>
- Tomasek, J. J., Gabbiani, G., Hinz, B., Chaponnier, C., & Brown, R. A. (2002). Myofibroblasts and mechano: Regulation of connective tissue remodelling. In *Nature Reviews Molecular Cell Biology* (Vol. 3, Issue 5, pp. 349–363). <https://doi.org/10.1038/nrm809>
- Tzahor, E. (2007). Wnt/ $\beta$ -Catenin Signaling and Cardiogenesis: Timing Does Matter. In *Developmental Cell* (Vol. 13, Issue 1, pp. 10–13). <https://doi.org/10.1016/j.devcel.2007.06.006>
- van Spreeuwel, A. C. C., Bax, N. A. M., van Nierop, B. J., Aartsma-Rus, A., Goumans, M.-J. T. H., & Bouten, C. V. C. (2017). Mimicking Cardiac Fibrosis in a Dish: Fibroblast Density Rather than Collagen Density Weakens Cardiomyocyte Function. *Journal of Cardiovascular Translational Research*, 10(2), 116–127. <https://doi.org/10.1007/s12265-017-9737-1>
- Vasquez, C., Benamer, N., & Morley, G. E. (2011). The cardiac fibroblast: Functional and electrophysiological considerations in healthy and diseased hearts. In *Journal of Cardiovascular Pharmacology* (Vol. 57, Issue 4, pp. 380–388). <https://doi.org/10.1097/FJC.0b013e31820cda19>
- Velayutham, N., & Yutzey, K. E. (2022). Porcine Models of Heart Regeneration. In *Journal of Cardiovascular Development and Disease* (Vol. 9, Issue 4). MDPI. <https://doi.org/10.3390/jcdd9040093>
- Velecela, V., Torres-Cano, A., García-Melero, A., Ramiro-Pareta, M., Müller-Sánchez, C., Segarra-Mondejar, M., Chau, Y.-Y., Campos-Bonilla, B., Reina, M., Soriano, F. X., Hastie, N. D., Martínez, F. O., & Martínez-Estrada, O. M. (2019). Epicardial cell shape and maturation are regulated by Wt1 via transcriptional control of Bmp4. *Development*, 146(20), dev178723. <https://doi.org/10.1242/dev.178723>
- Verheijen, M., Lienhard, M., Schrooders, Y., Clayton, O., Nudischer, R., Boerno, S., Timmermann, B., Selevsek, N., Schlapbach, R., Gmuender, H., Gotta, S., Geraedts, J., Herwig, R., Kleinjans, J., & Caiment, F. (2019). DMSO induces drastic changes in human cellular processes and epigenetic landscape in vitro. *Scientific Reports*, 9(1), 4641. <https://doi.org/10.1038/s41598-019-40660-0>
- von Bibra, C., Shibamiya, A., Bähr, A., Geertz, B., Köhne, M., Stuedemann, T., Starbatty, J., Horneffer-van der Sluis, V., Klostermeier, U. C., Hornaschewitz, N., Li, X., Wolf, E., Klymiuk, N., Krane, M., Kupatt, C., Hiebl, B., Eschenhagen, T., & Weinberger, F. (2023). Immature human engineered heart tissues engraft in a guinea pig chronic injury model. *Disease Models & Mechanisms*, 16(5), dmm049834. <https://doi.org/10.1242/dmm.049834>

- Walker, M., Godin, M., & Pelling, A. E. (2020). Mechanical stretch sustains myofibroblast phenotype and function in microtissues through latent TGF- $\beta$ 1 activation. *Integrative Biology*, 12(8), 199–210. <https://doi.org/10.1093/intbio/zyaa015>
- Wang, A. Y. L., & Loh, C. Y. Y. (2019). Episomal Induced Pluripotent Stem Cells: Functional and Potential Therapeutic Applications. In *Cell Transplantation* (Vol. 28, Issue 1\_suppl, pp. 112S-131S). SAGE Publications Ltd. <https://doi.org/10.1177/0963689719886534>
- Wang, L., Yue, Y., Yang, X., Fan, T., Mei, B., Hou, J., Liang, M., Chen, G., & Wu, Z. (2017). Platelet derived growth factor alpha (PDGFR $\alpha$ ) induces the activation of cardiac fibroblasts by activating c-kit. *Medical Science Monitor*, 23, 3808–3816. <https://doi.org/10.12659/MSM.906038>
- Wang, Q., Stacy, T., Bindert, M., Marin-Padillat, M., Sharpe, A. H., & Speck, N. A. (1996). Disruption of the Cbfa2 gene causes necrosis and hemorrhaging in the central nervous system and blocks definitive hematopoiesis. *Developmental Biology*, 93(8), 3444–3449. <https://www.pnas.org>
- Wang, Y., Li, Q., Tao, B., Angelini, M., Ramadoss, S., Sun, B., Wang, P., Krokhaleva, Y., Ma, F., Gu, Y., Espinoza, A., Yamauchi, K., Pellegrini, M., Novitch, B., Olcese, R., Qu, Z., Song, Z., & Deb, A. (2023). Fibroblasts in heart scar tissue directly regulate cardiac excitability and arrhythmogenesis. *Science*, 381(6665), 1480–1487. <https://doi.org/10.1126/science.adh9925>
- Wang, Y., Wang, M., Samuel, C. S., & Widdop, R. E. (2022). Preclinical rodent models of cardiac fibrosis. *British Journal of Pharmacology*, 179(5), 882–899. <https://doi.org/https://doi.org/10.1111/bph.15450>
- Weber, K. T. (1997). Extracellular Matrix Remodeling in Heart Failure. *Circulation*, 96(11), 4065–4082. <https://doi.org/10.1161/01.CIR.96.11.4065>
- Wei, K., Nguyen, H. N., & Brenner, M. B. (2021). Fibroblast pathology in inflammatory diseases. *The Journal of Clinical Investigation*, 131(20). <https://doi.org/10.1172/JCI149538>
- Weinberger, F., Mannhardt, I., & Eschenhagen, T. (2017). Engineering Cardiac Muscle Tissue: A Maturing Field of Research. *Circulation Research*, 120(9), 1487–1500. <https://doi.org/10.1161/CIRCRESAHA.117.310738>
- Werner, T. (2018). *Humanes künstliches Herzgewebe aus mehreren Zelltypen zur Untersuchung kardialer Hypertrophie* [University Hamburg]. <http://ediss.sub.uni-hamburg.de/volltexte/2018/9072>
- Wijsenbeek, M. S., Kool, M., & Cottin, V. (2018). Targeting interleukin-13 in idiopathic pulmonary fibrosis: From promising path to dead end. In *European Respiratory Journal* (Vol. 52, Issue 6). European Respiratory Society. <https://doi.org/10.1183/13993003.02111-2018>
- Witty, A. D., Mihic, A., Tam, R. Y., Fisher, S. A., Mikryukov, A., Shoichet, M. S., Li, R. K., Kattman, S. J., & Keller, G. (2014). Generation of the epicardial lineage from human pluripotent stem cells. *Nature Biotechnology*, 32(10), 1026–1035. <https://doi.org/10.1038/nbt.3002>
- Wojciechowski, M. C., Mahmutovic, L., Shu, D. Y., & Lovicu, F. J. (2017). ERK1/2 signaling is required for the initiation but not progression of TGF $\beta$ -induced lens epithelial to mesenchymal transition (EMT). *Experimental Eye Research*, 159, 98–113. <https://doi.org/https://doi.org/10.1016/j.exer.2017.03.012>



- Woodcock-Mitchell, J., Mitchell, J. J., Low, R. B., Kieny, M., Sengel, P., Rubbia, L., Skalli, O., Jackson, B., & Gabbiani, G. (1988).  $\alpha$ -Smooth muscle actin is transiently expressed in embryonic rat cardiac and skeletal muscles. *Differentiation*, 39(3), 161–166. <https://doi.org/https://doi.org/10.1111/j.1432-0436.1988.tb00091.x>
- Wulff, B. C., Pappa, N. K., & Wilgus, T. A. (2019). Interleukin-33 encourages scar formation in murine fetal skin wounds. *Wound Repair and Regeneration*, 27(1), 19–28. <https://doi.org/https://doi.org/10.1111/wrr.12687>
- Yang, M., Zhang, K., Li, J., Wang, L., Zhang, K., Qiu, Z., & Wang, X. (2019). *Effects of DMSO and DMF on myocardial cytotoxicity and STAT3 signaling pathway in H9C2*. 31(9), 1446–1452. <https://doi.org/10.3969/j.issn.1004-1524.2019.09.07>
- Yang, X., Chen, B., Liu, T., & Chen, XiaoHong. (2014). Reversal of myofibroblast differentiation: A review. *European Journal of Pharmacology*, 734, 83–90. <https://doi.org/https://doi.org/10.1016/j.ejphar.2014.04.007>
- Yeung, T., Georges, P. C., Flanagan, L. A., Marg, B., Ortiz, M., Funaki, M., Zahir, N., Ming, W., Weaver, V., & Janmey, P. A. (2005). Effects of substrate stiffness on cell morphology, cytoskeletal structure, and adhesion. *Cell Motility*, 60(1), 24–34. <https://doi.org/https://doi.org/10.1002/cm.20041>
- Ytrehus, K., Hulot, J.-S., Perrino, C., Schiattarella, G. G., Madonna, R., & Perivascular, R. M. (2018). Perivascular fibrosis and the microvasculature of the heart. Still hidden secrets of pathophysiology? *Vascular Pharmacology*, 107, 78–83. <https://doi.org/10.1016/j.vph.2018.04.007>
- Yuan, X., Pan, J., Wen, L., Gong, B., Li, J., Gao, H., Tan, W., Liang, S., Zhang, H., & Wang, X. (2019). MiR-144-3p Enhances Cardiac Fibrosis After Myocardial Infarction by Targeting PTEN. *Frontiers in Cell and Developmental Biology*, 7. <https://doi.org/10.3389/fcell.2019.00249>
- Yue, Y., Meng, K., Pu, Y., & Zhang, X. (2017). Transforming growth factor beta (TGF- $\beta$ ) mediates cardiac fibrosis and induces diabetic cardiomyopathy. *Diabetes Research and Clinical Practice*, 133, 124–130. <https://doi.org/https://doi.org/10.1016/j.diabres.2017.08.018>
- Zeisberg, E. M., Tarnavski, O., Zeisberg, M., Dorfman, A. L., McMullen, J. R., Gustafsson, E., Chandraker, A., Yuan, X., Pu, W. T., Roberts, A. B., Neilson, E. G., Sayegh, M. H., Izumo, S., & Kalluri, R. (2007). Endothelial-to-mesenchymal transition contributes to cardiac fibrosis. *Nature Medicine*, 13(8), 952–961. <https://doi.org/10.1038/nm1613>
- Zeisberg, M., Strutz, F., & Müller, G. A. (2000). Role of fibroblast activation in inducing interstitial fibrosis. *Journal of Nephrology*, 13 Suppl 3, S111-20. <http://europepmc.org/abstract/MED/11132027>
- Zhang, H., Shen, M., & Wu, J. C. (2022). Generation of Quiescent Cardiac Fibroblasts Derived from Human Induced Pluripotent Stem Cells. In *Methods in Molecular Biology* (Vol. 2454, pp. 109–115). Humana Press Inc. [https://doi.org/10.1007/7651\\_2020\\_300](https://doi.org/10.1007/7651_2020_300)
- Zhang, H., Tian, L., Shen, M., Tu, C., Wu, H., Gu, M., Paik, D. T., & Wu, J. C. (2019). Generation of quiescent cardiac fibroblasts from human induced pluripotent stem cells for in vitro modeling of

- cardiac fibrosis. *Circulation Research*, 125(5), 552–566. <https://doi.org/10.1161/CIRCRESAHA.119.315491>
- Zhang, J., Tao, R., Campbell, K. F., Carvalho, J. L., Ruiz, E. C., Kim, G. C., Schmuck, E. G., Raval, A. N., da Rocha, A. M., Herron, T. J., Jalife, J., Thomson, J. A., & Kamp, T. J. (2019). Functional cardiac fibroblasts derived from human pluripotent stem cells via second heart field progenitors. *Nature Communications*, 10(1), 2238. <https://doi.org/10.1038/s41467-019-09831-5>
- Zhang, T., Zhang, Z., Dong, Q., Xiong, J., & Zhu, B. (2020). Histone H3K27 acetylation is dispensable for enhancer activity in mouse embryonic stem cells. *Genome Biology*, 21(1), 45. <https://doi.org/10.1186/s13059-020-01957-w>
- Zhang, W.-W., Bai, F., Wang, J., Zheng, R.-H., Yang, L.-W., James, E. A., & Zhao, Z.-Q. (2017). Edaravone inhibits pressure overload-induced cardiac fibrosis and dysfunction by reducing expression of angiotensin II AT1 receptor. *Drug Design, Development and Therapy*, 11(null), 3019–3033. <https://doi.org/10.2147/DDDT.S144807>
- Zhao, H., Li, X., Zhao, S., Zeng, Y., Zhao, L., Ding, H., Sun, W., & Du, Y. (2014). Microengineered in vitro model of cardiac fibrosis through modulating myofibroblast mechanotransduction. *Biofabrication*, 6(4), 045009. <https://doi.org/10.1088/1758-5082/6/4/045009>
- Zhao, M. T., Ye, S., Su, J., & Garg, V. (2020). Cardiomyocyte Proliferation and Maturation: Two Sides of the Same Coin for Heart Regeneration. In *Frontiers in Cell and Developmental Biology* (Vol. 8). Frontiers Media S.A. <https://doi.org/10.3389/fcell.2020.594226>
- Zhou, T., Luo, M., Cai, W., Zhou, S., Feng, D., Xu, C., & Wang, H. (2018). Runx-Related Transcription Factor 1 (RUNX1) Promotes TGF- $\beta$ -Induced Renal Tubular Epithelial-to-Mesenchymal Transition (EMT) and Renal Fibrosis through the PI3K Subunit p110 $\delta$ . *EBioMedicine*, 31, 217–225. <https://doi.org/10.1016/j.ebiom.2018.04.023>
- Zile, M. R., Baicu, C. F., S. Ikonomidis, J., Stroud, R. E., Nietert, P. J., Bradshaw, A. D., Slater, R., Palmer, B. M., Van Buren, P., Meyer, M., M. Redfield, M., A. Bull, D., L. Granzier, H., & LeWinter, M. M. (2015). Myocardial Stiffness in Patients With Heart Failure and a Preserved Ejection Fraction. *Circulation*, 131(14), 1247–1259. <https://doi.org/10.1161/CIRCULATIONAHA.114.013215>
- Zimmermann, W.-H., Schneiderbanger, K., Schubert, P., Didié, M., Münzel, F., Heubach, J. F., Kostin, S., Neuhuber, W. L., & Eschenhagen, T. (2002). Tissue Engineering of a Differentiated Cardiac Muscle Construct. *Circulation Research*, 90(2), 223–230. <https://doi.org/10.1161/hh0202.103644>

## 8. Curriculum vitae

### Personal information

Name Aaltje Maria Stella Stoter  
Born 24th of August 1995, in Apeldoorn, the Netherlands

### Previous education

2016-2019 MSc BioMedical Engineering, University of Twente, Enschede, graduated in July 2019  
2017 Obtained the “Radiation Protection” certificate  
2013-2016 BSc Technical Medicine, University of Twente, Enschede, graduated in June 2016  
2007-2013 International Baccalaureate, Koninklijke Scholengemeenschap, Apeldoorn, graduated September 2013  
2007-2013 High school with a physics profile, cum laude, Koninklijke Scholengemeenschap, Apeldoorn, graduated July 2013

### Language skills

Dutch Fluent, native  
English Fluent  
German Proficient

### Publications

Stoter AMS, Hirt MN, Stenzig J, Weinberger F (2020). Assessment of cardiotoxicity with stem cell-based strategies. Clin Ther. 42(10):1892-1910.

Stenzig J, Lemoine MD, Stoter AMS, Wrona KM, Lemme M, Mulla W, Etzion Y, Eschenhagen T, Hirt MN (2022). Recapitulation of dyssynchrony-associated contractile impairment in asymmetrically paced engineered heart tissue. J Mol Cell Cardiol, 163:97-105.

Krause J, Nickel A, Madsen A, Aitken-Buck HM, Stoter AMS, et al. (2023). An arrhythmogenic metabolite in atrial fibrillation. J Transl Med. 21, 566.

### Conference participation

GPTS 7<sup>th</sup> Summit, 8<sup>th</sup> – 10<sup>th</sup> of March 2022, online; poster presentation “An Optimized Engineered Heart Tissue Model to Study Pro-Fibrotic Enhancers”

ERA-CVD symposium, 19<sup>th</sup> – 20<sup>th</sup> of September 2022, Riga, Latvia; poster presentation “Fibrosis Treatment by Enhancer Targeting (FIBER) – JTC2018”

TERMIS EU Chapter, 28<sup>th</sup> – 31<sup>st</sup> of March 2023, Manchester, UK; poster presentation “Creating a 3D Human Engineered Heart Tissue Fibrosis Model – Technical Perspectives”

AHA Scientific Sessions, 11<sup>th</sup> – 13<sup>th</sup> of November 2023, Philadelphia, USA; moderated poster session  
“Knock Out of a Fibrosis Related Enhancer Sequence in hiPSC-derived Fibroblasts Reduces Fibrosis in  
3D Engineered Cardiac Tissue”

**Other**

Co-authored an accepted DFG grant “How cardiac fibroblasts react to cardiomyocyte signaling – focus  
on epigenetic signal integration”, main author Dr. Justus Stenzig; STE2596/5-1

## 9. Acknowledgements

I am extremely grateful to the many people who have supported me during my PhD journey these last couple of years. This thesis would not have been possible without all of you, and I sincerely apologize that I am not able to list every single person who has helped me get to where I am.

Firstly, I would like to thank my supervisors. I would like to thank Prof. Thomas Eschenhagen for giving me the opportunity to perform my research in his institute. His input and critical thinking has greatly contributed to the success of my thesis. I would also like to thank Prof. Tanja Zeller and Prof. Boris Fehse for supervising my work and being a part of my thesis committee. I would like to express my sincere gratitude to Dr. Justus Stenzig for his day-to-day supervision of my work, for providing me with encouragement when I needed it and with constructive criticism when it was required.

I would additionally like to mention many people who have contributed to different parts of this thesis: Dr. Paola Cattaneo from the IRCCS in Italy and Dr. Luis Luna-Zurita from the CNIC in Spain for identifying *RUNX1* and the *RUNX1*-related enhancer *enh35232* as potentially interesting target regions for my research, Dr. Thomas Moore-Morris and Dr. Alenca Harrington from the IGF in France for providing the hiPSCs with either *RUNX1* or *enh35232* knocked out, Dr. Sandra Hemkemeyer and Prof. Maike Frye from the ICCLM, UKE for the nanoindentation measurements and subsequent discussions, Dr. Sigrid Fuchs from the IHG, UKE, for the karyotype analysis and June Uebeler from the IEPT, UKE for the mycoplasma analysis.

I want to express my sincere gratitude to multiple colleagues from the institute: Grit Höppner, both for her help with the protein analysis and many other experiments and for her mental support and listening ear, Dr. Bangfen Pan, Dr. Alexandra Madsen and Dr. Julia Krause for teaching me the ropes in the laboratory, Jessica Schrapers for her help with EHT culture and the many other great colleagues I have had the pleasure of working together with.

Furthermore, I would like to thank my family and friends, both the ones back in the Netherlands and the ones who made Hamburg my new home. I want to thank them for their interest in my work and for their distractions when I did not want to discuss it.

Though a few of these people have already been mentioned, I want to emphasize how important some people have been for me. These last 4.5 years have been some of the most challenging years of my life, but with your support I was able to cry when it was needed and to laugh whenever possible. There was a time after my accident where I was ready to give up on my scientific career as my health took complete precedence in my life, and I no longer felt like I was able to contribute anything to anything. Instead of giving up on me, Justus made me realise that I still had something to offer and for that I will be eternally grateful. Here's to everyone who visited me in the hospital, for all the cards and the well wishes, for everyone who helped, also when I didn't want to ask for help, and for everyone who didn't make me feel like a burden, you might not realise how much this meant to me, but it made all the difference. I will always remember my dad walking with me through those hospital walls and I can never thank my mom enough for moving in with us so we would not have to make it through on our own. And finally, to my husband, Matthias, for years you were the one taking care of me and of our home, when I could not do anything but sit on the couch and watch. Instead of being upset about all the extra work, you have always told me how proud you are of me and reminded me of how far I have come. Thank you for your unconditional love and support and for giving me a hug when I said I did not want one. Together, we can make it through anything.

## 10. Supplements

### 10.1 Supplementary figures

#### 10.1.1 Fibroblast differentiation

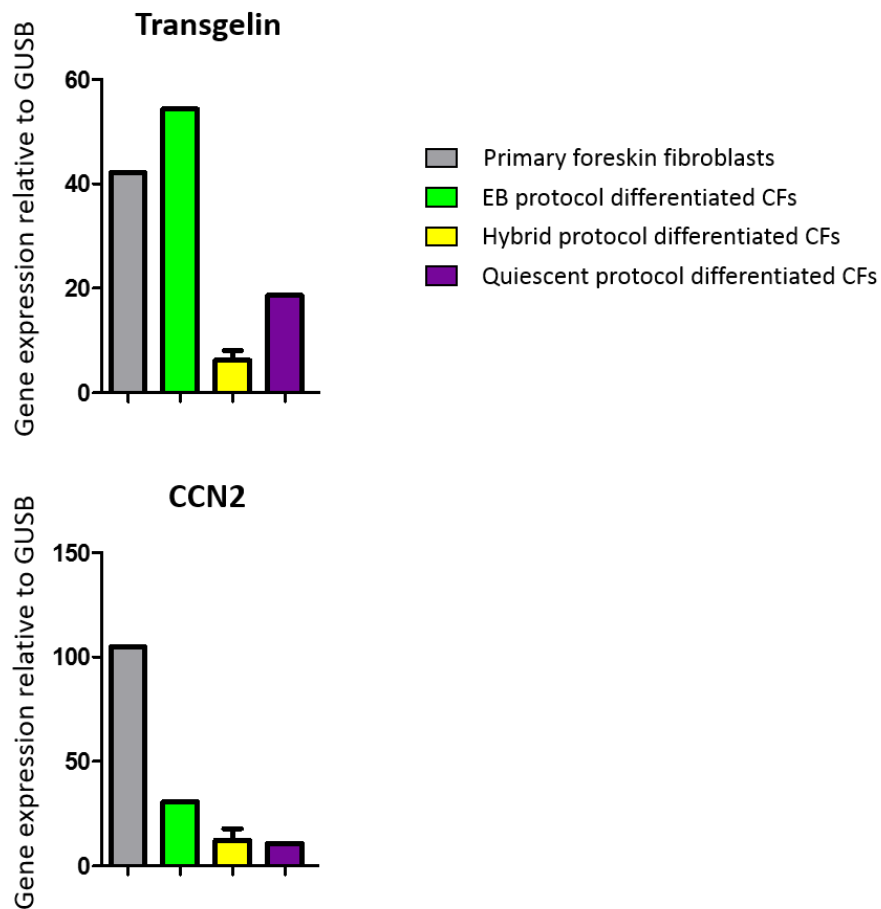


Figure 50: The mRNA abundance relative to GUSB of the fibroblast activation markers transgelin and CCN2 in CFs differentiated with the EB protocol, the hybrid protocol or the quiescent protocol. CFs were harvested on the last day of the respective differentiation protocol. When possible, data are presented as mean  $\pm$  SEM,  $n=1-4$  per group.

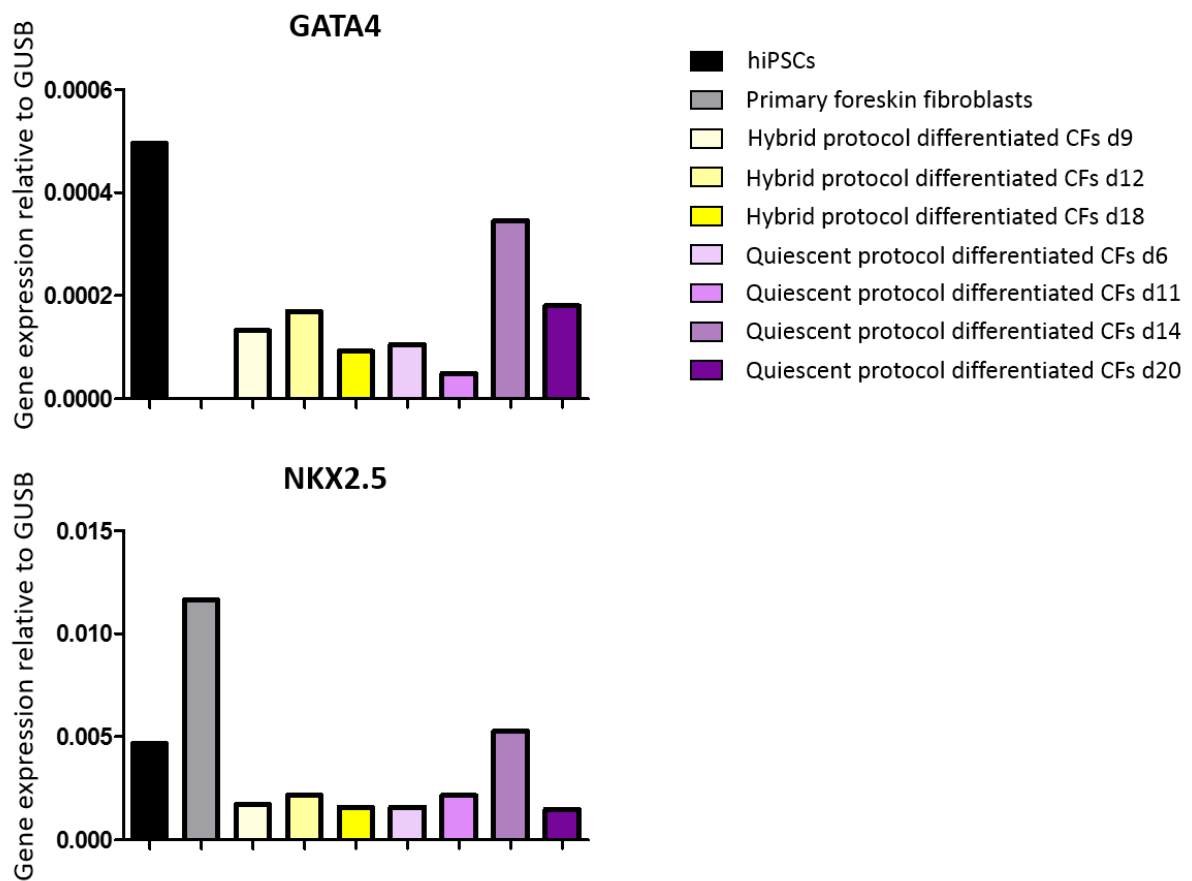
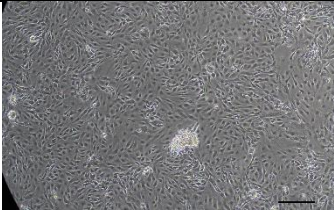
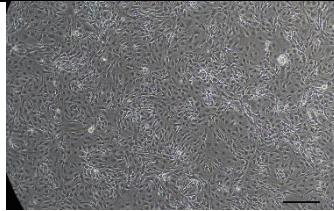
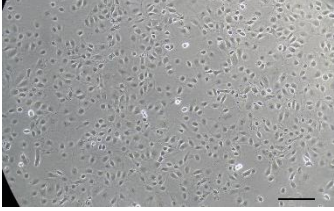
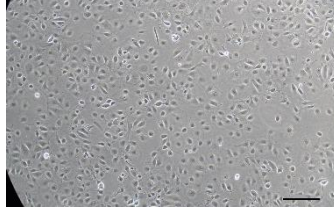


Figure 51: The mRNA abundance relative to GUSB of different markers present during and at the end of the development of cardiac fibroblasts: GATA4 and NKX2.5 (a cardiac lineage marker). The mRNA abundance was analysed in hiPSCs, primary foreskin fibroblasts and in cells sampled at different days of differentiation using either the hybrid or the quiescent protocol. For the hybrid protocol differentiation, cells were sampled on day 9, day 12 and on the last day of differentiation, day 18. For the quiescent protocol differentiation, cells were sampled on day 6, day 11, day 14 and on the last day of differentiation, day 20, n=1 per condition.

Table 16: Microscope images at 10x magnification, which show the morphology of cells undergoing the hybrid protocol on either MG coated or GTX coated T75 cell culture flasks, at various days of differentiation. A representative imagine is shown from n=2. Scale bar is 200  $\mu$ m.

	MG coating	GTX coating
Day 14		
Day 16		



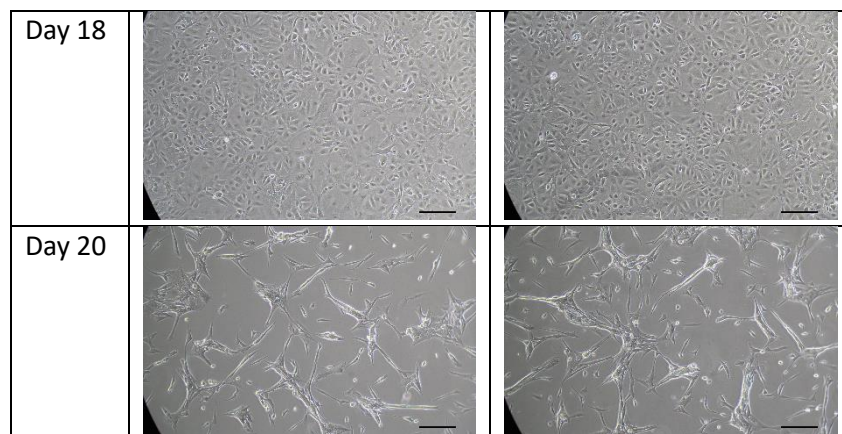
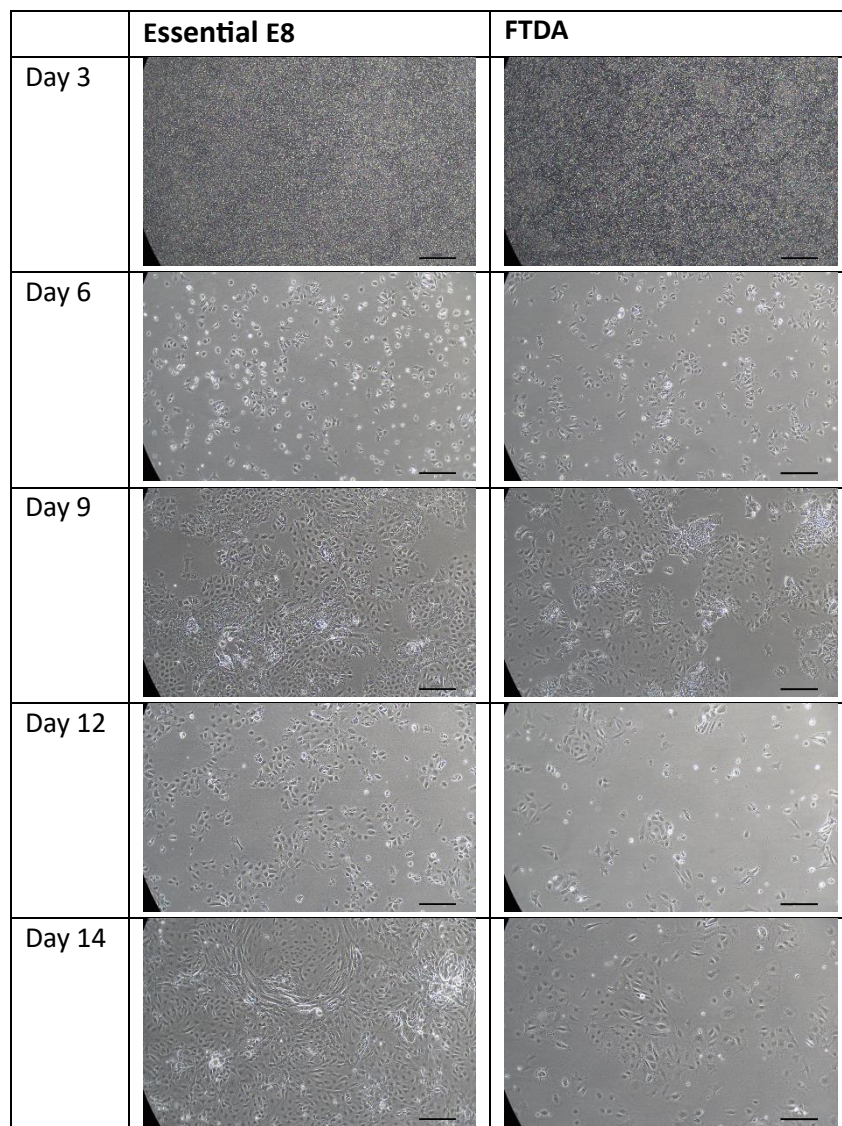
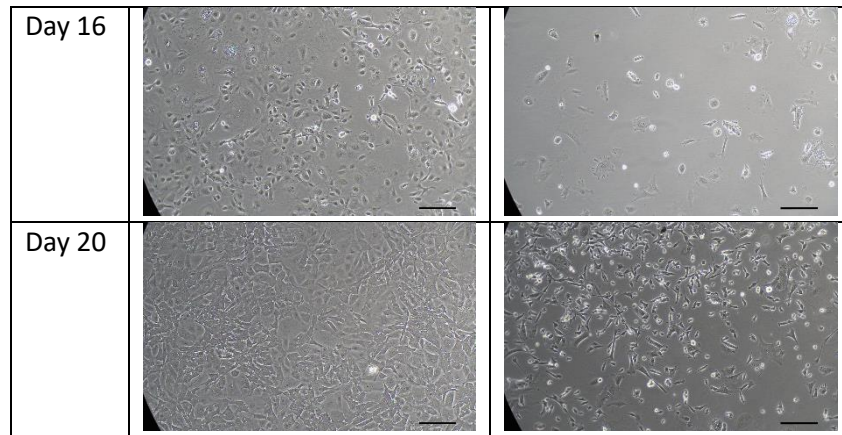


Table 17: Microscope images at 10x magnification, which show the morphology of cells undergoing the quiescent protocol, where the hiPSCs were cultivated in either Essential E8 or FTDA medium prior to the start of the differentiation, at various days of differentiation. A representative image is shown from n=2. Scale bar is 200  $\mu$ m.







### 10.1.2 Serum concentration

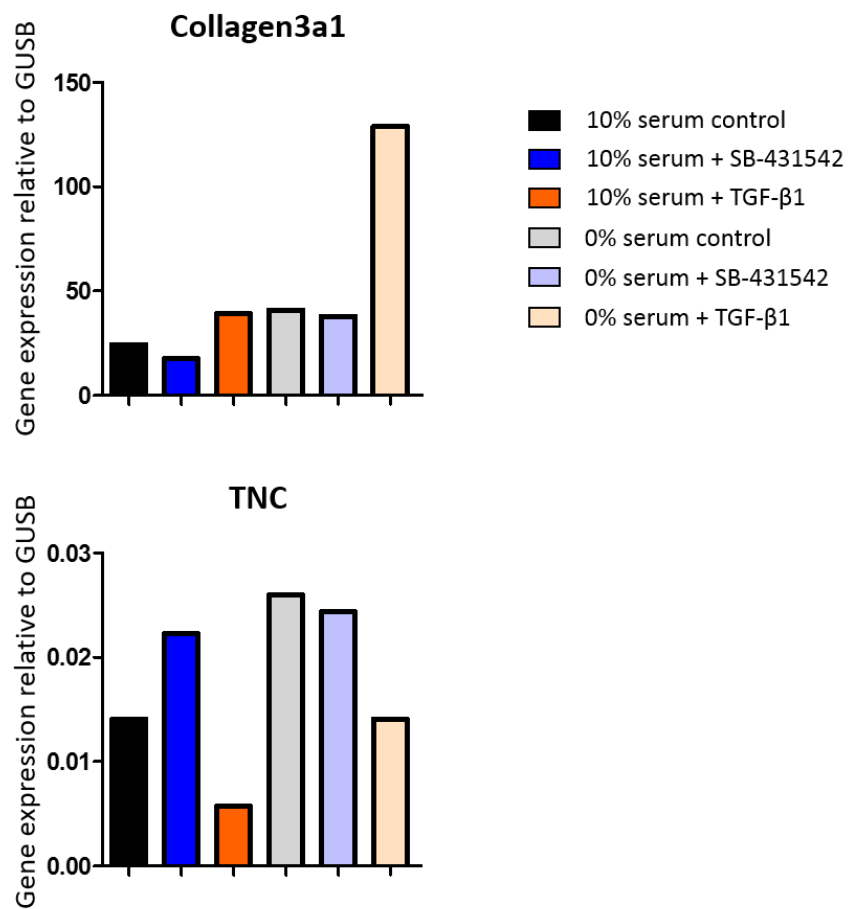


Figure 52: The mRNA abundance relative to GUSB of multiple fibroblast activation markers in 2D cultured primary foreskin fibroblasts: collagen3a1 and TNC. All fibroblasts were cultured in 10% serum containing medium until day 6, after which half of the fibroblasts were cultured in medium containing 0% serum. Additionally, the fibroblasts were assigned different exposure conditions, and either kept as control, treated with 5.4  $\mu$ M SB-431542 or treated with 48 ng/ml TGF- $\beta$ 1 for 5 days. Data are presented as mean,  $n=2$  per group.

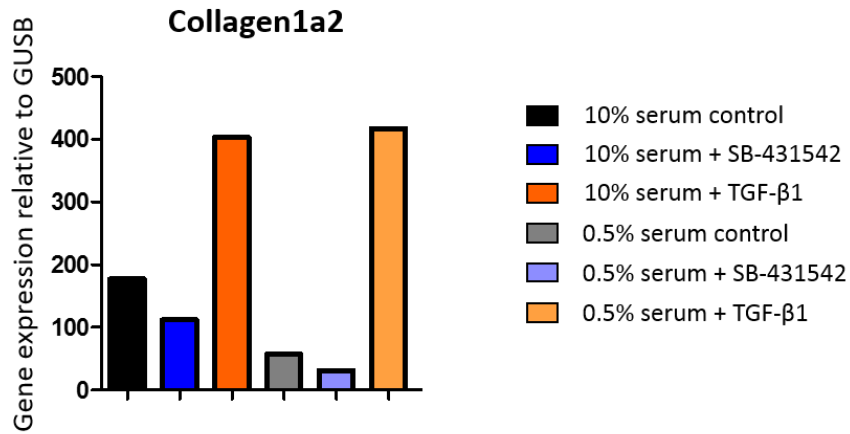


Figure 53: The mRNA abundance relative to GUSB of fibroblast activation marker collagen1a2 in 2D cultured primary foreskin fibroblasts. The fibroblasts were cultured in 10% serum containing medium until day 4, after which they were cultured in 0.5% serum containing medium. Additionally, the fibroblasts were assigned to different conditions, and either kept as control, treated with 5.4  $\mu$ M SB-431542 or treated with 48 ng/ml TGF- $\beta$ 1 for 3 days, n=1 per condition.

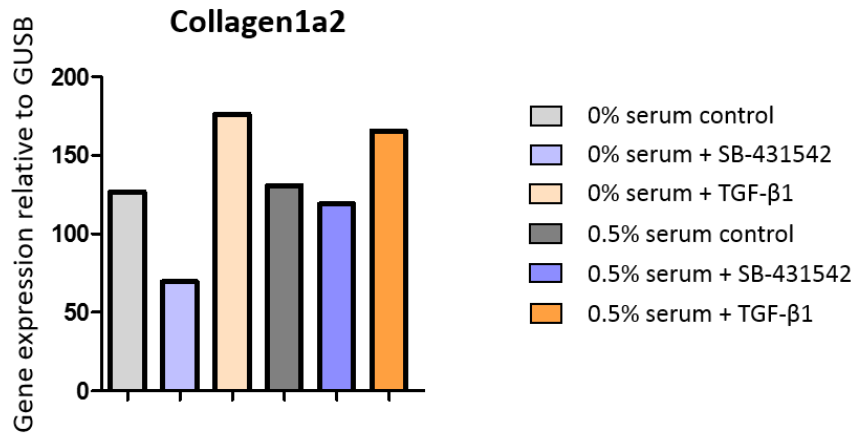


Figure 54: The mRNA abundance relative to GUSB of fibroblast activation marker collagen1a2 in 2D cultured primary foreskin fibroblasts. From day 0, half of the fibroblasts were cultured in medium containing 0% serum, the other half of the fibroblasts were cultured in 0.5% serum containing medium. Additionally, the fibroblasts were assigned to different conditions, and either kept as control, treated with 5.4  $\mu$ M SB-431542 or treated with 48 ng/ml TGF- $\beta$ 1 for 3 days, n=1 per condition.

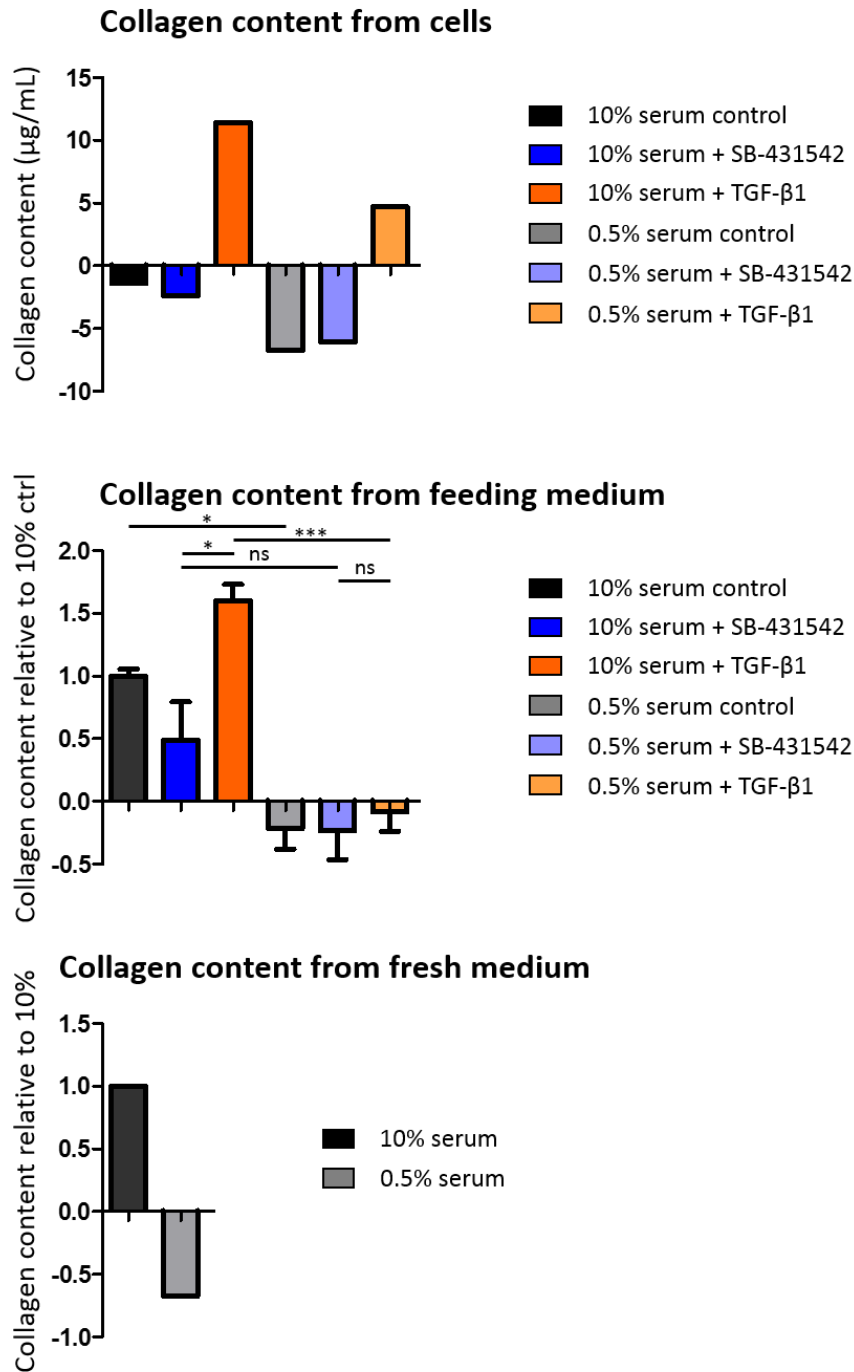


Figure 55: Collagen content, measured in either scraped off 2D cultured primary foreskin fibroblasts (top), used culture medium aspirated from the fibroblasts (middle) or from fresh culture medium (bottom). All fibroblasts were cultured in 10% serum containing medium until day 3 or 4, after which half of the fibroblasts were cultured in medium containing 0.5% serum. On day 6 or 7, respectively, the fibroblasts were assigned to different exposure conditions, and either kept as control, treated with 5.4  $\mu\text{M}$  SB-431542 or treated with 48 ng/ml TGF- $\beta$ 1 for 5 days. When possible, data are presented as mean  $\pm$  SEM. ns: not significant, \* $p < 0.05$ , \*\*\* $p < 0.001$  by one-way ANOVA plus Bonferroni's post-test for multiple comparisons,  $n = 2-3$  per group.

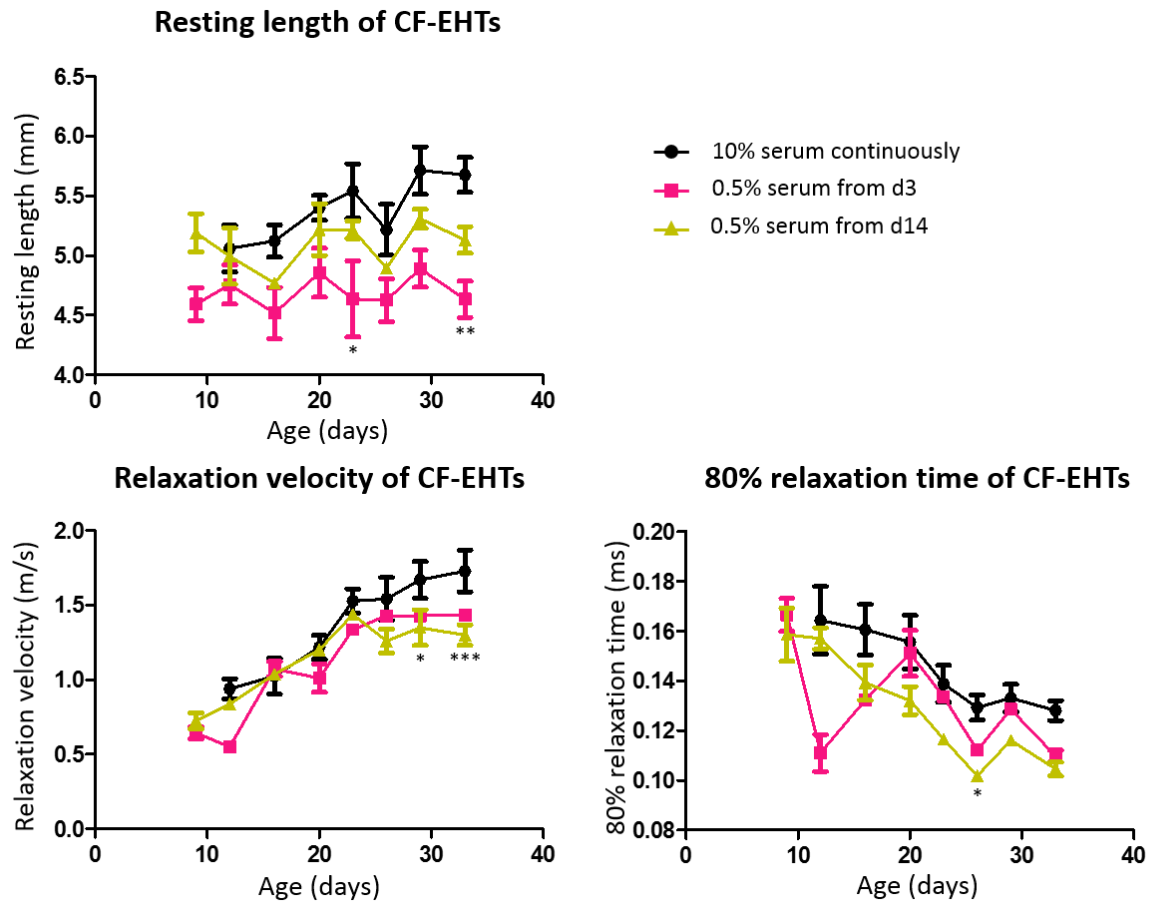


Figure 56: Contractility analyses of CF-EHTs. The development of the resting length, relaxation velocity and 80% relaxation time of the CF-EHTs are presented over time. The CF-EHTs were either continuously cultured in medium containing 10% serum or switched to medium containing 0.5% serum on either day 3 or day 14, CF-EHTs were harvested on day 33. Data are presented as mean  $\pm$  SEM, \* $p$ <0.05, \*\* $p$ <0.005, \*\*\* $p$ <0.001 by two-way ANOVA plus Bonferroni's post-test for multiple comparisons, only biologically meaningful comparisons are shown,  $n=4$  per group.

### 10.1.3 CF percentage

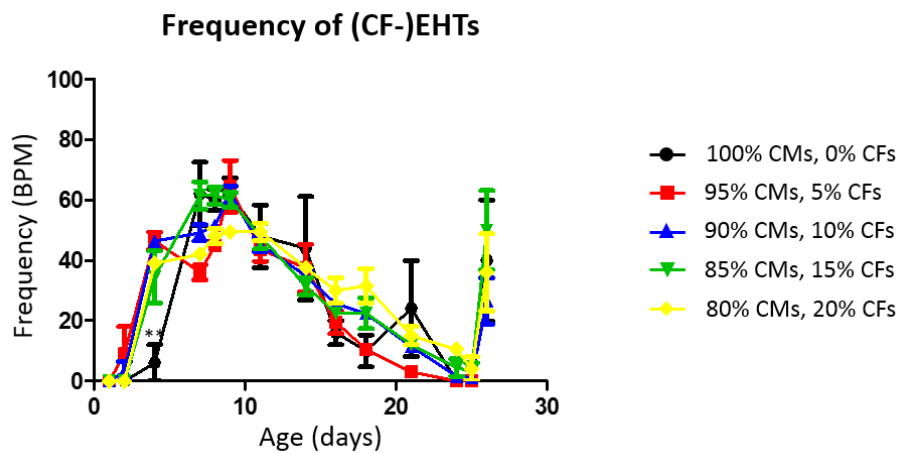


Figure 57: Contractility analyses of (CF-)EHTs containing 0%, 5%, 10%, 15% or 20% hiPSC-derived cardiac fibroblasts. The development of the beating frequency of the (CF-)EHTs is presented over time. The (CF-)EHTs were cultured in 10% serum containing medium until day 4, after which they were cultured in 0.5% serum containing medium. On the last day of culture, day 25, the contractility of the CF-EHTs was analysed under pacing, the results of which are presented as the fictional analysis

on day 26 here. Data are presented as mean  $\pm$  SEM,  $^{**}p<0.005$  by two-way ANOVA, only biologically meaningful comparisons are shown,  $n=4$  per group.

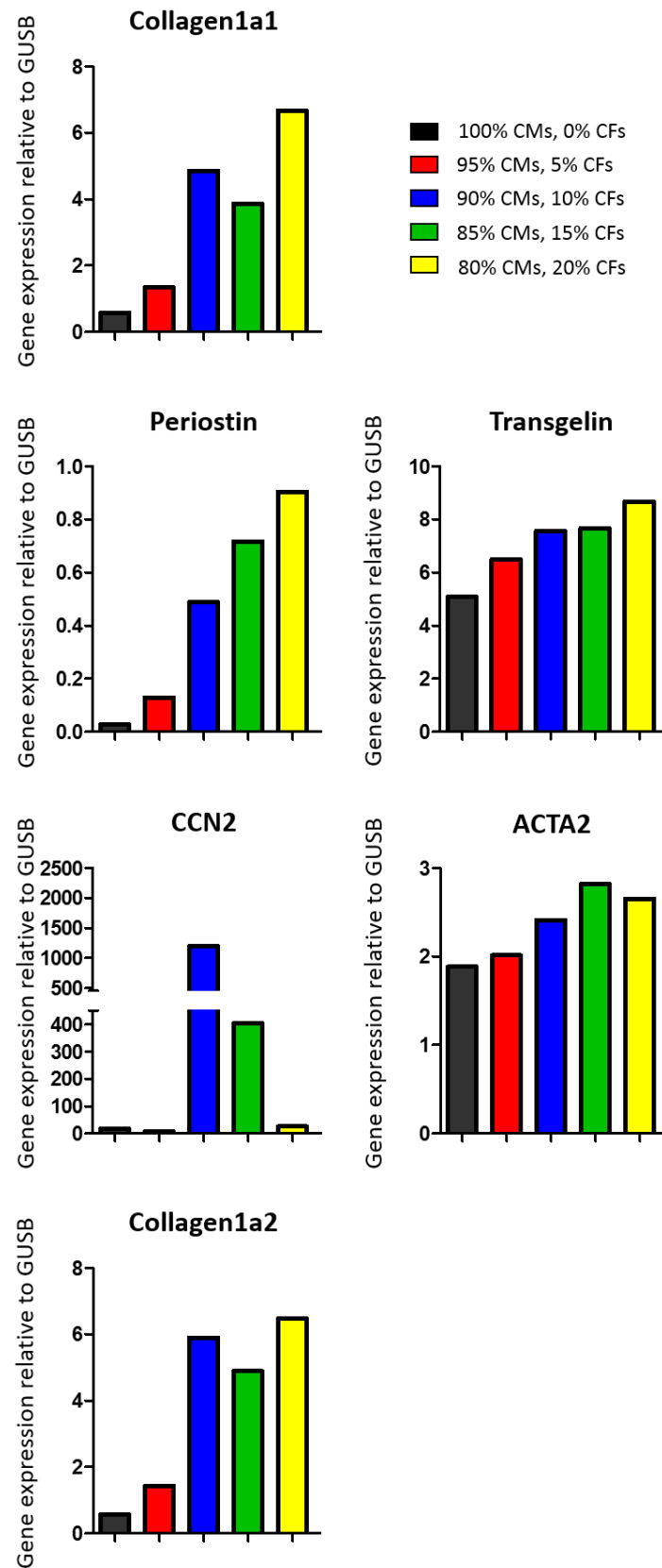


Figure 58: The mRNA abundance relative to GUSB of fibroblast activation markers collagen1a1, periostin, transgelin, CCN2, ACTA2 and collagen1a2 in (CF-)EHTs. The (CF-)EHTs contained either 0%, 5%, 10%, 15% or 20% hiPSC-derived cardiac

fibroblasts. The (CF-)EHTs were cultured in 10% serum containing medium until day 4, after which they were cultured in 0.5% serum containing medium, until they were harvested on day 25. When possible, data are presented as mean,  $n=1-2$  per group.

#### 10.1.4 2D fibroblast activation

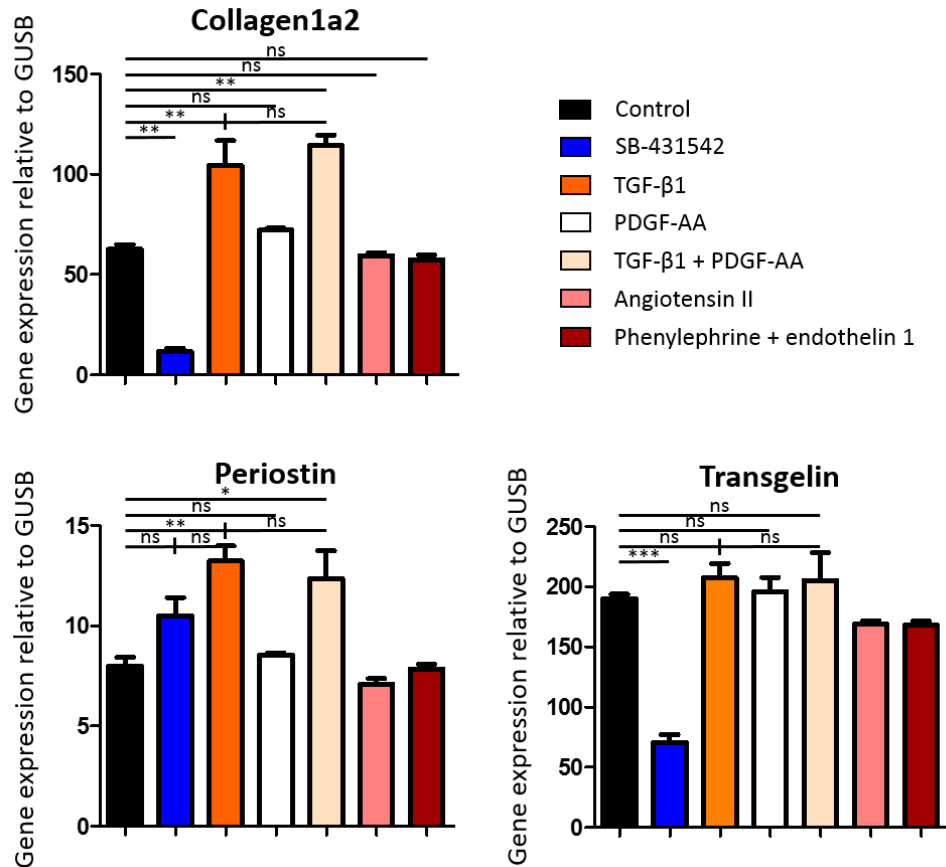


Figure 59: The mRNA abundance relative to GUSB of multiple fibroblast activation markers in 2D cultured hiPSC-derived cardiac fibroblasts: collagen1a2, periostin and transgelin. The 2D cultured cardiac fibroblasts were either assigned to a control group, an inhibited group, treated with SB-431542 or an activated group, treated with either TGF-β1, PDGF-AA, TGF-β1 + PDGF-AA, angiotensin II or phenylephrine + endothelin 1, respectively. Fibroblasts were cultured in 0.5% serum containing medium from day 0 on, assigned to their respective conditions on day 4 and kept on these conditions until they were harvested on day 11. Data are presented as mean  $\pm$  SEM. ns: not significant, \* $p<0.05$ , \*\* $p<0.005$ , \*\*\* $p<0.001$  by one-way ANOVA plus Bonferroni's post-test for multiple comparisons,  $n=3$  per group.

## 10.1.5 3D fibroblast activation

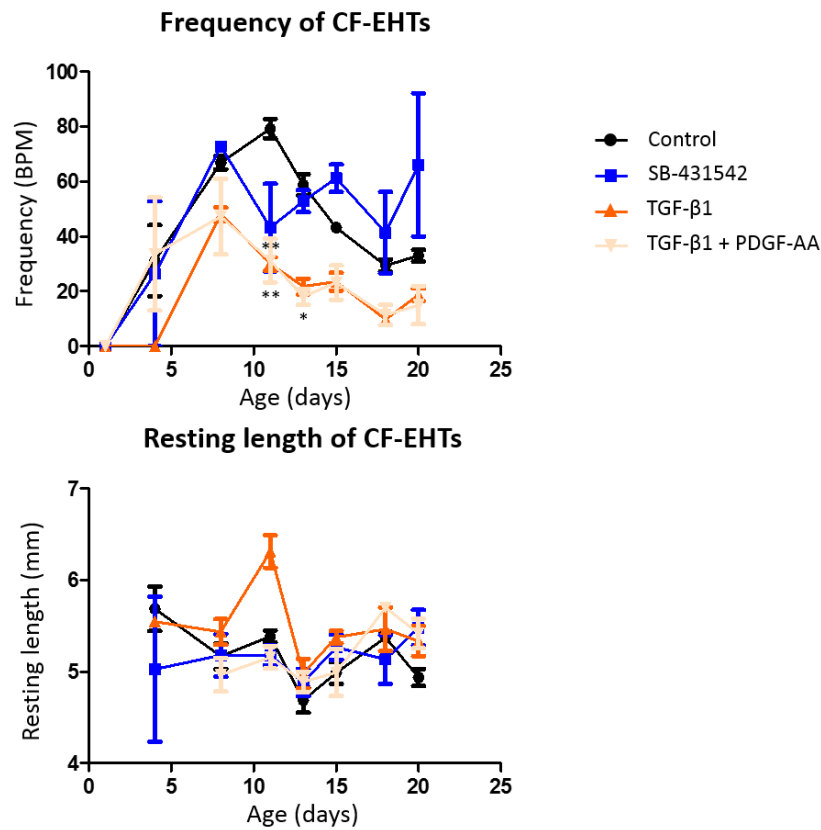


Figure 60: Contractility analyses of CF-EHTs assigned to either a control group, an inhibited group, treated with 1  $\mu$ M SB-431542 for 7 days and 5  $\mu$ M for the remainder of the culture period, or to 1 of 2 activated groups, treated with either 15 ng/ml TGF- $\beta$ 1 or 15 ng/ml TGF- $\beta$ 1 + 10 ng/ml PDGF-AA. The development of the beating frequency and resting length of the CF-EHTs are presented over time. The CF-EHTs were cultured in 10% serum containing medium until day 4, after which the CF-EHTs were cultured in 0.5% serum containing medium, assigned to their respective groups on day 8 and kept on these conditions until the last day of culture, day 21. Data are presented as mean  $\pm$  SEM, \* $p$ <0.05, \*\* $p$ <0.005, \*\*\* $p$ <0.001 by two-way ANOVA, only biologically meaningful comparisons are shown,  $n$ =4-5 per group.

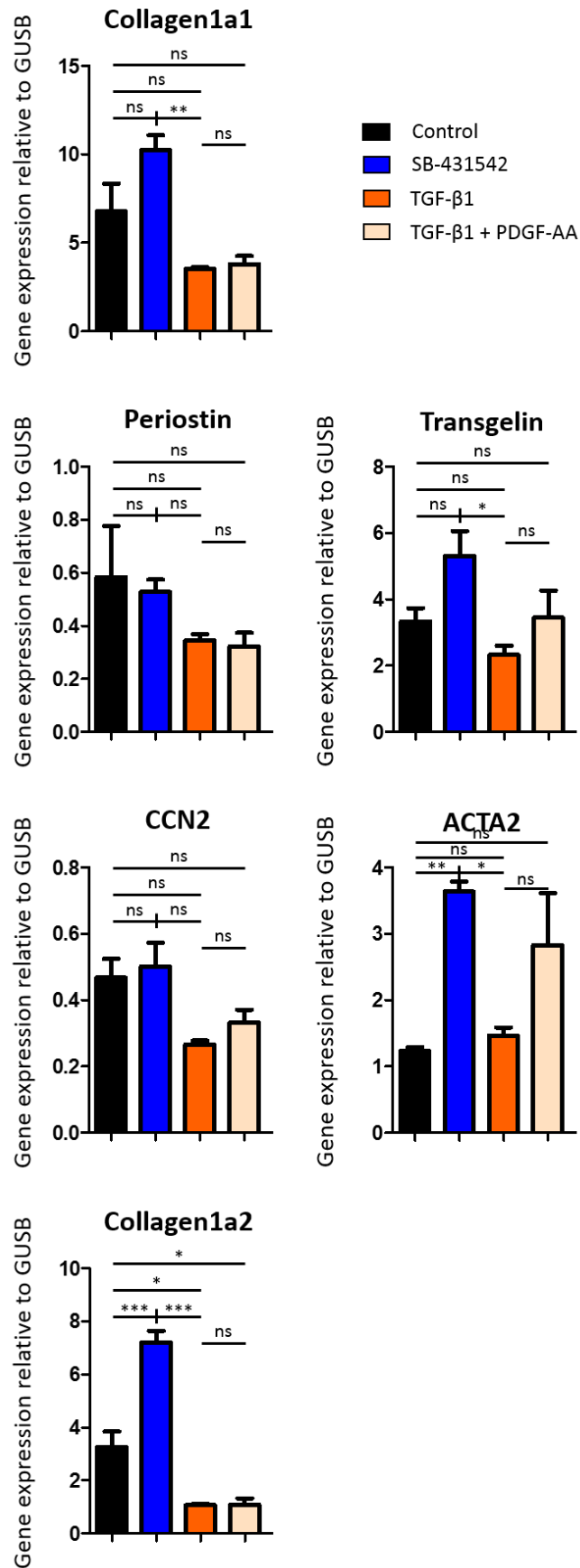


Figure 61: The mRNA abundance relative to GUSB of the fibroblast activation markers collagen1a1, periostin, transgelin, CCN2, ACTA2 and collagen1a2 in CF-EHTs. CF-EHTs were assigned to either a control group, an inhibited group, treated with 1  $\mu$ M



SB-431542 for 7 days and 5  $\mu\text{M}$  for the remainder of the culture period, or to 1 of 2 activated groups, treated with either 15 ng/ml TGF- $\beta$ 1 or 15 ng/ml TGF- $\beta$ 1 + 10 ng/ml PDGF-AA. The CF-EHTs were cultured in 10% serum containing medium until day 4, after which they were cultured in 0.5% serum containing medium, they were assigned to their respective groups on day 8 and kept on these conditions until the last day of culture, day 21. Data are presented as mean  $\pm$  SEM. ns: not significant, \* $p$ <0.05, \*\*\* $p$ <0.001 by one-way ANOVA plus Bonferroni's post-test for multiple comparisons,  $n$ =4-5 per group.

### 10.1.6 SB-431542 treatment

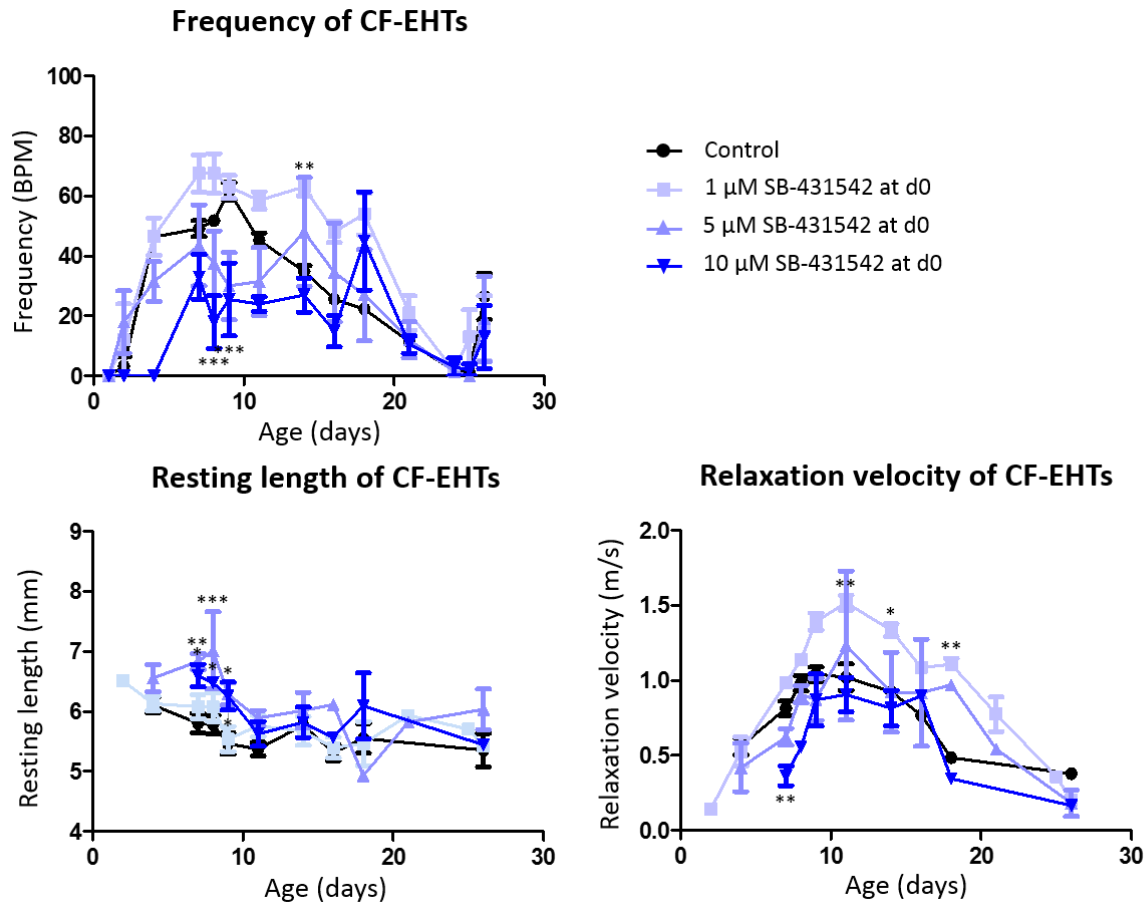


Figure 62: Contractility analyses of CF-EHTs treated with either no SB-431542 (control), 1  $\mu\text{M}$ , 5  $\mu\text{M}$ , or 10  $\mu\text{M}$  SB-431542 from day 0. The CF-EHTs were cultured in 10% serum containing medium until day 4, after which the CF-EHTs were cultured in 0.5% serum containing medium. The development of the beating frequency, resting length and relaxation velocity of the CF-EHTs are presented over time. On the last day of culture, day 25, the contractility of the CF-EHTs was analysed under pacing, the results of which are presented as the fictional analysis on day 26 here. Data are presented as mean  $\pm$  SEM, \* $p$ <0.05, \*\* $p$ <0.005, \*\*\* $p$ <0.001 by two-way ANOVA, only biologically meaningful comparisons are shown,  $n$ =4-11 per group.

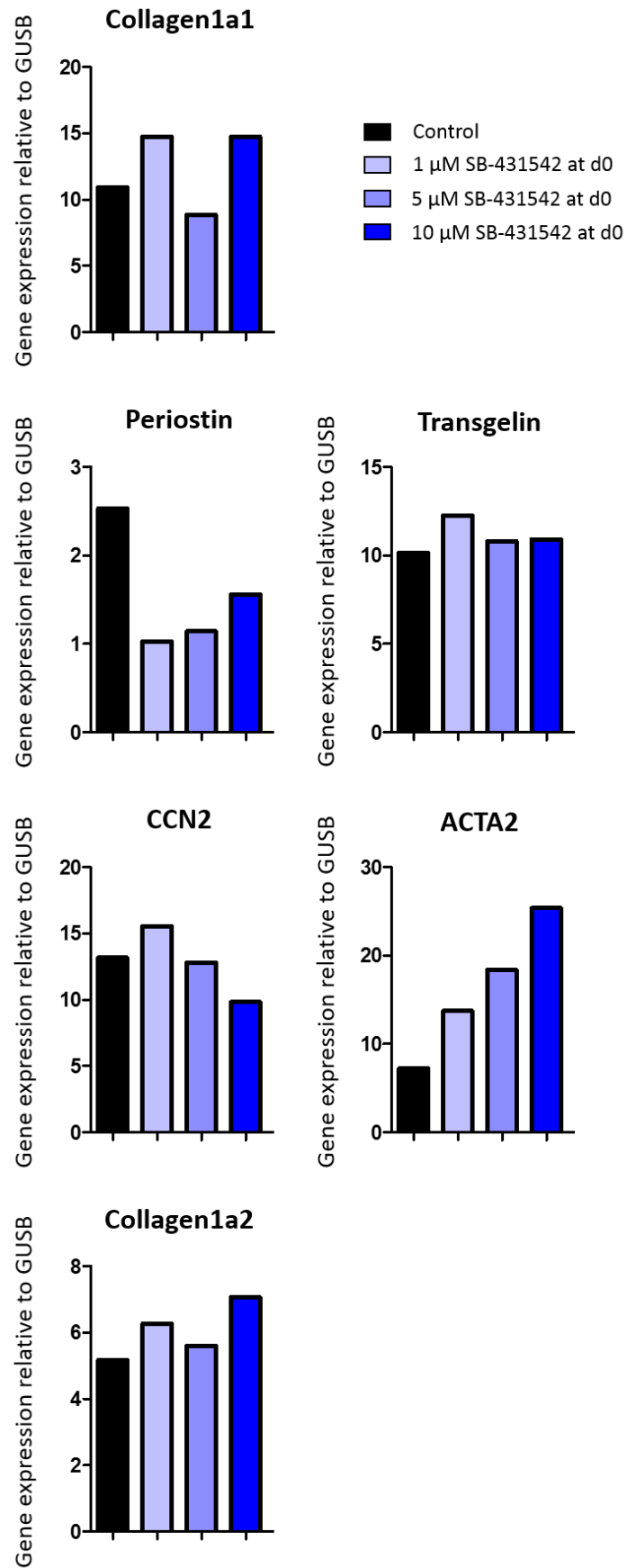


Figure 63: The mRNA abundance relative to GUSB of multiple fibroblast activation markers in CF-EHTs: collagen1a1, periostin, transgelin, CCN2, ACTA2 and collagen1a2. CF-EHTs were treated with no SB-431542 (control), 1 μM, 5 μM or 10 μM SB-431542,

from day 0. The CF-EHTs were cultured in 10% serum containing medium until day 4, after which they were cultured in 0.5% serum containing medium until they were harvested on day 25,  $n=1$  per condition.

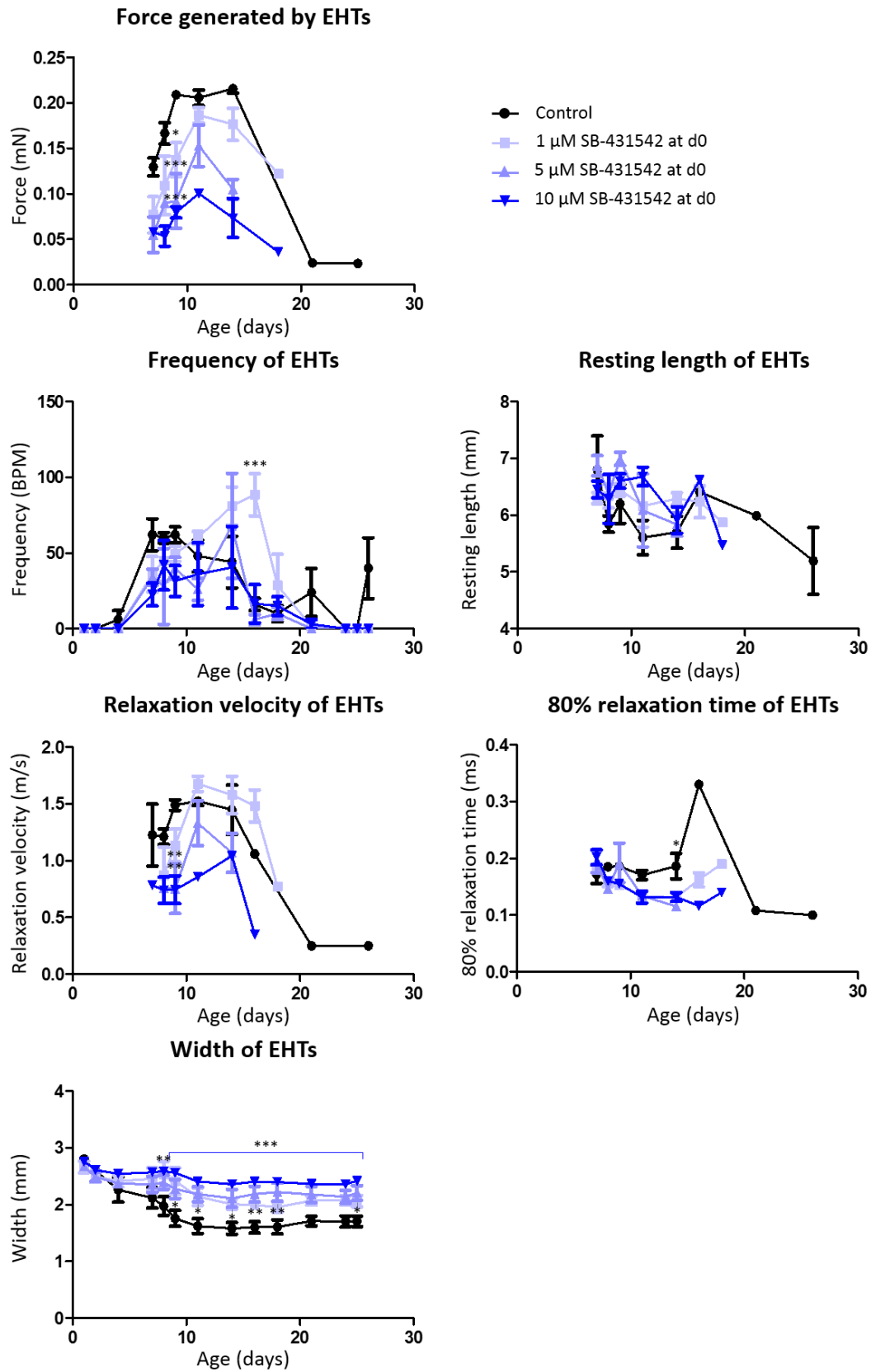


Figure 64: Contractility analyses of EHTs (containing no cardiac fibroblasts) treated with either no SB-431542 (control), 1  $\mu$ M, 5  $\mu$ M or 10  $\mu$ M SB-431542 from day 0. The EHTs were cultured in 10% serum containing medium until day 4, after which they

were cultured in 0.5% serum containing medium. The development of the generated force, beating frequency, resting length, relaxation velocity, 80% relaxation time and width of the CF-EHTs are presented over time. On the last day of culture, day 25, the contractility of the CF-EHTs was analysed under pacing, the results of which are presented as the fictional analysis on day 26 here. Data are presented as mean  $\pm$  SEM, \* $p$ <0.05, \*\* $p$ <0.005, \*\*\* $p$ <0.001 by two-way ANOVA, only biologically meaningful comparisons are shown. From day 16, only 1 control EHT spontaneously contracted, so from day 16 no statistical analysis could be performed,  $n$ =3-4 per group.

### 10.1.7 TGF- $\beta$ 1 treatment

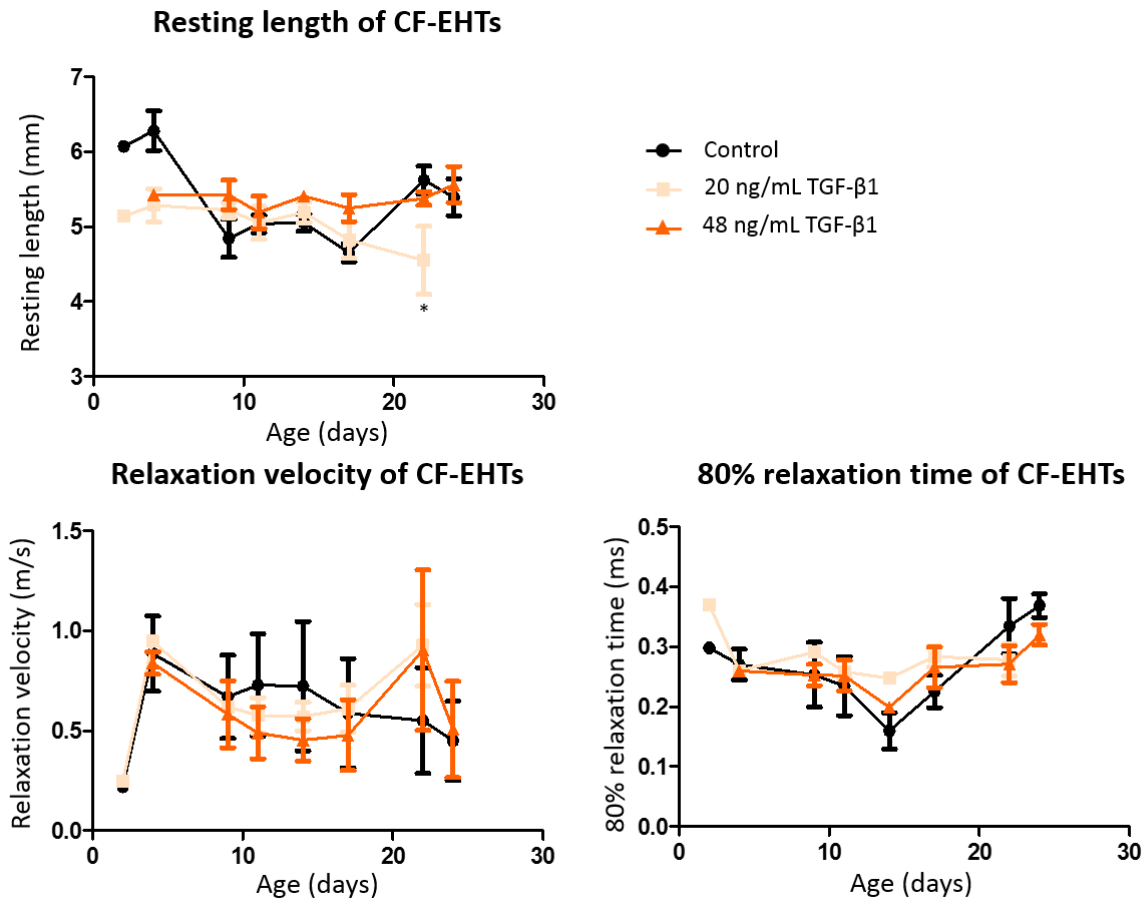


Figure 65: Contractility analyses of CF-EHTs treated with either no TGF- $\beta$ 1 (control), 20 ng/ml or 48 ng/ml TGF- $\beta$ 1 from day 0. The CF-EHTs were cultured in 10% serum containing medium until day 4, after which they were cultured in 0.5% serum containing medium. The development of the resting length, relaxation velocity and 80% relaxation time of the CF-EHTs are presented over time. The CF-EHTs were harvested on day 24. Data are presented as mean  $\pm$  SEM, \* $p$ <0.05 by two-way ANOVA, only biologically meaningful comparisons are shown,  $n$ =4 per group.

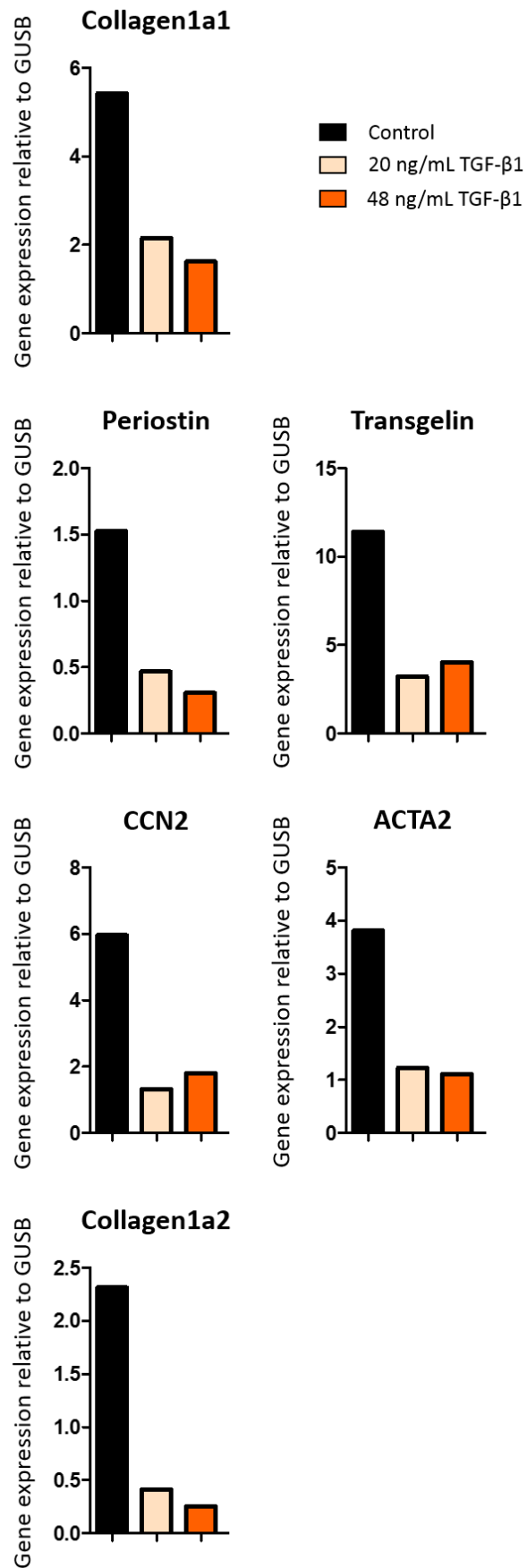


Figure 66: The mRNA abundance relative to GUSB of multiple fibroblast activation markers in CF-EHTs: collagen1a1, periostin, transgelin, CCN2, ACTA2 and collagen1a2. CF-EHTs were treated with either no TGF-β1 (control), 20 ng/ml or 48 ng/ml TGF-

61 from day 0. The CF-EHTs were cultured in 10% serum containing medium until day 4, after which the CF-EHTs were cultured in 0.5% serum containing medium until they were harvested on day 24, n=1 per condition.

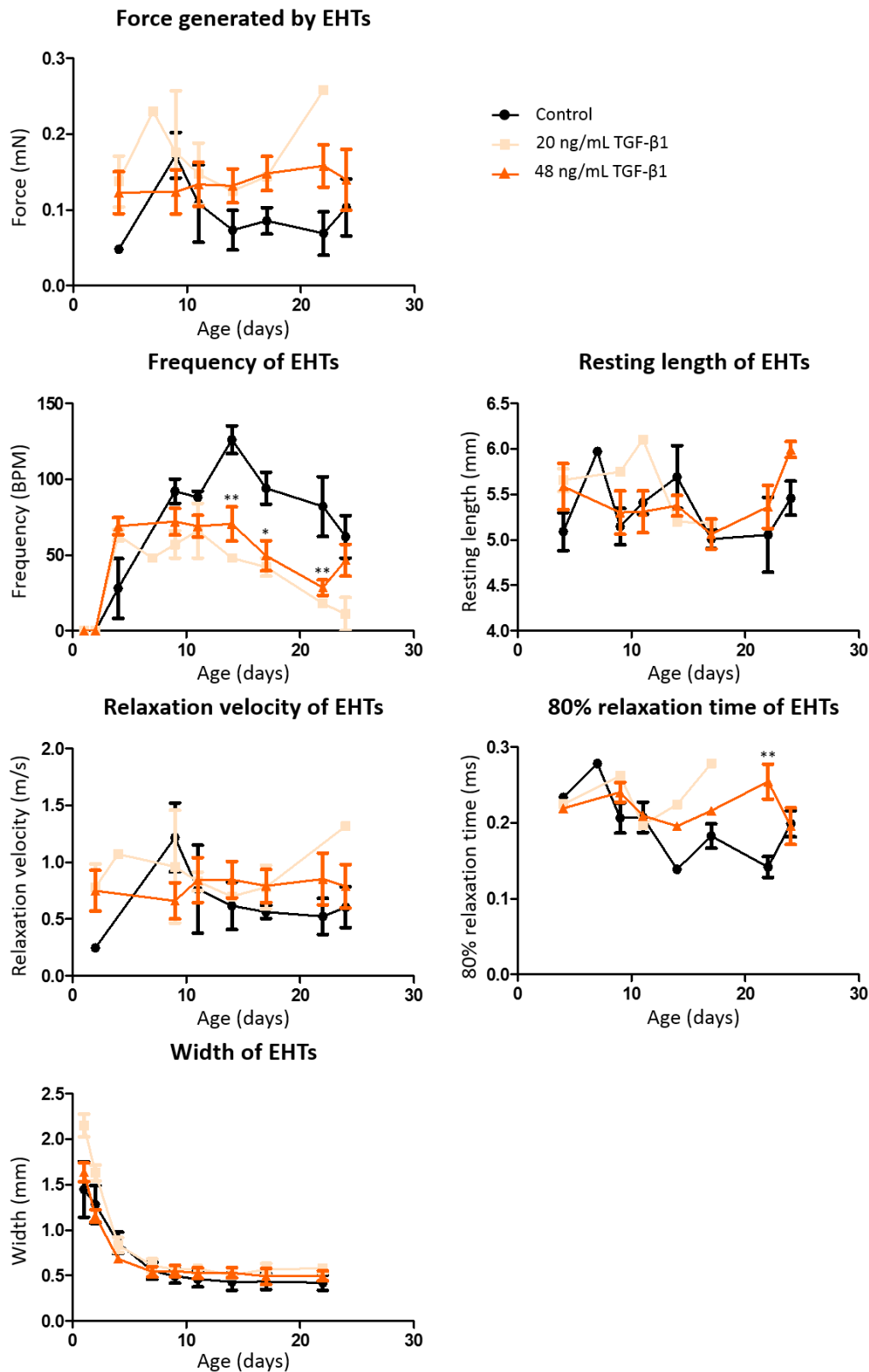


Figure 67: Contractility analyses of EHTs (containing no cardiac fibroblasts) treated with either no TGF- $\beta$ 1 (control), 20 ng/ml or 48 ng/ml TGF- $\beta$ 1 from day 0. The EHTs were cultured in 10% serum containing medium until day 4, after which they were cultured in 0.5% serum containing medium. The development of the generated force, beating frequency, resting length, relaxation velocity, 80% relaxation time and width of the EHTs are presented over time. The CF-EHTs were harvested on day

24. Data are presented as mean  $\pm$  SEM, \* $p$ <0.05, \*\* $p$ <0.005, by two-way ANOVA, only biologically meaningful comparisons are shown. No significance could be calculated with the 20 ng/ml TGF- $\beta$ 1 treated EHTs as all but 2 EHTs ruptured after day 4,  $n$ =3-4 per group.

### 10.1.8 Timing of treatment

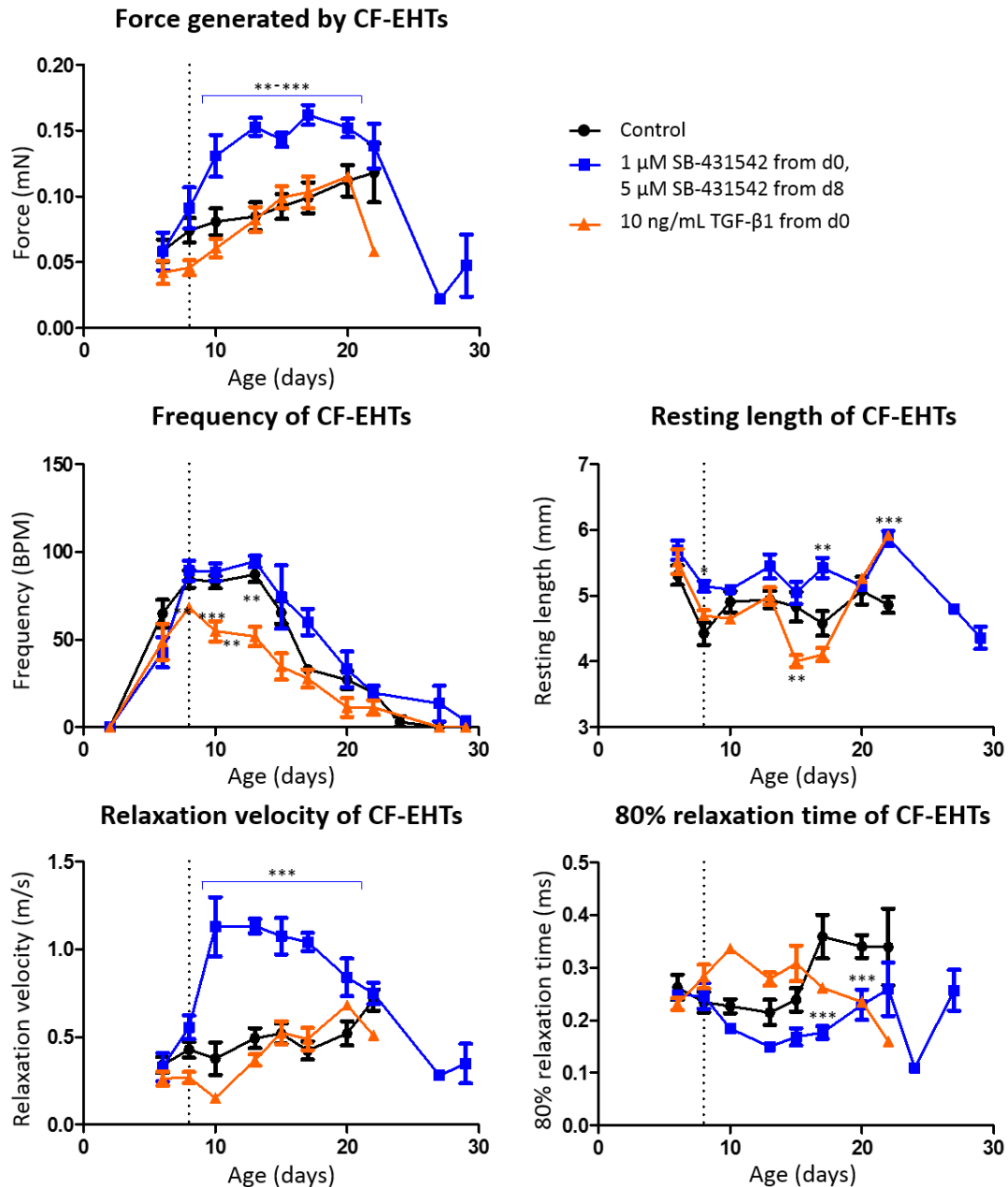


Figure 68: Contractility analyses of CF-EHTs assigned to either a control group; an inhibited group, treated with 1  $\mu$ M SB-431542 from day 0 and 5  $\mu$ M SB-431542 from day 8; or an activated group, treated with 10 ng/ml TGF- $\beta$ 1 from day 0. The CF-EHTs were cultured in 10% serum containing medium until day 3, after which they were cultured in 0.5% serum containing medium. The development of the generated force, beating frequency, resting length, relaxation velocity and 80% relaxation time of the CF-EHTs are presented over time. The CF-EHTs were harvested on day 29. Data are presented as mean  $\pm$  SEM, \*\* $p$ <0.005, \*\*\* $p$ <0.001 by two-way ANOVA, only biologically meaningful comparisons are shown,  $n$ =4-5 per group.

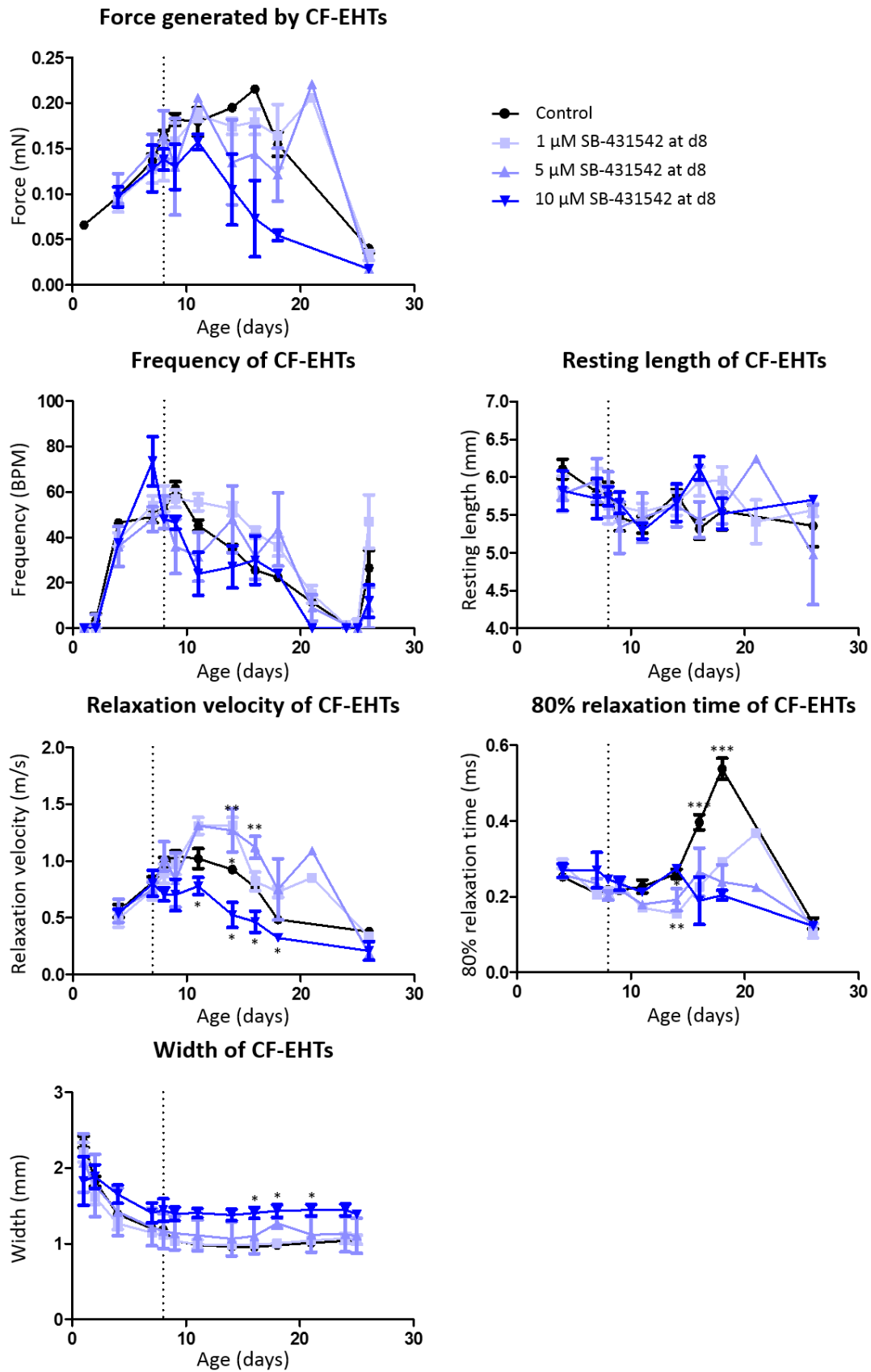


Figure 69: Contractility analyses of CF-EHTs treated with either no SB-431542 (control), 1  $\mu$ M, 5  $\mu$ M or 10  $\mu$ M SB-431542 from day 8. The CF-EHTs were cultured in 10% serum containing medium until day 4, after which they were cultured in 0.5% serum containing medium. The development of the generated force, beating frequency, resting length, relaxation velocity, 80%



relaxation time and width of the CF-EHTs are presented over time. On the last day of culture, day 25, contractility of CF-EHTs was analysed under pacing, the results are presented as the fictional analysis on day 26 here. Data are presented as mean  $\pm$  SEM, \* $p$ <0.05, \*\* $p$ <0.005, \*\*\* $p$ <0.001 by two-way ANOVA, only biologically meaningful comparisons are shown,  $n$ =4-11 per group.

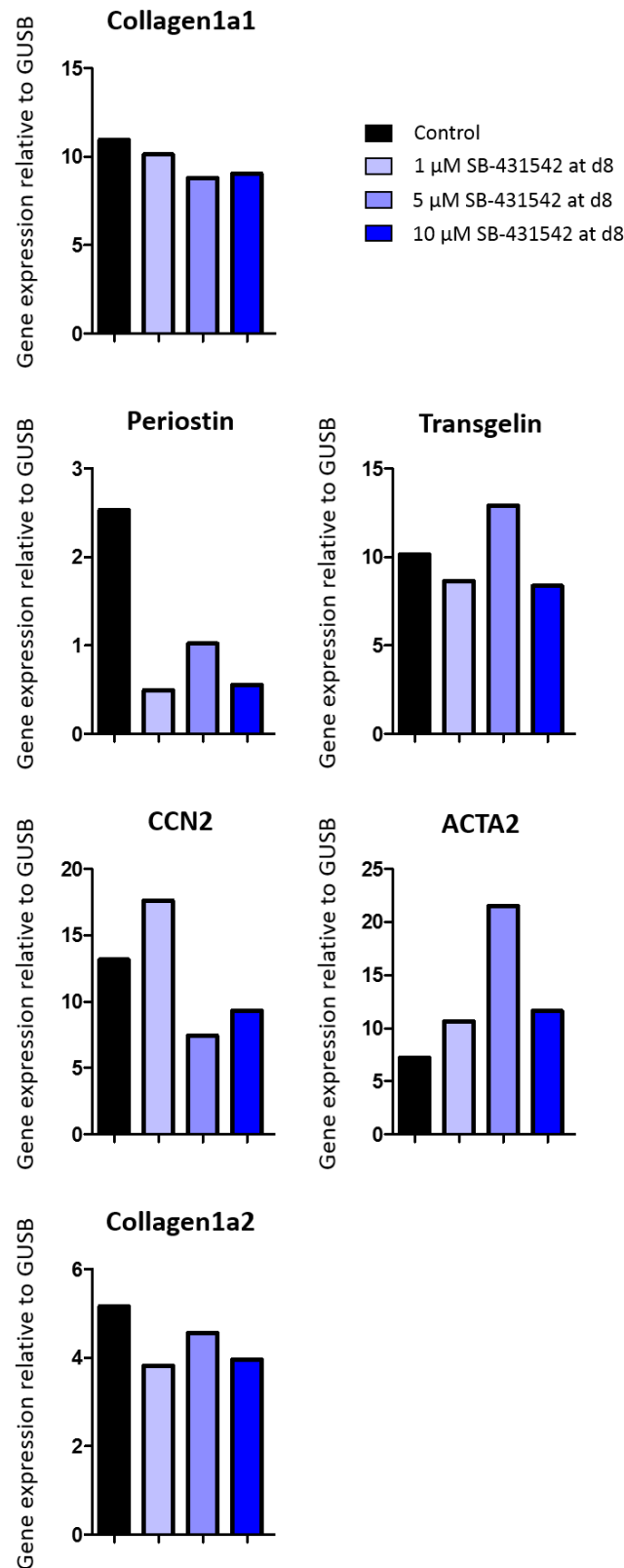


Figure 70: The mRNA abundance relative to GUSB of multiple fibroblast activation markers in CF-EHTs: collagen1a1, periostin, transgelin, CCN2, ACTA2 and collagen1a2. CF-EHTs were treated with either no SB-431542 (control), 1  $\mu$ M, 5  $\mu$ M or 10  $\mu$ M SB-

431542, from day 8. The CF-EHTs were cultured in 10% serum containing medium until day 4, after which the CF-EHTs were cultured in 0.5% serum containing medium. The CF-EHTs were harvested on day 25,  $n=1$  per condition.

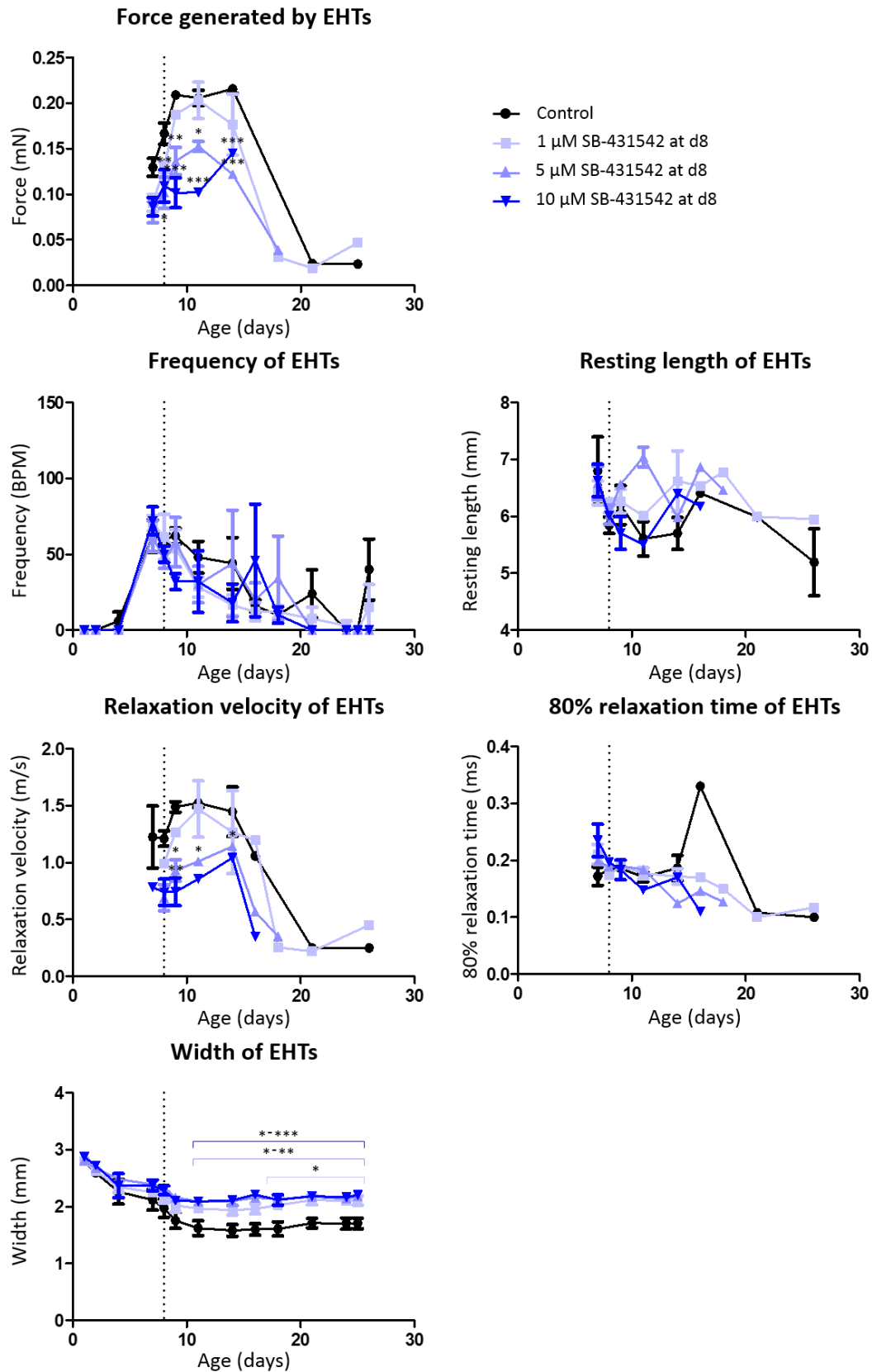


Figure 71: Contractility analyses of EHTs (containing no cardiac fibroblasts) treated with either no SB-431542 (control), 1  $\mu$ M, 5  $\mu$ M or 10  $\mu$ M SB-431542 from day 8. The EHTs were cultured in 10% serum containing medium until day 4, after which they

were cultured in 0.5% serum containing medium. The development of the generated force, beating frequency, resting length, relaxation velocity, 80% relaxation time and width of the CF-EHTs are presented over time. On the last day of culture, day 25, the contractility of the EHTs was analysed under pacing, the results of which are presented as the fictional analysis on day 26 here. Data are presented as mean  $\pm$  SEM, \* $p$ <0.05, \*\* $p$ <0.005, \*\*\* $p$ <0.001 by two-way ANOVA, only biologically meaningful comparisons are shown,  $n$ =3-4 per group.

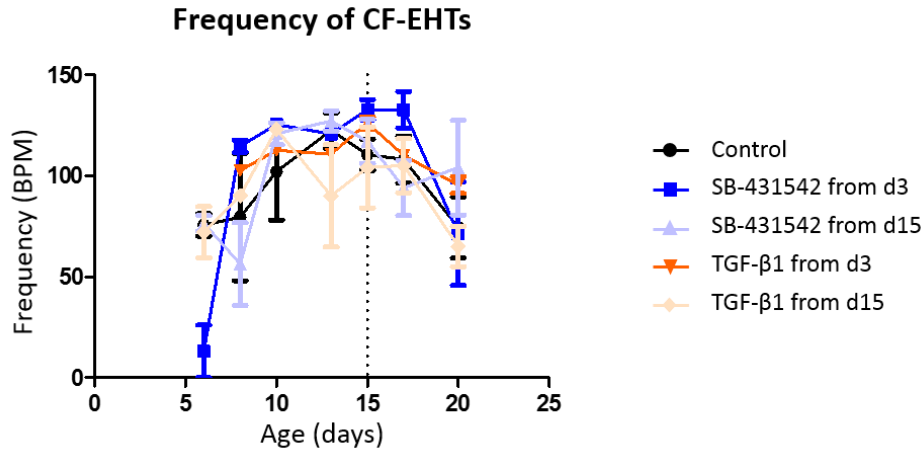


Figure 72: Contractility analyses of CF-EHTs assigned to either a control group, 1 of 2 inhibited groups, or 1 of 2 activated groups. The CF-EHTs were harvested on day 21. The CF-EHTs from 1 inhibited group were treated with 1  $\mu$ M SB-431542 from day 3 and 5  $\mu$ M SB-431542 from day 10 until they were harvested. The CF-EHTs from the other inhibited group were treated with 5  $\mu$ M SB-431542 from day 15 until they were harvested. The CF-EHTs from 1 activated group were treated with 10 ng/ml TGF- $\beta$ 1 from day 3 until they were harvested. The CF-EHTs from the other activated group were treated with 10 ng/ml TGF- $\beta$ 1 from day 15 until they were harvested. The CF-EHTs were cultured in 10% serum containing medium until day 3, after which they were cultured in 0.5% serum containing medium. The development of the beating frequency of the CF-EHTs is presented over time. On the second to last day of culture, day 20, the contractility of the CF-EHTs was analysed under pacing. Data are presented as mean  $\pm$  SEM, no significant differences were measured by two-way ANOVA plus Bonferroni's post-test for multiple comparisons,  $n$ =4-6 per group

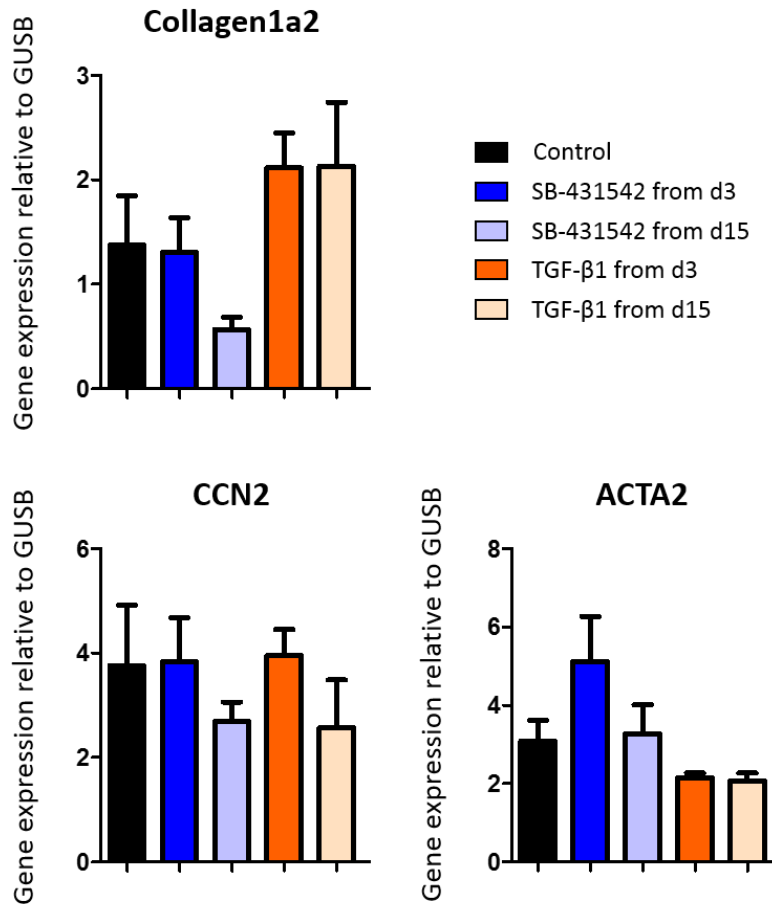


Figure 73: The mRNA abundance relative to GUSB of multiple fibroblast activation markers in CF-EHTs: collagen1a2, CCN2 and ACTA2. The CF-EHTs were assigned to either a control group, 1 of 2 inhibited groups, or 1 of 2 activated groups. The CF-EHTs were harvested on day 21. The CF-EHTs from 1 inhibited group were treated with 1  $\mu$ M SB-431542 from day 3 and 5  $\mu$ M SB-431542 from day 10 until they were harvested. The CF-EHTs from the other inhibited group were treated with 5  $\mu$ M SB-431542 from day 15 until they were harvested. The CF-EHTs from 1 activated group were treated with 10 ng/ml TGF- $\beta$ 1 from day 3 until they were harvested. The CF-EHTs from the other activated group were treated with 10 ng/ml TGF- $\beta$ 1 from day 15 until they were harvested. The CF-EHTs were all cultured in 10% serum containing medium until day 3, after which the CF-EHTs were cultured in 0.5% serum containing medium. Data are presented as mean  $\pm$  SEM. No significant differences were measured by one-way ANOVA plus Bonferroni's post-test for multiple comparisons,  $n=3-4$  per group.

10.1.9 The *in vitro* fibrosis model

## 10.1.9.1 A18945 CF-EHTs

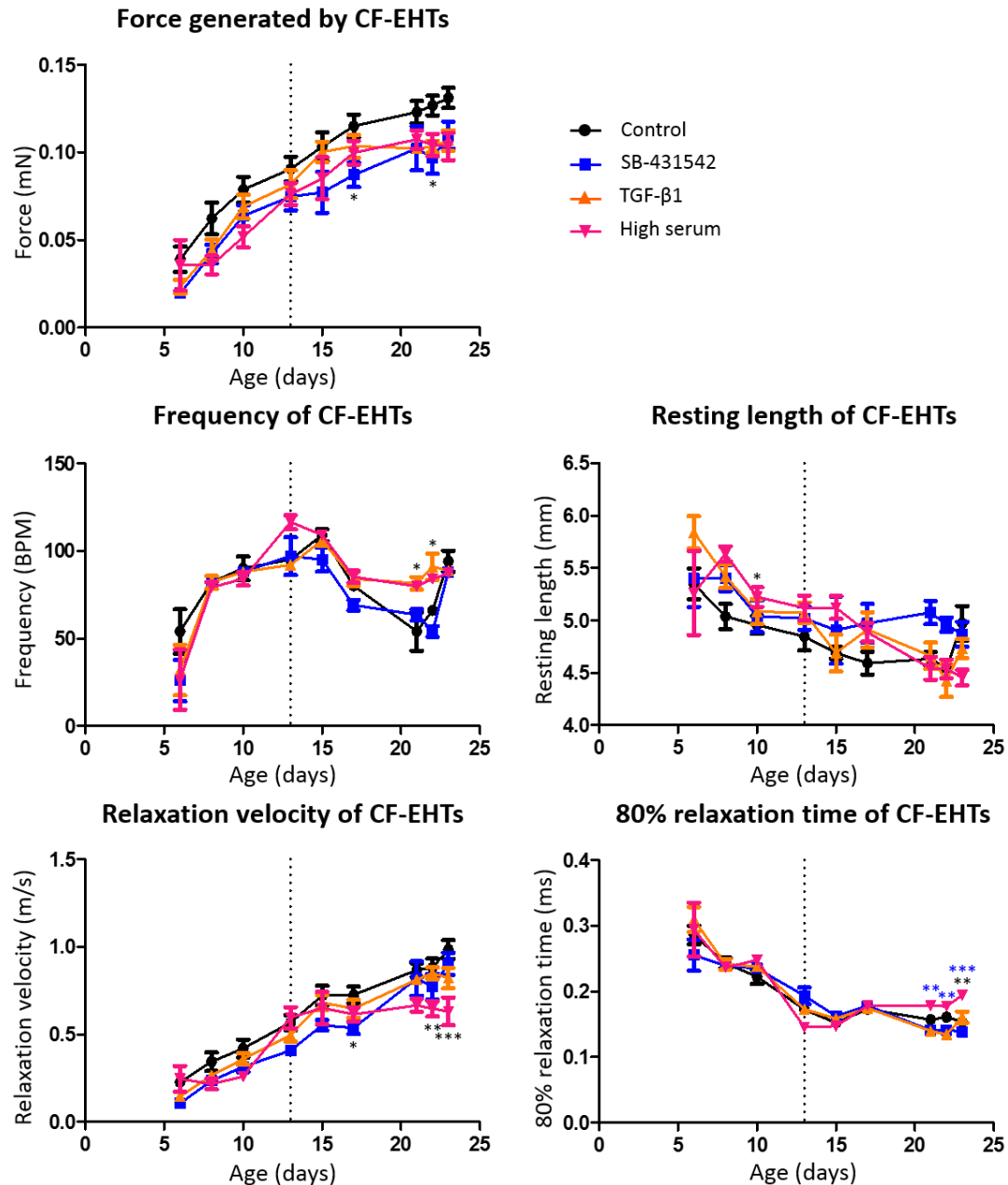


Figure 74: Contractility analyses of A18945 CF-EHTs, assigned to either a control group, an inhibited group, treated with 5  $\mu$ M SB-431542, or 1 of 2 activated groups. The CF-EHTs from 1 activated group were treated with 10 ng/ml TGF- $\beta$ 1, the CF-EHTs from the other activated group were exposed to 10% serum containing medium. All CF-EHTs were cultured in 10% serum containing medium until day 3, after which they were cultured in 0.5% serum containing medium. All CF-EHTs were cultured with 5  $\mu$ M SB-431542 from day 10 until day 13, after which they were assigned to their respective groups. All CF-EHTs were treated according to their group until day 22, when they were harvested. The development of the generated force, beating frequency, resting length, relaxation velocity and 80% relaxation time of the CF-EHTs are presented over time. On the last day of culture, day 22, the contractility of the CF-EHTs was analysed under electrical pacing, the results of which are presented as the fictional analysis on day 23 here. Data are presented as mean  $\pm$  SEM, \* $p$ <0.05, \*\* $p$ <0.005, \*\*\* $p$ <0.001 by two-way ANOVA plus Bonferroni's post-test for multiple comparisons, only biologically meaningful comparisons are shown,  $n$ =5-6 per group.

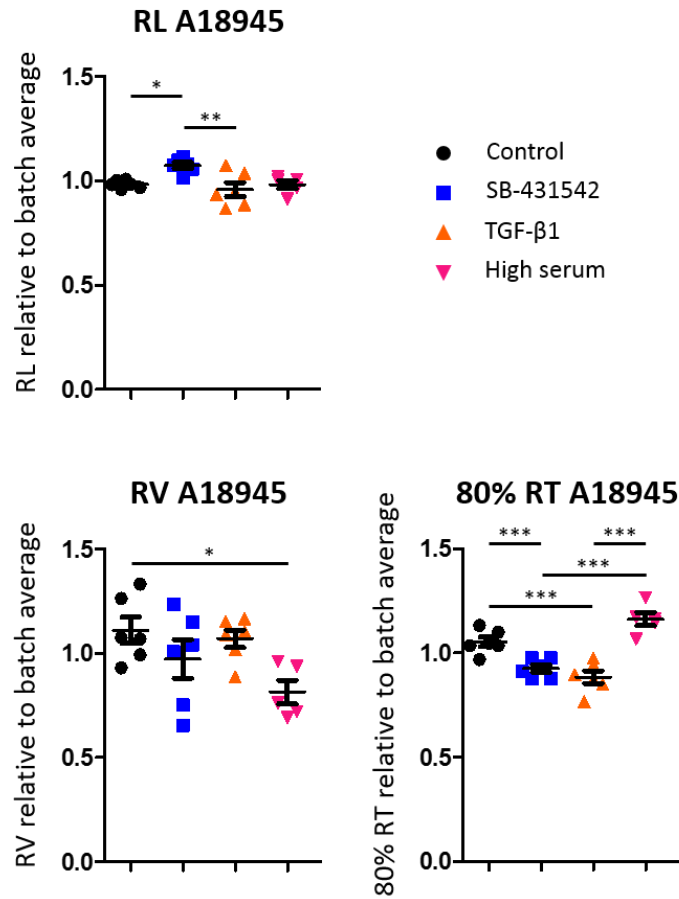


Figure 75: Contractility analyses of A18945 CF-EHTs, assigned to either a control group, an inhibited group, or 1 of 2 activated groups, and treated as previously described. The resting length, relaxation velocity and 80% relaxation time of the spontaneous contractions of the CF-EHTs on the last day of culture, day 22, relative to the batch average are presented. Data are presented as mean  $\pm$  SEM. \* $p < 0.05$ , \*\* $p < 0.005$ , \*\*\* $p < 0.001$  by one-way ANOVA plus Bonferroni's post-test for multiple comparisons,  $n = 5-6$  per group.

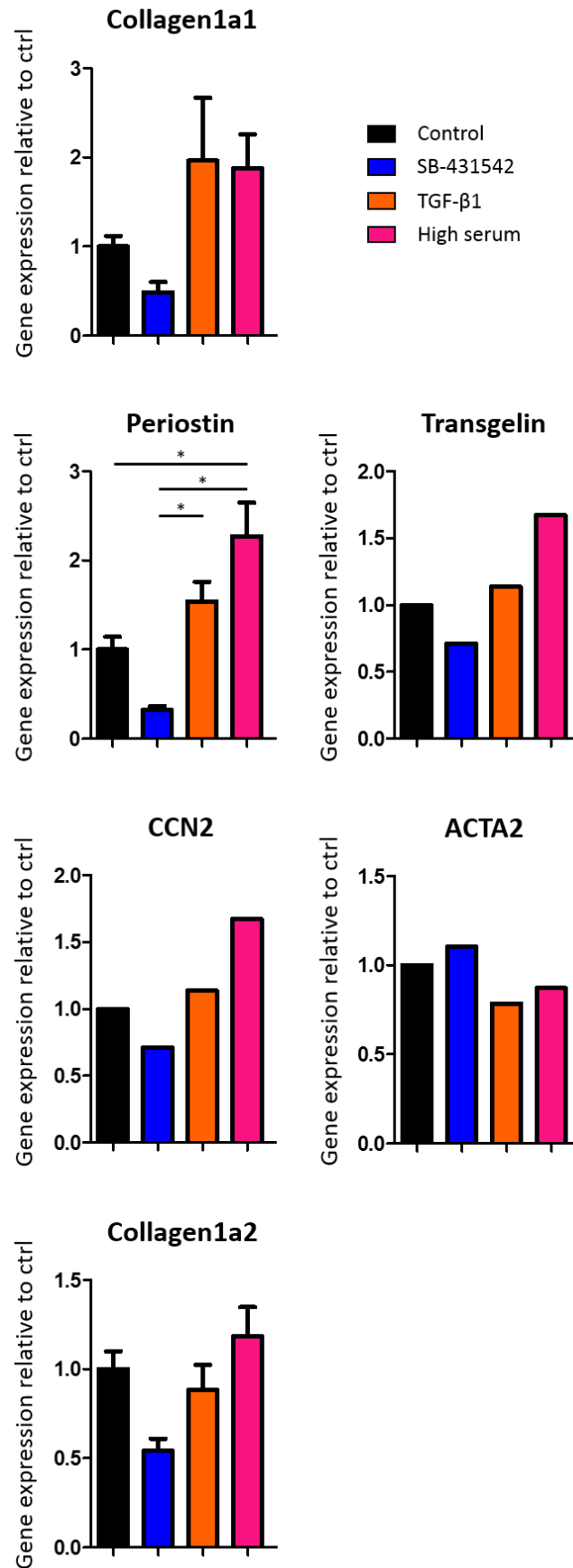


Figure 76: The mRNA abundance relative to GUSB and the control CF-EHTs of multiple fibroblast activation markers in A18945 CF-EHTs. Collagen1a1, periostin, transgelin, CCN2, ACTA2 and collagen1a2 are presented. The CF-EHTs were assigned to either

a control group, an inhibited group, or 1 of 2 activated groups, and treated as previously described. The CF-EHTs were harvested on day 22. When possible, data are presented as mean  $\pm$  SEM. \* $p < 0.05$  by one-way ANOVA plus Bonferroni's post-test for multiple comparisons,  $n = 2-4$  per group.

#### 10.1.9.2 UKEi001-A/ERC001 CF-EHTs

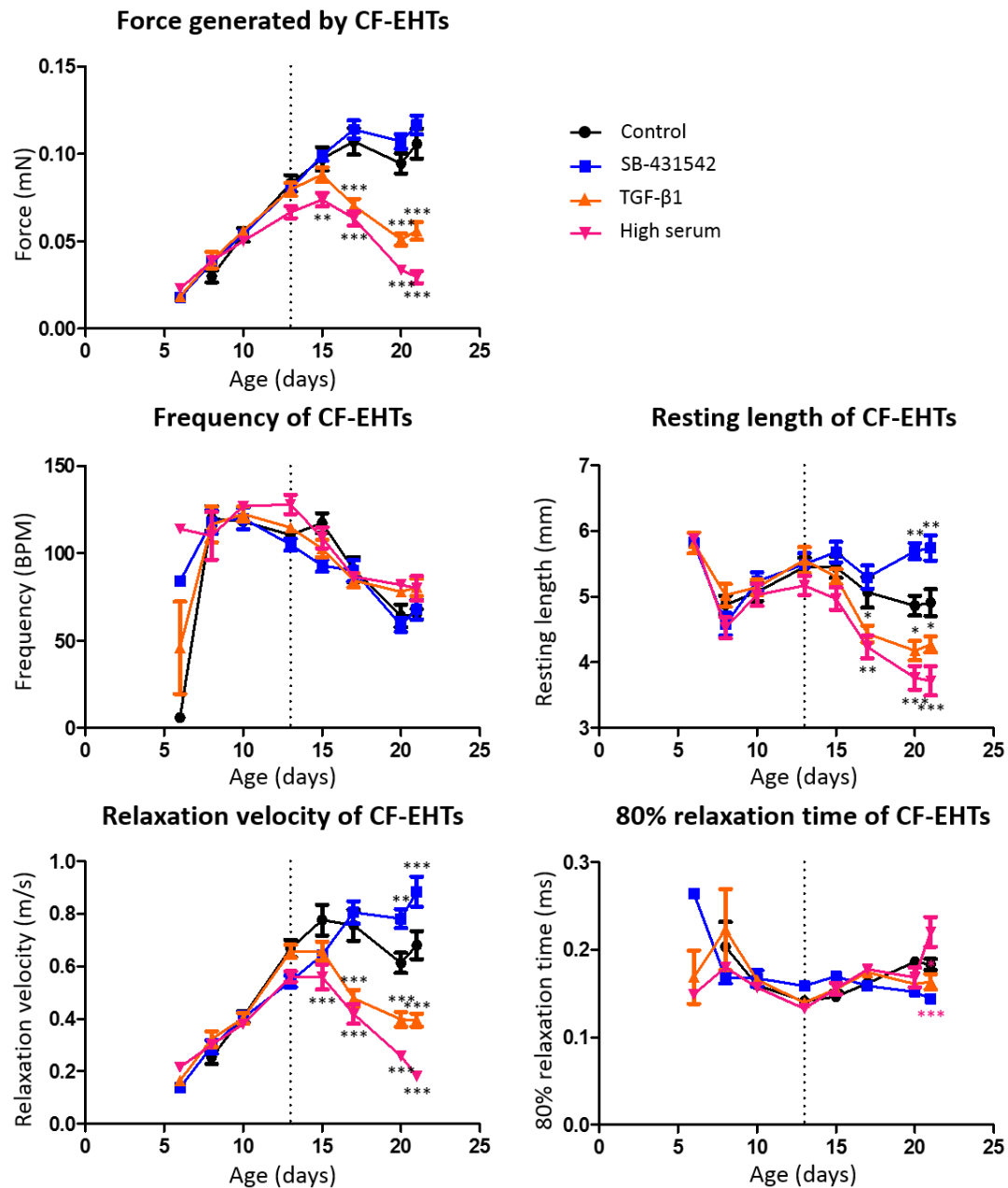


Figure 77: Contractility analyses of ERC001 CF-EHTs, assigned to either a control group, an inhibited group, or 1 of 2 activated groups, and treated as previously described. The CF-EHTs were harvested on day 21. The development of the generated force, beating frequency, resting length, relaxation velocity and 80% relaxation time of the CF-EHTs are presented over time. Data are presented as mean  $\pm$  SEM, \* $p < 0.05$ , \*\* $p < 0.005$ , \*\*\* $p < 0.001$  by two-way ANOVA plus Bonferroni's post-test for multiple comparisons, only biologically meaningful comparisons are shown,  $n = 6-7$  per group.



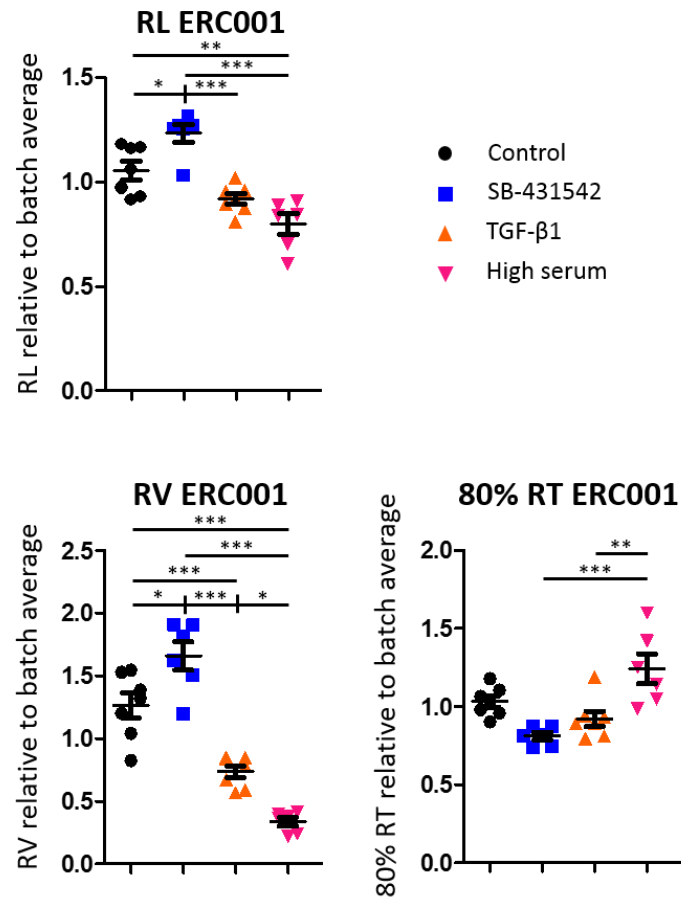


Figure 78: Contractility analyses of ERC001 CF-EHTs, assigned to either a control group, an inhibited group, or 1 of 2 activated groups, and treated as previously described. The resting length, relaxation velocity and 80% relaxation time of the spontaneous contractions of the CF-EHTs on the last day of culture, day 21, relative to the batch average are presented. Data are presented as mean  $\pm$  SEM. \* $p < 0.05$ , \*\* $p < 0.005$ , \*\*\* $p < 0.001$  by one-way ANOVA plus Bonferroni's post-test for multiple comparisons,  $n = 6-7$  per group.

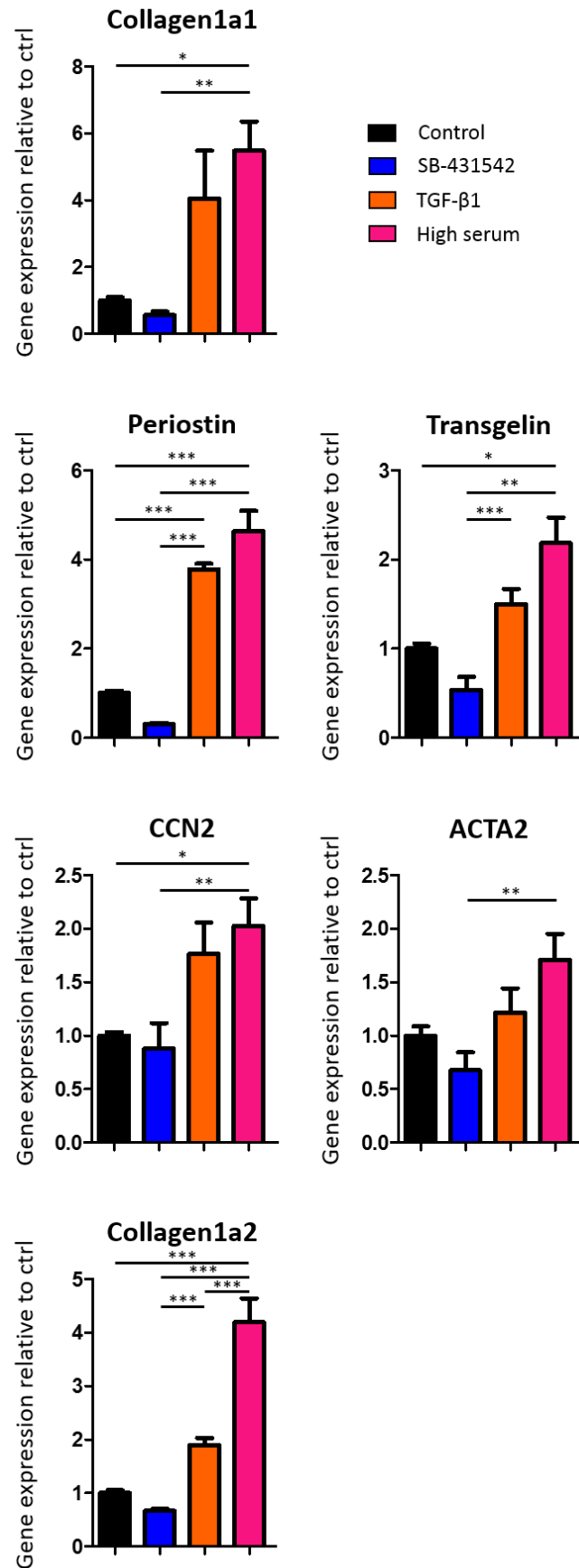


Figure 79: The mRNA abundance relative to GUSB and control CF-EHTs of multiple fibroblast activation markers in ERC001 CF-EHTs: collagen1a1, periostin, transgelin, CCN2, ACTA2 and collagen1a2. The CF-EHTs were assigned to either a control group,

an inhibited group, or 1 of 2 activated groups, and treated as previously described. The CF-EHTs were harvested on day 21. Data are presented as mean  $\pm$  SEM. \* $p$ <0.05, \*\* $p$ <0.005, \*\*\* $p$ <0.001 by one-way ANOVA plus Bonferroni's post-test for multiple comparisons,  $n$ =4 per group.

### 10.1.9.3 UKEi003-C/ERC018 CF-EHTs

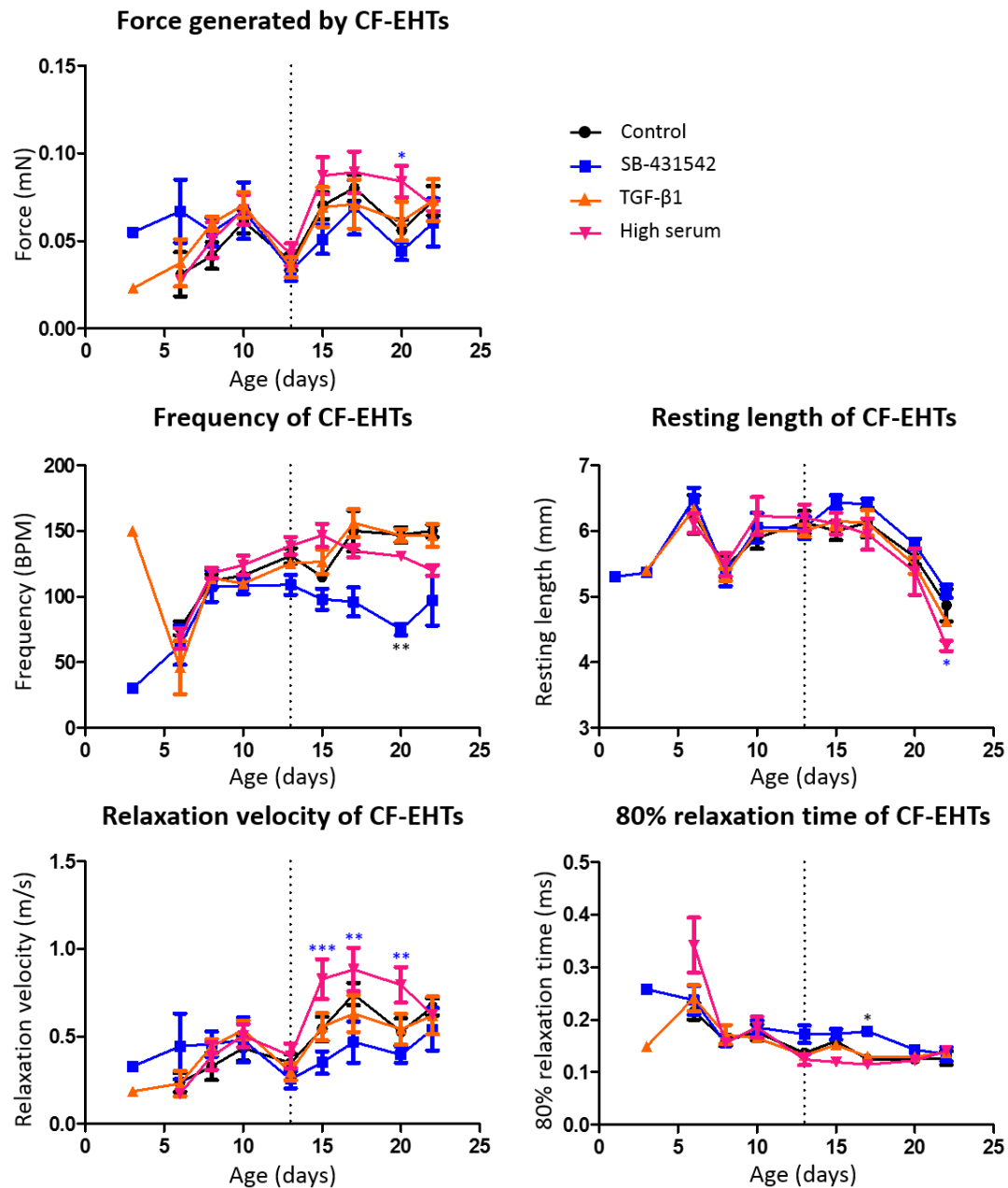


Figure 80: Contractility analyses of ERC018 CF-EHTs, assigned to either a control group, an inhibited group, or 1 of 2 activated groups, and treated as previously described. The CF-EHTs were harvested on day 22. The development of the generated force, beating frequency, resting length, relaxation velocity and 80% relaxation time of the CF-EHTs are presented over time. Data are presented as mean  $\pm$  SEM, \* $p$ <0.05, \*\* $p$ <0.005, \*\*\* $p$ <0.001 by two-way ANOVA plus Bonferroni's post-test for multiple comparisons, only biologically meaningful comparisons are shown,  $n$ =4-6 per group.

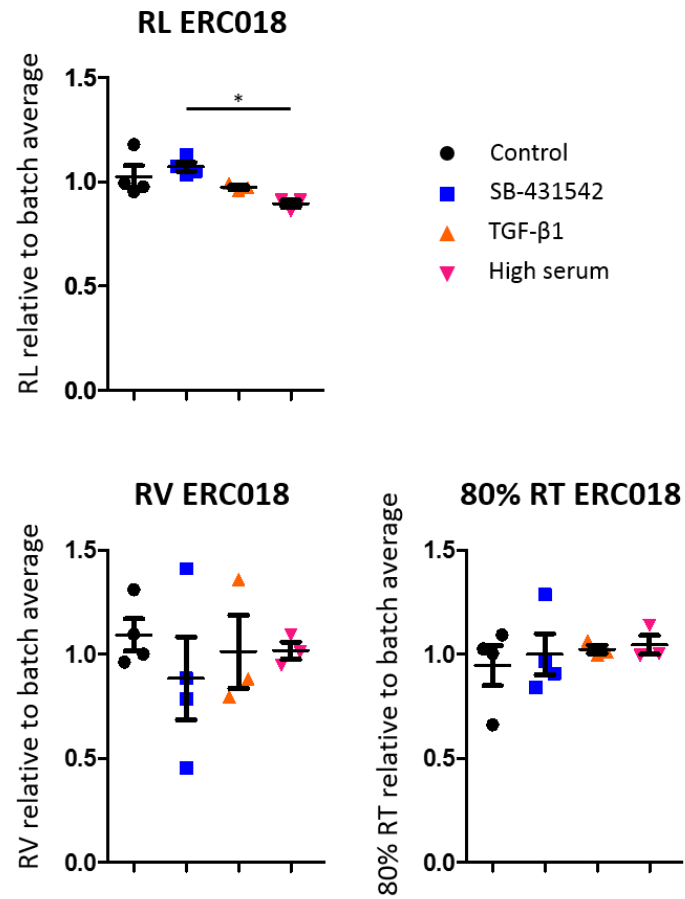


Figure 81: Contractility analyses of ERC018 CF-EHTs, assigned to either a control group, an inhibited group, or 1 of 2 activated groups, and treated as previously described. The resting length, relaxation velocity and 80% relaxation time of the spontaneous contractions of the CF-EHTs on the last day of culture, day 22, relative to the batch average are presented. Data are presented as mean  $\pm$  SEM. \* $p < 0.05$  by one-way ANOVA plus Bonferroni's post-test for multiple comparisons,  $n = 3-4$  per group.

## 10.1.9.4 Combined analysis

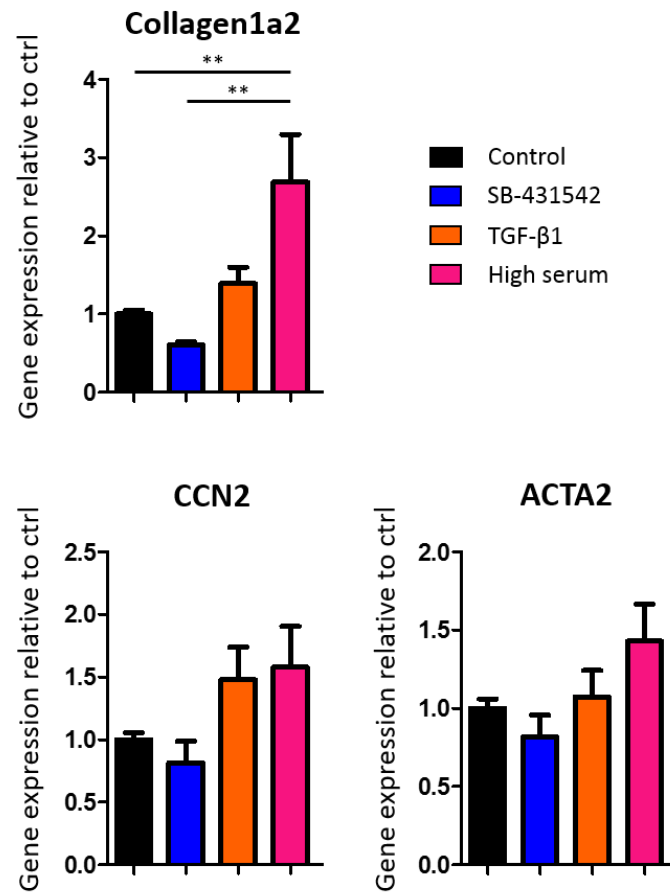


Figure 82: Combined mRNA abundance analyses relative to GUSB and control CF-EHTs of multiple fibroblast activation markers in A18945 and ERC001 CF-EHTs: collagen1a2, CCN2 and ACTA2. The CF-EHTs were assigned to either a control group, an inhibited group, or 1 of 2 activated groups, and treated as previously described. The CF-EHTs were harvested on day 21 or day 22. Data are presented as mean  $\pm$  SEM. \*\* $p < 0.005$  by one-way ANOVA plus Bonferroni's post-test for multiple comparisons,  $n = 6-8$  per group.

## 10.1.10 Quality control

## 10.1.10.1 Karyogram

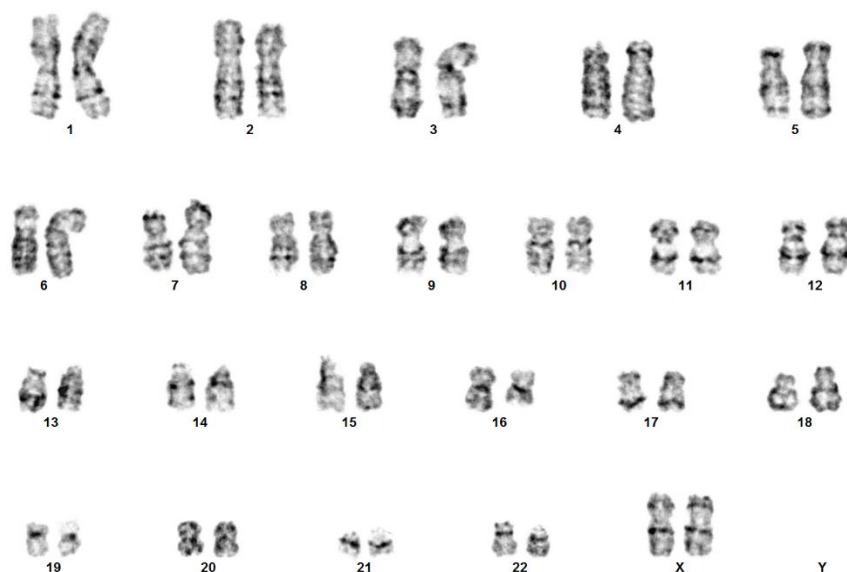


Figure 83: Cytogenetic analysis by Giemsa-banding produced a visible karyogram of A18945 hiPSCs with the enh35232 knocked out, which showed a normal, female karyotype (46, XX), with no visible aberrations.



Figure 84: Cytogenetic analysis by Giemsa-banding produced a visible karyogram of A18945 hiPSCs with the RUNX1 gene knocked out, which showed a normal, female karyotype (46, XX), with no visible aberrations.

## 10.1.10.2 Cardiac fibroblast differentiation

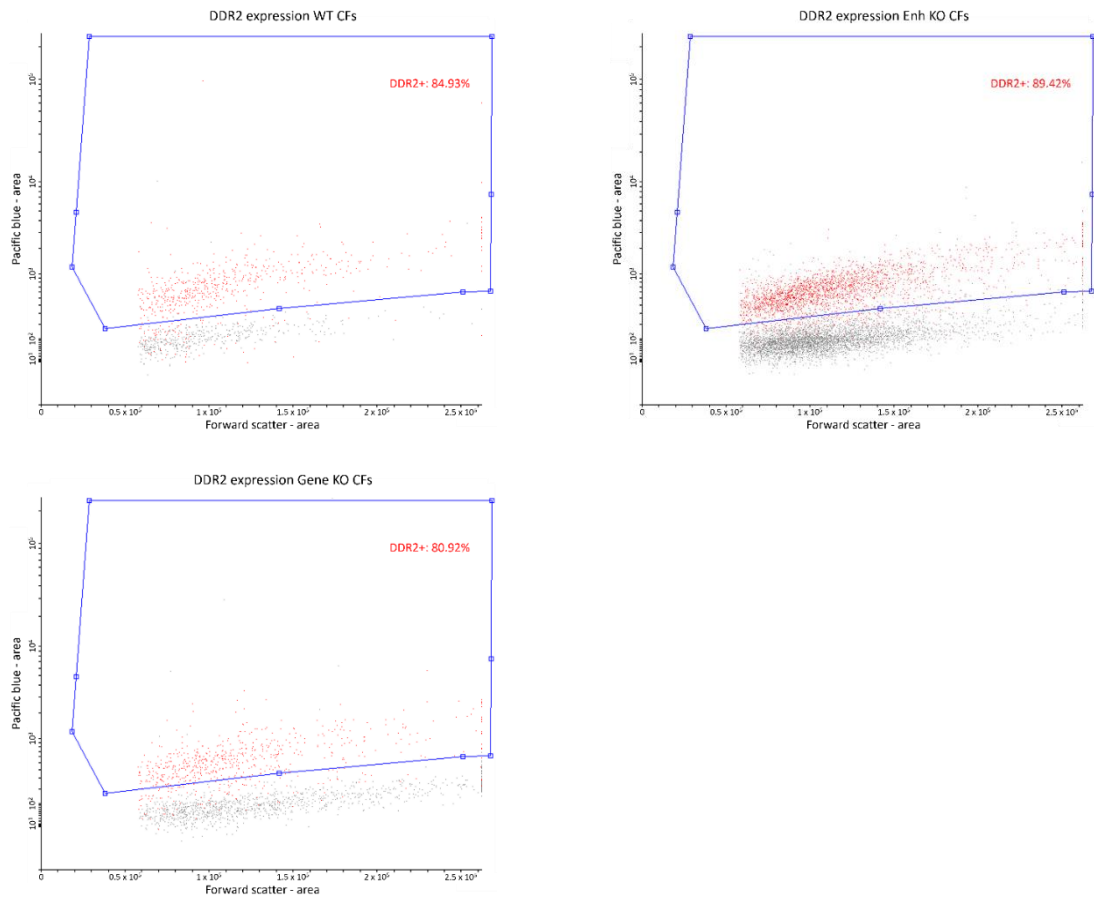


Figure 85: Top left, DDR2 expression in hiPSC-derived A18945 WT CFs (red), top right, DDR2 expression in hiPSC-derived A18945 Enh KO CFs (red), bottom left, DDR2 expression in hiPSC-derived A18945 Gene KO CFs (red). In all 3 images, unstained isotype control hiPSC-derived CFs (grey) were used to determine the gating.

## 10.1.10.3 KO CM

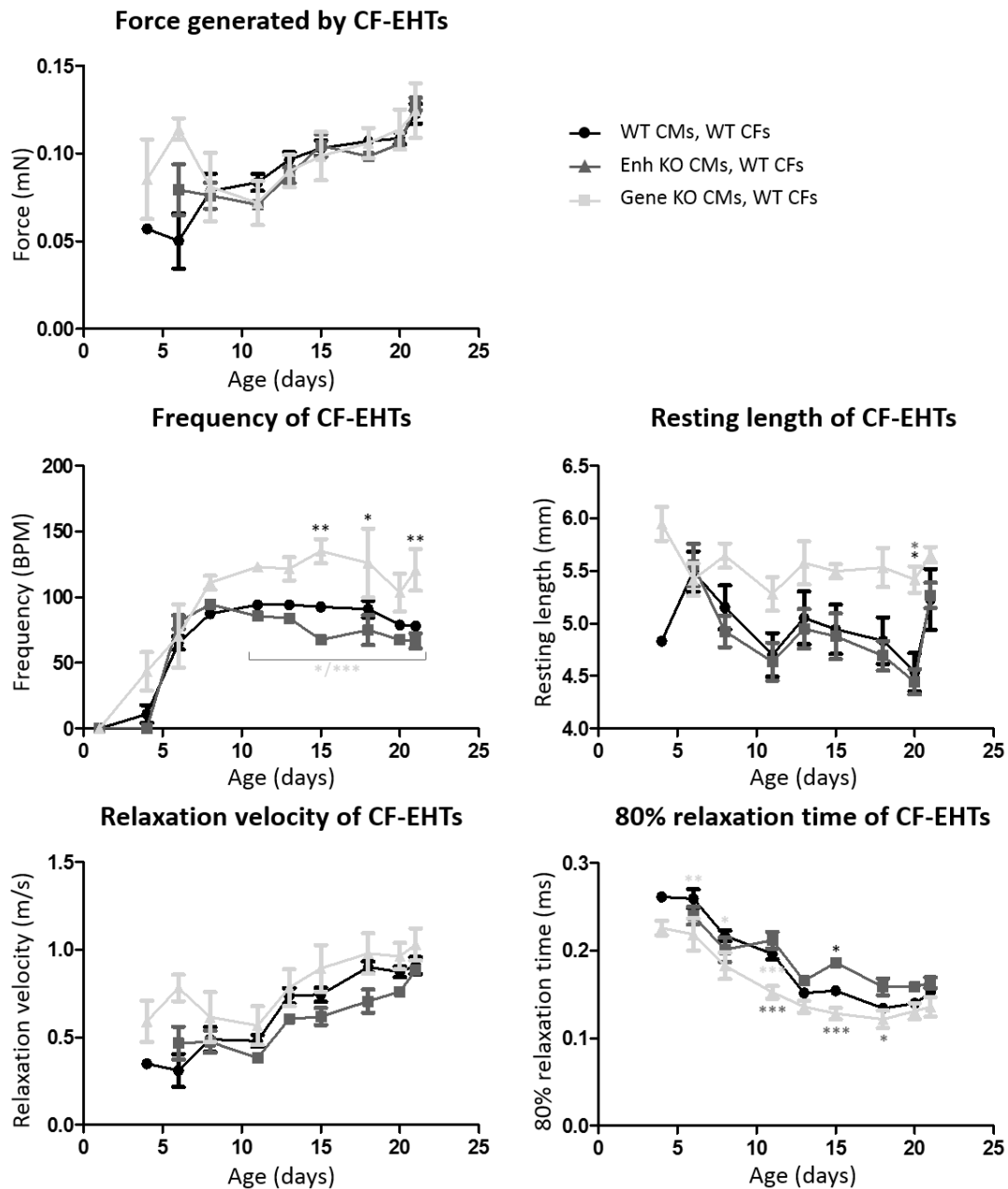


Figure 86: Contractility analysis of CF-EHTs composed of 90% either WT, Enh KO or Gene KO cardiomyocytes and 10% WT cardiac fibroblasts. All CF-EHTs were cultured in 10% serum containing medium until day 3, after which they were cultured in 0.5% serum containing medium. All CF-EHTs were cultured with 5  $\mu$ M SB-431542 from day 10 until day 13, after which they were cultured in 0.5% serum containing medium without SB-431542 until day 21, when they were harvested. The development of the generated force, beating frequency, resting length, relaxation velocity and 80% relaxation time of the CF-EHTs are presented over time. Data are presented as mean  $\pm$  SEM, \* $p$ <0.05, \*\* $p$ <0.005, \*\*\* $p$ <0.001 by two-way ANOVA plus Bonferroni's post-test for multiple comparisons, only biologically meaningful comparisons are shown,  $n$ =4-7 per group.



10.1.11 Effects of an *enh35232* or *RUNX1* knockout in 2D culture

## 10.1.11.1 The mRNA abundance

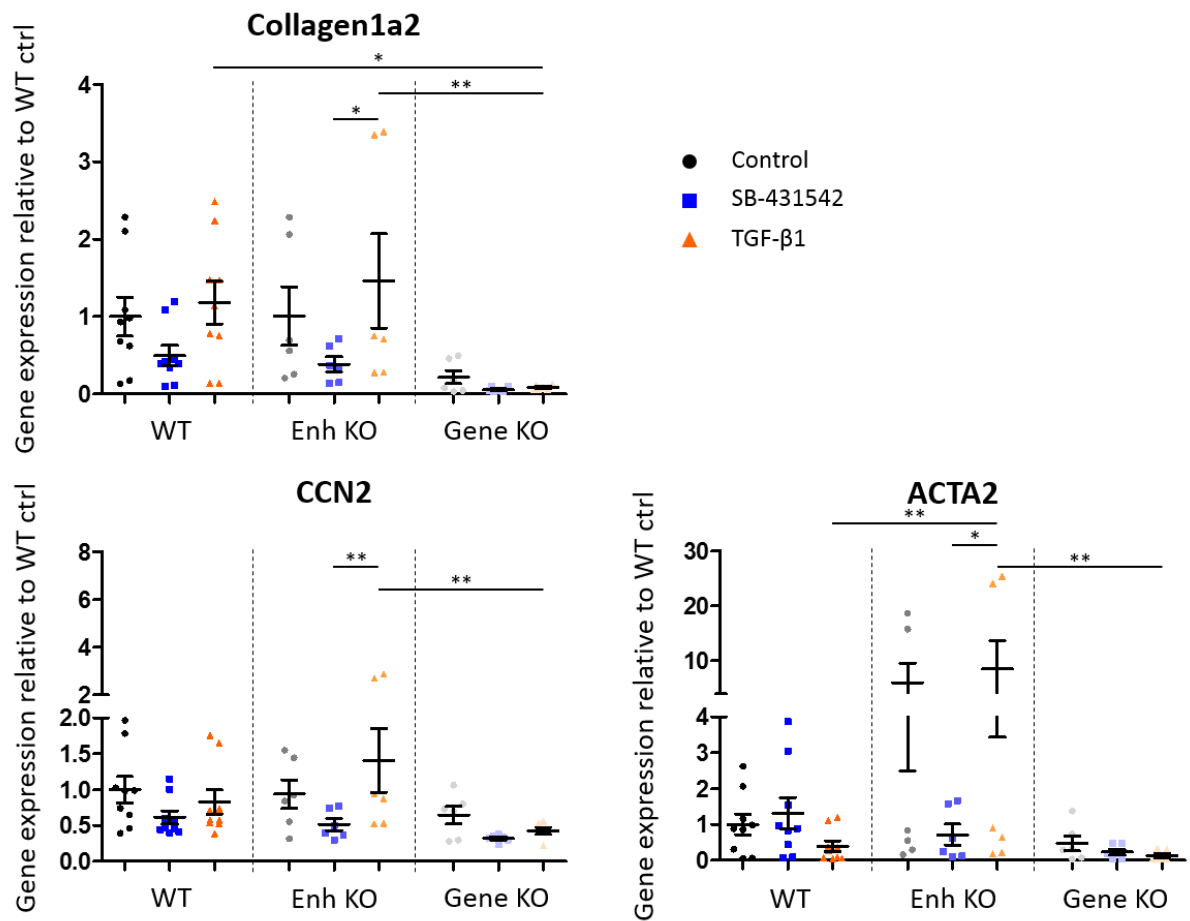


Figure 87: The mRNA abundance relative to GUSB and WT control of the fibrosis markers collagen1a2, CCN2 and ACTA2 in A18945 WT CFs, Enh KO CFs and Gene KO CFs. The CFs were assigned to either a control group, an inhibited group, treated with 5  $\mu$ M SB-431542, or an activated group treated with 10 ng/ml TGF- $\beta$ 1. All CFs were cultured in 10% serum containing medium until day 3, after which they were cultured in 0.5% serum containing medium + 5  $\mu$ M SB-431542 until day 7, when they were assigned to their respective groups. The CFs were treated according to their group until day 10, when they were harvested. Data are presented as mean  $\pm$  SEM. \* $p$ <0.05, \*\* $p$ <0.005, \*\*\* $p$ <0.001 by two-way ANOVA plus Bonferroni's post-test for multiple comparisons,  $n$ =6-9 per group.

## 10.1.11.2 Flowcytometry

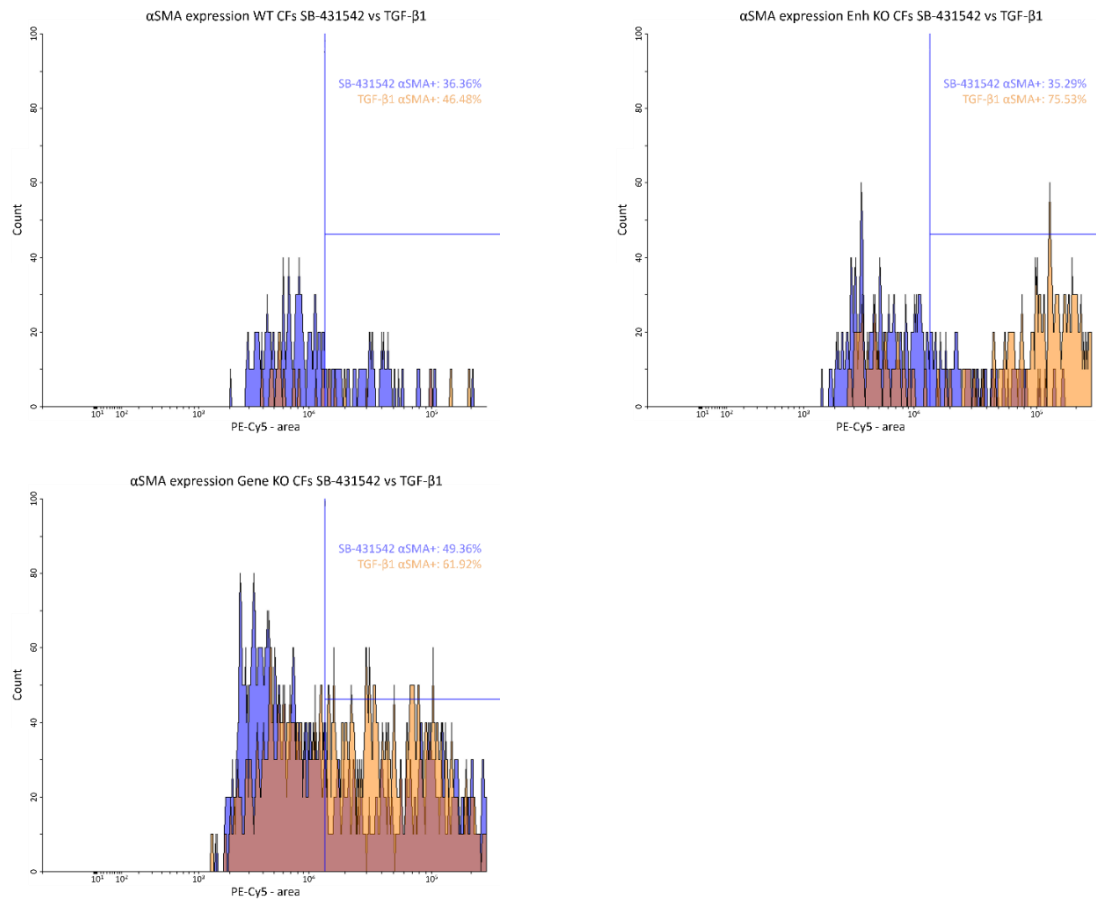


Figure 88: Top left, αSMA expression in DDR2<sup>+</sup> inhibited, SB-431542 treated A18945 WT CFs (blue) compared to αSMA expression in DDR2<sup>+</sup> activated, TGF-β1 treated A18945 WT CFs (orange). Top right, αSMA expression in DDR2<sup>+</sup> inhibited, SB-431542 treated A18945 Enh KO CFs (blue) compared to αSMA expression in DDR2<sup>+</sup> activated, TGF-β1 treated A18945 Enh KO CFs (orange). Bottom left, αSMA expression in DDR2<sup>+</sup> inhibited, SB-431542 treated A18945 Gene KO CFs (blue) compared to αSMA expression in DDR2<sup>+</sup> activated, TGF-β1 treated A18945 Gene KO CFs (orange). In all 3 figures, the area right of the blue line was defined as αSMA<sup>+</sup>, as determined by unstained isotype controls. All CFs were cultured in 10% serum containing medium until day 3, after which they were cultured in 0.5% serum containing medium + 5 μM SB-431542 until day 6, when they were assigned to their respective groups (SB-431542 treated or TGF-β1 treated). The CFs were treated according to their group until day 10, when they were harvested.

10.1.12 Effects of an *enh35232* or *RUNX1* knockout in 3D culture

## 10.1.12.1 Contractility of A18945 CF-EHTs

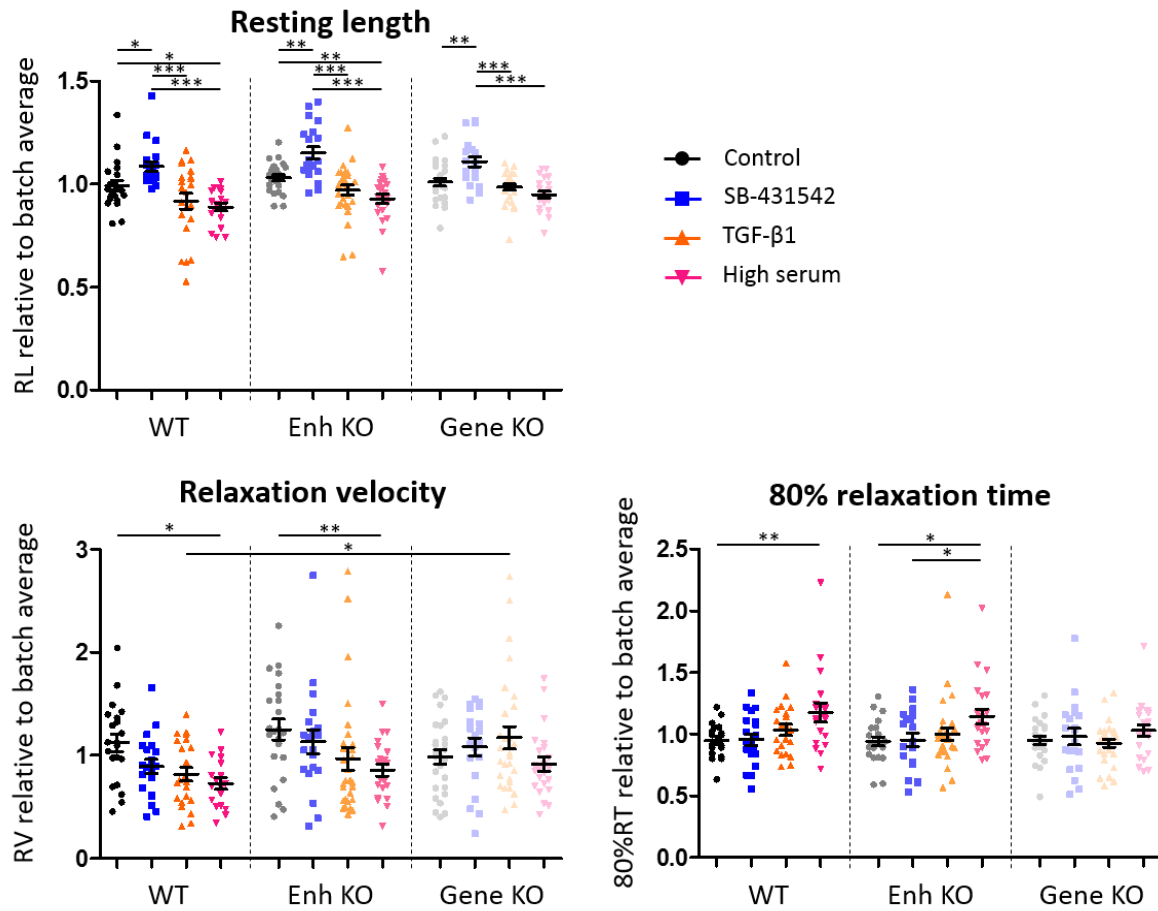


Figure 89: Contractility analysis of A18945 WT, Enh KO and Gene KO CF-EHTs, assigned to either a control group, an inhibited group, or 1 of 2 activated groups, and treated as previously described. The resting length, relaxation velocity and 80% relaxation time of the spontaneous contractions of the CF-EHTs on the last day of culture, day 21, relative to the batch average, are presented. Data are presented as mean  $\pm$  SEM, \* $p$ <0.05, \*\* $p$ <0.005, \*\*\* $p$ <0.001 by two-way ANOVA plus Bonferroni's post-test for multiple comparisons, only biologically meaningful comparisons are shown,  $n$ =19-29 per group, from 4 different batches.

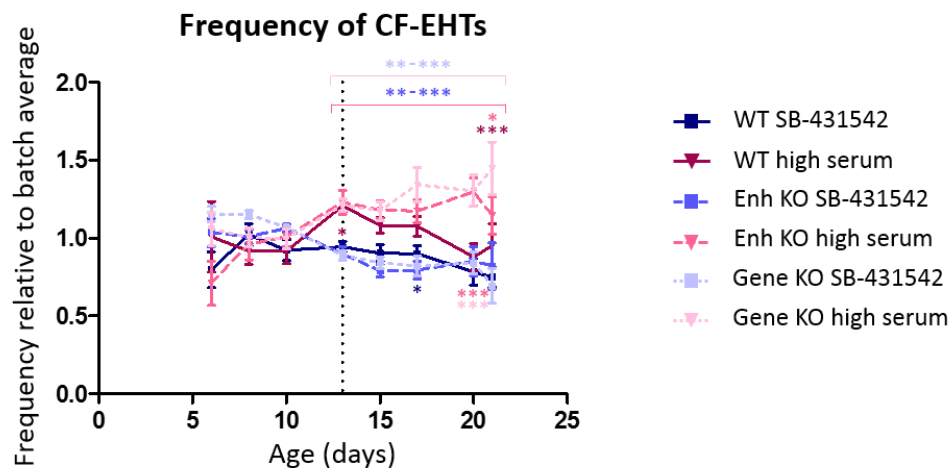


Figure 90: Contractility analysis of A18945 WT, Enh KO and Gene KO CF-EHTs, assigned to either an inhibited group, treated with 5  $\mu$ M SB-431542, or an activated group, exposed to 10% serum containing medium, and treated as previously described.

The CF-EHTs were harvested on day 21. The development of the beating frequency of the CF-EHTs is presented over time, relative to batch average. Data are presented as mean  $\pm$  SEM, \* $p$ <0.05, \*\* $p$ <0.005, \*\*\* $p$ <0.001 by two-way ANOVA plus Bonferroni's post-test for multiple comparisons, only biologically meaningful comparisons are shown,  $n$ =20-25 per group, from 4 different batches.

#### 10.1.12.2 The mRNA abundance of A18945 CF-EHTs

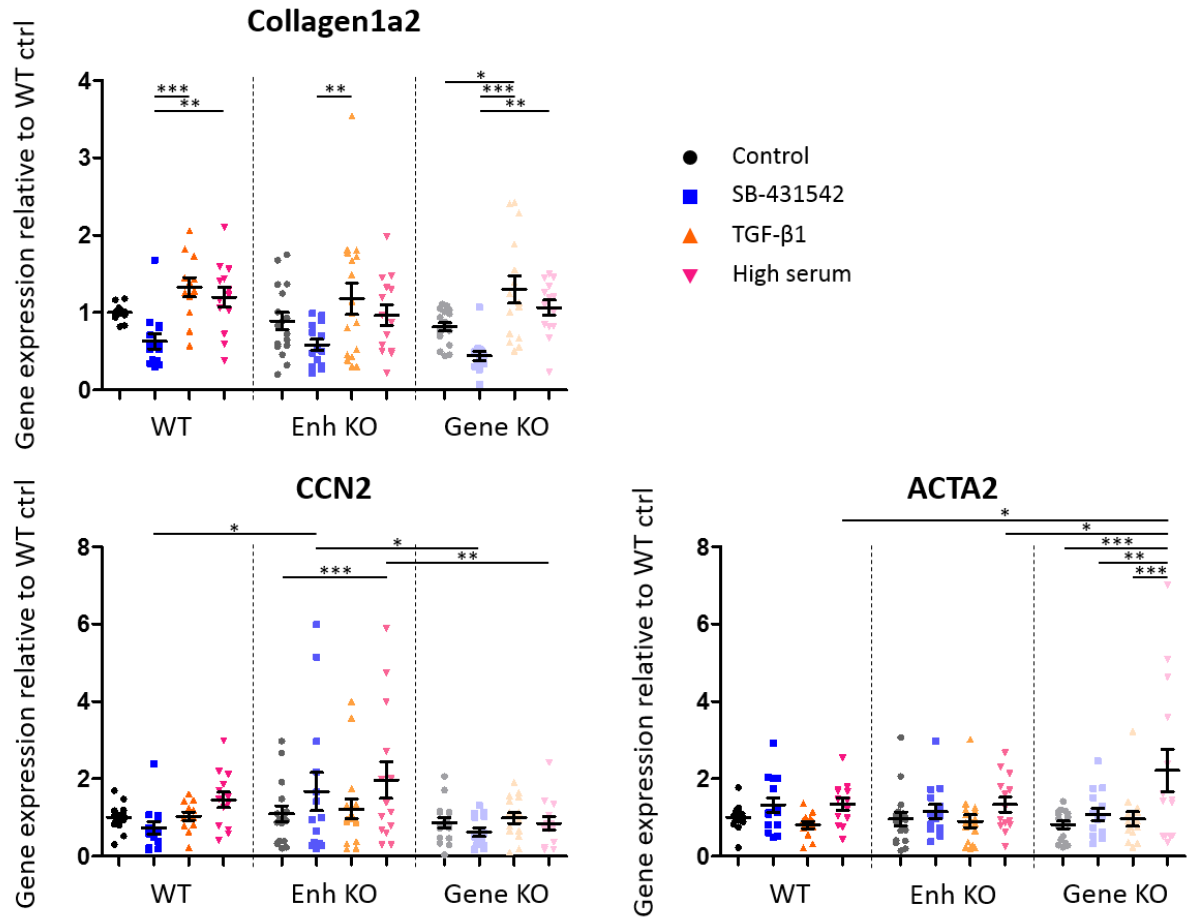


Figure 91: The mRNA abundance relative to GUSB and WT control of the fibrosis markers collagen1a2, CCN2 and ACTA2 in A18945 WT, Enh KO and Gene KO CF-EHTs. The CF-EHTs were assigned to either a control group, an inhibited group, or 1 of 2 activated groups, and treated as previously described. The CF-EHTs were harvested on day 21. Data are presented as mean  $\pm$  SEM, \* $p$ <0.05, \*\* $p$ <0.005, \*\*\* $p$ <0.001 by two-way ANOVA plus Bonferroni's post-test for multiple comparisons,  $n$ =12-17 per group, from 4 different batches.

## 10.1.13 CF-EHTs composed of 75% cardiomyocytes and 25% cardiac fibroblasts

## 10.1.13.1 Contractility

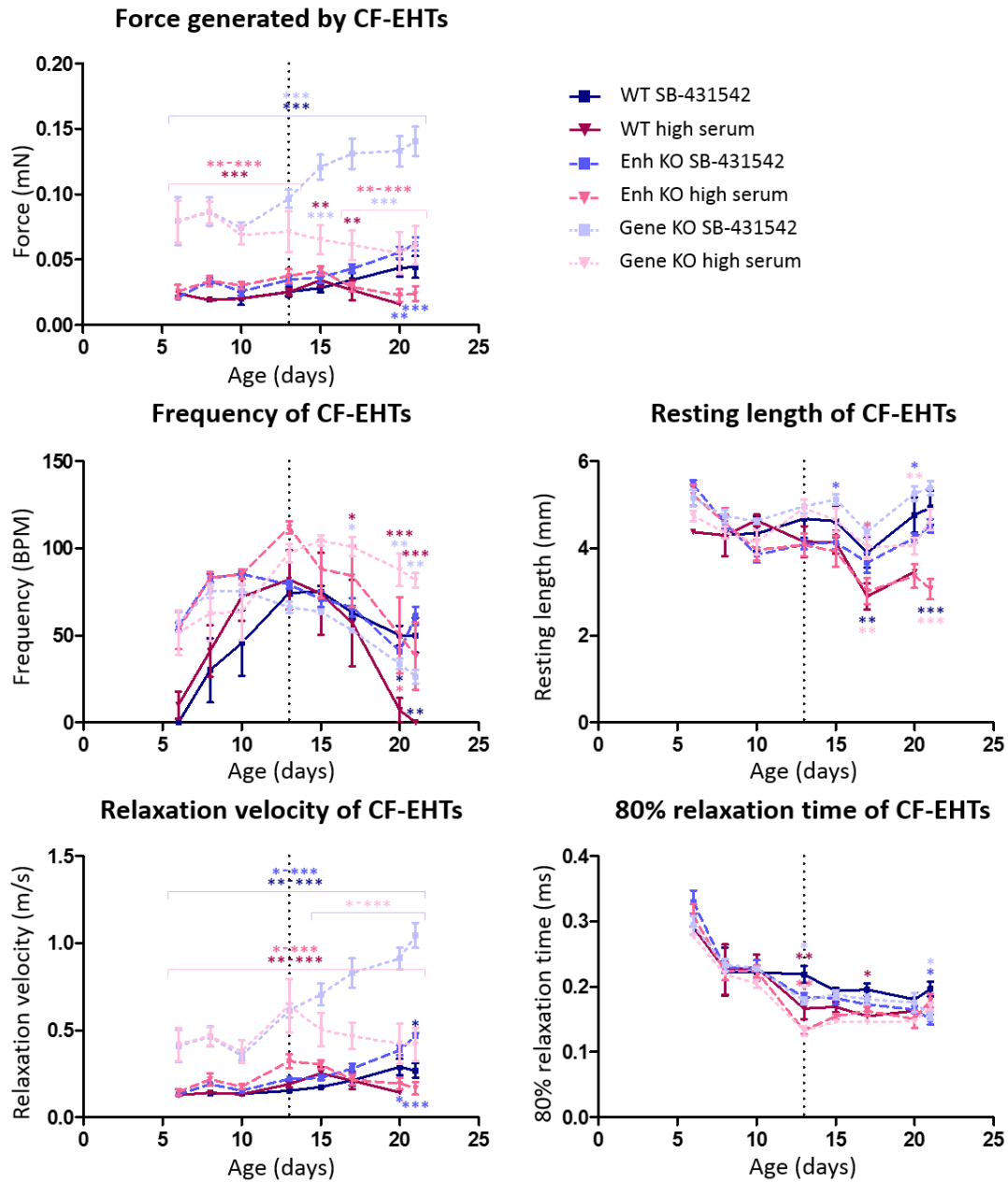


Figure 92: Contractility analysis of CF-EHTs composed of 75% A18945 WT cardiomyocytes and 25% A18945 WT, Enh KO or Gene KO cardiac fibroblasts, assigned to either an inhibited group, treated with 5  $\mu$ M SB-431542, or an activated group, exposed to 10% serum containing medium, and treated as previously described. The CF-EHTs were harvested on day 21. The development of the generated force, beating frequency, resting length, relaxation velocity and 80% relaxation time of the CF-EHTs are presented over time. Data are presented as mean  $\pm$  SEM, \* $p$ <0.05, \*\* $p$ <0.005, \*\*\* $p$ <0.001 by two-way ANOVA plus Bonferroni's post-test for multiple comparisons, only biologically meaningful comparisons are shown,  $n$ =5-6.

## 10.1.13.2 The mRNA abundance

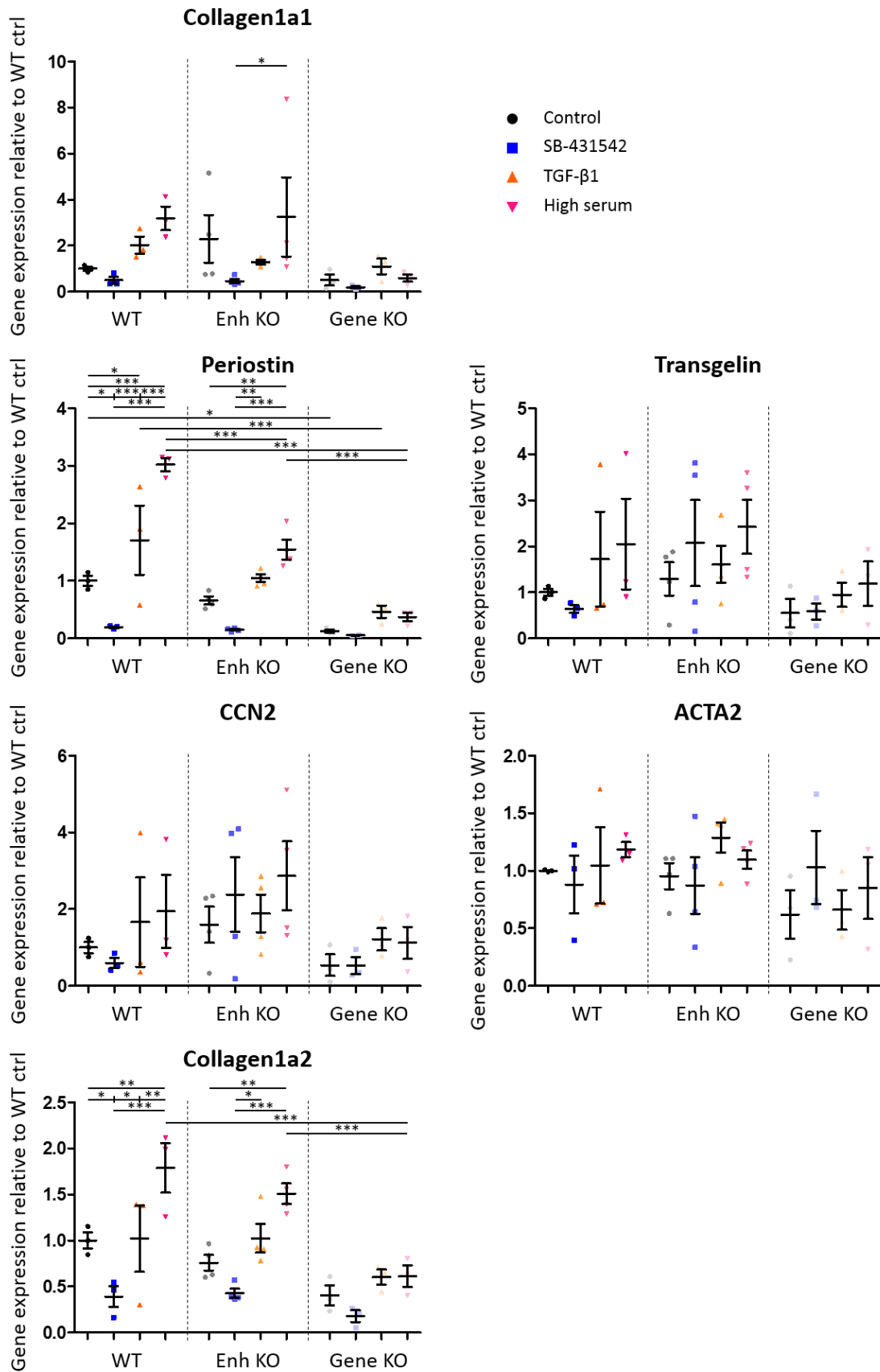


Figure 93: The mRNA abundance relative to GUSB and WT control of the fibrosis markers collagen1a1, periostin, transgelin, CCN2, ACTA2 and collagen1a2 in CF-EHTs composed of 75% A18945 WT cardiomyocytes and 25% A18945 WT, Enh KO or Gene

KO cardiac fibroblasts. The CF-EHTs were assigned to either a control group, an inhibited group, or 1 of 2 activated groups, and treated as previously described. The CF-EHTs were harvested on day 21. Data are presented as mean  $\pm$  SEM, \* $p$ <0.05, \*\* $p$ <0.005, \*\*\* $p$ <0.001 by two-way ANOVA plus Bonferroni's post-test for multiple comparisons, only biologically meaningful comparisons are shown,  $n=3-4$ .

#### 10.1.14 Effects of an *enh35232* or *RUNX1* knockout in ERC001

##### 10.1.14.1 Quality control

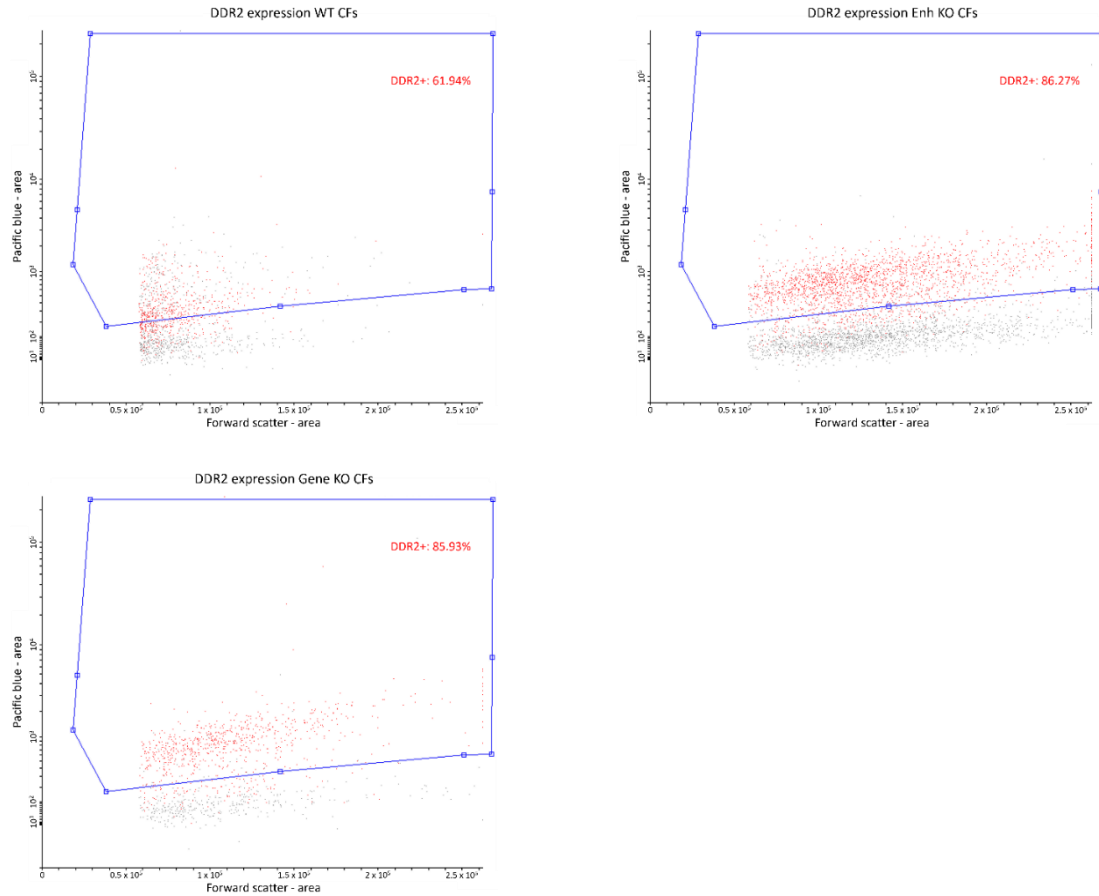


Figure 94: Top left, DDR2 expression in ERC001 hiPSC-derived WT CFs (red), top right, DDR2 expression in ERC001 hiPSC-derived Enh KO CFs (red), bottom left, DDR2 expression in ERC001 hiPSC-derived Gene KO CFs (red). In all 3 images, unstained isotype control hiPSC-derived CFs (grey) were used to determine the gating.

## 10.1.14.2 2D culture; flowcytometry

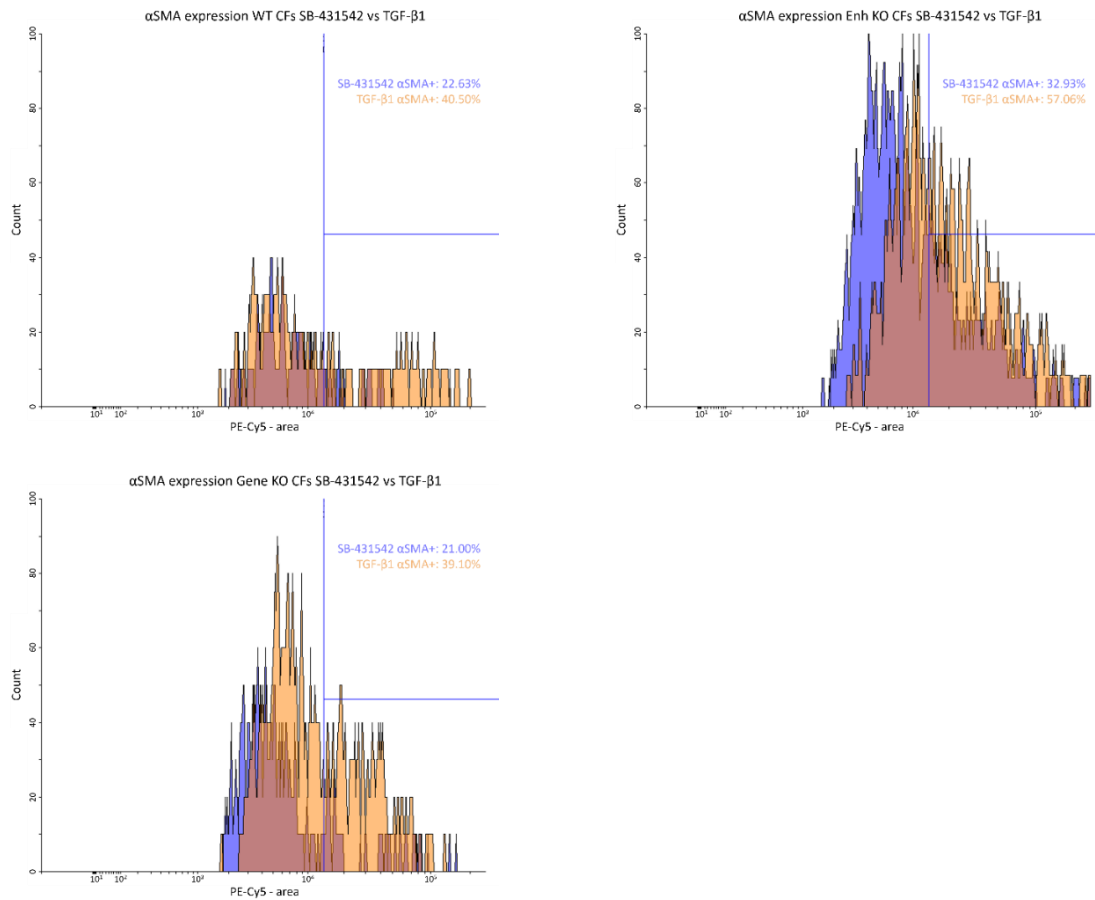


Figure 95: Top left, αSMA expression in DDR2<sup>+</sup> inhibited, SB-431542 treated ERC001 WT CFs (blue) compared to αSMA expression in DDR2<sup>+</sup> activated, TGF-β1 treated ERC001 WT CFs (orange). Top right, αSMA expression in DDR2<sup>+</sup> inhibited, SB-431542 treated ERC001 Enh KO CFs (blue) compared to αSMA expression in DDR2<sup>+</sup> activated, TGF-β1 treated ERC001 Enh KO CFs (orange). Bottom left, αSMA expression in DDR2<sup>+</sup> inhibited, SB-431542 treated ERC001 Gene KO CFs (blue) compared to αSMA expression in DDR2<sup>+</sup> activated, TGF-β1 treated ERC001 Gene KO CFs (orange). In all 3 figures, the area right of the blue line was defined as αSMA<sup>+</sup>, as determined by unstained isotype controls. All CFs were cultured in 10% serum containing medium until day 3, after which they were cultured in 0.5% serum containing medium + 5 μM SB-431542 until day 6, when they were assigned to their respective groups (SB-431542 treated or TGF-β1 treated). The CFs were treated according to their group until day 10, when they were harvested.



## 10.1.14.3 Contractility of ERC001 CF-EHTs

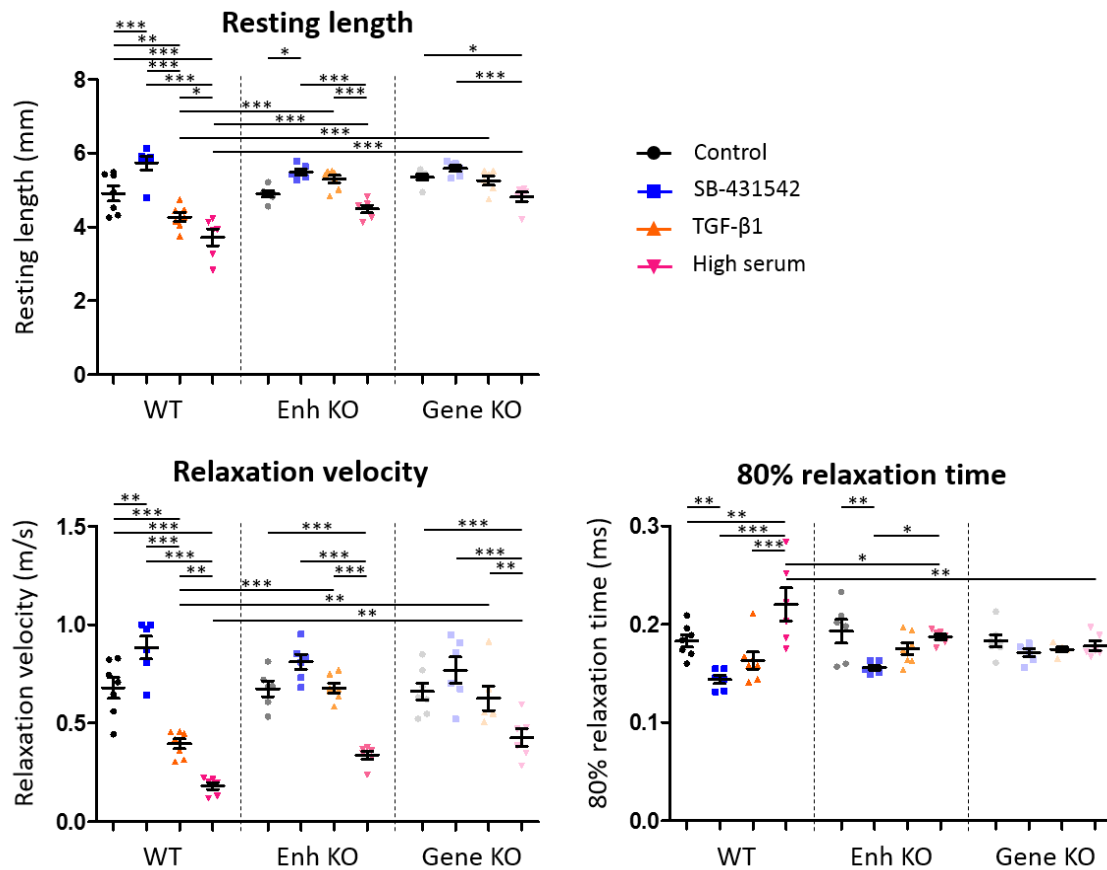


Figure 96: Contractility analysis of ERC001 WT, Enh KO and Gene KO CF-EHTs, assigned to either a control group, an inhibited group, or 1 of 2 activated groups, and treated as previously described. The resting length, relaxation velocity and 80% relaxation time of the spontaneous contractions of the CF-EHTs on the last day of culture, day 21, are presented. Data are presented as mean  $\pm$  SEM, \* $p$ <0.05, \*\* $p$ <0.005, \*\*\* $p$ <0.001 by two-way ANOVA plus Bonferroni's post-test for multiple comparisons, only biologically meaningful comparisons are shown,  $n$ =6-7

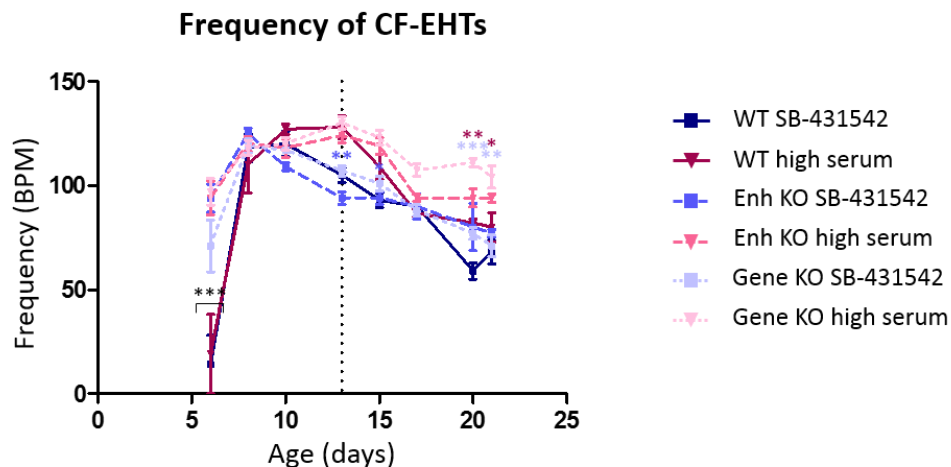


Figure 97: Contractility analysis of ERC001 WT, Enh KO and Gene KO CF-EHTs, assigned to either an inhibited group, treated with 5  $\mu$ M SB-431542, or an activated group, exposed to 10% serum containing medium, and treated as previously described. The CF-EHTs were harvested on day 21. The development of the beating frequency of the CF-EHTs is presented over time. Data are presented as mean  $\pm$  SEM, \* $p$ <0.05, \*\* $p$ <0.005, \*\*\* $p$ <0.001 by two-way ANOVA plus Bonferroni's post-test for multiple comparisons, only biologically meaningful comparisons are shown,  $n$ =6 per group.

## 10.1.14.4 The mRNA abundance of ERC001 CF-EHTs

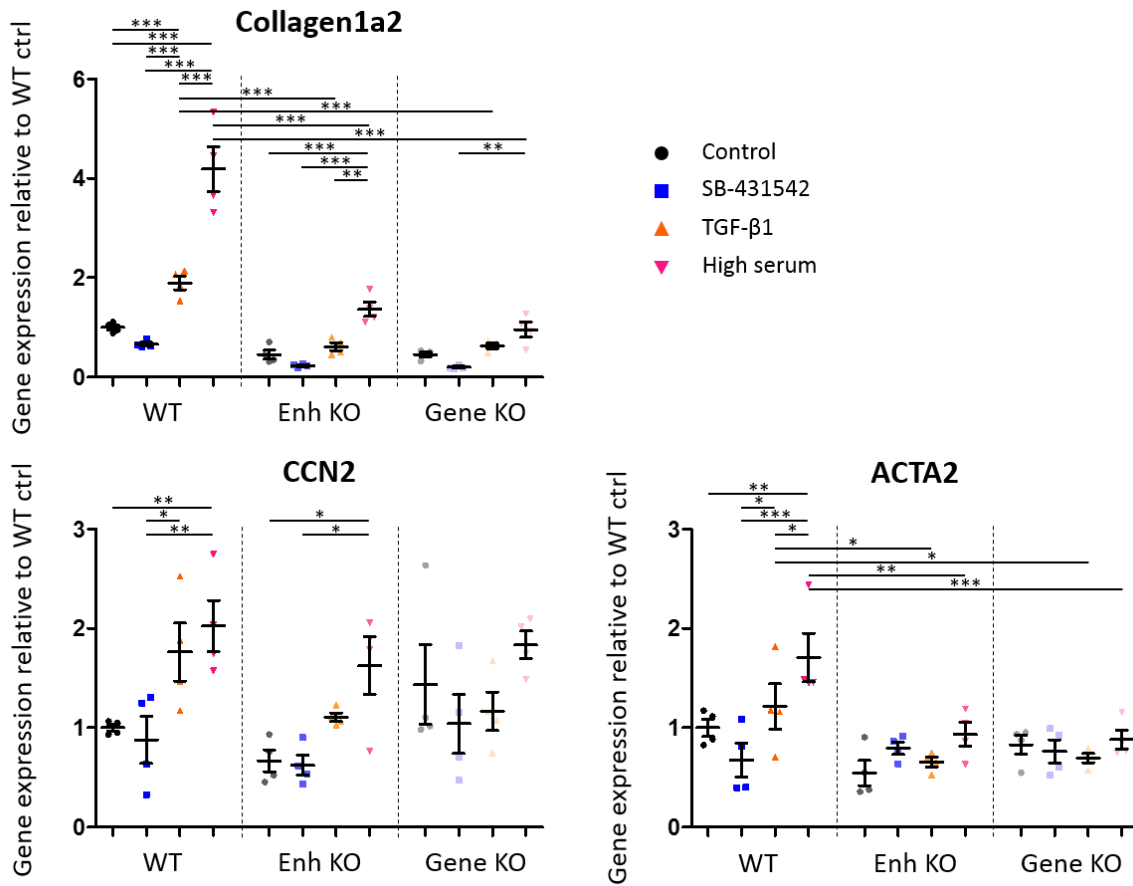


Figure 98: The mRNA abundance relative to GUSB and WT control of the fibrosis markers collagen1a2, CCN2 and ACTA2 in ERC001 WT, Enh KO and Gene KO CF-EHTs. The CF-EHTs were assigned to either a control group, an inhibited group, or 1 of 2 activated groups, and treated as previously described. The CF-EHTs were harvested on day 21. Data are presented as mean  $\pm$  SEM, \* $p$ <0.05, \*\* $p$ <0.005, \*\*\* $p$ <0.001 by two-way ANOVA plus Bonferroni's post-test for multiple comparisons, only biologically meaningful comparisons are shown,  $n$ =4 per group.

10.1.15 *Enh35232* sequence data

ATGAATTTATGTCATACCAAGTTTCCAGAAGATTAAAAACATGATAAAATGACTTGGAAGATGCATGCTATTCTTTT  
 CGCACACATACCCCCTGTTTAGATTTGGTAGTCTTCTCTAAGGATGCTGCAGAGGGTAGCCTCTACATAGGCACCTT  
 CCACAACACTGGTATTTCTTTAAAAGCAAAAGTCTGTCCTTTAAAGCAATGTAGAGGGAGAAGGATAAAGAGGT  
 AGAAACTGGGGAGAATTATCCCAGCAAACAAATATGCCTTGACCAAATATATTACAATTATTAACCAGATGA  
 TTAGAAGTAATAGCTTATCACCTCCACCAATGGGAACATGGACCAACCAACCGGAGACTCATAAAAGGAAGGGG  
 AACATGAAAGCATAATCTCAATCCAGAGTCAAATCCAATATATACCTTTCTAGAGAAAAATGAACAGTCTTTCTTT  
 CTCAAATAAGACTACTCTTTTCATTTTCTAAATAACCTTCTCAATCTGAGCTATAGTATGTCTGGATGCTAATTGTCTA  
 GTAGTCTAGACAGTGATGATATTATGACCAAGTTATGCACAGATAATCACTGTGTCACTGTTTCCAAAGCTGCCTAC  
 ACGTATTGCTTCACTGGACACACTTGGCATGTGTGATTATTCTCTGATATTATTTTCACCATGTAAAGTAGAGAATG  
 CTTACTTAATCAAACCATCCAGTGAAGTGAAGTGTGAGTGTGTTTATAATTCAAATGCAATATGAGAGTCTTGAAGCTAAG  
 AAAAAAATTATGTTAATGTAGCCCATACTTTCTGTATTCTGGGGCAAGGAACCTGTGGCATTGCTCGCTTCAT  
 TCGCTAGGGATGCATCTTGCCAGGTCCCTCCAGTATTACCTCTGCAAATCATTCTACCCAGATGGGTTGGCTTAA  
 CCAAACCATTCTGATCAAGGAGTTCCAGGAATCTCTCCGGAGAGGTCTTTTCTGCAGCCTGGTCCAATGCACAG  
 GTTACAATAAAGTGGATGACTATATGGTTCTCTGGCTTTTCAAATGACACATTTGTTTTTAAAAACCACCATCTT  
 AACGAAGCATATGGGCAACGATGTCATGACACCCTTAACCCACCCGAAGGAGGGAGACTGAAATCAATGCAGA  
 AATGAAAAACAGTATGGTTTGGAAAGTA

In yellow, the minimum enhancer sequence is highlighted. In red, the different guide RNAs (gRNAs) are highlighted; guide 1 (ACCAACCGGAGACTCATAAA), guide 2 (TCACTGGACACACTTGGCA) and guide 3 (ACCCAGATGGGTTGGCTTAA). In the A18945 hiPSC line, guides 1 and 2 were targeted. In the ERC001 hiPSC line, guides 2 and 3 were targeted. Primers to assess for knockout and WT sequences are highlighted in blue and purple, respectively.

## 10.2 Devices, materials and substances

## 10.2.1 Devices

ABI PRISM 7900HT Sequence Detection System	Thermo Fisher Scientific
Accu-jetR pro	Brand
Analytic Scale Genius	Sartorius AG
BD FACSCanto II	BD Biosciences
C25 Incubator Shaker	New Brunswick Scientific
Cell culture incubator CB 220	Binder
Cell culture incubator HERAcell 240	Thermo Fisher Scientific
Cell culture incubators MCO-19M & MCO-20AIC	Sanyo
Centrifuge Avanti JXN-26	Beckmann
Centrifuges 5415 R & 5810 R	Eppendorf
Centrifuges Rotanta/RP & Universal 30 RF	Hettich
Chiaro Nanoindenter	Optics11 Life
ChemiDoc Touch Imaging System	Bio-Rad Laboratories
Combispin FVL-2400N & with vortex function	PeqLab
Electrophoretic Transfer Cell Mini Trans-Blot cell	Bio-Rad Laboratories
Gel electrophoresis cell Mini-PROTEAN 3 Cell	Bio-Rad Laboratories
Gel electrophoresis tank Sub-cell GT	Bio-Rad Laboratories
GeneAMP PCR System 9700 thermocycler	Thermo Fisher Scientific
Magnetic stirring and heating plate IKA	Janke & Kunkel GmbH & Co.KG
Combimag RET	
Magnetic stirring plate Variomag / Cimagrec	Thermo Scientific
Biosystem 4 Direct	
Magnetic stirring plate Variomag / Cimagrec	Thermo Scientific
Biosystem Direct	
Megafuse 1.0 R	Heraeus
Microscope Nikon Eclipse TS2	Nikon
Microscope T1-SM Nikon Eclipse TS100	Nikon
Nanodrop 1000 Spectrophotometer	Thermo Fisher Scientific
pH meter, digital	Mettler Toledo
Pipettes 10/100/1000 µl	Eppendorf
Pipetus	Hirschmann
Power supply PowerPac Basic	Bio-Rad Laboratories
Precision Advanced Scale	Ohaus
QuantStudio 5	Thermo Fisher Scientific
S88X dual output square pulse stimulator	Grass/Natus Neurology
Safety workbench HeraSafe KS9 & HS12 & HSP12	Heraeus
Safety workbench Safe 2020	Thermo Fischer Scientific
Safire <sup>2</sup> Multi Detection Plate Reader	Tecan
Scale EK-4000H	A&D Weighing
Thermal cycler Hybaid PCR Sprint	Thermo Fischer Scientific

TissueLyser	QIAGEN
Video-optical EHT analysis system	EHT Technologies GmbH
Vortex Genie 2	Scientific Industries
Vortex Reax 2000	Heidolph
Vortex vibrofix	Janke & Kunkel GmbH & Co.KG
Warming cabinet 37 °C	Custom made at UKE, Hamburg
Warming cabinet Kelvitron	T Heraeus
Water bath WB-12	Phoenix Instruments

### 10.2.2 Software

BioRender	BioRender
Consulting Team Machine Vision	CTMV Pforzheim
FACSDiva 9.0	BD Biosciences
Flowing software 2.5.1	Turku Bioscience
Image Lab Version 5.2.1	Bio-Rad Laboratories
ImageJ 1.37	Wayne Rasband
Nanodrop 1000 3.8.1	Thermo Fisher Scientific
NIS-Elements D 4.60.00	Nikon
Office 365	Microsoft
Prism 5	GraphPad
QuantStudio Design & Analysis 1.5.2	Applied Biosystems
SDS 2.4.1	Applied Biosystems

### 10.2.3 Materials and equipment

10 ml Wide Tip Stripette	Corning, 4492
250 ml Vacuum Filtration "rapid"-Filtermax	TPP, 99250
500 ml Vacuum Filtration "rapid"-Filtermax	TPP, 99500
Aspiration pipette 2 ml	Sarstedt, 86.1252.011
Carbon pacing electrode	EHT Technologies GmbH, P0001
Cell culture flask T175 for suspension culture	Sarstedt, 83.3912.502
Cell culture flask T75 for suspension culture	Sarstedt, 83.3911.502
Cell culture plate 6 / 12 / 24 -well	Nunc
Cell culture tube 12 ml, round bottom (for EHT generation)	GreinerBio One, 163160
Cell scraper	Sarstedt, 83.1830
Cell strainer 100 µm	Falcon, 352360
Comb 10 well 1.0 mm	Bio-Rad Laboratories, 165-3359
Cryovial CryoPure 1.6 ml	Sarstedt, 72.380
EHT PDMS rack (24-well format)	EHT Technologies GmbH, C0001
Falcon tube, graduated, 15 ml	Sarstedt, 62.554.502
Flow cytometry tubes	Sarstedt, 55.1579
Gel casting chamber	Bio-Rad

Gel electrophoresis chamber	Bio-Rad, 37S/740
Hydrolysis tubes, screw-capped	Quickzyme Biosciences
Medical Face Masks Type IIR	Farstar medical GmbH
Microtiter 96-well plate	Quickzyme Biosciences
Nalgene Mr. Frosty Cryo 1 °C Freezing Container	Thermo Fischer Scientific
Neubauer counting chamber	Karl-Hecht
Nitrile examination gloves	Dermagrip
Nitrocellulose blotting membrane 0.45 µM	Sigma-Aldrich, GE10600002
Nunc EasyFlask Cell Culture Flasks T175 cm <sup>2</sup>	Thermo Fisher Scientific, 156340
Nunclon Delta Surface	
Nunc EasyFlask Cell Culture Flasks T75 cm <sup>2</sup>	Thermo Fisher Scientific, 156499
Nunclon Delta Surface	
Pacing adapter/cables	EHT Technologies GmbH, P0002
Pipette tips	Sarstedt, 70.762, 70.760.002
Pipette tips with Biosphere filter	Sarstedt, 70.1130.210, 70.1116.210 70.760.212, 70.762.211
PTFE spacer	EHT Technologies, C0002
Reaction tubes conical 15 / 50 ml	Sarstedt
Reaction tubes Safe Lock 0.2 - 2 ml	Eppendorf
Scalpel Blade	Bayha GmbH
Serological pipettes 2 / 5 / 10 / 25 / 50 ml	Sarstedt
Spinner flasks 1000 ml	Integra Biosciences, 182101
Syringe filtration unit Filtrapur S 0.2 µm	Sarstedt, 83.1826.001
TissueLyser steel beads	QIAGEN, 69989
V-shaped sedimentation rack	Custom made at UKE, Hamburg

#### 10.2.4 Cell culture medium and serum

Advanced DMEM/F12	Gibco, 12634010
Basal Medium (Neurobasal)	Thermo Fisher Scientific, 21103-049
Bovine serum albumin	Fisher Scientific, 30036578
DMEM powder for 2x DMEM	Gibco, 52100-021
DMEM/F-12 without Glutamine	Gibco, 21331-046
DMEM-low glucose	Sigma, D5546-500ML
Essential E8 medium + supplements	Gibco, A1517001
Foetal Bovine Serum	Biochrom, S0615
Fibroblast Growth Medium 3 + supplements	PromoCell, C-23025
Horse serum	Life Technologies, 26050-088
Human serum albumin	Biological Industries, 05-720-1B
RPMI 1640	Gibco, 21875-034

## 10.2.5 Reagents

1,4-Dithiothreitol (DTT)	Roth, 6908.2
1-Thioglycerol	Sigma-Aldrich, M6145
2-Mercaptoethanol	Sigma-Aldrich, M6250
2-Propanol	Merck Millipore, 107022
Accutase Cell Dissociation Reagent	Sigma-Aldrich, A6964
Acrylamide/Bis 40%	Bio-Rad Laboratories, 161-0146
Activin A	R&D Systems, 338-AC
Agarose	Invitrogen, 15510-027
Ammonium persulfate (APS)	Bio-Rad Laboratories, 161-0700
Angiotensin II (human)	Abcam, 120183
Aprotinin	Genaxxon bioscience, M6361.1010
bFGF	R&D Systems, 233-FB
Biotin	Sigma-Aldrich, B4639-100MG
BMP4	R&D Systems, 314-BP
Bromophenol blue	Merck, 115-39-9
BTS (N-benzyl-p-toluenesulfonamide)	TCI, B3082-25G
Catalase	Sigma-Aldrich, C40-100MG
CHIR99021	Cayman, 13122
Chloroform	J.T. Baker, 7368
Collagenase II	Worthington, LS004176
Corticosterone	Sigma-Aldrich, C2505-500MG
D(+)-Galactose	Sigma-Aldrich, G0625-100G
D(+)-Glucose anhydrous	Roth, X997.2
DL-alpha tocopherol	Sigma-Aldrich, T3251-5G
DL-alpha tocopherol acetate	Sigma-Aldrich, T3001-10G
DMSO	Sigma-Aldrich, D4540
DNase II type V	Sigma-Aldrich, D8764
Dorsomorphin	Tocris, 3093
DPBS	Gibco, 14190250
EDTA	Roth, 8043.2
Endothelin-1	Sigma-Aldrich, E7764
Ethanol, absolute	Chemsolute, 2246.1000
Ethanolamine	Sigma-Aldrich, E9508-100ML
Fibrinogen	Sigma-Aldrich, F8630
Geltrex	Gibco, A1413302
GlutaMax Supplement	Gibco, 35050061
Glutathione	Sigma-Aldrich, G6013-5G
Glycerol	Roth, 56-81-5
Glycine	Roth, 56-40-6
HBSS (-) Ca <sup>2+</sup> /Mg <sup>2+</sup>	Gibco, 14175-053
HEPES	Roth, 9105.4
Human Holo-Transferrin	Sigma-Aldrich, T0665-500MG
Hydrochloride	Supelco/Merck 1.00317.2500

Hydrocortisone	Sigma-Aldrich, H4001
Insulin	Sigma-Aldrich, I9278
IWR-1	Selleckchem, S7086
Laminin	Sigma-Aldrich, 11243217001
L-Carnitine	Sigma-Aldrich, C0283-1G
L-Glutamine	Gibco, 25030-081
Linoleic acid	Sigma-Aldrich, L1012-100MG
Linolenic acid	Sigma-Aldrich, L2376-500MG
Lipid mix	Sigma-Aldrich, L5146
Magnesium chloride (MgCl <sub>2</sub> )	Sigma Aldrich, M0250
Matrigel Basement Membrane Matrix	Corning, 354234
Methanol	J. Baker, 8045
Milk powder	Roth, T145.2
N,N,N',N'-Tetramethylethylenediamine (TEMED)	Bio-Rad Laboratories, 161-0801
Nitrogen, liquid	TMG
Non-essential amino acids	Gibco, 11140
Papain	Sigma-Aldrich, 76220
Paraffin	Sigma-Aldrich, 327204
Penicillin / streptomycin	Gibco, 15140
Phenylephrine	Sigma-Aldrich, 59-42-7
Phosphoascorbate (2-Phospho-L-ascorbic acid trisodium salt, PAA)	Sigma-Aldrich, 49752
Pluronic F-127	Sigma-Aldrich, P2443
Polyvinyl alcohol	Sigma-Aldrich, P8136
Ponceau S solution	Sigma-Aldrich, P7170-1L
Progesterone	Sigma-Aldrich, P8783-1G
Puromycin	Invivogen, QLL-38-04B
Putrescine	Sigma-Aldrich, P5780-5G
Recombinant human PDGF-AA	PeproTech, 100-13A
Retinoid acid	Sigma-Aldrich, 302-79-4
Retinyl acetate	Sigma-Aldrich, R7882-1G
Roti-Histofix 4%	Roth, P087.3
Saponin	Merck, 558255
SB-431542	MedChemExpress, HY-10431
Sodium azide	Sigma-Aldrich, 71290
Sodium chloride solution 0.9%	B. Braun, 3570210
Sodium dodecyl sulfate (SDS)	Roth, 151-21-3
Sodium fluoride	Merck, 106449
Sodium hydroxide	Roth, 6771.1
Sodium selenite	Sigma-Aldrich, T8158
TBS	Sigma-Aldrich, T6664
TGF- $\beta$ 1	Peprtech, 100-21
Thrombin	Sigma-Aldrich, T7513
Trans-4-(Aminomethyl)cyclohexanecarboxylic Acid (TA)	Sigma-Aldrich, 857653-50G



Transferrin	Sigma-Aldrich, S5261
Triiodo-L-thyronine sodium salt	Sigma-Aldrich, T2877-100MG
TRIS-hydrochloride	Roth, 9090.2
Triton X-100	Roth, 3051.3
Trizma base	Sigma-Aldrich, T1503
Trypan Blue	Biochrom, L 6323
Trypsin-EDTA 0.5%	Gibco, 15400054
Tween 20	Sigma-Aldrich, P1379
VEGF	R&D Systems, 293-VE
Water	B. Braun
XAV-939	Tocris, 3748
Y-27632	Biaffin, PKI-Y27632-010

### 10.2.6 Kits

5x HOT FIREPol EvaGreen qPCR Mix Plus ROX	Solis BioDyne, 08-24-00008
High-Capacity cDNA Reverse Transcription kit	Applied Biosystems, 4368813
Pierce ECL Western Blotting Substrate	Thermo Fisher, 32106
RNeasy Mini kit	QIAGEN, 74904
Total Collagen Assay kit	QuickZyme Biosciences
TRIzol Reagent	Life Technologies, 15596026

### 10.2.7 Composition of reagents and solutions

Table 18: Composition of used reagents and solutions

Reagent/solution	Composition
Agarose for EHT casting	2% (w/v) Agarose 300 ml 1 x DPBS Sterilised by autoclaving
Agarose for nanoindentation	4% (w/v) Agarose 300 ml 1 x DPBS
Aprotinin	33 mg/ml Aprotinin Dissolved in sterile water
BTS solution	30 mM BTS in DMSO
DNase solution	100 mg DNase II, type V 50 ml DPBS Filter-sterilised (0.2 µm filter)
EDTA	0.5 mM EDTA DPBS
Fibrinogen	200 mg/ml Fibrinogen 100 µg/ml Aprotinin 0.9% NaCl solution
HEPES stock solution	1 M HEPES

	DPBS Sodium hydroxide for adjustment of pH to 7.4
Pluronic F-127 solution	0.1% (v/v) Pluronic F-127 DPBS Filter-sterilised (0.2 µm filter)
Polyvinyl alcohol (50X)	20 g Polyvinyl alcohol Add water to 100 ml
SB-431542	10 µM SB-431542 in DMSO
Thrombin	100 U/ml Thrombin 60% (v/v) DPBS 40% (v/v) Water
Tris 0.5 M (pH 6.8)	60.6 g Trizma base Add water to 1 l
Tris 1.5 M (pH 8.8)	181.7 g Trizma base Add water to 1 l

### 10.2.8 Antibody list

Table 19: Primary and secondary antibodies for flow cytometry

Antibody	Dilution	Company and #
Anti-SSEA3 Alexa Fluor 647	1:50	BD Pharmingen, 561145
Isotype control Alexa Fluor 647	1:50	BD Pharmingen, 557714
Anti-cardiac troponin T FITC	1:50	Miltenyi Biotec, 130-119-575
Isotype control FITC	1:50	Miltenyi Biotec, 130-113-437
Anti-DDR2	1:210	Thermo Fisher, PA5-27752
Goat anti-rabbit Alexa Fluor 405	1:200	Invitrogen A-31556
Anti-αSMA	1:100	Dako, M0851
Goat anti-mouse Alexa Fluor 633	1:100	Invitrogen A-21050

Table 20: Primary and secondary antibodies for Western blot analysis

Antibody	Dilution	Company and #
Anti-periostin	1:500	Invitrogen, PA5-34641
Anti-rabbit IgG peroxidase-conjugated secondary antibody	1:10000	Sigma-Aldrich, A0545
Anti-αSMA	1:2000	Dako, M0851
Anti-α-tubulin	1:5000	Cell Signaling, #3873
Anti-lamin A/C	1:1000	Santa Cruz, sc-376248
Anti-mouse IgG peroxidase-conjugated secondary antibody	1:10000	Sigma-Aldrich, A9044

## 11. Declaration of academic integrity – Eidesstattliche Versicherung

I hereby declare that I have performed my work independently without outside help, aside from the references and aids indicated in my work. The passages taken from the consulted works, either verbatim or rewritten, are individually listed according to edition (issue and year of publication), volume and page, when applicable.

I further declare that this thesis was not submitted in any other form to any other University or board of examiners.

I agree that my thesis can be checked with a commonly employed software for plagiarism by the dean of the medical faculty.

Signature: .....

---

Ich versichere ausdrücklich, dass ich die Arbeit selbständig und ohne fremde Hilfe verfasst, andere als die von mir angegebenen Quellen und Hilfsmittel nicht benutzt und die aus den benutzten Werken wörtlich oder inhaltlich entnommenen Stellen einzeln nach Ausgabe (Auflage und Jahr des Erscheinens), Band und Seite des benutzten Werkes kenntlich gemacht habe.

Ferner versichere ich, dass ich die Dissertation bisher nicht einem Fachvertreter an einer anderen Hochschule zur Überprüfung vorgelegt oder mich anderweitig um Zulassung zur Promotion beworben habe.

Ich erkläre mich einverstanden, dass meine Dissertation vom Dekanat der Medizinischen Fakultät mit einer gängigen Software zur Erkennung von Plagiaten überprüft werden kann.

Unterschrift: .....